

The Preserve: Lehigh Library Digital Collections

Assessing Coral Biodiversity Through Environmental DNA

Citation

McCartin, Luke. *Assessing Coral Biodiversity Through Environmental DNA*. 2024, https://preserve.lehigh.edu/lehigh-scholarship/graduate-publications-theses-dissertations/theses-dissertations/assessing-coral.

Find more at https://preserve.lehigh.edu/

This document is brought to you for free and open access by Lehigh Preserve. It has been accepted for inclusion by an authorized administrator of Lehigh Preserve. For more information, please contact preserve@lehigh.edu.

Assessing Coral Biodiversity Through Environmental DNA

by

Luke
McCartin

Presented to the Graduate and Research
Committee of Lehigh University
in Candidacy for
the Degree of
Doctor of
Philosophy

in

Biology

Lehigh
University

August 2024

© 2024 Copyright
Luke McCartin

Dissertation is accepted and approved in partial fulfillment of the requirements for the PhD in Biology in the Department of Biological Sciences.

Dissertation Committee Members:

Dr. Santiago Herrera

Dr. Annette Govindarajan

Dr. Jill McDermott

Dr. Wynn Meyer

Dr. Amber Rice

ACKNOWLEDGEMENTS

My passion for understanding the distribution and evolution of life on Earth began during my childhood on Cape Cod. Here, in a place defined by seasonal change, I found joy exploring forests, ponds, salt marshes and beaches. Southwesterly winds in the summer revitalized the landscape and brought a suite of migratory species from both the air and sea. When the last school of bluefish, *Pomatomus saltatrix*, departed ahead of an October nor'easter, the landscape reset.

I am forever grateful to my parents, Janet and Paul, for raising me and my sister Madelyn in such a naturally interesting place, and for always supporting my love to learn about and explore the outdoors. My father taught me the joy of finding snakes, salamanders, and most of all birds at home on the Cape and on road trips. We explored places like the White Mountains to the north and Shenandoah to the south. I am reminded of venturing far back into the Great Smoky Mountains on dirt roads in our minivan and successfully finding a reintroduced population of Elk. These experiences formed the bedrock of my passion to understand the natural world that has evolved into a career and life full of deep personal reward.

I could not have accomplished this goal without the support and guidance of so many people during this academic journey that began when I was just eighteen years old. I thank Dr. Daniel Fornari and Dr. Timothy Shank who first opened my eyes to the possibility of a life as a scientist and oceanographer at the Woods Hole Oceanographic Institution. For their guidance during my undergraduate years, I thank Dr. Juli Gould at the USDA in Buzzards Bay, and Dr. Alison Brody and Dr. Nabil Nasseri at the University of Vermont. It was working under their mentorship that I began to fully

express my research interests and hone my skills. During these years and in Woods Hole afterwards, I thank Lizzie McElwee for her selfless encouragement and support, and for sharing with me her love of exploring truly wild places like Dolly Sods. I am also grateful for my friends during winter in Woods Hole, Joe Mangiafico, Rory Egan, Sarah Weiss and Jenny Vaccaro.

The experience that lit a fire in me to pursue a career as a deep-sea biologist was the participation in my first research cruise to the Phoenix Islands Protected Area in 2017. For inviting me to participate in that incredible expedition, I thank Dr. Timothy Shank and Dr. Erik Cordes. Here, I also met Dr. Alexis Weinnig, who took me under her wing and continues to show me the ropes as I navigate my career. I am forever thankful for her continued investment in my success as both a scientist and in life in general.

I certainly would not have achieved this much during my PhD if not for my advisor Dr. Santiago Herrera. Reconnecting with Santiago in 2019 as I explored my options for graduate school ended up being the best possible choice for my career. During these five years, I have been afforded more opportunities than I could have envisioned, and I have grown as a scientist in a way that I could not have fathomed before I started in the lab. His infectious enthusiasm for deep-sea research has propelled me forward to accomplish all my research goals.

I also owe deep gratitude to my dissertation committee. I started my PhD with limited molecular biology experience. Dr. Annette Govindarajan welcomed me to her lab to visit during the first year of my PhD in 2019. Under Annette's mentorship I became a competent molecular biologist and eDNA analyst, defining the pace at which I was able to complete all this work. Annette's guidance during my visit and afterwards has been

vital to my success. I am thankful to have been lucky enough to have learned from Dr. Jill McDermott, in the classroom and at sea, and for her belief in my abilities as a researcher. As one example, she believed in me to dive in *Alvin*, to the chimneys at YBW of all places, settling my nerves and allowing me to experience a day that I consider the highlight of my career. In Dr. Wynn Meyer's class, she challenged us to think about the societal implications of our science and how to be a moral scientist. I am grateful for that perspective and for her continued support, feedback, and excitement to point me in the right direction as I forge onward in my career. It has been a pleasure to learn from Dr. Amber Rice both as her teaching assistant and as her student, and to collaborate with her and her lab members. I am also thankful for her guidance through various aspects of our PhD program.

My five years of research have been made more fun by working alongside members of Lehigh Oceans and specifically the Herrera Lab including Susan Ambrose, Penny Demetriades, Syrmalenia Kotronaki, Nicole Pittoors, Milan Sengthep, Dr. Samuel Vohsen, and Liz Whitson. I would like to specifically thank Sam, who has always been willing to share his wealth of knowledge with me, and who has been instrumental in my success as a graduate student and as a vegetable gardener. Adventure is par for the course as a member of the Lehigh Oceans team. I am reminded of specific memories like our road trip to Mississippi and celebrating our dives in *Alvin* at the East Pacific Rise. These memories and so many more have defined my time as graduate student at Lehigh, and I look forward to another year of fun experiences at sea and in the lab as a member of Lehigh Oceans.

My fellowship at the Smithsonian Museum of Natural History (NMNH) was both productive and truly enjoyable. I thank my fellowship mentors Dr. Andrea Quattrini and Dr. Allen Collins for welcoming me into their labs and for teaching me so much in such a short time. In the Department of Invertebrate Zoology at NMNH I would also like to thank Dr. Sarah Tweedt, Dr. Chris Meyer, Dr. Herman Wirshing, and LAB staff for their helpful discussion and technical assistance. I'd also like to thank members of the NMNH coral lab, especially Annemarie Wood, Dr. Jeremy Horowitz, Dr. Claudia Vaga, Dr. Declan Morrissey, Dr. Michael Connelly, Nina Ramos, Dr. Sonia Rowley, and Dr. Adela Roa-Varón for our productive collaborations and discussions.

I'd like to acknowledge my other co-authors, Dr. Michael Layden, Dr. Catherine McFadden and Emma Saso, and our collaborators who have helped me in my dissertation research through our discussions regarding all things marine eDNA: Dr. Eily Allan, Dr. Cheryl Morrison, Dr. Dana Yoerger, and Dr. Meredith Everett. I would also like to thank several undergraduate students who I was fortunate to work with over the years and contributed significantly to data collection for the work in Chapter 3: Penny Demetriades, Luis Caceres, Mary Mahoney, Maia Clayton, Carly Hecht, and Petra Oganovich. None of this work would have been possible without the help of members in the department of Biological Sciences, especially Erin Curtolo, Maria Brace, and Lee Graham, whose technical expertise allowed me to learn new techniques like fluorescence microscopy. I'd also like to thank Dr. Greg Lang and Dr. Mike Burger for their investment in our experience as graduate students in the department and college, respectively.

Various aspects of this work were funded by NOAA Office of Ocean Exploration award #NA180AR0110289, and the CYCLE Project, funded by NOAA's National

Centers for Coastal Ocean Science competitive research program under award NA18NOS4780166. Chapter 5 was also part of the Woods Hole Oceanographic Institution's Ocean Twilight Zone Project, funded as part of the Audacious Project housed at TED. I am grateful to the Smithsonian Institution Fellowship Program and the Thorne Fellowship in the Department of Biological Sciences at Lehigh for each funding me for one semester of my PhD, the Department of Biological Sciences for funding me as a teaching assistant for four semesters, and to NOAA's Mesophotic and Deep Benthic Communities project for funding me for one year through a video analysis contract.

For the field work components of this research, I thank the Flower Garden Banks National Marine Sanctuary and the sanctuary staff; the captains and crew of the *R/V Manta* and *R/V Point Sur*; the *Mesobot* team, and the *Global Explorer* ROV team. For their help with library preparation and sequencing, I thank the Genomics Research Core at the University of Illinois Chicago; the Genomics and Microbiome Core Facility at Rush University; and specifically, Dr. Stefan Green, Kevin Kuntsman, Weihua Wang, and Cecilia Chau. For their instruction in microbiome and phylogenetic analysis, I thank the instructors and teaching assistants of the STAMPS and Molecular Evolution courses at the Marine Biological Laboratory.

Last but certainly not least, I'd like to thank my loved ones and friends whose support underlies my accomplishments. My success over the past five years would not have been possible in isolation, something that I learned the hard way during the initial COVID lockdown. These five years have come with hardship and tested my ability to continue onward towards this goal. My parents support and guidance has been unwavering, even when they have had to bear their own hardships over the past few

years. For always being there for me throughout these moments, I also thank my sister Madelyn. I look forward to brighter days ahead with you and Dan; you both brighten my life. For lifting me up during the harder moments of the past two years, helping me regain my sense of place, pushing me over the finish line, and always showing me love and kindness, I am grateful to Sam Temples.

I am so fortunate to have made so many great friends over these five years, at Lehigh, in D.C., and beyond. Allison and Artemiza, thank you both for being there with me through huge milestones in our program, like our qualifying exam, and for being fantastic office mates. I can't wait to celebrate you both too. Austin, Nicole, Slam, Milan, Sam, Mac, Jess, Allison and Arpana, all our good times have lifted me up over the past few years. You've been there for me when I needed it, whether that was pushing me to hike the Devil's Path or helping me simply survive a weekend of Musikfest. For making the trip out to Bethlehem numerous times and joining for some of our most memorable days, I thank lifelong friend Mike Dombrowski. I am also grateful for everyone in the Invertebrate Zoology department at NMNH, for welcoming me in during my visit, and for happy hours and excursions to D.C. museums and Nats games. Lastly, one of the greatest joys of being a scientist is traveling for conferences, field expeditions, and courses like those offered at the MBL in Woods Hole. I'll cherish all these experiences and the people that I've met over these five years.

TABLE OF CONTENTS

Title page i

Copyright ii

Certificate of approval iii

ACKNOWLEDGEMENTS iv

TABLE OF CONTENTS x

LIST OF TABLES xiv

LIST OF FIGURES xix

ABSTRACT 1

Chapter 1: INTRODUCTION 3

1.1 Mesophotic and Deep-sea Coral Communities 3

1.2 Environmental DNA (eDNA) Quantification and Sequencing 5

1.3 eDNA Analysis for Coral Biodiversity Assessment 6

1.4 Marine eDNA Fate and Transport 8

1.5 Objectives 10

1.6 References 11

Chapter 2: TEMPERATURE CONTROLS EDNA PERSISTENCE ACROSS PHYSICOCHEMICAL CONDITIONS IN SEAWATER 25

2.1 Abstract 25

2.2 Introduction 26

2.3 Methods 29

2.4 Results and Discussion 43

2.5 Acknowledgements 55

2.6 References 55

Chapter 3: INFLUENCE OF THE BACTERIAL COMMUNITY ON EDNA DEGRADATION IN EXPERIMENTS ACROSS PHYSICOCHEMICAL CONDITIONS IN SEAWATER 69

3.1 Abstract 69

3.2 Introduction 70

3.3 Methods 72

3.4 Results and Discussion 83

3.5 Concluding remarks 100

3.6 Acknowledgements 101

3.7 References 102

Chapter 4: NUCLEAR EDNA METABARCODING PRIMERS FOR ANTHOZOAN CORAL BIODIVERSITY ASSESSMENT 113

4.1 Abstract 113

4.2 Introduction 114

4.3 Methods 116

4.4 Results and Discussion 134

4.5 Concluding remarks 149

4.6 Acknowledgements 150

4.7 References 151

Chapter 5: TRANSPORT OF BENTHIC MARINE EDNA AT AN OFFSHORE MESOPHOTIC BANK IN THE NORTHWESTERN GULF OF MEXICO 164

5.1 Abstract 164

5.2 Introduction 165

5.3 Methods 170

5.4 Results 185

5.5 Discussion 201

5.6 Acknowledgments 211

5.7 References 212

Chapter 6: CONCLUSION 223

Publication and co-authorship notes 226

Appendix A: Supporting information for Chapter 2 227

A.1 Supplementary Methods 227

A.2 Supplementary Figures 234

A.3 Supplementary Tables 236

A.4 References 239

Appendix B: Supporting information for Chapter 3 240

B.1 Supplementary Figures 241

B.2 Supplementary Tables 242

Appendix C: Supporting information for Chapter 4 244

C.1 Supplementary Methods 244

C.2 Supplementary Figures 251

C.3 Supplementary Tables 255

C.4 References 257

Appendix D: Supporting information for Chapter 5 259

D.1 Supplementary Figures 259

VITA 261

LIST OF TABLES

Table 3.1: Coefficients and Type III Analysis of Variance results for a linear mixed model with log-transformed eDNA concentrations as the response variable, and the interaction of time with cell counts as a fixed effect along with physicochemical conditions 95

Table 3.2: Coefficients and Type III Analysis of Variance results for a linear mixed model with log-transformed eDNA concentrations as the response variable, and the interaction of time with estimated Shannon alpha diversity as a fixed effect along with physicochemical conditions 95

Table 3.3: Coefficients and Type III Analysis of Variance results for a linear mixed model with log-transformed eDNA concentrations as the response variable, and the interaction of time with PCoA axes as fixed effects along with physicochemical conditions. 96

Table 4.1: Primer sequences designed for anthozoan coral eDNA metabarcoding of the nuclear *28S* gene. The *Anth-28S-eDNA* primers were designed to target black coral and octocoral sequences, and the *Scler-28S-eDNA* primers target scleractinian sequences. For metabarcoding, the forward and reverse primers were synthesized with CS1 and CS2 universal adapters, respectively, at the 5' ends to facilitate the binding of Access Array (Standard BioTools) indices unique to each sample during library preparation. The CS1 universal adapter is 5'-ACACTGACGACATGGTTCTACA-3', and the CS2 universal

adapter is 5'-TACGGTAGCAGAGACTTGGTCT-3'. The %GC content reported for primers with ambiguities is the average of the possible primer sequences. 121

Table A.1: Statistics summarizing the fits of linear models and segmented linear models to log-transformed eDNA concentration data over time to estimate exponential decay rate constants for single-phase and biphasic decay models. Between single-phase and biphasic models, lower BIC values and non-significant P-values are bolded. *pH for each experiment was measured at the ambient temperature in the cold room set for each experiment and at 1 bar. 236

Table A.2: Parameters for simple and biphasic exponential models of eDNA decay among 22 eDNA persistence experiments conducted under 11 unique sets of physicochemical factors. *pH for each experiment was measured at the ambient temperature in the cold room set for each experiment and at 1 bar. **Decay rate constants for the initial and second phases of eDNA degradation, as given by the fit of a biphasic exponential model, are separated by commas in that order. 236

Table A.3: Summary of the linear mixed model fit to the first phase data for twenty-one eDNA persistence experiments to investigate the role of temperature, pH, [DO] and relevant covariates in controlling eDNA degradation rate. The model formula was LN(eDNA Conc.) ~ Temp.*Time + pH*Time + [DO]*Time + ORP*Time + (1 + Time | Experiment). 237

Table A.4: Summary of the linear mixed model fit to the second phase data for twenty-one eDNA persistence experiments to investigate the role of temperature, pH, [DO] and relevant covariates in controlling eDNA degradation rate. The model formula was LN(eDNA Conc.) ~ Temp.*Time + pH*Time + [DO]*Time + ORP*Time + LN(Max total DNA concentration + 1)*Time + (1 + Time | Experiment). 237

Table A.5: Summary of the linear mixed model fit to the second phase data for eDNA persistence experiments conducted at pH 8.2, 4°C, and 20°C to investigate the role of [DO] on eDNA degradation rate. The model formula was LN(eDNA Conc.) ~ Temp.*Time + [DO]*Time + ORP*Time + LN(Max total DNA concentration + 1)*Time + (1 + Time | Experiment). 237

Table A.6: Summary of the linear mixed model fit to the second phase data for eDNA persistence experiments conducted at 4°C and 10°C, to investigate the role of pH and relevant covariates in controlling eDNA degradation rate. The model formula was LN(eDNA Conc.) ~ Temp.*Time + pH*Time + [DO]*Time + ORP*Time + LN(Max total DNA concentration + 1)*Time + (1 + Time | Experiment). 238

Table A.7: Data from previous studies and this study included in the analysis of $T_{99.9\%}$, or the calculated time point at which 99.9% of the starting concentration of eDNA degrades. 238

Table A.8: Concentrations of caryophylliid eDNA from seawater samples at Viosca Knoll 826, ~ 470 meters depth in the Gulf of Mexico. "ND" represents no detection or the instance wherein a qPCR triplicate did not amplify. 238

Table A.9: Measured concentrations of undiluted and diluted eDNA samples to test for PCR inhibition. 239

Table B.1: Bacteria detected in *16S* metabarcoding data from samples taken during twenty-two eDNA persistence experiments. 242

Table C.1: Sample metadata for collections of corals made from field sites in the northwestern Gulf of Mexico that were DNA barcoded through conventional PCR/Sanger sequencing and/or genome skimming. 255

Table C.2: *28S* barcode sequences of anthozoan corals generated in this study and downloaded from GenBank for taxonomic classification, as well as analyses of primer complementary and the ability of the *28S* barcode amplified with the primers described herein to delineate taxonomic groups. 255

Table C.3: *mtMutS* sequences of octocorals generated in this study or downloaded from GenBank for taxonomic classification, as well as analyses of the ability of the *mtMutS* barcode amplified with the primers described in Everett and Park (2018) to delineate taxonomic groups. 256

Table C.4: eDNA sample metadata for eDNA samples analyzed using the *28S rRNA* and *mtMutS* primers in this study. 256

LIST OF FIGURES

Figure 2.1: (A) Matrix of target conditions for 11 combinations of temperature, pH, and [DO] investigated to determine the persistence of eDNA from the coral *Lophelia* among a range of marine physicochemical states. Two replicate experiments were conducted for each combination of temperature, pH, and [DO]. 20°C temperature, half and fully saturated oxygen experiments (shaded green) represent conditions characteristic of subtropical subsurface environments. 4°C temperature, half-saturated conditions (shaded dark blue) represent conditions characteristic of the subtropical deep-sea environment. Remaining cells (shaded light blue) represent other conditions characteristic of the global subsurface and deep ocean. (B) Schematic examples of experimental conditions. Compressed air and nitrogen gas flow rates were adjusted to reach target [DO]. Small doses of 0.5 M HCl were automatically administered to the tanks when desired pH values were exceeded. Physicochemical measurements were monitored by suspending probes in the tanks. Caps were secured with O-rings to control the oxygen concentration in the above headspace. All tubing and probes were placed through small openings in these caps. A photograph of the experimental setup is presented in Figure S1. (C) Measurements of temperature, pH, and [DO] over the 22 eDNA persistence experiments. Points indicate individual measurements, and paths are drawn through daily averages. All measurements were recorded daily and at each sampling time point. Temperature measurements were made using a laser thermometer. pH and [DO] measurements were made with probes in each of twenty-two individual experimental tanks. 30

Figure 2.2: Degradation of *Lophelia* eDNA in 22 persistence experiments among a range of marine physicochemical states. eDNA concentration was measured as the concentration of a 154 base pair fragment of the *Lophelia* mitochondrial COI gene. The natural log-transformed concentration of eDNA (y-axis) is plotted against time (x-axis). Different colors represent the two experimental replicates at each experimental condition. Points represent the average of three qPCR replicate measurements for two samples at a given time point. Lines represent the fit to a biphasic model. Thin lines connecting points to the line of best fit represent the distance from the observed to the fitted values at each time point (the residuals). Panels are arranged by temperature (descending top to bottom) and [DO] (increasing left to right). Values shown on top of each panel indicate the target experimental conditions. Points below the limit of quantification of the qPCR assay (the natural log of 77.8 copies/reaction or 130 copies/mL seawater filtered) are not plotted. The limit of quantification is indicated by the dashed line. 44

Figure 2.3: Decay rate constant estimates for the initial (A) and second (B) phases of eDNA degradation for 22 experiments conducted across 11 combinations of temperature, pH and [DO]. Decay rate constants were estimated by fitting an exponential decay equation with initial and second degradation phases with different rates (biphasic). Decay rate constants are arranged on the x-axis by the average pH over the course of each experiment. Vertical error bars represent 95% confidence intervals for the decay rate constants. The color of each point represents the average [DO] over the course of each experiment. 48

Figure 2.4: eDNA persistence time (times until degradation of 99.9% of starting eDNA concentration), estimated using decay rate constants from our study and other published marine studies, as a function of temperature. The line of best fit is fit only to points derived from the simple exponential model. The shaded region represents the 95% confidence interval for the slope. Points are dodged slightly from actual recorded temperatures to improve visualization. (Inset) Comparison of calculated persistence times when fitting a single exponential versus a biphasic model to the data in this study. Data are reported in **Table A.7**. 52

Figure 3.1: Relative abundance of bacterial ASVs that comprised at least 1% of the sequencing reads in any single sample in 22 eDNA persistence experiments. Genus-level taxonomic classifications of the bacterial ASVs are visualized. Shannon alpha diversity and cell counts are plotted in the upper panels. Shannon alpha diversity is plotted as the black line through each estimate at each timepoint. Each individual cell count observation, and a smoothing curve fit through the average cell count at each timepoint are plotted. The right y-axis (cell counts) is $\log_{10}$ transformed. 86

Figure 3.2: Distance-based redundancy analysis (dbRDA) ordination plots of *16S* bacterial communities visualized by time, temperature, dissolved oxygen concentration, and pH in eDNA persistence experiments. Bray-Curtis distances between samples were calculated based on a matrix of relative abundances of genera represented by ASVs that comprised at least 1% of sequence read abundance in any sample. Axes labels represent the percentage of constrained variation that is accounted for by each axis. 88

Figure 3.3: Relationships between decay rate constants and the maximum number of cells counted at any one time point in eDNA persistence experiments. Error bars represent the standard error of the decay rate constant estimate. 94

Figure 3.4: Changes in [PO_4^{3-}] over time in eDNA persistence experiments plotted by temperature. Each point represents the average concentration from duplicate samples analyzed from each time point in each experiment. A smoothing function was fit to the data, and the highlighted region represents the standard error. 98

Figure 4.1: Sequence alignment of the barcoding region of the *28S* targeted for eDNA metabarcoding from a selection of zoantharian, octocoral, black coral, and scleractinian species. Sequences were aligned with MAFFT. The similarity of the aligned sequences was calculated as the percent identity shared at each position across all sequences. The scale bar represents the number of substitutions per site. The tree is rooted at the node representing the most recent common ancestor of hexacorals and octocorals. The tree was modeled using IQ-TREE2 (Minh et al., 2020) without bootstrapping. The best substitution model was found with modelfinder (Kalyaanamoorthy et al., 2017) based on Bayesian Information Criterion. The model is a transition model where AC=CG and AT=GT and base frequencies were unequal (TIM3), with empirical base frequencies (+F), and rate heterogeneity modeled using a gamma function (+G4). 118

Figure 4.2: (A) eDNA sampling sites (white points) across the Northern Gulf of Mexico. Water sampling was conducted with Niskin bottles during remotely operated vehicle (ROV) dives and Niskin bottle rosette (CTD) casts. Bathymetry data is from the Global Multi-Resolution Topography Data Synthesis (GMRT.org), and contours represent 100-meter isobaths. EFGB stands for Eastern Flower Garden Bank. **(B)** At Bright Bank and to its east, eDNA samples were collected at three proximate sites at differing depths. Navigational fixes during ROV dives are shown in black and intersect contour lines. The spatial extent of the highlighted area on the right is indicated as the yellow shaded area on the map of Bright Bank on the left panel. Bathymetry data is from the USGS Multibeam Mapping of Selected Areas of the Outer Continental Shelf, Northwestern Gulf of Mexico (https://pubs.usgs.gov/of/2002/0411/index.html). Contours represent 10-meter and 2-meter isobaths. Sampling sites at EFGB and at 67 and 85-meters depth at Bright Bank were conducted within the boundaries of the Flower Garden Banks National Marine Sanctuary (highlighted in red). The bathymetric map was created with QGIS. 125

Figure 4.3: Matrices of pairwise identities between *28S rRNA* barcode sequences generated in this study and downloaded from GenBank. Boxes with thick black borders highlight comparisons within families, and boxes with thin black borders highlight comparisons within genera. Only families represented by the largest numbers of barcode sequences are labeled to highlight these comparisons and improve readability. 139

Figure 4.4: Octocoral eDNA sequence read abundances from replicate water samples taken during ROV dives and CTD casts near coral communities in the Northern Gulf of

Mexico. Data are separated by the primer set used (*Anth-28S-eDNA* vs. *mtMutS*). Variable x-axis scales are used to aid in data visualization for all taxa. 146

Figure 4.5: Black coral and scleractinian eDNA sequence read abundances from replicate water samples taken during ROV dives and CTD casts near coral communities in the Northern Gulf of Mexico. Data generated using both the *Anth-28S-eDNA* and *Scler-28S-eDNA* primers are summed. Sequence libraries from East Flower Garden Bank were only generated using the *Scler-28S-eDNA* primers. Variable x-axis scales are used to aid data visualization. Sequence reads classified to the genus *Tubastraea* are not visible due to the low sequence read abundance. 147

Figure 5.1: A) Bathymetric map of Bright Bank and nearby mesophotic banks in the northwestern Gulf of Mexico. Bathymetry data includes data from the USGS Multibeam Mapping of Selected Areas of the Outer Continental Shelf, Northwestern Gulf of Mexico (https://pubs.usgs.gov/of/2002/0411/index.html) (Gardner et al., 1998) and the General Bathymetric Chart of the Oceans (GEBCO; https://www.gebco.net/). 10-meter isobaths at depths from 100 to 60 meters in the high resolution data are indicated with contour lines. 60 and 80-meter isobaths are emboldened and labeled. The extent of the color ramp is from 300 to 60 meters, and all depths shallower than 60 meters are indicated by the same, light blue color. B) Bathymetric map of Bright Bank, the study site at the shelf edge in the northwestern Gulf of Mexico. Contour lines represent the 40, 60, 80, 100 and 120 meter isobaths. Colors of the stations correspond their distances from the center of Bright Bank, except for casts at the "*Swiftia"* and "mooring" stations. C) Downcast profiles of

temperature from Niskin bottle rosette casts at distances away from the center of Bright Bank. 173

Figure 5.2: Rarefaction curves visualizing amplicon sequence diversity (ASV) in samples at steps of 2,500 sequencing reads for libraries generated using an *18S* and *28S* barcode. Each path line represents a single sample from a Niskin bottle collected during Niskin bottle rosette casts at the center or some distance from the center of Bright Bank in the northwestern Gulf of Mexico (visualized as the color of each path). 186

Figure 5.3: Relative abundances of eDNA sequencing reads from invertebrate animal classes across sampling replicates at different sampling depths, distances and directions from the center of Bright Bank. X axis labels indicate direction from the center of Bright Bank (C = Center, E = east, NE = northeast, NW = northwest, SE = southwest, and SW = southeast). Gray bars on the x axis indicate samples taken as close to the seafloor as possible. 189

Figure 5.4: Visualizations of the first two PCoA axes for eDNA samples amplified using *18S* and *28S* primer sets. Ordinations are based on Bray-Curtis dissimilarities between samples calculated from the relative abundances (upper plots) and presence/absence (lower plots) of animal ASVs. Each point represents data across all sample replicates collected at each sampling station and depth. 192

Figure 5.5: Relative abundances of eDNA from benthic invertebrate families across sampling replicates at different sampling depths, distances and directions from the center of Bright Bank. Note that relative abundances are plotted with different y-axis scales for large volume samples that correspond to each marker and taxonomic grouping. X-axis labels indicate direction from the center of Bright Bank (C = Center, E = east, NE = northeast, NW = northwest, SE = southwest, and SW = southeast). Gray bars on the x axis indicate samples taken as close to the seafloor as possible. 197

Figure 5.6: Modeled $\log_2$ fold changes in the sequence abundances of eDNA from benthic invertebrate families in samples taken below the surface mixed layer. Benthic families with sequence abundances that were significantly correlated ($\alpha = 0.05$) with distance from the center and/or sampling depth are shown. Error bars represent one standard error. 198

Figure 5.7: Taxonomic richness of benthic invertebrates detected in eDNA samples taken at 60 meters depth and at increasing distances from the center of Bright Bank. Each point represents a single sample replicate, and points are colored by their direction away from the bank's center. 199

Figure 5.8: Detections of coral eDNA at depths of 60 and 80 meters at distances away from the center of Bright Bank. 60 and 80-meter isobath contours are emboldened and labeled. The boundaries of the FGBNMS are indicated with the red polygon. Points highlighted in yellow indicate sampling locations where coral eDNA was detected across

all sample replicates at 60 meters depth. X-axis labels indicate direction from the center of Bright Bank (C = Center, E = east, NE = northeast, NW = northwest, SE = southwest, and SW = southeast). Gray bars on the x axis indicate samples taken as close to the seafloor as possible. 200

Figure A.1: Photograph of the experimental setup in the controlled-temperature room. Up to four experiments, and a sampling negative control, were conducted simultaneously. 234

Figure A.2: Residuals over time from a simple exponential model fit as a linear model to natural-log transformed eDNA concentration data over the course of 22 eDNA persistence experiments. Points are colored by the temperature at which each experiment was conducted. 235

Figure A.3: Plots of total DNA concentrations (from any source) measured using Qubit fluorometry over the time course of 22 eDNA persistence experiments among a range of temperatures, pH and [DO]. Each point represents a measurement from an individual DNA extraction. Points are fit with a loess smoothing curve to aid in the visualization of trends over time. 236

Figure B.1: Representative images of bacterial cells from eDNA persistence experiments conducted at temperatures of 20°C (top left), 10°C (top right), 4°C (bottom left), and in a sampling negative control tank at 20°C (bottom right). The bottom two images are

stacked composites of multiple images taken at the same location with slight differences in focus. Composite images were generated using Adobe photoshop and the brightness/contrast were adjusted using the auto setting. Each image was taken at 100X magnification with a 10 µm scale bar included, and scale bars are consistent across the images. The scale bar on the bottom left with enlarged text is superimposed to aid in visualization. 240

Figure B.2: Visualization of principal coordinates analysis (PCoA) of Bray-Curtis distances between experimental and field samples calculated based on the proportion of sequencing reads from each classified Genus in the dataset. 241

Figure C.1: Results of *in silico* taxonomic specificity testing of the *Anth-28S-eDNA* and *Scler-28S-eDNA* primers against the SILVA large subunit ribosomal RNA database. Amplicons were predicted by querying the database with the primers using *cutadapt* and zero, one, and two permitted mismatches to the primer sequences. 251

Figure C.2: Matrices of pairwise identities between predicted *mtMutS* barcode sequences amplified using the PCR primers described in Everett and Park (2018). Boxes with thick black lines delineate comparisons within families, and boxes with thin black lines delineate comparisons within genera. Only families represented by the largest numbers of barcode sequences are labeled to highlight these comparisons and improve readability. 252

Figure C.3: Percentage of sequencing reads identified as coral across libraries generated from eDNA water samples taken at different altitudes from the seafloor. ASVs were identified as corals if the top BLASTN hit for that ASV was at least 90% identical to an anthozoan coral sequence in GenBank. 253

Figure C.4: Maximum-likelihood phylogenetic tree of amplicon sequence variants (ASVs) recovered from eDNA samples collected in the Gulf of Mexico and amplified using the *28S* primers described herein. ASVs were aligned with *MAFFT* and the phylogenetic tree was constructed using *IQTree* and *modelfinder* without bootstrapping. The model with the lowest BIC is a General Time Reversible model with empirical base frequencies (+F), and rate heterogeneity modeled using a gamma function (+G4). Tips are labeled with the *28S* primer set used, ASV numerical identifier and their taxonomic classification. The tree is rooted at the note representing the most recent common ancestor to hexacorals and octocorals. 254

Figure D.1: Profiles of temperature, salinity, oxygen concentration, fluorescence, and turbidity by depth collected during downcasts of Niskin bottle deployments at and near Bright Bank. 259

Figure D.2: Hindcasted currents at approximately 24 hour intervals over the course of eDNA sampling. Data are from the HYCOM + NCODA Gulf of Mexico 1/25° Analysis (https://www.hycom.org/data/gomu0pt04/expt-90pt1m000). The spatial extent along the shelf edge includes Bright Bank as well as West Flower Garden Bank and East Flower

Garden Bank to the west. Contour lines represent 100 meter isobaths. Times are in universal coordinated time. 260

ABSTRACT

The ocean provides humanity with many benefits including commercial, recreational, and subsistence fisheries; tourism economies; and natural resources and is a vital component of many human cultures. These benefits do not end in the surface ocean and coastal seas but extend to the ocean's deepest depths and most remote locales. Diverse biological communities, including mesophotic and deep-sea coral communities, exist in the deep sea, provide ecosystem services, and are impacted by human activities. However, compared to shallow reefs, the fates of these deep coral communities in the face of these anthropogenic impacts receive comparatively less attention. Further, the biodiversity of deep coral communities and their distribution are less understood, largely due to the technical challenges in studying life at the depths that they occur. To rapidly assess and monitor coral biodiversity and its distribution, novel approaches are needed to complement conventional methods. One promising approach is the analysis of environmental DNA (eDNA), the DNA that all organisms release into their environments. However, to fully harness the power of this new technology, the spatiotemporal scales over which eDNA can be detected after it is shed from an organism into the ocean must be constrained.

This dissertation research addresses this knowledge gap through a combination of experimental and field studies. Chapter 2 reports the results of eDNA persistence experiments conducted across combinations of temperatures, pH, and dissolved oxygen concentrations that reflect natural conditions in the subsurface open ocean. Coral eDNA degradation was accelerated at 20°C as compared to 10°C and 4°C, and degradation rates were weakly correlated with pH and not correlated with dissolved oxygen concentration.

Acknowledging that temperature controls eDNA degradation rate, eDNA persistence times across the range of ocean temperatures can be approximated, informing the timescales over which eDNA may be transported in the field. In Chapter 3, bacterial community composition, assessed by sequencing the *16S* gene, and bacterial abundance, measured with fluorescence microscopy, were measured from the experiments reported in Chapter 2. Experiments conducted at 20°C exhibited higher bacterial diversity, along with repeatable and faster rates of bacterial community turnover and bacterial growth than experiments conducted at lower temperatures. These results suggest that microbial processes, in synergy with temperature, govern eDNA degradation rate.

In Chapter 4, new PCR primers and an accompanying reference sequence database for targeted eDNA metabarcoding of anthozoan corals at all depths are presented. These new PCR primers, which target the *28S* gene, distinguish the vast majority of anthozoan corals at the genus level and enrich coral DNA from water samples. In Chapter 5, the transport of eDNA in the open ocean is practically investigated by sequencing eDNA at multiple depths and distances away from an offshore community of benthic invertebrates. Stratification in the water column resulted in limited detection of eDNA in the surface mixed layer and across depth zones in the thermocline. In sequencing data generated using the PCR primers for corals presented in Chapter 4, there was strong evidence for the horizontal transport of eDNA at distances up to ~1.5 kilometers from likely sources. This finding highlights the importance of interpreting species' detections from eDNA data as a function of the sensitivity of the detection or sequencing protocol used. In whole, this dissertation provides new molecular tools and develops a conceptual framework for using eDNA analysis to conserve life in the ocean.

CHAPTER 1

INTRODUCTION

1.1 Mesophotic and Deep-sea Coral Communities

Corals in the subphylum Anthozoa (Phylum: Cnidaria) are foundational species that provide vital ecosystem services, and the benefits they provide extend from shallow, coastal reefs to mesophotic and deep-sea coral communities (Thurber et al., 2014; Soares et al., 2020; Woodhead et al., 2021). Mesophotic coral communities are characterized by their presence in transitional depths where sunlight attenuates nearly completely (Lesser et al., 2009). At mesophotic reefs, light is sufficient for photosynthesis, and zooxanthellate stony corals (Order: Scleractinia) provide reef structure and habitat for fishes and invertebrates as they do in shallow waters. At greater depths in the mesophotic where light is further attenuated, heterotrophy dominates, and arborescent octocorals (Orders: Malacalcyonacea and Scleralcyonacea) and black corals (Order: Antipatharia) tend to increase in abundance along with sponges (Rezak et al., 1985; Kahng et al., 2010). Like stony corals, octocorals and black corals in the mesophotic interact with and provide habitat for invertebrates and fish and are ecosystem engineers through interactions with sponges (Wicksten et al., 2014; Slattery & Lesser, 2021; Bosch et al., 2023). In the deep sea where sunlight attenuates completely (defined as depths of 200 meters and below) azooxanthellate stony coral reefs occur globally, providing important habitats for benthic invertebrates and deep-sea fishes (Roberts et al., 2006; Lessard-Pilon et al., 2010; Cordes et al., 2023). Deep-sea octocorals and black corals also engage in symbioses with other invertebrates and serve as nurseries for teleost fish and

elasmobranchs (Buhl-Mortensen & Mortensen, 2004; Etnoyer & Warrenchuk, 2007; Baillon et al., 2012).

Anthropogenic activities threaten the conservation of mesophotic and deep-sea corals. However, impacts to corals at these depths have received comparatively less attention than impacts to corals at shallow reefs. Threats to mesophotic and deep-sea coral communities include invasive species, rising sea surface temperatures, ocean acidification, destructive fisheries practices, and natural resource extraction (Lesser & Slattery, 2011; Clark et al., 2015; Etnoyer et al., 2016; Rocha et al., 2018; Girard & Fisher, 2018). The potential threat of deep-sea mining to corals also looms (Carreiro-Silva et al., 2022). Despite these threats, understanding the distribution of mesophotic and deep-sea coral biodiversity at regional and global scales is hindered by the technical challenges of observing life on the seafloor in the deep. Nondestructively surveying and sampling corals at mesophotic and deep-sea depths relies on either technical diving or accessing limited submersible assets, whether remotely operated (ROVs), autonomous (AUVs), or human occupied (HOVs) (Heirtzler & Grassle, 1976; Fornari et al., 1997; Pyle, 2019; Armstrong et al., 2019). To further complicate matters, anthozoan corals are difficult if not impossible to identify at meaningful taxonomic levels (genus or better yet species level) from imagery data alone. Therefore, physical collections of specimens are required for their morphological and genetic identification. As a result, the time from data collection in the field to the generation of deep coral species occurrence records is lengthy.

1.2 Environmental DNA (eDNA) Quantification and Sequencing

One method that shows promise to rapidly assess and monitor coral biodiversity in the deep and determine its distribution is the analysis of environmental DNA (eDNA). As its name implies, eDNA refers to the genetic material that is shed by organisms into their environment, typically soil, sediment, or water, but more recently even air (e.g. Lynggaard et al., 2022). The analysis of eDNA from water samples usually involves filtering the sample, and then DNA is isolated from captured DNA and particulates using standard protocols (e.g. phenol-chloroform extraction) or specialized kits. Next, one of two approaches is commonly used, 1) eDNA quantification with quantitative or digital droplet polymerase chain reaction (PCR), or 2) PCR amplification and sequencing with high throughput technologies, such as Illumina (Taberlet et al., 2018).

Quantitative PCR (qPCR) uses primers that are highly specific to a target species or taxon. Standards of known concentrations are analyzed in parallel with samples of unknown concentrations to accurately quantify the concentration of eDNA in a sample down to low concentrations where variability between technical replicates is acceptable (the limit of quantification of the qPCR assay) and detection is consistent (the limit of detection) (Klymus et al., 2020). While qPCR is quantitative and highly accurate, quantifying concentrations of eDNA from more than a few different species or taxa in a sample is impractical, because each species or taxon requires separate PCR primers.

High throughput sequencing of PCR products, a technique referred to as eDNA metabarcoding, is typically used to analyze eDNA from a mixed community of taxa. For eDNA metabarcoding, primers can be designed to broadly amplify a DNA barcode from many taxa (e.g. Amaral-Zettler, 2009; Leray et al., 2013) or specifically amplify a

barcode from a taxon of interest (e.g. Miya et al., 2015). eDNA metabarcoding protocols typically target mitochondrial and ribosomal RNA genes due to their high copy number in the environment and the existence of reference barcode databases from conventional DNA barcoding and molecular phylogenetic studies. eDNA sequences are identified by comparison to sequences from specimens in reference barcode databases. These databases have been conventionally populated with sequences generated using PCR and Sanger sequencing, but more recently reference barcodes are being generated from shallow coverage genome sequencing ("genome skimming") data (e.g. Hoban et al., 2022; Quattrini et al., 2024).

1.3 eDNA Analysis for Coral Biodiversity Assessment

Ficetola et al. (2008) first demonstrated the efficacy of analyzing eDNA for detecting animals, in their case the invasive American bullfrog, *Lithobates catesbeianus*, in European ponds. Since this foundational study, eDNA analysis has been rapidly implemented for animal species detection and biodiversity assessment in freshwater and marine ecosystems (Ficetola et al., 2008; Taberlet et al., 2018; Gaither et al., 2022). In the ocean, the analysis of eDNA from seawater samples has been applied for a multitude of applications and in virtually all marine habitats. eDNA metabarcoding methods have been developed to assess biodiversity in coral reefs, targeting reef-building stony corals themselves as well as the invertebrates and fish that these reefs support (Alexander et al., 2020; Dugal et al., 2020; Shinzato et al., 2021; West et al., 2022). eDNA assays have been developed for the detection of marine invasive species where early detection is challenging (Whitaker et al., 2021). The potential utility of eDNA analysis for fisheries

stock assessments continues to be investigated, and models to make eDNA metabarcoding more quantitative with this goal in mind have been developed (Stoeckle et al., 2020; Yates et al., 2022). In addition, eDNA sequencing protocols have been extended from species detection and biodiversity assessment to analyses of population genetics by using target capture rather than PCR to enrich targets across the genome instead of a single barcode (Jensen et al., 2021).

The analysis of eDNA shows exceptional promise for studying biology at the deep sea, where observations are limited due to the inherent challenges of obtaining imagery data and physical collections for genetic analysis. While eDNA analysis requires expertise in molecular biology and bioinformatics, water sampling is cost effective and time efficient as compared to technical diving and deploying submersibles. The rise of eDNA analysis has also corresponded with a sampling technology boom, and new samplers can filter tens of liters of deep-sea water *in situ*, detecting greater biodiversity than smaller volume samples (Govindarajan, et al. 2022). eDNA sequencing generates data from many species in a single water sample, potentially circumventing the need for comprehensive physical collections from a community to confirm identifications. eDNA analysis is also inherently non-invasive and is thus ideally suited for working in marine sanctuaries (e.g. the Flower Garden Banks National Marine Sanctuary) or at sensitive deep-sea communities, such as those impacted by the Deepwater Horizon oil spill in the northern Gulf of Mexico (Girard & Fisher, 2018).

Indeed, with all these potential benefits, eDNA metabarcoding has been widely adopted for biodiversity assessment in the deep sea, and more specifically at mesophotic and deep-sea coral communities (Everett et al., 2018; Kutti et al., 2018; Laroche et al.,

2020; Canals et al., 2021; Govindarajan et al., 2021; Merten et al., 2021; Govindarajan et al., 2023; Hoban et al., 2023; Nishitsuji et al., 2024). Kutti et al., (2020) developed a qPCR assay for the deep-sea scleractinian *Desmophyllum pertusum*, and Everett & Park (2018) designed PCR primers to amplify a mitochondrial barcode in octocorals. Taxonomically specific PCR primer sets for metabarcoding, like those developed by Everett & Park (2018), permit the targeted enrichment of eDNA from corals, making these methods more sensitive for detecting coral eDNA. PCR primers can also be designed to amplify barcoding regions that are particularly taxonomically informative in corals, instead of relying on the varied taxonomic resolution of a single barcode across many taxa with different evolutionary histories. Prior to this dissertation research, PCR primer sets that specifically target eDNA from corals were designed only to single species (e.g. Kutti et al., 2018), octocorals (Everett & Park, 2018), and shallow scleractinians (Brian et al., 2019; Nichols & Marko, 2019; Alexander et al., 2020; Shinzato et al., 2021).

1.4 Marine eDNA Fate and Transport

eDNA sequencing promises to be a cost effective and sensitive tool for detecting the presence of corals in the deep and assessing their biodiversity and its distribution. However, interpreting species detections from eDNA quantification and sequencing data generated from seawater samples is not straightforward. eDNA may be shed into the marine environment in the form of mucus, skin, scales, gametes and/or waste, and its shedding rate depends on metabolic rate, ontogeny, activity, and environmental factors including temperature (Maruyama et al., 2014; Klymus et al., 2015; Andruszkiewicz

Allan et al., 2021; Ostberg et al., 2021; Thalinger et al., 2021; Kwong et al., 2021). After eDNA is shed from an organism into the surrounding seawater, it is subject to transport by ocean currents until it degrades into fragments that are too short for PCR amplification or settles to the benthos (reviewed in Harrison et al., 2019). Depending on the timescales that eDNA persists, detectable concentrations of eDNA may be transported far from their sources.

Comprehensively determining how physicochemical factors influence the degradation rate of eDNA is vital to constraining the spatiotemporal scale of eDNA detections across environments in the ocean. Multiple experimental studies have pointed to the influence of temperature on marine eDNA degradation (Tsuji et al., 2017; Collins et al., 2018; Jo et al., 2019; Kasai et al., 2020; Andruszkiewicz Allan et al., 2021; Caza-Allard et al., 2021). However, these studies did not concurrently consider other relevant physicochemical factors, namely pH and dissolved oxygen concentration, nor the influence of the microbial community on eDNA degradation.

Predicting the timescales of eDNA persistence is vital to accurately estimating the distances that eDNA may be transported by currents in the ocean. To this end, modeling studies are particularly useful at large spatial scales, and predict the transport of detectable concentrations of eDNA over distances of tens of kilometers by implementing eDNA decay rate estimates from simple exponential models (Andruszkiewicz et al., 2019; Kutti et al., 2020). Even though eDNA transport distances may be substantial, several eDNA metabarcoding studies have distinguished biological communities over small spatial scales in connected environments (e.g. Port et al., 2016; West et al., 2020). By using known point sources of eDNA in the field, transport distances can be better

constrained in both the horizontal and vertical dimensions, but these studies have been limited in scope (Murakami et al., 2019; Ely et al, 2021).

1.5 Objectives

The objectives of this dissertation research were broadly to provide new tools for sequencing eDNA from deep anthozoan corals and to develop a conceptual framework for interpreting the spatiotemporal resolution of data generated using these methods. Towards this goal, the objective of Chapters 2 and 3 was to determine the physicochemical and microbial controls on the degradation rate of coral eDNA in a controlled laboratory setting. The objective of Chapter 4 was to design and test new PCR primers and an accompanying reference barcode database for metabarcoding eDNA from all anthozoan corals, including scleractinians, octocorals, and black corals. The objective of Chapter 5 was to determine the detectable extents of eDNA transport in the vertical and horizontal dimensions in metabarcoding data using both taxonomically broad and taxonomically specific PCR primers.

1.6 References

Alexander, J. B., Bunce, M., White, N., Wilkinson, S. P., Adam, A. A. S., Berry, T., Stat, M., Thomas, L., Newman, S. J., Dugal, L., & Richards, Z. T. (2020). Development of a multi-assay approach for monitoring coral diversity using eDNA metabarcoding. *Coral Reefs, 39*(1), 159–171.

Allan, E. A., DiBenedetto, M. H., Lavery, A. C., Govindarajan, A. F., & Zhang, W. G. (2021). Modeling characterization of the vertical and temporal variability of environmental DNA in the mesopelagic ocean. *Scientific Reports*, *11*(1), 21273.

Amaral-Zettler, L. A., McCliment, E. A., Ducklow, H. W., & Huse, S. M. (2009). A method for studying protistan diversity using massively parallel sequencing of V9 hypervariable regions of small-subunit ribosomal RNA genes. *PloS One*, *4*(7), e6372.

Andruszkiewicz, E. A., Koseff, J. R., Fringer, O. B., Ouellette, N. T., Lowe, A. B., Edwards, C. A., & Boehm, A. B. (2019). Modeling Environmental DNA Transport in the Coastal Ocean Using Lagrangian Particle Tracking. *Frontiers in Marine Science*, *6*. https://doi.org/10.3389/fmars.2019.00477

Andruszkiewicz Allan, E., Zhang, W. G., C. Lavery, A., & F. Govindarajan, A. (2021). Environmental DNA shedding and decay rates from diverse animal forms and thermal regimes. *Environmental DNA (Hoboken, N.J.)*, *3*(2), 492–514.

Armstrong, R. A., Pizarro, O., & Roman, C. (2019). Underwater Robotic Technology for Imaging Mesophotic Coral Ecosystems. In Y. Loya, K. A. Puglise, & T. C. L. Bridge (Eds.), *Mesophotic Coral Ecosystems* (pp. 973–988). Springer International Publishing.

Bosch, N. E., Espino, F., Tuya, F., Haroun, R., Bramanti, L., & Otero-Ferrer, F. (2023). Black coral forests enhance taxonomic and functional distinctiveness of mesophotic fishes in an oceanic island: implications for biodiversity conservation. *Scientific Reports*, *13*(1), 4963.

Brian, J. I., Davy, S. K., & Wilkinson, S. P. (2019). Elevated Symbiodiniaceae richness at Atauro Island (Timor-Leste): a highly biodiverse reef system. *Coral Reefs, 38*(1), 123–136.

Buhl-Mortensen, L., & Mortensen, P. (2004). Symbiosis in deep-water corals. *Symbiosis, 37*, 33–61.

Canals, O., Mendibil, I., Santos, M., Irigoien, X., & Rodríguez-Ezpeleta, N. (2021). Vertical stratification of environmental DNA in the open ocean captures ecological patterns and behavior of deep-sea fishes. *Limnology and Oceanography Letters*, *6*(6), 339–347.

Carreiro-Silva, M., Martins, I., Riou, V., Raimundo, J., Caetano, M., Bettencourt, R., Rakka, M., Cerqueira, T., Godinho, A., Morato, T., & Colaço, A. (2022). Mechanical and toxicological effects of deep-sea mining sediment plumes on a habitat-forming cold-water octocoral. *Frontiers in Marine Science*, *9*. https://doi.org/10.3389/fmars.2022.915650

Caza-Allard, I., Laporte, M., Côté, G., April, J., & Bernatchez, L. (2022). Effect of biotic and abiotic factors on the production and degradation of fish environmental DNA: An experimental evaluation. *Environmental DNA (Hoboken, N.J.)*, *4*(2), 453–468.

Clark, M. R., Althaus, F., Schlacher, T. A., Williams, A., Bowden, D. A., & Rowden, A. A. (2015). The impacts of deep-sea fisheries on benthic communities: a review. *ICES Journal of Marine Science: Journal Du Conseil*, *73*(suppl_1), i51–i69.

Collins, R. A., Wangensteen, O. S., O'Gorman, E. J., Mariani, S., Sims, D. W., & Genner, M. J. (2018). Persistence of environmental DNA in marine systems. *Communications Biology*, *1*, 185.

Cordes, E. E., Demopoulos, A. W. J., Davies, A. J., Gasbarro, R., Rhoads, A. C., Lobecker, E., Sowers, D., Chaytor, J. D., Morrison, C. L., Weinnig, A. M., Brooke, S., Lunden, J. J., Mienis, F., Joye, S. B., Quattrini, A. M., Sutton, T. T., McFadden, C. S., Bourque, J. R., McClain-Counts, J. P., … Adams, C. (2023). Expanding our view of the

cold-water coral niche and accounting of the ecosystem services of the reef habitat. *Scientific Reports*, *13*(1), 19482.

Dugal, L., Thomas, L., Wilkinson, S. P., Richards, Z. T., Alexander, J. B., Adam, A. A. S., Kennington, W. J., Jarman, S., Ryan, N. M., Bunce, M., & Gilmour, J. P. (2022). Coral monitoring in northwest Australia with environmental DNA metabarcoding using a curated reference database for optimized detection. *Environmental DNA (Hoboken, N.J.)*, *4*(1), 63–76.

Ely, T., Barber, P. H., Man, L., & Gold, Z. (2021). Short-lived detection of an introduced vertebrate eDNA signal in a nearshore rocky reef environment. *PloS One*, *16*(6), e0245314.

Etnoyer, P., & Warrenchuk, J. (2007). A catshark nursery in a deep gorgonian field in the Mississippi Canyon, Gulf of Mexico. *Bulletin of Marine Science*, *81*, 553–559.

Etnoyer, P. J., Wickes, L. N., Silva, M., Dubick, J. D., Balthis, L., Salgado, E., & MacDonald, I. R. (2016). Decline in condition of gorgonian octocorals on mesophotic reefs in the northern Gulf of Mexico: before and after the Deepwater Horizon oil spill. *Coral Reefs, 35*(1), 77–90.

Everett, M. V., & Park, L. K. (2018). Exploring deep-water coral communities using environmental DNA. *Deep-Sea Research. Part II, Topical Studies in Oceanography*, *150*, 229–241.

Ficetola, G. F., Miaud, C., Pompanon, F., & Taberlet, P. (2008). Species detection using environmental DNA from water samples. *Biology Letters*, *4*(4), 423–425.

Fornari, D. J., Perfit, M. R., & Humphris, S. E. (1997). Deep submergence science takes a new approach. *Eos, Transactions, American Geophysical Union, 38(78),* 402-408.

Gaither, M. R., DiBattista, J. D., Leray, M., & Heyden, S. (2022). Metabarcoding the marine environment: from single species to biogeographic patterns. *Environmental DNA (Hoboken, N.J.)*, *4*(1), 3–8.

Girard, F., & Fisher, C. R. (2018). Long-term impact of the Deepwater Horizon oil spill on deep-sea corals detected after seven years of monitoring. *Biological Conservation*, *225*, 117–127.

Govindarajan, A. F., Francolini, R. D., Jech, J. M., Lavery, A. C., Llopiz, J. K., Wiebe, P. H., & Zhang, W. (gordon). (2021). Exploring the Use of Environmental DNA (eDNA) to Detect Animal Taxa in the Mesopelagic Zone. *Frontiers in Ecology and Evolution*, *9*. https://doi.org/10.3389/fevo.2021.574877

Govindarajan, A. F., Llopiz, J. K., Caiger, P. E., Jech, J. M., Lavery, A. C., McMonagle, H., Wiebe, P. H., & Zhang, W. (2023). Assessing mesopelagic fish diversity and diel vertical migration with environmental DNA. *Frontiers in Marine Science*, *10*. https://doi.org/10.3389/fmars.2023.1219993

Govindarajan, A.F., McCartin, L., Adams, A., Allan, E., Belani, A., Francolini, R., Fujii, J., Gomez-Ibañez, D., Kukulya, A., Marin, F. and Tradd, K. (2022). Improved biodiversity detection using a large-volume environmental DNA sampler with in situ filtration and implications for marine eDNA sampling strategies. *Deep Sea Research Part I: Oceanographic Research Papers*, *189*, 103871.

Harrison, J. B., Sunday, J. M., & Rogers, S. M. (2019). Predicting the fate of eDNA in the environment and implications for studying biodiversity. *Proceedings. Biological Sciences / The Royal Society*, *286*(1915), 20191409.

Heirtzler, J. R., & Grassle, J. F. (1976). Deep-sea research by manned submersibles. *Science*, *194*(4262), 294–299.

Hoban, M. L., Bunce, M., & Bowen, B. W. (2023). Plumbing the depths with environmental DNA (eDNA): Metabarcoding reveals biodiversity zonation at 45-60 m on mesophotic coral reefs. *Molecular Ecology*, *32*(20), 5590–5608.

Jensen, M. R., Sigsgaard, E. E., Liu, S., Manica, A., Bach, S. S., Hansen, M. M., Møller, P. R., & Thomsen, P. F. (2021). Genome-scale target capture of mitochondrial and nuclear environmental DNA from water samples. *Molecular Ecology Resources*, *21*(3), 690–702.

Jo, T., Murakami, H., Yamamoto, S., Masuda, R., & Minamoto, T. (2019). Effect of water temperature and fish biomass on environmental DNA shedding, degradation, and size distribution. *Ecology and Evolution*, *9*(3), 1135–1146.

Kahng, S. E., Garcia-Sais, J. R., Spalding, H. L., Brokovich, E., Wagner, D., Weil, E., Hinderstein, L., & Toonen, R. J. (2010). Community ecology of mesophotic coral reef ecosystems. *Coral Reefs, 29*(2), 255–275.

Kasai, A., Takada, S., Yamazaki, A., Masuda, R., & Yamanaka, H. (2020). The effect of temperature on environmental DNA degradation of Japanese eel. *Fisheries Science: FS*, *86*(3), 465–471.

Klymus, K. E., Merkes, C. M., Allison, M. J., Goldberg, C. S., Helbing, C. C., Hunter, M. E., Jackson, C. A., Lance, R. F., Mangan, A. M., Monroe, E. M., Piaggio, A. J., Stokdyk, J. P., Wilson, C. C., & Richter, C. A. (2020). Reporting the limits of detection and quantification for environmental DNA assays. *Environmental DNA (Hoboken, N.J.)*, *2*(3), 271–282.

Klymus, K. E., Richter, C. A., Chapman, D. C., & Paukert, C. (2015). Quantification of eDNA shedding rates from invasive bighead carp Hypophthalmichthys nobilis and silver carp Hypophthalmichthys molitrix. *Biological Conservation*, *183*, 77–84.

Kutti, T., Johnsen, I. A., Skaar, K. S., Ray, J. L., Husa, V., & Dahlgren, T. G. (2020). Quantification of eDNA to Map the Distribution of Cold-Water Coral Reefs. *Frontiers in Marine Science*, *7*. https://doi.org/10.3389/fmars.2020.00446

Laroche, O., Kersten, O., Smith, C. R., & Goetze, E. (2020). Environmental DNA surveys detect distinct metazoan communities across abyssal plains and seamounts in the western Clarion Clipperton Zone. *Molecular Ecology*, *29*(23), 4588–4604.

Leray, M., Yang, J. Y., Meyer, C. P., Mills, S. C., Agudelo, N., Ranwez, V., Boehm, J. T., & Machida, R. J. (2013). A new versatile primer set targeting a short fragment of the mitochondrial COI region for metabarcoding metazoan diversity: application for characterizing coral reef fish gut contents. *Frontiers in Zoology*, *10*(1), 34.

Lessard-Pilon, S. A., Podowski, E. L., Cordes, E. E., & Fisher, C. R. (2010). Megafauna community composition associated with Lophelia pertusa colonies in the Gulf of Mexico. *Deep-Sea Research. Part II, Topical Studies in Oceanography*, *57*(21), 1882–1890.

Lesser, M. P., & Slattery, M. (2011). Phase shift to algal dominated communities at mesophotic depths associated with lionfish (Pterois volitans) invasion on a Bahamian coral reef. *Biological Invasions*, *13*(8), 1855–1868.

Lesser, M. P., Slattery, M., & Leichter, J. J. (2009). Ecology of mesophotic coral reefs. *Journal of Experimental Marine Biology and Ecology*, *375*(1), 1–8.

Lynggaard, C., Bertelsen, M. F., Jensen, C. V., Johnson, M. S., Frøslev, T. G., Olsen, M. T., & Bohmann, K. (2022). Airborne environmental DNA for terrestrial vertebrate community monitoring. *Current Biology: CB*, *32*(3), 701–707.e5.

Kwong, S. L. T., Villacorta-Rath, C., Doyle, J., & Uthicke, S. (2021). Quantifying shedding and degradation rates of environmental DNA (eDNA) from Pacific crown-of-thorns seastar (Acanthaster cf. solaris). *Marine Biology*, *168*(6), 85.

Maruyama, A., Nakamura, K., Yamanaka, H., Kondoh, M., & Minamoto, T. (2014). The release rate of environmental DNA from juvenile and adult fish. *PloS One*, *9*(12), e114639.

Merten, V., Bayer, T., Reusch, T. B. H., Puebla, O., Fuss, J., Stefanschitz, J., Lischka, A., Hauss, H., Neitzel, P., Piatkowski, U., Czudaj, S., Christiansen, B., Denda, A., & Hoving, H.-J. T. (2021). An Integrative Assessment Combining Deep-Sea Net Sampling, in situ Observations and Environmental DNA Analysis Identifies Cabo Verde as a Cephalopod

Biodiversity Hotspot in the Atlantic Ocean. *Frontiers in Marine Science*, *8*. https://doi.org/10.3389/fmars.2021.760108

Miya, M., Sato, Y., Fukunaga, T., Sado, T., Poulsen, J. Y., Sato, K., Minamoto, T., Yamamoto, S., Yamanaka, H., Araki, H., Kondoh, M., & Iwasaki, W. (2015). MiFish, a set of universal PCR primers for metabarcoding environmental DNA from fishes: detection of more than 230 subtropical marine species. *Royal Society Open Science*, *2*(7), 150088.

Murakami, H., Yoon, S., Kasai, A., Minamoto, T., Yamamoto, S., Sakata, M. K., Horiuchi, T., Sawada, H., Kondoh, M., Yamashita, Y., & Masuda, R. (2019). Dispersion and degradation of environmental DNA from caged fish in a marine environment. *Fisheries Science: FS*, *85*(2), 327–337.

Nichols, P. K., & Marko, P. B. (2019). Rapid assessment of coral cover from environmental DNA in Hawai'i. *Environmental DNA (Hoboken, N.J.)*, *1*(1), 40–53.

Nishitsuji, K., Nagahama, S., Narisoko, H., Shimada, K., Okada, N., Shimizu, Y., & Satoh, N. (2024). Possible monitoring of mesophotic scleractinian corals using an underwater mini-ROV to sample coral eDNA. *Royal Society Open Science*, *11*(2), 221586.

Ostberg, C. O., & Chase, D. M. (2022). Ontogeny of eDNA shedding during early development in Chinook Salmon (*Oncorhynchus tshawytscha*). *Environmental DNA (Hoboken, N.J.)*, *4*(2), 339–348.

Port, J. A., O'Donnell, J. L., Romero-Maraccini, O. C., Leary, P. R., Litvin, S. Y., Nickols, K. J., Yamahara, K. M., & Kelly, R. P. (2016). Assessing vertebrate biodiversity in a kelp forest ecosystem using environmental DNA. *Molecular Ecology*, *25*(2), 527–541.

Pyle, R. L. (2019). Advanced Technical Diving. In Y. Loya, K. A. Puglise, & T. C. L. Bridge (Eds.), *Mesophotic Coral Ecosystems* (pp. 959–972). Springer International Publishing.

Quattrini, A. M., McCartin, L. J., Easton, E. E., Horowitz, J., Wirshing, H. H., Bowers, H., Mitchell, K., González-García, M. D. P., Sei, M., McFadden, C. S., & Herrera, S. (2024). Skimming genomes for systematics and DNA barcodes of corals. *Ecology and Evolution*, *14*(5), e11254.

Rezak, R., Bright, T. J., & Mcgrail, D. (1985). Reefs and banks of the northwestern Gulf of Mexico: Their geological, biological, and physical dynamics.

Roberts, J. M., Wheeler, A. J., & Freiwald, A. (2006). Reefs of the deep: the biology and geology of cold-water coral ecosystems. *Science*, *312*(5773), 543–547.

Rocha, L. A., Pinheiro, H. T., Shepherd, B., Papastamatiou, Y. P., Luiz, O. J., Pyle, R. L., & Bongaerts, P. (2018). Mesophotic coral ecosystems are threatened and ecologically distinct from shallow water reefs. *Science*, *361*(6399), 281–284.

Shinzato, C., Narisoko, H., Nishitsuji, K., Nagata, T., Satoh, N., & Inoue, J. (2021). Novel Mitochondrial DNA Markers for Scleractinian Corals and Generic-Level Environmental DNA Metabarcoding. *Frontiers in Marine Science*, *8*. https://doi.org/10.3389/fmars.2021.758207

Slattery, M., & Lesser, M. P. (2021). Gorgonians Are Foundation Species on Sponge-Dominated Mesophotic Coral Reefs in the Caribbean. *Frontiers in Marine Science*, *8*. https://doi.org/10.3389/fmars.2021.654268

Soares, M. de O., Araújo, Jorge Thé de, Ferreira, S. M. C., Santos, B. A., Boavida, J. R. H., Costantini, F., & Rossi, S. (2020). Why do mesophotic coral ecosystems have to be protected? *The Science of the Total Environment*, *726*, 138456.

Stoeckle, M. Y., Adolf, J., Charlop-Powers, Z., Dunton, K. J., Hinks, G., & VanMorter, S. M. (2020). Trawl and eDNA assessment of marine fish diversity, seasonality, and relative abundance in coastal New Jersey, USA. *ICES Journal of Marine Science: Journal Du Conseil*, *78*(1), 293–304.

Taberlet, P., Bonin, A., Zinger, L., & Coissac, E. (2018). *Environmental DNA: For Biodiversity Research and Monitoring*. Oxford University Press.

Thalinger, B., Rieder, A., Teuffenbach, A., Pütz, Y., Schwerte, T., Wanzenböck, J., & Traugott, M. (2021). The Effect of Activity, Energy Use, and Species Identity on Environmental DNA Shedding of Freshwater Fish. *Frontiers in Ecology and Evolution*, *9*. https://doi.org/10.3389/fevo.2021.623718

Thurber, A. R., Sweetman, A. K., Narayanaswamy, B. E., Jones, D. O. B., Ingels, J., & Hansman, R. L. (2014). Ecosystem function and services provided by the deep sea. *Biogeosciences* , *11*(14), 3941–3963.

Tsuji, S., Ushio, M., Sakurai, S., Minamoto, T., & Yamanaka, H. (2017). Water temperature-dependent degradation of environmental DNA and its relation to bacterial abundance. *PloS One*, *12*(4), e0176608.

West, K. M., Stat, M., Harvey, E. S., Skepper, C. L., DiBattista, J. D., Richards, Z. T., Travers, M. J., Newman, S. J., & Bunce, M. (2020). eDNA metabarcoding survey reveals fine-scale coral reef community variation across a remote, tropical island ecosystem. *Molecular Ecology*, *29*(6), 1069–1086.

West, K. M., Adam, A. A. S., White, N., Robbins, W. D., Barrow, D., Lane, A., & Richards, Z. (2022). The applicability of eDNA metabarcoding approaches for sessile

benthic surveying in the Kimberley region, north-western Australia. *Environmental DNA (Hoboken, N.J.)*, *4*(1), 34–49.

Whitaker, J. M., Brower, A. L., & Janosik, A. M. (2021). Invasive lionfish detected in estuaries in the northern Gulf of Mexico using environmental DNA. *Environmental Biology of Fishes*, *104*(11), 1475–1485.

Wicksten, M. K., Nuttall, M. F., & Hickerson, E. L. (2014). Crustaceans from antipatharians on banks of the northwestern Gulf of Mexico. *ZooKeys*, *457*, 45–54.

Woodhead, A. J., Hicks, C. C., Norström, A. V., Williams, G. J., & Graham, N. A. J. (2019). Coral reef ecosystem services in the Anthropocene. *Functional Ecology*, *33*(6), 1023–1034.

Yates, M. C., Wilcox, T. M., Stoeckle, M. Y., & Heath, D. D. (2022). Interspecific allometric scaling in eDNA production among northwestern Atlantic bony fishes reflects physiological allometric scaling. *Environmental DNA (Hoboken, N.J.)*. https://doi.org/10.1002/edn3.381

CHAPTER 2

TEMPERATURE CONTROLS EDNA PERSISTENCE ACROSS PHYSICOCHEMICAL CONDITIONS IN SEAWATER

2.1 Abstract

Environmental DNA (eDNA) quantification and sequencing are emerging techniques for assessing biodiversity and species abundances in marine ecosystems. Environmental DNA may be transported by ocean currents and remain at detectable concentrations far from its source, depending on the duration that these concentrations persist. Thus, determining how accurately an eDNA sample reflects the biological community where it is taken hinges on understanding the factors that control eDNA persistence. To investigate the relative effects of physicochemical factors on eDNA degradation rate, we performed persistence experiments at temperature, pH, and oxygen conditions relevant to the subsurface open ocean and the deep sea. We found that the eDNA degradation process was best explained by a model with two phases with different decay rate constants. During the initial phase, eDNA degraded rapidly and the rate was independent of physicochemical factors. During the second phase, eDNA degraded slowly and the rate was strongly controlled by temperature, weakly controlled by pH, and not controlled by dissolved oxygen concentration. We demonstrate that marine eDNA can persist at quantifiable concentrations for over two weeks at low temperatures (≤10°C) but a week or less at ≥20°C. The relationship between temperature and eDNA persistence is independent of the source species. We propose a general temperature-dependent model to estimate the maximum persistence time of eDNA detected through single-species eDNA quantification methods.

2.2 Introduction

Anthropogenic impacts are causing species extinctions and population abundance declines globally (Barnosky et al., 2011; Dirzo et al., 2014; McCauley et al., 2015). Molecular biology methods accelerate the pace at which the diversity and distribution of vulnerable biological communities are measured, informing conservation and ecosystem restoration efforts (Thomsen et al., 2015; Breed et al., 2019). Environmental DNA (eDNA) sequencing and quantification complement conventional methods for assessing biodiversity and the distribution of invasive and ecologically important species in marine habitats (Port et al., 2016; Everett & Park, 2018; Kutti et al., 2020; Whitaker et al., 2021; Keller et al., 2022). However, the utility of eDNA methods hinges on understanding the factors that control the distribution and abundance of eDNA across spatiotemporal scales (Barnes et al., 2016).

Aqueous eDNA is DNA shed from an organism that is dissolved in solution or associated with larger suspended particles, such as cells, organelles, or aggregates (Mauvisseau et al., 2022). eDNA may be shed into the environment through several processes, and the shedding rate depends on factors like biomass, metabolic rate, ontogeny, and activity (Maruyama et al., 2014; Klymus et al., 2015; Lacoursiere-Roussel et al., 2016; Sansom et al., 2017; Jo et al., 2019a; Ostberg et al., 2021; Thalinger et al., 2021). Once shed from an organism, eDNA changes from intracellular to sub-cellular states (Jo et al., 2019b; Jo et al., 2019c). eDNA degrades at rates influenced by physicochemical and biotic factors, and the influence of these factors on degradation rate may depend on eDNA state (Weltz et al., 2017; Collins et al., 2018; Jo et al., 2020; Mauvisseau et al., 2022). Before completely degrading into short fragments that

molecular methods cannot detect, marine eDNA can be transported away from its source by ocean currents (Harrison et al., 2019; Andruszkiewicz et al., 2019). Determining how the persistence of eDNA is influenced by physicochemical conditions is vital to constraining when and where it was shed from the source organism. This knowledge is essential to define the spatiotemporal resolution of the ecological information derived from eDNA quantification and sequencing.

Experimental studies using freshwater and marine animals have established that eDNA degrades beyond the detection limit of PCR-based methods over timescales spanning hours to weeks. These studies have indicated that temperature, pH, and dissolved oxygen concentration may influence the degradation rate and thus the persistence of environmental DNA. Temperature controls the degradation rate of eDNA shed from diverse organisms (Jo et al., 2019a; Joe et al., 2019c; Collins et al., 2018; Strickler et al., 2015; Eichmiller et al., 2016; Lance et al., 2017; Tsuji et al., 2017; Kasai et al., 2020; Andruszkiewicz Allan et al., 2021; Caza-Allard et al., 2022). Higher temperatures increase the kinetics of many processes responsible for DNA degradation, including cell and organelle lysis, hydrolysis and oxidation of DNA molecules, and breakdown by extracellular enzymes. The stability of the DNA molecules is affected by pH (Lindahl & Nyberg, 1972; Cheng & Pettitt, 1992; Lindahl, 1993). Consistently, experiments have indicated that the rate of eDNA degradation is also affected by pH (Strickler et al., 2015; Lance et al., 2017; Seymour et al., van Bochove et al., 2020). However these experimental inquiries have been limited to freshwater systems where pH ranges widely, from 5.0 to 9.0. No study has experimentally tested the effect of pH on eDNA degradation in seawater, which has a narrower range between 7.5 and 8.3.

Dissolved oxygen concentration (hereafter abbreviated as [DO]) is another potentially important physicochemical parameter that has received comparatively little attention. Dissolved oxygen concentration is biologically relevant due to its importance to microbial metabolism. Oxygen is also chemically relevant due to the susceptibility of DNA molecules to oxidation. To date, only one study has experimentally manipulated [DO] to determine its effect on eDNA decay in seawater (Weltz et al., 2017). That study found that the decay rate of eDNA was slower at a dissolved oxygen saturation of 20% versus 55%. To fully determine the effect of [DO] on eDNA degradation, it is necessary to perform experiments across the range of oxygenation states in marine ecosystems, from fully oxygenated to nearly anoxic.

In the open ocean, temperature, pH and [DO] vary considerably with location and depth. Temperature decreases from ~30°C in the tropical surface ocean to near freezing in the deep sea, and pH typically changes with depth from approximately 8.3 to 7.5 (Lalli & Parsons, 1997). Seawater is usually nearly saturated with oxygen in the surface ocean, decreases to a minimum at mesopelagic depths, and increases with higher solubility at lower temperatures in the deep sea (Paulmier et al., 2009). Considering the potentially interactive effects of these abiotic factors on the persistence of marine eDNA is necessary for the application of eDNA methodologies to study ocean biodiversity.

Here we test the relative effects of temperature, pH, and [DO] on the degradation rate of eDNA across conditions that reflect the subtropical open ocean, spanning subsurface waters to the deep sea. We developed an experimental setup that allows tight control of physicochemical conditions and produces reproducible results. We used the deep-sea coral *Desmophyllum pertusum* (Linnaeus 1758) as the source of eDNA.

Desmophyllum pertusum is hereafter referred to as *Lophelia* for consistency with abundant literature that uses its synonymized name *Lophelia pertusa* (Addamo et al., 2016). *Lophelia* is an ecologically important reef-forming coral with a cosmopolitan distribution in cold and deep waters of the Atlantic and Pacific Ocean basins (Cordes et al., 2008; Lessard-Pilon et al., 2010). We hypothesized that temperature, pH, and [DO] would have interactive effects controlling the decay rate of eDNA.

2.3 Methods

2.3.1 Experimental Conditions

To test our hypothesis, we conducted eDNA persistence experiments under 11 fixed combinations of temperature (set to either 4°C, 10°C or 20°C), [DO] (set to either nearly anoxic, 0.1 mg/L; half saturated, 3.6 mg/L; or fully saturated, 7.2 mg/L), and pH (set to either 7.6, 7.9 or 8.2). These discrete sets of conditions were chosen to reflect the range of physicochemical conditions found in the subtropical open ocean, spanning subsurface waters to the deep sea. Each set of conditions was investigated in duplicate experiments (22 experiments total) to assess reproducibility in estimating the eDNA decay rate. We maintained these conditions at target values throughout the experiments with accuracy (**Figure 2.1**).

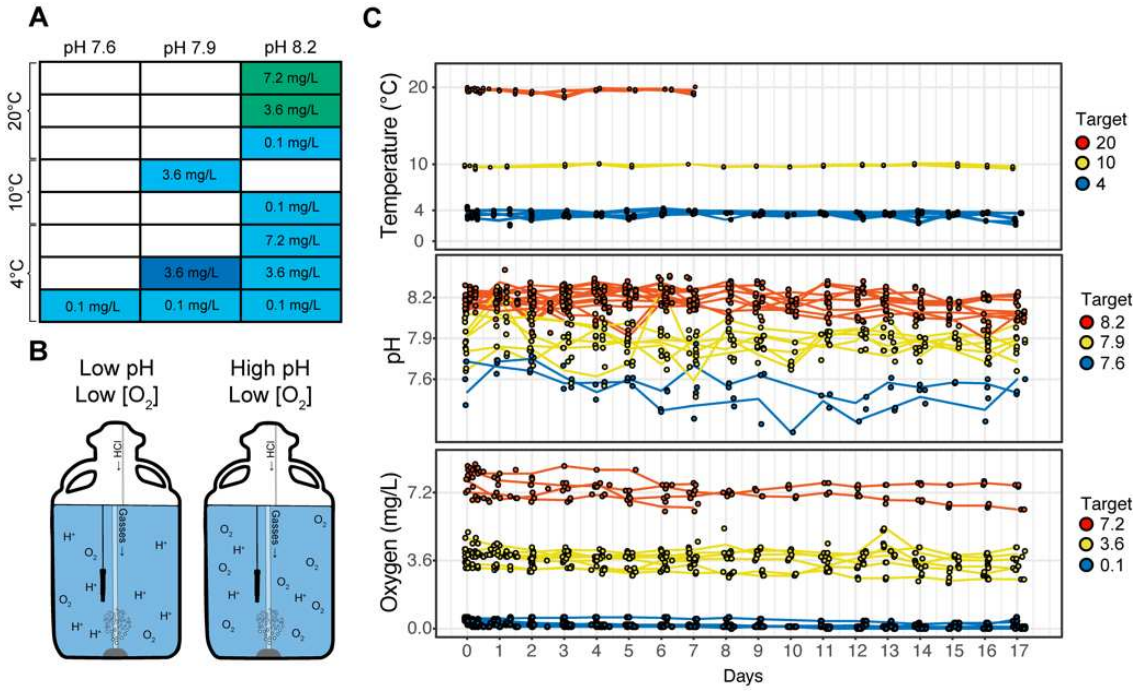

Figure 2.1: (A) Matrix of target conditions for 11 combinations of temperature, pH, and [DO] investigated to determine the persistence of eDNA from the coral *Lophelia* among a range of marine physicochemical states. Two replicate experiments were conducted for each combination of temperature, pH, and [DO]. 20°C temperature, half and fully saturated oxygen experiments (shaded green) represent conditions characteristic of subtropical subsurface environments. 4°C temperature, half-saturated conditions (shaded dark blue) represent conditions characteristic of the subtropical deep-sea environment. Remaining cells (shaded light blue) represent other conditions characteristic of the global subsurface and deep ocean. (B) Schematic examples of experimental conditions. Compressed air and nitrogen gas flow rates were adjusted to reach target [DO]. Small doses of 0.5 M HCl were automatically administered to the tanks when desired pH values were exceeded. Physicochemical measurements were monitored by suspending probes in the tanks. Caps were secured with O-rings to control the oxygen concentration in the above headspace. All tubing and probes were placed through small openings in these

caps. A photograph of the experimental setup is presented in Figure S1. (C) Measurements of temperature, pH, and [DO] over the 22 eDNA persistence experiments. Points indicate individual measurements, and paths are drawn through daily averages. All measurements were recorded daily and at each sampling time point. Temperature measurements were made using a laser thermometer. pH and [DO] measurements were made with probes in each of twenty-two individual experimental tanks.

2.3.2 Experimental Setup

Experiments were conducted in a controlled-temperature room (KE2 Therm Solutions Inc., Washington, MO, USA) set to the target temperature. Ambient temperature in the cold room was monitored using a HOBO data logger (Onset Computer Corporation, Bourne, MA, USA). The temperature of each tank was also measured daily and at each sampling time point using an Etekcity infrared laser thermometer (Vesync Co., Anaheim, CA, USA).

Experiments were conducted in opaque polypropylene carboys in the controlled temperature room with no windows, and artificial fluorescent lights were only turned on during sampling. These conditions removed the potential effect of UV light on eDNA degradation rate in the experiments. Natural levels of UV radiation from sunlight have not been found to have a significant effect on marine eDNA degradation (Andruszkiewicz et al., 2017). Therefore, eliminating UV light should have a negligible effect on the interpretation of results from experiments that may reflect conditions in the surface ocean (high pH and oxygenated) where UV radiation penetrates (Tedetti & Sempéré, 2006).

We continuously monitored pH using a BlueLab pH Controller Connect System (BlueLab, New Zealand) with a single-junction pH electrode (Oakton, Vernon Hills, IL, USA) and an RTD temperature probe (BlueLab) for automatic temperature compensation. Target pH values were maintained by automated dosing with small volumes of 0.5M hydrochloric acid whenever the controller pH reading exceeded 0.1 pH unit over the target value (approximately hourly). We manually added small volumes (< 5 mL) of 0.5M sodium hydroxide if the pH reading dropped below 0.1 pH unit of the target value. Duplicate, small-volume samples (~ 50 mL) were removed at each sampling time point to obtain independent pH measurements using an Orion PerpHect Log R meter (ThermoFisher Scientific, Waltham, MA, USA) with a single-junction pH electrode (Oakton). The pH monitoring systems were calibrated at the start of each experiment using a three-point calibration with pH 4.01, 7.00, and 10.01 solutions (Oakton). The pH meter used for daily sampling measurements was calibrated before each measurement using a two-point calibration with pH 7.00 and 10.01 solutions (Oakton). pH measurements were temperature-compensated manually by setting the monitor to the ambient temperature of the cold room.

We controlled [DO] by manipulating the flow rates of compressed air and high purity nitrogen gas. Compressed air and nitrogen flow rates were set with Aalborg GFC Mass Flow Controllers (Aalborg, Orangeburg, NY, USA). Before each experiment, gas flow rates were independently verified using a soap film bubble flowmeter. Gasses were delivered to each experimental tank using independent gas lines capped with air stones placed at the bottom of each tank. Dissolved oxygen concentrations and oxidative reductive potential (ORP) were monitored within the experimental tanks and recorded

daily and at each sampling time point with Pinpoint II Dissolved Oxygen and Pinpoint ORP monitors, respectively (American Marine, Ridgefield, CT, USA). Dissolved oxygen concentration and ORP monitors were calibrated at the start of each experiment, following the manufacturer's instructions. The [DO] monitors were calibrated to atmospheric oxygen concentration. The ORP monitors were calibrated using the manufacturer-supplied 400 ORP AgCl reference standard (American Marine).

2.3.3 eDNA Persistence Experiments

For each experiment, 42 liters of artificial seawater at 35 PSU salinity were prepared in a polypropylene carboy (Foxx Life Sciences, Salem, NH, USA) using the B-Ionic Artificial Seawater (ASW) System (ESV Aquarium Products, Hicksville, NY, USA). Seawater was prepared with ultra-pure deionized water using a Milli-Q system with an attached LC-Pak Polisher (MilliporeSigma, Burlington, MA, USA). The LC-Pak Polisher removes trace organics from water. We chose to make ASW from Milli-Q water to restrict organic material sources to the B-Ionic ASW components and our eDNA source.

We prepared a tissue homogenate from freshly frozen *Lophelia* fragments as the source of eDNA. Fragments approximately 10 cm in length with 8-10 polyps were collected at two sites at ~700 and ~760 meters depth at the Richardson Reef Complex off the coast of South Carolina, USA (31.98°N, 77.41°W; 31.88°N, 77.37°W, respectively). Collection details are presented in the Supplementary Methods. *Lophelia* tissue was removed from the skeleton with a strong stream of ASW using a water jet dental flosser. The resulting mixture of tissue and ASW was collected in a sterile Whirl-Pak. This

mixture was homogenized using a FisherBrand 150 rotor-stator homogenizer with a 5 mm fine saw-tooth probe (ThermoFisher Scientific, Waltham, MA, USA). The homogenate was aliquoted into 15 mL sterile centrifuge tubes (Celltreat, Pepperell, MA, USA), frozen, and stored at -80°C. One aliquot was thawed on ice immediately before each experiment. Details about the preparation and choice of source eDNA are presented in the Appendix A.

Between 12 and 15 mL of tissue homogenate were added to each tank at the beginning of each experiment. The concentration was adjusted based on the measured concentration of coral eDNA in each preparation to keep starting concentrations consistent among experiments (see Supplementary Methods). From this point onwards, seawater from each experiment was serially sampled at increasing time intervals to quantify the concentration of coral eDNA over time. The first sample was taken between 30 and 45 minutes after adding the homogenate to allow mixing. After conducting pilot experiments, we determined that sampling over eight days was sufficient for experiments at 20°C, since the limit of quantification of our qPCR assay was reached in less than a week in some experiments. However, this timeframe was insufficient to capture the entire degradation process at lower temperatures. Thus, sampling for experiments at 10°C and 4°C was conducted less frequently over the first two days and extended to 17 days. Sampling timepoints for each experiment are shown in Figure 2. We sampled coral eDNA by filtering approximately 1 liter of water (mean = 1,008 mL, standard deviation = 74 mL, range = 404 to 1145 mL) through a 0.22 μm pore-size polyethersulfone Sterivex filter (Millipore-Sigma). Water was pumped through the filter using an L/S peristaltic pump, Easy-load II pump heads, and L/S 15 high-performance precision tubing

(Masterflex, Vernon Hills, IL, USA). The pump was set to a rate of 100 RPM. The tubing was primed with tank water before a filter was attached. The effluent from each filtered sample was weighed using a balance to adjust measured concentrations of eDNA by mass (in grams) of water filtered. Any water remaining in the tubing was pumped back into the experimental tanks once filtration was complete and the filter was removed. Following filtration, Sterivex filters were stored in sterile Whirl-pak bags and frozen at -80°C immediately after eDNA filtration until DNA extraction, which occurred within one month.

2.3.4 DNA Extraction and Quantitative PCR

DNA was extracted from each filter using a Qiagen DNEasy Blood & Tissue Kit (Hilden, Germany) following methods initially developed by Spens *et al.* with modifications described in Govindarajan *et al.* (Spens et al., 2017; Govindarajan et al., 2022). DNA was eluted in two separate volumes of 50 µL AE buffer for a total volume of 100 µL per extraction. The total concentration of DNA in each extract was quantified using the Qubit 1X High-sensitivity double-stranded DNA Assay (ThermoFisher Scientific, Waltham, MA, USA). The average DNA concentration was 3.40 ng/µL and the range was < 0.1 (too low to quantify) to 52.0 ng/µL. After this assay, DNA was stored frozen at -20°C.

We developed a new qPCR assay to amplify and quantify a 154 base pair fragment of the Lophelia mitochondrial COI gene (*Lop-COI*) using primers that match the COI gene of caryophylliid corals. The forward primer sequence is 5'-CTGGGGGACGATCATCTTTA-3,' and the reverse primer sequence is 5'-

TGTTTAATCGGGGGAAAGC-3'. Primers were synthesized by Eurofins Genomics (Louisville, KY, USA), purified by standard desalting, and normalized at 100 µM in TE buffer (pH 8.0). Quantitative PCR reactions were performed in 20 µL volumes using the Quantabio PerfecTa SYBR Green Fastmix (Beverly, MA, USA) and a Qiagen RotorGene 6000 Thermal Cycler with either the 72-well or 36-well ring. We used clear Qiagen 0.1 mL four-strip tubes (for the 72-well ring) or 0.2 mL single tubes (for the 36-well ring) designed for the RotorGene. DNA extracts were diluted 10-fold in Buffer AE (Qiagen, Germany), and 6 µL of this dilution was used in each reaction (effectively 0.6 µL of DNA template). Primer stocks in TE buffer were diluted to 10 µM using molecular-grade water, and 6 picomoles of both the forward and reverse primers were added to each reaction for a final concentration of 300 nM for each primer. We used molecular-grade water to complete the 20 µL volume of each reaction. Cycling conditions were as follows: initial denaturation at 95°C for 10 minutes, then 35 cycles of denaturation at 95°C for 15 seconds, annealing at 55°C for 15 seconds, and elongation at 72°C for 20 seconds. Amplification was followed by melting curve analysis, conducted with pre-melt conditioning at 72°C for 90 seconds, followed by a ramp from 72°C to 95°C, with holds of 5 seconds per 0.5°C increase in temperature. The details regarding primer design and qPCR assay optimization are presented in the Supplementary Methods. The qPCR assay's quantification (LOQ) and detection limits (LOD) were calculated and visualized using code adapted from Klymus *et al.* (2020) (see Supplementary Methods for further details). The LOQ was determined to be 77.8 copies/reaction, which is equivalent to 130 copies/mL of seawater filtered using our sampling and eDNA extraction methods. The

LOD with three qPCR replicates is 3.4 copies/reaction or 5.7 copies/mL of seawater filtered.

Each qPCR run consisted of 19 samples in triplicate, four ten-fold dilutions of purified plasmids containing the target fragment (778,000 to 778 copies/reaction or 1,300,000 to 1,300 copies/mL seawater filtered) in triplicate, and three PCR negative controls. Because triplicate reactions were conducted with 0.6 µL template each, the total volume of DNA extract used was 1.8 µL. Considering variation in the volumes filtered across samples, an average of 18.1 mL (standard deviation = 1.3 mL) from each seawater sample was analyzed. A sample was determined to have amplified if the characteristic exponential amplification curve was visualized in the log(RFU) and C_q value graph and if there was a distinct peak in the melting curve at 78°C, which corresponded to the peak of the plasmid standard PCR products. The C_q-threshold was set using the auto-threshold setting in the RotorGene software. The amplified samples' concentrations were determined by fitting the line of best fit to the standard curve in each run. The standard curves' average R^2 and doubling efficiencies for the 33 qPCR runs were 0.99236 ± 0.01502 (SD) and 85.4% ± 4.7% (SD), respectively. The average slope of the standard curves was -3.7391 ± 0.155 (SD) C_q/order of magnitude decrease in concentration and the average intercept was 7.4540 ± 2.5069 (SD) C_q.

2.3.5 Contamination controls

Before each experiment, tanks were sterilized with a solution of 10% household bleach (6% sodium hypochlorite) and deionized water and were subsequently rinsed with Milli-Q water. Sampling tubes (Cole Parmer, Antylia Scientific, Vernon Hills, IL, USA)

were sterilized by pumping a 10% bleach solution through them for 15 minutes and subsequently rinsed with at least 1 liter of Milli-Q water. Luer fittings, air stones, and air stone tubing were sterilized by soaking in 10% bleach for at least an hour and rinsed by soaking in Milli-Q water. Temperature, pH, [DO], and ORP probes were rinsed thoroughly with Milli-Q water. All tubing and probe wiring exteriors were wiped with 10% bleach followed by Milli-Q water before placing them in the tanks. Experimental controls (42 liters of ASW) without added tissue homogenate were conducted simultaneously with each set of persistence experiments (up to four at once). The physicochemical conditions in these controls were set and maintained the same way as the persistence experiments. This tank was sampled at each time point alongside the experiments, serving as a sampling negative control to monitor for contamination during sampling. Sampling negative control samples were processed similarly to the experimental samples in all subsequent laboratory steps. All laboratory work was conducted in a laboratory adjacent to, but separated from, the refrigerated room where experiments were conducted. DNA extractions were conducted at a dedicated bench where no tissue DNA extractions had occurred. Pipettes for eDNA extraction were wiped with 10% bleach solution and UV irradiated before each set of extractions. In each set of extractions, an extraction negative control was also processed to monitor for contamination at this step. Quantitative PCR (qPCR) preparation was conducted in a My-PCR Prep Station (Mystaire, Creedmoor, NC, USA) hood with positive airflow, air filtration through a HEPA filter, and an overhead UV lamp. Sterile filter tips were used at all stages of laboratory work. qPCR was conducted at a bench for qPCR cycling and post-

PCR work. qPCR products were disposed of in this lab area, and PCR products were not brought into any other part of the lab.

Of all sampling negative controls, extraction negative controls, and PCR negative controls measured, a single qPCR replicate from one extraction negative control and one PCR negative control amplified (both below the LOQ). The estimated concentrations of these two samples were 9.6 and 5.6 copies per reaction, or 16.0 and 9.3 copies per mL seawater filtered, respectively. No replicates from any other triplicates of the 204 negative control samples amplified. This results in a false positive rate of just 0.9%, if the amplification of a single qPCR triplicate at concentrations below the LOQ is considered a positive signal. Thus, we have high confidence that our experiments were free of contamination that would affect the interpretation of our results.

2.3.6 Statistical Analyses

All data analyses and visualizations were conducted using R version 4.1.0 (R Core Team) in RStudio. Plots were created with *ggplot2* in the *tidyverse* (Wickham et al., 2019) and edited in Adobe Illustrator. Decay models were fitted to the mean of qPCR triplicates for each eDNA sample to determine decay rate constants for each experiment. All three replicates were averaged in all cases, and we did not remove any potential outlying qPCR replicates. We only analyzed experimental time points where the mean concentration of the three qPCR triplicates was above the LOQ.

A simple exponential model was fit as a linear model to natural log transformed data from each experiment using the *lm* function. The linear model is defined as $LN(Y) = -kt + LN(Y_0)$. Here, the slope is mathematically equivalent to an

exponential model's decay rate constant, *k*. A decreasing rate of eDNA degradation over time has been observed in other studies (Eichmiller et al., 2016; Allan et al., 2021; Shogren et al., 2018; Bylemans et al., 2018). Therefore, we also fit a biphasic model to natural log transformed data as two linear models, allowing for a change in the decay rate constant over time. The bi-phasic linear model is defined as $LN(Y) = \{-k_1 t + LN(Y_1), if\ t < b\ -k_2 t + LN(Y_2),\ if\ t \geq b$ where k_1 is the initial decay rate constant, and k_2 is the second decay rate constant defined for time points, *t*, after a breakpoint, *b*, in the model. The natural log of Y_1 and Y_2 indicate the intercepts of each model (in natural log eDNA copies per reaction) during the initial and second phases of eDNA decay, respectively. The optimal breakpoint time for each model was estimated using the R package *segmented* (Muggeo, 2003). The number of breakpoints to be estimated was set to 1, and the starting value for estimation was set to 24 hours To avoid over-parameterization, we chose to fit a biphasic model over other more complex nonlinear models. This model choice also allows for direct comparisons of the decay rate constant estimates from each phase among experiments and the calculation of decay rate constants reported in most other studies to date. For each experiment, we calculated the log-likelihood and Bayesian Information Criterion (BIC) of the linear and biphasic models. A likelihood ratio test and comparison of BICs were conducted to determine which model was better at describing the data.

We fit a linear mixed model (LMM) on eDNA concentrations from each phase separately and considered the influence of temperature, pH, [DO] and relevant covariates on eDNA degradation. One outlier experiment, which exhibited a breakpoint in the biphasic model that was substantially later than the others (discussed more in depth in the

Results & Discussion section), was omitted from these analyses. Linear mixed models were fit to the data using the R package *lme4* (Bates et al., 2014). The significance of each coefficient was assessed with T-tests using Satterthwaite's method to determine degrees of freedom as implemented in the package *lmertest* (Kuznetsova et al., 2017). We also determined the effect size of each model term from the Type III sum of squares of an ANOVA with Satterthwaite's method using the package *effectsize* (Ben-Shachar et al., 2020).

Linear mixed models were formulated to test a priori hypotheses regarding the relative influence of temperature, pH and [DO] on eDNA degradation rate. The response variables in all LMM were the natural log-transformed Lophelia eDNA concentrations (triplicate qPCR averages in copies per reaction) for each of the duplicate eDNA samples taken at each time point. The experiments were considered as random intercepts to account for the non-independence of concentration measurements from the same experiment. Time (in days) was included as a random slope to permit variation in the degradation rate (the slope of the relationship between eDNA concentration and time) across the experimental groups (Harrison et al., 2018).

Fixed effects included time and the average temperature, pH, [DO] and ORP over the course of each experiment when eDNA concentrations were quantifiable. In addition, the natural-log plus one transformed concentration of total DNA was included as a fixed effect in the second phase models. In some experiments, total DNA concentration (presumably of microbial origin) increased over time (**Figure A.3**). The interactions of time with average temperature, pH, [DO], ORP and total DNA concentration were included to determine the effect of these factors on eDNA degradation.

Two additional LMM were also fit to second phase data from subsets of experiments to control for the unbalanced nature of our experimental conditions. One model only used the subset of experiments conducted at 4°C and 10°C to determine the influence of pH while eliminating the potentially confounding effects of experiments conducted at 20°C, which were all conducted at pH 8.2. Temperature [DO], ORP, total DNA concentration, and the interactions of these variables with time were included as fixed effects. Another model only included experiments conducted at 20°C, 4°C, at pH 8.2, to further investigate the influence of [DO]. This data subset represents a fully factorial design nested within our larger experimental framework.

2.3.7 Literature Search and Comparison to Other Studies

To place our results in a broader context, we compared our eDNA persistence time estimates to those from other marine eDNA studies that have fit a simple exponential model to their data. A literature search was conducted using the Web of Science database and the search terms "(eDNA OR "environmental DNA") AND (persist* OR decay OR degrad*)". This search was also supplemented by reviewing all publications from the journal *Environmental DNA*. Only studies that conducted experiments with marine organisms and reported decay rate constants derived from time series of individual eDNA persistence experiments using exponential models were included in the analysis. In total, 11 studies fit the search criteria (**Table A.7**). To compare across studies with variable starting eDNA concentrations, we calculated persistence time as the time until degradation of 99.9% of eDNA using the formula $T_{99.9\%} = \frac{LN(0.001)}{-k}$, in the case of the simple exponential model, where (k) is the decay

rate constant. In the case of the biphasic model, we used the formula $T_{99.9\%} = \frac{LN\left(0.001 \times \frac{Y_1}{Y_2}\right)}{-k_2}$, where Y_1 and Y_2 are concentrations corresponding to the intercepts of each phase of the biphasic model and k_2 is the decay rate constant for the second phase. This 1,000-fold decrease in initial eDNA concentrations reflects the approximate decrease from the eDNA starting concentration to the LOQ or LOD that is typical of eDNA persistence studies and is thus ecologically and methodologically relevant.

2.4 Results and Discussion

2.4.1 Modeling eDNA degradation

eDNA degradation did not show a trend consistent with a simple exponential decay process in our experiments. Instead, it showed a general trend of decreasing degradation rate over time. A simple exponential model consistently underestimated measured eDNA concentrations at earlier time points and overestimated them at intermediate time points (**Figure A.2**). Lower BIC and significant likelihood ratio tests indicated that the biphasic model better fit the data from 20 of the 22 experiments (**Table A.1**). We report the results of the biphasic model for the two experiments in which the biphasic model did not have a significantly better fit because the slopes of the initial and second phases were similar. The biphasic model's average breakpoint, parameter b, was 38.9 ± 18.6 hours. One experiment exhibited a substantially later breakpoint than the rest (227.1 hours; Table S2). In all experiments, the decay rate constant was greater during the initial phase (steeper slope) than during the second phase (**Figure 2.2**).

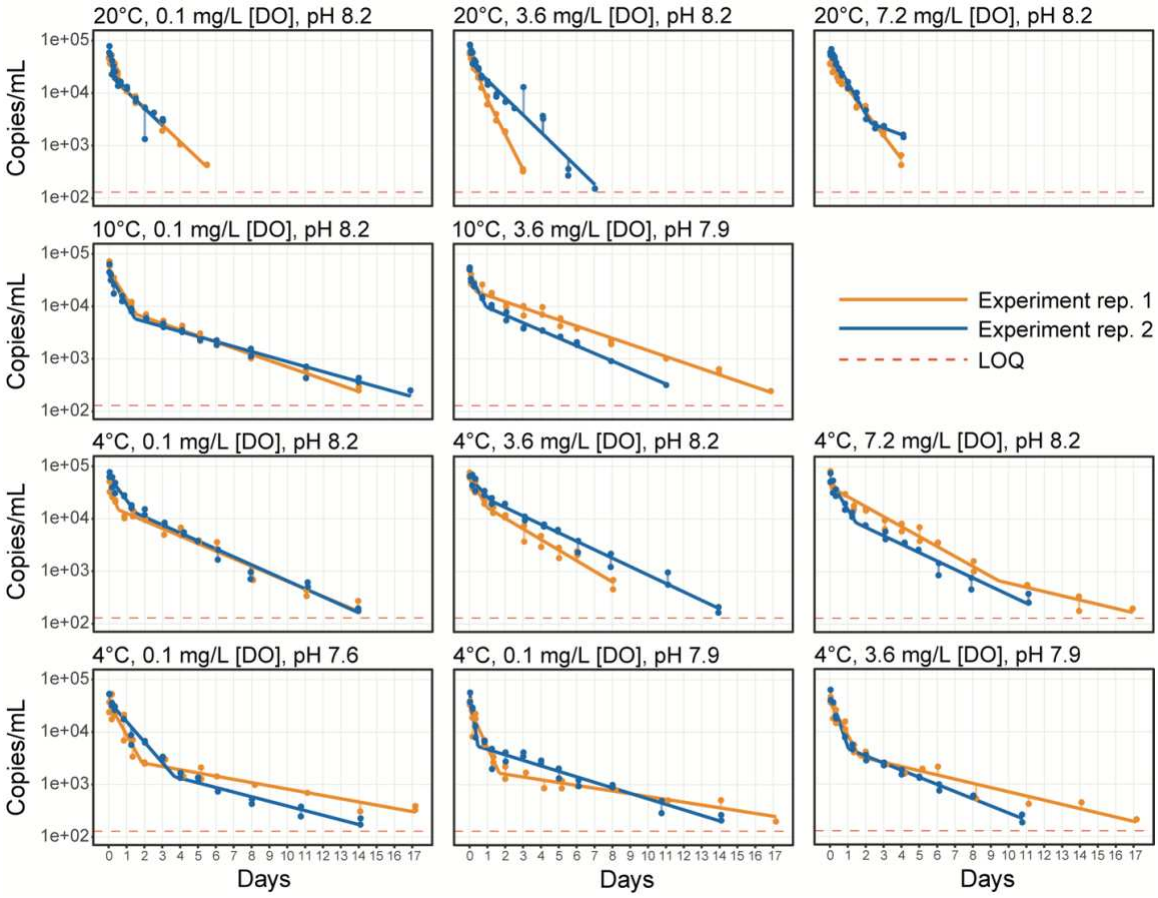

Figure 2.2: Degradation of *Lophelia* eDNA in 22 persistence experiments among a range of marine physicochemical states. eDNA concentration was measured as the concentration of a 154 base pair fragment of the *Lophelia* mitochondrial COI gene. The natural log-transformed concentration of eDNA (y-axis) is plotted against time (x-axis). Different colors represent the two experimental replicates at each experimental condition. Points represent the average of three qPCR replicate measurements for two samples at a given time point. Lines represent the fit to a biphasic model. Thin lines connecting points to the line of best fit represent the distance from the observed to the fitted values at each time point (the residuals). Panels are arranged by temperature (descending top to bottom) and [DO] (increasing left to right). Values shown on top of each panel indicate the target experimental conditions. Points below the limit of quantification of the qPCR assay (the

natural log of 77.8 copies/reaction or 130 copies/mL seawater filtered) are not plotted. The limit of quantification is indicated by the dashed line.

A decreasing rate of eDNA degradation may be explained by a decrease in the size of particles that the eDNA is associated with over time (Jo et al., 2019b; Jo et al., 2019c; Jo et al., 2022). Field and experimental studies show that eDNA is present primarily in relatively large size fractions, between 1 - 10 μm, which would include whole cells and mitochondria (Sassoubre et al., 2016; Turner et al., 2014; Wilcox et al., 2015). Experimental work indicates that the proportion of eDNA in large-size fractions decreases rapidly. However, the proportion of eDNA in size fractions smaller than 3 μm increases over time, and its degradation is slower than the degradation of eDNA in larger size fractions (Jo et al., 2019b; Jo et al., 2019c). Our observations that the degradation rate decreased over time may reflect a change in the association of eDNA with larger particles (e.g., cells or organelles) to smaller particles (Jo et al., 2019b; Jo et al., 2019c; Jo et al., 2022).

Since tissue homogenization and freezing likely lysed most *Lophelia* cells in our study, most of the eDNA at early timepoints in our experiments may have not been contained within cells but likely included free DNA or in mitochondria. We assume that it is unlikely that eDNA was adsorbed to foreign particulates in our experiments, because we used filtered, artificial seawater. It seems likely that free DNA would pass through the 0.22 μm pore size, non-polar membrane we used in our experiments. However, a recent study found that a 0.45 μm non-charged membrane can recover measurable concentrations of eDNA from free DNA molecules in filtered seawater (Zaiko et al.,

2022). In our experiments, the rapid initial decrease of eDNA we observed may be explained not only by the degradation of DNA in mitochondria, but also by the lysis of mitochondria and the loss of dissolved DNA that passes through the filter. Persistent, low concentrations of eDNA at later time points may reflect mitochondria that are not lysed, free DNA that is captured on the filter, or free DNA associated with material from the *Lophelia* tissue, such as mucus.

In addition to spawning and the release of gametes, it is likely that eDNA from corals is also shed through mucus production. *Lophelia* maintains a protective mucus layer, sheds mucus in response to disturbance, and may also produce mucus nets as a strategy to capture prey (Bythell & Wild, 2011; Murray et al., 2019). Previous studies have quantified eDNA shedding for *Lophelia* and two species of hydrozoans (Kutti et al., 2020; Allan et al., 2021; Minamoto et al., 2017). However, we lack an understanding of the state of eDNA that *Lophelia* and other cnidarians shed through processes such as mucus secretion. Experiments with corals that concurrently quantify eDNA shedding and mucus secretion would be informative, especially if the state of shed eDNA is determined.

2.4.2 Effects of temperature, pH, and oxygen concentration on eDNA degradation

Temperature

Our findings support the hypothesis that temperature is the most significant controlling factor of eDNA decay rate in seawater. The effect of temperature was substantial in the second phase of eDNA degradation but not in the initial phase. During the initial phase of eDNA degradation, the estimated decay rates among experiments

conducted at 20°C (mean ± 1 SD = 0.084 ± 0.016 hour^{-1}) were on average higher than those conducted at 10°C (0.070 ± 0.014 hour^{-1}) and 4°C (0.073 ± 0.013 hour^{-1}; **Figure 2.3A**). However, there was no significant effect of any predictor variable when fitting an LMM to the initial phase dataset (**Table A.3**). Therefore, we find no evidence that eDNA degradation is influenced by temperature, pH or [DO] over the course of early time points before the model breakpoints.

Decay rate constants during the second phase in experiments conducted at 20°C (0.0355 ± 0.0171 hour^{-1}) were substantially higher than those at 10°C (0.0113 ± 0.0021 hour^{-1}) and 4°C (0.0183 ± 0.0044 hour^{-1}; **Figure 2.3B**). In the second phase, the interaction between temperature and time (in days) was the most significant predictor (*P = 0.0025)* of eDNA concentration fitting the LMM to experiments from all conducted combinations of temperature, pH and [DO] (**Table A.4**). Consistently, the interaction between temperature and time was the only significant predictor (*P = 0.0348*) of eDNA concentration among the subset of experiments conducted at pH 8.2, excluding those at 10°C (**Table A.5**). In addition, the effect size for the interaction of temperature and time was greater than the effect size for any other model term (**Tables A.4 & A.5)**. These results imply that the temperature of an experiment and the time since the addition of eDNA are the strongest predictors of eDNA concentration in our experiments. We interpret that temperature more strongly controls the degradation rate and persistence of eDNA than pH or [DO].

The fact that temperature strongly controlled eDNA degradation rate during the second phase of the experiments but not the initial phase suggests that this effect may depend on eDNA state. As stated previously, we propose that faster degradation during

the initial phase in our experiments may reflect the lysis of mitochondria. Degradation of eDNA in smaller size fractions may be dominant in the second phase. If this is the case, our results contrast with a recent meta-analysis that found that the effect of temperature on eDNA degradation rate is stronger in studies using filter pore sizes > 0.7 μm than pore sizes < 0.45 μm (Jo et al., 2021). Our results suggest that the persistence of eDNA in smaller size fractions may have been more affected by temperature than the persistence of larger size fractions.

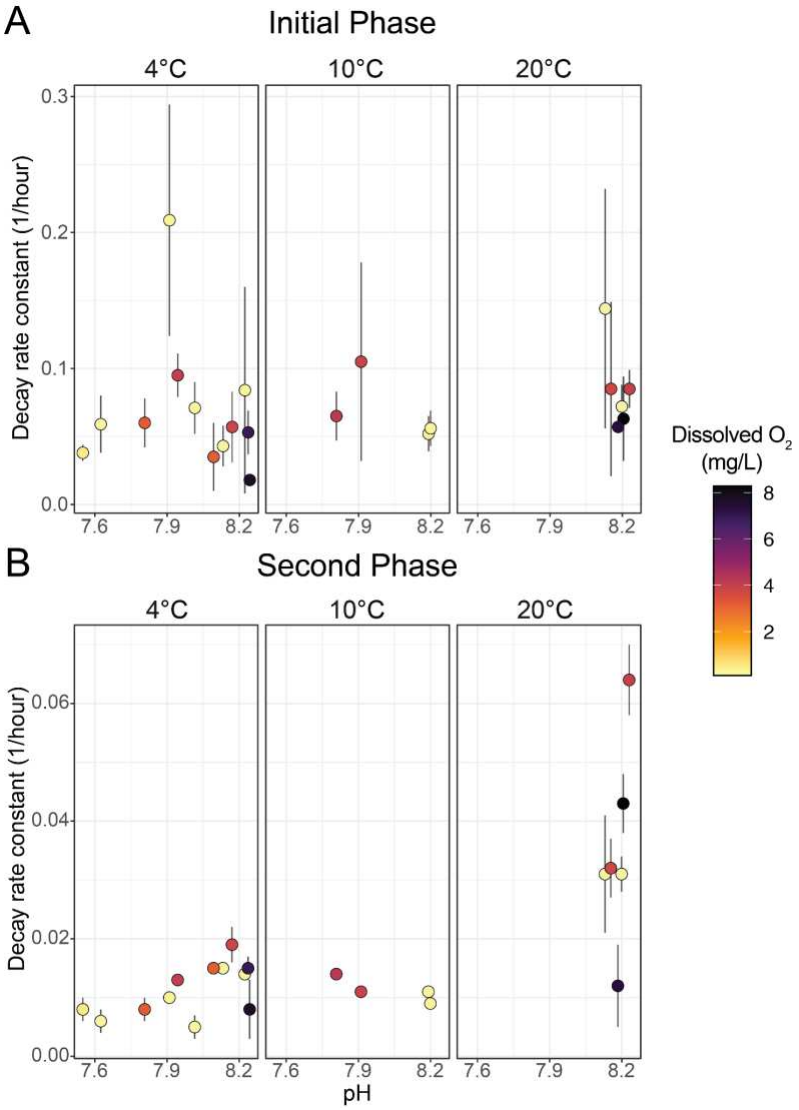

Figure 2.3: Decay rate constant estimates for the initial (A) and second (B) phases of eDNA degradation for 22 experiments conducted across 11 combinations of temperature, pH and [DO]. Decay rate constants were estimated by fitting an exponential decay equation with initial and second degradation phases with different rates (biphasic). Decay rate constants are arranged on the x-axis by the average pH over the course of each experiment. Vertical error bars represent 95% confidence intervals for the decay rate constants. The color of each point represents the average [DO] over the course of each experiment.

pH

Our findings tentatively support the hypothesis that pH may influence eDNA degradation rate in seawater. In the second phase, pH was a marginally significant predictor of eDNA concentration (*P = 0.0478;* **Table A.4**). The effect size of pH was substantially smaller than the effect size of the interaction between time and temperature (**Table A.4**). The LMM fit to the subset of the second-phase data that excluded experiments conducted at 20°C indicated that the interaction of time and pH is a nearly significant predictor of eDNA concentration (**P = 0.069; Table A.6**). Indeed, higher pH among experiments conducted at 4°C was associated with faster decay rate constants (Pearson's r = *0.601,* P = 0.0387; **Figure 2.3B**). We infer from these results that pH may affect the \persistence of eDNA among the range of marine conditions that we tested. However, this effect is small compared to that of temperature.

Previous work in freshwater systems has demonstrated that eDNA degrades faster at more acidic pH values (Strickler et al., 2015; Lance et al., 2017; Seymour et al., 2018;

van Bochove et al., 2020). Lance *et al.* investigated a pH range similar to our study's (7.5 and 8.0) and found that lower pH was associated with faster eDNA degradation in freshwater (Lance et al., 2017). Here, we present data suggesting that relatively more acidic seawater with pH near 7.6 may prolong the persistence of eDNA compared to seawater at higher pH. Our results suggest that the influence of pH on eDNA degradation in seawater may need to be further considered.

Dissolved oxygen concentration

Our findings do not support the hypothesis that [DO] is a significant controlling factor of eDNA degradation in seawater. We conducted experiments in a fully factorial design with a full range of [DO] at two temperatures (4°C and 20°C) and pH 8.2. In the LMMs fit to this subset of the data and the full second-phase dataset, neither average [DO], average ORP, nor the interaction of these factors with time were significant predictors of eDNA concentration (**Tables A.4 & A.5**). From these results, we infer that [DO] and the oxidative state of seawater have the least influence on eDNA degradation rate and persistence among the conditions we tested. Thus, it is possible that eDNA degradation is driven by oxygen-independent processes.

2.4.3 Temperature Dependence of eDNA Degradation in the Marine Environment

Environmental DNA persistence times estimated from our study are comparable to previous marine studies performed at similar temperatures regardless of the source species (**Figure 2.4**). For example, eDNA persistence times from a skate at 4°C ($T_{99.9\%}$ = 14.4 and 26.2 days) (Weltz et al., 2017) fall within our range of calculated persistence

times for Lophelia ($T_{99.9\%}$ range = 12.5 to 28.8 days). Further, persistence times from our experiments at 10°C ($T_{99.9\%}$ range = 16.0 to 24.0 days) are comparable to a previous study of *Lophelia* eDNA degradation using natural seawater and live coral at 8°C ($T_{99.9\%}$ = 16.9 days) (Kutti et al., 2020).

We fit a linear model to eDNA persistence time (time until degradation of 99.9% of starting eDNA concentration), estimated using decay rate constants from our study and other published marine studies, and temperature (**Figure 2.4**). We found that this model has a satisfactory fit (Adjusted $R^2 = 0.4792$, $P < 0.001$). The model predicts that eDNA persistence decreases by ~0.74 days for each increase in a degree Celsius. Our results align with findings by Allan *et al.* (2021), who demonstrated a positive linear relationship between temperature and decay rate constants in most studies that have investigated eDNA degradation at multiple temperatures. Similarly, Mauvisseau *et al.* 2022 found a linear relationship between increased temperature and faster decay rate constant in studies of freshwater and marine fish. Further investigations at intermediate (~8 to 12°C) and high temperatures (greater than ~ 25°C), and more studies of invertebrate taxa would improve confidence in the generality of this model. This model does not consider other factors that may influence eDNA quantification or detection in the ocean, including microbial activity, pH, UV radiation, advection, or diffusion. However, it serves as a resource to approximate maximum eDNA persistence times, constrained by temperature, in the marine environment.

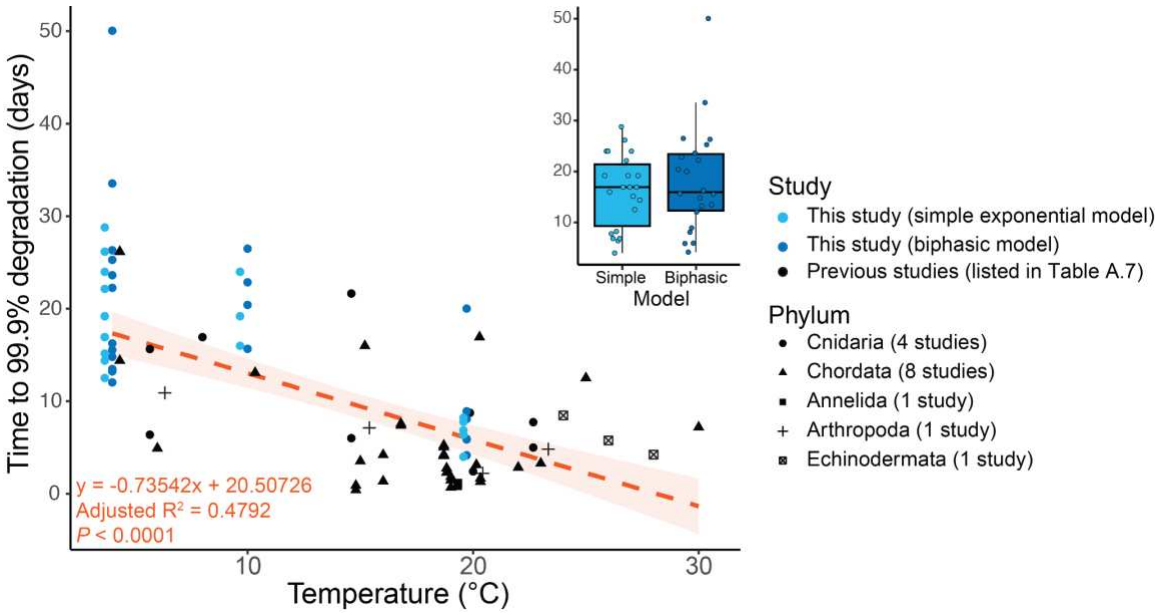

Figure 2.4: eDNA persistence time (times until degradation of 99.9% of starting eDNA concentration), estimated using decay rate constants from our study and other published marine studies, as a function of temperature. The line of best fit is fit only to points derived from the simple exponential model. The shaded region represents the 95% confidence interval for the slope. Points are dodged slightly from actual recorded temperatures to improve visualization. (Inset) Comparison of calculated persistence times when fitting a single exponential versus a biphasic model to the data in this study. Data are reported in **Table A.7**.

2.4.4 Implications for eDNA quantification and sequencing in the marine environment

Investigating the spatiotemporal scale of eDNA in the marine environment is critical to defining the spatiotemporal resolution of ecological information derived from eDNA quantification or detection. Recent studies have found that eDNA abundance can exhibit strong vertical stratification, among wide depth ranges from just 5 meters below the surface to 2,000 meters deep in the mesopelagic open ocean, and within just the first

10 meters below the surface at nearshore habitats (Govindarajan et al., 2021; Canals et al., 2021; Monuki et al., 2021). Further, model simulations have suggested that eDNA in the ocean remains within tens of meters from the depth where it is shed (Allan et al., 2021). Field data from eDNA sampling along short, horizontal transects has revealed discrete eDNA community profiles at a fine scale in diverse shallow-water habitats, including coral reefs and kelp forest ecosystems (Port et al., 2016; West et al., 2020; Lamy et al., 2021). Together, these results suggest that eDNA community profiles, obtained using techniques such as meta-barcoding, can accurately reflect biological communities structured by depth. However, the ability of eDNA meta-barcoding to distinguish communities in deep-sea environments is less clear. eDNA sequencing efforts in the deep sea have resulted in benthic community composition profiles that agree with expected differences due to habitat at sites ~15 km apart (Laroche et al., 2020). However, eDNA sampling paired with video analyses revealed remarkable disparities between video observations and sequence read abundances from deep-sea corals (Everett & Park, 2018). Some coral species were observed in video surveys but were not detected in eDNA, and many sequence reads were recovered from species not observed in videos.

Modeling studies suggest that the extent of horizontal transport of eDNA at concentrations detectable through single-species quantitative methods can be substantial, on the order of tens of kilometers, in the surface ocean and at depth (Andruzkiewicz et al., 2019; Kutti et al., 2020). These models provide valuable insights for understanding the horizontal spatial scale of eDNA in the ocean. However, studies modeling eDNA transport have utilized decay rate constants derived from simple exponential models. We found that at low temperatures of ≤10°C, a simple exponential model can substantially

underestimate the persistence of eDNA. Environmental DNA persistence time, defined as the time to degradation of 99.9% of the starting eDNA concentration, was up to 75% longer when fitting the data with the biphasic model rather than the simple exponential model (**Figure 2.4**, **Table A.7**). Thus, in cold marine environments, including the deep sea, detectable eDNA may be transported over longer distances than predicted by simulations that assume a simple exponential decay.

The interpretation of eDNA data from deep-sea corals in the field is complicated, because eDNA may persist for longer durations at cold temperatures and may be shed infrequently or at low concentrations. We conducted field sampling within 1 meter of a large aggregation of live *Lophelia* and at altitudes of 5, 10, and 20 meters above the seafloor in the Gulf of Mexico. We found that caryophylliid eDNA could be detected (positive qPCR amplification) within 10 meters above the seafloor. However, copy number estimates were below the LOQ of our qPCR assay (**Table A.8**; see Appendix A). Kutti *et al.* (2020) also measured relatively low concentrations of *Lophelia* eDNA in the Norwegian Sea (up to 1,000s of copies per liter of seawater filtered), demonstrating that *Lophelia* eDNA is present at low concentrations in its environment.

If eDNA in nature is shed at low concentrations, it may be diluted rapidly and degrade past the detectable limit more quickly than in an experimental setting. Thus, an eDNA sample may provide an accurate signal of the proximate biological community. However, our experiments demonstrate that eDNA can persist for weeks at low temperatures, so detectable concentrations may be transported over large distances. When using single-species quantitative methods, such as qPCR or digital-droplet PCR, considerable care should be taken when interpreting the source of a positive eDNA

amplification. We suggest that a range of possible sources must be considered for an observed eDNA signal. This range can be constrained by coupling estimated persistence times and hydrodynamic models.

2.5 Acknowledgments

We would like to thank members of the Herrera lab for their assistance with aspects of the laboratory work; Dylan Faltine-Gonzalez for his advice and help with the qPCR assay; Elizabeth Andruszkiewicz Allan for her advice regarding persistence experiment methods; and Alexis Weinnig and Adam Hallaj for their help providing *Lophelia* samples for the experiment. We also thank the captains and crew of the *NOAA Ship Ronald Brown* and the *R/V Point Sur* and the ROV *Jason* and ROV *Global Explorer* teams.

This research was funded by the National Oceanic and Atmospheric Administration's Oceanic and Atmospheric Research, Office of Ocean Exploration and Research, under award NA18OAR0110289 to SH and JMM at Lehigh University, and subawards to EC at Temple University and to CSM at Harvey Mudd College.

2.6 References

Addamo, A. M., Vertino, A., Stolarski, J., García-Jiménez, R., Taviani, M., & Machordom, A. (2016). Merging scleractinian genera: the overwhelming genetic similarity between solitary Desmophyllum and colonial Lophelia. *BMC Evolutionary Biology*, *16*(1), 108.

Andruszkiewicz Allan, E., Zhang, W. G., C. Lavery, A., & F. Govindarajan, A. (2021). Environmental DNA shedding and decay rates from diverse animal forms and thermal regimes. *Environmental DNA (Hoboken, N.J.)*, *3*(2), 492–514.

Andruszkiewicz, E. A., Koseff, J. R., Fringer, O. B., Ouellette, N. T., Lowe, A. B., Edwards, C. A., & Boehm, A. B. (2019). Modeling Environmental DNA Transport in the Coastal Ocean Using Lagrangian Particle Tracking. *Frontiers in Marine Science*, *6*. https://doi.org/10.3389/fmars.2019.00477

Andruszkiewicz, E. A., Sassoubre, L. M., & Boehm, A. B. (2017). Persistence of marine fish environmental DNA and the influence of sunlight. *PloS One*, *12*(9), e0185043.

Barnes, M. A., & Turner, C. R. (2016). The ecology of environmental DNA and implications for conservation genetics. *Conservation Genetics, 17*(1), 1–17.

Bates, D., Mächler, M., Bolker, B., & Walker, S. (2014). Fitting Linear Mixed-Effects Models using lme4. In *arXiv [stat.CO]*. arXiv. http://arxiv.org/abs/1406.5823

Barnosky, A. D., Matzke, N., Tomiya, S., Wogan, G. O. U., Swartz, B., Quental, T. B., Marshall, C., McGuire, J. L., Lindsey, E. L., Maguire, K. C., Mersey, B., & Ferrer, E. A. (2011). Has the Earth's sixth mass extinction already arrived? *Nature*, *471*(7336), 51–57.

Ben-Shachar, M., Lüdecke, D., & Makowski, D. (2020). Effectsize: Estimation of effect size indices and standardized parameters. *Journal of Open Source Software*, *5*(56), 2815.

Breed, M. F., Harrison, P. A., Blyth, C., Byrne, M., Gaget, V., Gellie, N. J. C., Groom, S. V. C., Hodgson, R., Mills, J. G., Prowse, T. A. A., Steane, D. A., & Mohr, J. J. (2019). The potential of genomics for restoring ecosystems and biodiversity. *Nature Reviews. Genetics*, *20*(10), 615–628.

Bylemans, J., Furlan, E. M., Gleeson, D. M., Hardy, C. M., & Duncan, R. P. (2018). Does Size Matter? An Experimental Evaluation of the Relative Abundance and Decay Rates of Aquatic Environmental DNA. *Environmental Science & Technology*, *52*(11), 6408–6416.

Bythell, J. C., & Wild, C. (2011). Biology and ecology of coral mucus release. *Journal of Experimental Marine Biology and Ecology*, *408*(1), 88–93.

Canals, O., Mendibil, I., Santos, M., Irigoien, X., & Rodríguez-Ezpeleta, N. (2021). Vertical stratification of environmental DNA in the open ocean captures ecological patterns and behavior of deep-sea fishes. *Limnology and Oceanography Letters*, *6*(6), 339–347.

Caza-Allard, I., Laporte, M., Côté, G., April, J., & Bernatchez, L. (2022). Effect of biotic and abiotic factors on the production and degradation of fish environmental DNA: An experimental evaluation. *Environmental DNA (Hoboken, N.J.)*, *4*(2), 453–468.

Cheng, Y. K., & Pettitt, B. M. (1992). Stabilities of double- and triple-strand helical nucleic acids. *Progress in Biophysics and Molecular Biology*, *58*(3), 225–257.

Collins, R. A., Wangensteen, O. S., O'Gorman, E. J., Mariani, S., Sims, D. W., & Genner, M. J. (2018). Persistence of environmental DNA in marine systems. *Communications Biology*, *1*, 185.

Cordes, E. E., McGinley, M. P., & Podowski, E. L. (2008). Coral communities of the deep Gulf of Mexico. *Deep Sea Research Part I: Oceanographic Research Papers*, *55(6)*, 777-787.

Dirzo, R., Young, H. S., Galetti, M., Ceballos, G., Isaac, N. J. B., & Collen, B. (2014). Defaunation in the Anthropocene. *Science*, *345*(6195), 401–406.

Eichmiller, J. J., Best, S. E., & Sorensen, P. W. (2016). Effects of Temperature and Trophic State on Degradation of Environmental DNA in Lake Water. *Environmental Science & Technology*, *50*(4), 1859–1867.

Everett, M. V., & Park, L. K. (2018). Exploring deep-water coral communities using environmental DNA. *Deep-Sea Research. Part II, Topical Studies in Oceanography*, *150*, 229–241.

Yang, N., Jin, D., & Govindarajan, A. F. (2024). Applying environmental DNA approaches to inform marine biodiversity conservation: The case of the Ocean Twilight Zone. *Marine Policy*, *165*, 106151.

Govindarajan, A. F., McCartin, L., Adams, A., Allan, E., Belani, A., Francolini, R., Fujii, J., Gomez-Ibañez, D., Kukulya, A., Marin, F., Tradd, K., Yoerger, D. R., McDermott, J. M., & Herrera, S. (2022). Improved biodiversity detection using a large-volume environmental DNA sampler with in situ filtration and implications for marine eDNA sampling strategies. *Deep Sea Research Part I: Oceanographic Research Papers*, *189*, 103871.

Harrison, J. B., Sunday, J. M., & Rogers, S. M. (2019). Predicting the fate of eDNA in the environment and implications for studying biodiversity. *Proceedings. Biological Sciences / The Royal Society*, *286*(1915), 20191409.

Harrison, X. A., Donaldson, L., Correa-Cano, M. E., Evans, J., Fisher, D. N., Goodwin, C. E. D., Robinson, B. S., Hodgson, D. J., & Inger, R. (2018). A brief introduction to mixed effects modelling and multi-model inference in ecology. *PeerJ*, *6*, e4794.

Jo, T., & Minamoto, T. (2021). Complex interactions between environmental DNA (eDNA) state and water chemistries on eDNA persistence suggested by meta-analyses. *Molecular Ecology Resources*, *21*(5), 1490–1503.

Jo, T., Arimoto, M., Murakami, H., Masuda, R., & Minamoto, T. (2019). Particle Size Distribution of Environmental DNA from the Nuclei of Marine Fish. *Environmental Science & Technology*, *53*(16), 9947–9956.

Jo, T., Murakami, H., Yamamoto, S., Masuda, R., & Minamoto, T. (2019). Effect of water temperature and fish biomass on environmental DNA shedding, degradation, and size distribution. *Ecology and Evolution*, *9*(3), 1135–1146.

Kasai, A., Takada, S., Yamazaki, A., Masuda, R., & Yamanaka, H. (2020). The effect of temperature on environmental DNA degradation of Japanese eel. *Fisheries Science: FS*, *86*(3), 465–471.

Keller, A. G., Grason, E. W., McDonald, P. S., Ramón-Laca, A., & Kelly, R. P. (2022). Tracking an invasion front with environmental DNA. *Ecological Applications: A Publication of the Ecological Society of America*, *32*(4), e2561.

Kirtane, A., Wieczorek, D., Noji, T., Baskin, L., Ober, C., Plosica, R., Chenoweth, A., Lynch, K., & Sassoubre, L. (2021). Quantification of Environmental DNA (eDNA) shedding and decay rates for three commercially harvested fish species and comparison

between eDNA detection and trawl catches. *Environmental DNA (Hoboken, N.J.)*, *3*(6), 1142–1155.

Klymus, K. E., Merkes, C. M., Allison, M. J., Goldberg, C. S., Helbing, C. C., Hunter, M. E., Jackson, C. A., Lance, R. F., Mangan, A. M., Monroe, E. M., Piaggio, A. J., Stokdyk, J. P., Wilson, C. C., & Richter, C. A. (2020). Reporting the limits of detection and quantification for environmental DNA assays. *Environmental DNA (Hoboken, N.J.)*, *2*(3), 271–282.

Klymus, K. E., Richter, C. A., Chapman, D. C., & Paukert, C. (2015). Quantification of eDNA shedding rates from invasive bighead carp *Hypophthalmichthys nobilis* and silver carp *Hypophthalmichthys molitrix*. *Biological Conservation*, *183*, 77–84.

Kutti, T., Johnsen, I. A., Skaar, K. S., Ray, J. L., Husa, V., & Dahlgren, T. G. (2020). Quantification of eDNA to Map the Distribution of Cold-Water Coral Reefs. *Frontiers in Marine Science*, *7*. https://doi.org/10.3389/fmars.2020.00446

Kuznetsova, A., Brockhoff, P. B., & Christensen, R. H. B. (2017). LmerTest package: Tests in linear mixed effects models. *Journal of Statistical Software*, *82*(13). https://doi.org/10.18637/jss.v082.i13

Kwong, S. L. T., Villacorta-Rath, C., Doyle, J., & Uthicke, S. (2021). Quantifying shedding and degradation rates of environmental DNA (eDNA) from Pacific crown-of-thorns seastar (*Acanthaster* cf. *solaris*). *Marine Biology*, *168*(6), 85.

Lacoursière-Roussel, A., Rosabal, M., & Bernatchez, L. (2016). Estimating fish abundance and biomass from eDNA concentrations: variability among capture methods and environmental conditions. *Molecular Ecology Resources*, *16*(6), 1401–1414.

Lalli, C., & Parsons, T. R. (1997). *Biological Oceanography: An Introduction*. Elsevier.

Lamy, T., Pitz, K. J., Chavez, F. P., Yorke, C. E., & Miller, R. J. (2021). Environmental DNA reveals the fine-grained and hierarchical spatial structure of kelp forest fish communities. *Scientific Reports*, *11*(1), 14439.

Lance, R., Klymus, K., Richter, C., Guan, X., Farrington, H., Carr, M., Thompson, N., Chapman, D., & Baerwaldt, K. (2017). Experimental observations on the decay of environmental DNA from bighead and silver carps. *Management of Biological Invasions: International Journal of Applied Research on Biological Invasions*, *8*(3), 343–359.

Laroche, O., Kersten, O., Smith, C. R., & Goetze, E. (2020). Environmental DNA surveys detect distinct metazoan communities across abyssal plains and seamounts in the western Clarion Clipperton Zone. *Molecular Ecology*, *29*(23), 4588–4604.

Lessard-Pilon, S. A., Podowski, E. L., Cordes, E. E., & Fisher, C. R. (2010). Megafauna community composition associated with *Lophelia pertusa* colonies in the Gulf of Mexico. *Deep-Sea Research. Part II, Topical Studies in Oceanography*, *57*(21), 1882–1890.

Lindahl, T., & Nyberg, B. (1972). Rate of depurination of native deoxyribonucleic acid. *Biochemistry*, *11*(19), 3610–3618.

Lindahl, T. (1993). Instability and decay of the primary structure of DNA. *Nature*, *362*(6422), 709–715.

Mauvisseau, Q., Harper, L. R., Sander, M., Hanner, R. H., Kleyer, H., & Deiner, K. (2022). The Multiple States of Environmental DNA and What Is Known about Their Persistence in Aquatic Environments. *Environmental Science & Technology*, *56*(9), 5322–5333.

Maruyama, A., Nakamura, K., Yamanaka, H., Kondoh, M., & Minamoto, T. (2014). The release rate of environmental DNA from juvenile and adult fish. *PloS One*, *9*(12), e114639.

McCauley, D. J., Pinsky, M. L., Palumbi, S. R., Estes, J. A., Joyce, F. H., & Warner, R. R. (2015). Marine defaunation: animal loss in the global ocean. *Science*, *347*(6219), 1255641.

Minamoto, T., Fukuda, M., Katsuhara, K. R., Fujiwara, A., Hidaka, S., Yamamoto, S., Takahashi, K., & Masuda, R. (2017). Environmental DNA reflects spatial and temporal jellyfish distribution. *PloS One*, *12*(2), e0173073.

Monuki, K., Barber, P. H., & Gold, Z. (2021). eDNA captures depth partitioning in a kelp forest ecosystem. *PloS One*, *16*(11), e0253104.

Muggeo, V. M. R. (2003). Estimating regression models with unknown break-points. *Statistics in Medicine*, *22*(19), 3055–3071.

Murray, F., De Clippele, L. H., Hiley, A., Wicks, L., Murray Roberts, J., & Hennige, S. (2019). Multiple feeding strategies observed in the cold-water coral *Lophelia pertusa*. *Journal of the Marine Biological Association of the United Kingdom. Marine Biological Association of the United Kingdom*, *99*(6), 1281–1283.

Ostberg, C. O., & Chase, D. M. (2022). Ontogeny of eDNA shedding during early development in Chinook Salmon (*Oncorhynchus tshawytscha*). *Environmental DNA (Hoboken, N.J.)*, *4*(2), 339–348.

Paulmier, A., & Ruiz-Pino, D. (2009). Oxygen minimum zones (OMZs) in the modern ocean. *Progress in Oceanography*, *80*(3), 113–128.

Port, J. A., O'Donnell, J. L., Romero-Maraccini, O. C., Leary, P. R., Litvin, S. Y., Nickols, K. J., Yamahara, K. M., & Kelly, R. P. (2016). Assessing vertebrate biodiversity in a kelp forest ecosystem using environmental DNA. *Molecular Ecology*, *25*(2), 527–541.

Sansom, B. J., & Sassoubre, L. M. (2017). Environmental DNA (eDNA) Shedding and Decay Rates to Model Freshwater Mussel eDNA Transport in a River. *Environmental Science & Technology*, *51*(24), 14244–14253.

Sassoubre, L. M., Yamahara, K. M., Gardner, L. D., Block, B. A., & Boehm, A. B. (2016). Quantification of Environmental DNA (eDNA) Shedding and Decay Rates for Three Marine Fish. *Environmental Science & Technology*, *50*(19), 10456–10464.

Seymour, M., Durance, I., Cosby, B. J., Ransom-Jones, E., Deiner, K., Ormerod, S. J., Colbourne, J. K., Wilgar, G., Carvalho, G. R., de Bruyn, M., Edwards, F., Emmett, B. A., Bik, H. M., & Creer, S. (2018). Acidity promotes degradation of multi-species environmental DNA in lotic mesocosms. *Communications Biology*, *1*, 4.

Shogren, A. J., Tank, J. L., Egan, S. P., August, O., Rosi, E. J., Hanrahan, B. R., Renshaw, M. A., Gantz, C. A., & Bolster, D. (2018). Water Flow and Biofilm Cover Influence Environmental DNA Detection in Recirculating Streams. *Environmental Science & Technology*, *52*(15), 8530–8537.

Spens, J., Evans, A. R., & Halfmaerten, D. (2017). Comparison of capture and storage methods for aqueous macrobial eDNA using an optimized extraction protocol: advantage of enclosed filter. *Methods in Ecology and Evolution / British Ecological Society*. https://doi.org/10.1111/2041-210X.12683

Strickler, K. M., Fremier, A. K., & Goldberg, C. S. (2015). Quantifying effects of UV-B, temperature, and pH on eDNA degradation in aquatic microcosms. *Biological Conservation*, *183*, 85–92.

Tedetti, M., & Sempéré, R. (2006). Penetration of ultraviolet radiation in the marine environment. A review. *Photochemistry and Photobiology*, *82*(2), 389–397.

Thalinger, B., Rieder, A., Teuffenbach, A., Pütz, Y., Schwerte, T., Wanzenböck, J., & Traugott, M. (2021). The Effect of Activity, Energy Use, and Species Identity on Environmental DNA Shedding of Freshwater Fish. *Frontiers in Ecology and Evolution*, *9*. https://doi.org/10.3389/fevo.2021.623718

Thomsen, P. F., Kielgast, J., Iversen, L. L., Møller, P. R., Rasmussen, M., & Willerslev, E. (2012). Detection of a diverse marine fish fauna using environmental DNA from seawater samples. *PloS One*, *7*(8), e41732.

Thomsen, P. F., & Willerslev, E. (2015). Environmental DNA – An emerging tool in conservation for monitoring past and present biodiversity. *Biological Conservation*, *183*, 4–18.

Turner, C. R., Barnes, M. A., & Xu, C. C. Y. (2014). Particle size distribution and optimal capture of aqueous macrobial eDNA. *Methods in Ecology and Evolution / British Ecological Society*. https://doi.org/10.1111/2041-210X.12206

van Bochove, K., Bakker, F. T., Beentjes, K. K., Hemerik, L., Vos, R. A., & Gravendeel, B. (2020). Organic matter reduces the amount of detectable environmental DNA in freshwater. *Ecology and Evolution*, *10*(8), 3647–3654.

Weltz, K., Lyle, J. M., Ovenden, J., Morgan, J. A. T., Moreno, D. A., & Semmens, J. M. (2017). Application of environmental DNA to detect an endangered marine skate species in the wild. *PloS One*, *12*(6), e0178124.

West, K. M., Stat, M., Harvey, E. S., Skepper, C. L., DiBattista, J. D., Richards, Z. T., Travers, M. J., Newman, S. J., & Bunce, M. (2020). eDNA metabarcoding survey reveals fine-scale coral reef community variation across a remote, tropical island ecosystem. *Molecular Ecology*, *29*(6), 1069–1086.

Wickham, H., Averick, M., Bryan, J., Chang, W., McGowan, L., François, R., Grolemund, G., Hayes, A., Henry, L., Hester, J., Kuhn, M., Pedersen, T., Miller, E.,

Bache, S., Müller, K., Ooms, J., Robinson, D., Seidel, D., Spinu, V., … Yutani, H. (2019). Welcome to the tidyverse. *Journal of Open Source Software*, *4*(43), 1686.

Wilcox, T. M., McKelvey, K. S., Young, M. K., Lowe, W. H., & Schwartz, M. K. (2015). Environmental DNA particle size distribution from Brook Trout (*Salvelinus fontinalis*). *Conservation Genetics Resources*, *7*(3), 639–641.

Whitaker, J. M., Brower, A. L., & Janosik, A. M. (2021). Invasive lionfish detected in estuaries in the northern Gulf of Mexico using environmental DNA. *Environmental Biology of Fishes*, *104*(11), 1475–1485.

Wood, S. A., Biessy, L., Latchford, J. L., Zaiko, A., von Ammon, U., Audrezet, F., Cristescu, M. E., & Pochon, X. (2020). Release and degradation of environmental DNA and RNA in a marine system. *The Science of the Total Environment*, *704*, 135314.

Zaiko, A., von Ammon, U., Stuart, J., Smith, K. F., Yao, R., Welsh, M., Pochon, X., & Bowers, H. A. (2022). Assessing the performance and efficiency of environmental DNA/RNA capture methodologies under controlled experimental conditions. *Methods in Ecology and Evolution / British Ecological Society*, *13*(7), 1581–1594.

CHAPTER 3

INFLUENCE OF THE BACTERIAL COMMUNITY ON EDNA DEGRADATION IN EXPERIMENTS ACROSS PHYSICOCHEMICAL CONDITIONS IN SEAWATER

3.1 Abstract

We previously reported the results of a series of eDNA persistence experiments designed to test the relative influences of temperature, pH, and dissolved oxygen concentration on the degradation rate of coral eDNA in seawater. We found that eDNA degradation was accelerated at temperatures of 20°C as compared to 10°C and 4°C, weakly controlled by pH, and not controlled by dissolved oxygen concentration. Here, we report the bacterial community composition, assessed with *16S* metabarcoding, and bacterial cell abundance, assessed with cell counts using fluorescence microscopy, in these same experiments. In addition, we measured phosphate [PO_4^{3-}] concentrations. Across experiments conducted at temperatures of 20°C, where we measured the fastest rates of eDNA degradation, increases in bacterial diversity, turnover in the bacterial community, and increases in bacterial cells happened with a higher frequency and more quickly than in experiments conducted at lower temperatures. We also found that [PO_4^{3-}] concentrations in these experiments were not limited. These results suggest that microbial processes, in synergy with temperature, drive eDNA degradation. Further, we find that microbial degradation of eDNA is important even when ambient concentrations of [PO_4^{3-}], which are frequently scarce in the ocean, are not limiting.

3.2 Introduction

After aquatic environmental DNA (eDNA) is shed from an organism, it remains detectable in the surrounding water and sediment until it degrades into fragments that are too short for PCR amplification (Mauvisseau et al., 2022). The rate at which eDNA degrades depends on complex interactions between physicochemical conditions, biological factors, and its form (i.e. intracellular eDNA versus dissolved DNA molecules) (Jo and Minamoto, 2021; Mauvisseau et al., 2022). Higher temperature accelerates the degradation of aqueous eDNA (Strickler et al, 2015; Eichmiller et al, 2016; Tsuji et al., 2017; Lance et al, 2017; Collins et al., 2018; Jo et al., 2019; Jo et al., 2020; Kasai et al., 2020; Andruszkiewicz Allan et al., 2021; Caza-Allard et al., 2022; McCartin et al., 2022). Temperature likely contributes to eDNA degradation through interactions with microbial processes, such as the degradation of DNA by extracellular nucleases (Mauvisseau et al., 2022).

To determine the role of microbes on eDNA degradation, several studies have experimentally manipulated bacterial communities in various ways. By altering the density of goldfish, Barnes et al. (2014) found that eDNA degradation rate *decreased* with eutrophic conditions and higher concentrations of bacterial DNA (Barnes et al., 2014). However, several subsequent studies have found that higher productivity and increased microbial density accelerate eDNA degradation, and that this effect may be additive to the effect of increased temperature (Eichmiller et al., 2016; Lance et al., 2017; Shogren et al., 2018; Zulkefli et al., 2019; Zhao et al., 2022). Higher temperatures tend to quicken microbial metabolism, growth rates, and generation times. These findings indicate that higher temperatures stimulate faster bacterially mediated breakdown of

eDNA, and that eDNA degrades largely through microbial processes (e.g. the production of extracellular nucleases) that are strengthened with higher temperature.

In addition to temperature, several other physicochemical factors may interact with microbially-mediated processes resulting in eDNA degradation. pH modulates bacterial community composition, potentially altering the functional capabilities of heterotrophic bacterial communities to degrade and metabolize nucleic acids (Krause et al., 2012). Likewise, higher dissolved oxygen concentrations may enhance the proliferation of aerobic, heterotrophic bacteria contributing to the degradation of eDNA. In addition to pH and dissolved oxygen concentration, the concentration of nutrients may also impact eDNA degradation rate, since microbes can utilize DNA as sources of essential nutrient elements, including carbon [C], nitrogen [N], and phosphorus [P]. Concentrations of inorganic dissolved phosphate [PO_4^{3-}] are often low and frequently limit microbial growth in the marine environment, compared to concentrations of carbon and nitrogen-bearing compounds (Redfield, 1958; Karl, 2014). Dissolved DNA molecules and nucleotides comprise a substantial portion of the total bioavailable P pool in the water column and sediments of P-limited marine habitats (Björkman and Karl, 1994; Björkman et al., 2000; Björkman and Karl, 2003; Dell'Anno and Danovaro, 2005; Karl and Björkman, 2015). In a landmark study, Salter et al. (2017) demonstrated that natural marine microbial communities exhibited a faster turnover rate of labeled P in dissolved eDNA under conditions of P-limitation, highlighting the importance of considering nutrient availability when assessing eDNA degradation rate in the marine environment.

We previously reported findings from a series of eDNA persistence experiments conducted to determine the relative influence of temperature, pH, and dissolved oxygen

concentration [DO] on the degradation rate of marine eDNA (McCartin et al., 2022). We found that eDNA degradation rate was strongly controlled by temperature, weakly controlled by pH, and not controlled by [DO]. To investigate the possibility that the strong effect of temperature was driven by microbial processes, we assessed bacterial community composition and abundance in those experiments by conducting *16S rRNA* metabarcoding to analyze community composition and epifluorescence microscopy to determine bacterial abundance. We also determined the abundance of dissolved, inorganic phosphate at each time point. Here, we present these data and integrate them with models of eDNA degradation rate to determine the influence of microbial processes on eDNA degradation rate in response to varying physicochemical conditions.

3.3 Methods

3.3.1 eDNA Persistence Experiments

A detailed account of the eDNA persistence experiments referred to herein is reported in McCartin et al. (2022). Briefly, we conducted duplicate experiments at 11 combinations of temperatures (4, 10, or 20°C), pH (7.6, 7.9, or 8.2), and dissolved oxygen concentrations (0.1 mg/L, 3.6 mg/L, or 7.2 mg/L). The combinations we chose reflect the range of conditions in the subtropical ocean at near-surface and deep waters. Experiments were conducted using B-Ionic artificial seawater (ESV Aquarium Products, Hicksville, NY, USA). The artificial seawater was prepared using ultrapure deionized water using a Milli-Q system with an attached LC-Pak Polisher (Millipore Sigma, Burlington, MA, USA). At the start of each experiment, homogenized coral tissue was added to each experimental tank. After the addition of the homogenized tissue, duplicate

one-liter (mean = 1.008 L; SD = .074 L; range = 0.404 to 1.145 L) water samples were filtered through 0.22 μm pore-size polyethersulfone Sterivex filters (Millipore-Sigma) at set time intervals to assess coral eDNA persistence and to quantify eDNA degradation rates. In experiments conducted at 20°C, eDNA samples were taken at 0.5, 2, 4, 6, 8, 10, 12, 16, 24, 36, 48, 72, 96, 132 and 168 hours. In experiments conducted at 4°C and 10°C, eDNA samples were taken at 0.5, 4, 8, 20, 32, 48, 72, 96, 120, 144, 192, 264, 336, and 408 hours. DNA was extracted from these filters using the Qiagen DNEasy Blood & Tissue Kit with a modified protocol to extract DNA directly from the filter capsule (Spens et al., 2017; Govindarajan et al., 2021). Coral eDNA concentrations were quantified with qPCR using primers specific to the mitochondrial COI gene of the coral (McCartin et al., 2022). The total concentration of DNA (including the coral and any other source) in each sample was also quantified using the Qubit 1X dsDNA high-sensitivity assay (Invitrogen, Waltham, MA, USA).

Concurrent with running each set of experiments, a control tank of artificial seawater was prepared and sampled over time. Homogenized coral tissue was not added to these control tanks. These tanks primarily served as sampling negative controls to monitor for contamination. However, in the negative controls sampled concurrently with experiments at 20°C and 4°C, dissolved oxygen concentration and pH were maintained and monitored just as they were in the experimental tanks. This experimental design permitted direct comparisons between the microbial communities in tanks at select temperature, [DO], and pH regimes in the presence and absence of the homogenized coral tissue and, thus, in the presence and absence of coral eDNA.

3.3.2 Bacterial Community 16S Metabarcoding

The bacterial communities in each experiment and in the negative sampling controls were analyzed by metabarcoding DNA extracts from each sampling day of the experiments. For metabarcoding, the V1 and V2 regions of the *16S rRNA* gene were amplified using the *27F* and *355R* primers (Muyzer et al., 1993; Rodriguez-Lanetty et al., 2013). The primers were ordered from Eurofins Genomics with salt-free purification in TE buffer (100 µM concentration) and included the CS1 (forward primer) and CS2 (reverse primer) sequences for compatibility with Fluidigm Access Array indices. The primer sequences were ACACTGACGACATGGTTCTACAAGAGTTTGATCCTGGCTCAG (16S_27F+CS1) and TACGGTAGCAGAGACTTGGTCTGCTGCCTCCCGTAGGAGT (16S_355R+CS2). Primers were diluted to 10 µM in molecular-grade water for PCR.

A 2.5 µL aliquot of each DNA extract was amplified in a total volume of 25 µL using KAPA HiFi HotStart ReadyMix, a 0.300 µM final concentration of each primer, and molecular-grade water. PCR cycling conditions included an initial denaturation at 95°C for 3 minutes; 30 cycles of 98°C for 20 seconds, 51°C for 15 seconds, and 72°C for 15 seconds; and a final extension at 72°C for 1 minute. Duplicate PCR reactions were performed for each sample. PCR reactions were prepared in a MyStaire clean PCR hood with a UV light, positive airflow, and a HEPA filter. All work surfaces and pipettes were sterilized by wiping with a solution of 10% household bleach, rinsing with Milli-Q water, and irradiation with the UV light for 15 minutes before PCR reactions were prepared. Sterile filter tips and nitrile gloves were used during all steps. No-template controls (NTC) were included during each set of PCR reactions, which consisted of the reaction

master mix with molecular-grade water in place of DNA extract. Following PCR amplification, 1 µL of each PCR product was visualized on a 1% agarose gel in TBE buffer stained with 1X GelRed to confirm the presence of an amplicon with the expected length. PCR duplicates for each sample, negative sampling control, and NTC were pooled and sent to the Genome Research Core at the University of Illinois at Chicago for further library preparation and sequencing.

To index each sample, PCR products were amplified in a total volume of 10 µL using the MyTaq HS mastermix combined with sample indices from the Access Array Barcode Library for Illumina (Fluidigm, South San Francisco, CA; Item# 100-4876) and molecular grade water. PCR cycling included an initial denaturation at 95°C for 5 minutes; 8 cycles of 95°C for 30 seconds, 60°C for 30 seconds, and 72°C for 30 seconds; and a final extension at 72°C for 7 minutes. The indexed products were pooled with equal volumes and sequenced on an Illumina MiniSeq. For sequencing on a subsequent Illumina MiSeq run, the volumes of each sample that were pooled were adjusted based on the number of reads yielded for each sample from the MiniSeq run to normalize the number of reads obtained per sample. The MiSeq run was conducted with paired-end 250 bp reads using V2 chemistry and a 15% spike-in of phiX. Before sequencing, the pooled libraries were bead cleaned with a 1.0X ratio of Ampure beads to remove residual primers and primer-dimers.

3.3.3 Bioinformatic analysis

Forward and reverse primer sequences were trimmed from the sequencing reads using *cutadapt* (Martin, 2011) with the following flags: -n 1, -O 5, and --minimum-length

5. Any read pair in which either the forward or reverse primer was not trimmed from the 5' ends of the reads was discarded. The reverse complements of the reverse and forward primer sequences were optionally trimmed from the 3' ends of the forward and reverse reads, respectively, if identified. The trimmed data was filtered and denoised using *DADA2* (Callahan et al., 2016). After visualizing the quality profiles of the reads along their lengths in a subset of the samples, forward and reverse reads were truncated to 225 and 125 bp, respectively, and quality trimmed using the default settings with the *filterAndTrim* function. Denoising and chimera removal were performed using the default settings to construct a table of the sequence read counts of each denoised amplicon sequence variant (ASV) across the samples. ASVs were taxonomically classified using *assignTaxonomy*, and any ASVs with 100% matches to reference sequences were made using *addSpecies*. The default settings, with the "allowMultiple" argument set to "FALSE" were used, so that species assignments were only reported if an ASV matched exactly one unique sequence in the reference database. The SILVA 138.1 curated reference database files formatted for taxonomic classification using these functions in *DADA2* were used (https://benjjneb.github.io/dada2/training.html). After ASV tables were constructed and ASVs were taxonomically classified, we used *decontam* (Davis et al., 2018) with the prevalence method to remove contaminant ASVs identified in the extraction negative controls and no-template controls. Fifteen ASVs were identified as contaminants and removed from the ASV table for downstream analyses.

3.3.4 Microbial cell counts

On each sampling day of the experiments, water samples were taken for cell counts. A 47.5 mL aliquot of the seawater from each tank was collected in a sterile, 50 mL centrifuge tube (Celltreat Scientific Products, Pepperell, MA, USA) using a peristaltic pump and Masterflex L/S 15 platinum-cured silicone tubing. The tubing was bleach-sterilized at the start of each experiment for eDNA sampling and flushed with water from the experiments before microbial sampling. Each sample was treated with 2.5 mL of 50% (v/v) glutaraldehyde , and samples were mixed by inversion to fix microorganisms. Samples were then stored at 4°C until they were processed.

The entire volume of each sample was filtered over a 0.20 μm pore size, 25 mm diameter Whatman cyclopore polycarbonate filter (Cytiva, Marlborough, MA. USA) by vacuum filtration with a vacuum pump and a 12-position vacuum filtration sampling manifold (Millipore Sigma, Burlington, MA, USA). The molecular-grade water used to prepare the reagents was filtered through one filter alongside the samples to serve as filtration blanks. Several filtration blanks were processed and imaged the same way as the experimental samples to confirm that the reagents were not contaminated. Before each filtration, the apparatus was sterilized by wiping it with a 10% solution of household bleach, allowing it to air dry, and then rinsing it with deionized water. 4′,6-diamidino-2-phenylindole (DAPI) was used to stain nucleic acids in bacterial cells for fluorescence microscopy. After filtration, filters were submerged in 1 mL of 10 mg/mL DAPI for 10 minutes in the dark. The DAPI solution was then filtered through the filters, the filters were submerged in 1X phosphate-buffered saline (PBS) for 1 minute to rinse, and the 1X PBS was filtered through. Slides were prepared by adding a drop of immersion oil to a glass slide. The filter was then applied to the center of the slide with flame-sterilized

forceps, another drop of immersion oil was added to the filter, and then a glass coverslip was firmly placed over the filter. Slides were then stored in an opaque box in 4°C in a dark refrigerator until they were imaged. Filtration and staining were conducted in a fume hood with positive airflow to minimize the risk of contamination.

Slides were imaged using either a Nikon Eclipse E1000 or Eclipse TE2000-U microscope at 100X magnification using excitation wavelengths from 385 to 400 nm and 360 to 370 nm, respectively. Using the E1000, fluorescence in the range of 450 to 465 nm was observed and photographed using a Nikon camera and the Nikon NIS-S Elements Software. Using the TE2000-U, fluorescence of 420 nm using a long pass filter was observed and photographed using a SPOT RT sCMOS camera and SPOT Advanced imaging software. Ten locations on each filter were randomly selected and photographed for image analysis using the auto-exposure setting. A scale bar of 10 µm was included in each image. In some cases, it was necessary to take multiple images of a location with very slight adjustments in focus in order to capture the entire area of the photograph clearly. In these cases, a composite image of the location was created using either the ImageJ plugin *stackfocuser* using the default settings or Adobe Photoshop. The brightness and contrast of images were adjusted as necessary to facilitate accurate cell counting, typically when a low abundance (tens) of cells were present in an image and thus overall fluorescence was weak. Cells in each image or composite image were counted in *ImageJ* using the multi-point tool. The number of cells per milliliter of seawater was estimated by extrapolating the area imaged (~0.01178 mm^2 for images taken with the E1000 and ~0.012444 mm^2 with the E2000-TU) to the total area of the filter membrane (490.9 mm^2) and dividing by the number of ml filtered (47.5 ml).

3.3.5 Quantification of Dissolved Inorganic Phosphate Concentration

At each time point, samples of approximately 20 mL of the filtrate from the 0.2 µm pore-size Sterivex filters were collected in duplicate into glass scintillation vials and frozen at -20°C. To quantify inorganic dissolved [PO_4^{3-}], we used a colorimetric method by reacting the samples with a mixed reagent comprised of ammonium molybdate, sulfuric acid, ascorbic acid, and potassium antimonyl-tartrate (Strickland & Parsons, 1972).

All reagents and standards were prepared in glassware or plasticware (HDPE) that was treated overnight with 5% w/v nitric acid at 60°C to remove any trace organophosphates. Pipet tips were acid-treated in the same manner. All reagents and standards were prepared with ultrapure MilliQ water. The ammonium molybdate solution was prepared by dissolving 2 grams of $(NH_4)_6Mo_7O_{24}$ $4H_2O$ in 1 L of water; the sulfuric acid solution was prepared by diluting concentrated H_2SO_4 1:100 in water; the ascorbic acid solution was prepared by dissolving 1.75 grams of ascorbic acid in 0.5 L water; and the potassium antimonyl-tartrate was prepared by dissolving 0.09 g of $KSbC_4H_4O_7$ $1/2H_2O$ in 1 L water. The ascorbic acid solution was refrigerated and replaced weekly, while the other solutions were stored at room temperature. A primary standard was prepared by dissolving 0.87185 g K_2PO_4 in 0.5 L water to create a 0.01 M solution, and a secondary standard was prepared by diluting the primary standard, adding 1 ml of the primary standard, and topping off the volume to 100 ml in a volumetric flask. The concentration of this secondary standard, in µm/L, was calculated from the exact amount

of K_2PO_4 added to the primary standard. The primary and secondary standards were stored in glass bottles and refrigerated.

The night before analysis, water samples were thawed at 4°C. The mixed reagent was prepared before each run by combining the four reagents at a ratio of 1:2.5:1:0.5 in the order described above. Five standards of known and increasing concentrations were prepared by diluting 0.5, 1, 2, 3.5, and 4.5 mls of the secondary standard in 100 ml water, and these standards were run along with each run of samples daily. A standard that only consisted of MilliQ water (i.e. 0 µM PO_4^{3-}) was also run as a blank alongside each set of samples. For each reaction, 6.5 ml of each sample or standard was added to 13 ml of the mixed reagent in a new, clean scintillation vial. After at least thirty minutes, the reaction was transferred to a 10 cm long quartz glass cell, and absorbance at 885 nm was measured using a Shimadzu UV-1601 spectrophotometer. The cell was flushed with a small sample volume before the remainder was transferred to the cell for measurement to prevent crossover between measurements conducted after one another. A standard curve for each day of analysis was created by fitting a linear model in R (function *lm*) to the standard data from each day with the known concentrations of the standards as the response variable and their measured absorbances as the predictor variable. The intercept and slope of these linear models were then used to calculate the known concentrations of each of the samples. The calculated concentrations for the duplicate samples from each experiment at each timepoint were averaged to obtain a single value in µm/L. The analytical uncertainty (2s) was ± 5% for PO_4^{3-}.

3.3.6 Statistical Analysis and Data Visualization

Statistical analysis and data visualization were conducted in R (version 4.3.1 *Beagle Scouts*) using primarily *tidyverse* packages (Wickham et al., 2019), as well as *phyloseq* (McMurdie & Holmes, 2013) and *vegan* (Okansen, 2013). Shannon alpha diversity in each sample was estimated using the *estimate_richness* function from *phyloseq*. For all other analyses of community composition, the dataset was subset to ASVs that occurred at a relative abundance of sequencing reads of at least 1% in any sample. Hereafter, we refer to these ASVs as "abundant ASVs". Barplot visualizations of the abundant ASVs were generated using the *plot_bar* function from *phyloseq*. To analyze the correlation of the community distances with physicochemical conditions, Bray-Curtis dissimilarities were calculated using the relative abundances of the abundant ASVs as the genus level, and a distance-based redundancy analysis (dbRDA) was performed using *dbRDA* from *vegan*. Time (in days), average temperature, dissolved oxygen concentration, and pH over the course of the experiments were included as the explanatory variables. A Principal Coordinates Analysis (PCoA) was conducted from the same dissimilarity matrix using the *plot_ordination* function from *vegan* with *justDF* set to TRUE to obtain principal coordinates to represent bacterial community composition in models of eDNA degradation.

To determine if specific bacterial genera were significantly different in their abundances over time across experiments of different conditions, we used Analysis of Compositions of Microbiomes with Bias Correction 2 (*ANCOM-BC2*) (Lin & Das Peddada, 2020). We fit a model using the function *ancombc2* that included time, temperature, oxygen concentration, and pH as fixed effects; and each experiment as a random intercept. To investigate differences in abundance across experimental

temperatures, we conducted multiple pairwise comparison tests of significance using Dunnett's tests.

To incorporate the cell counts data with the *16S* rRNA metabarcoding and coral eDNA quantification data, the cell counts data were merged with the *16S* and eDNA quantifications by the day of the experiment when they were taken. The time of eDNA sampling was used for statistical analyses. Since sampling for eDNA and cell counts occurred within ~2 hours of one another, we deemed these small differences in sampling time negligible for interpreting statistically significant effects.

To identify statistically significant relationships between Shannon alpha diversity, bacterial community composition, and cell counts (response variables), with time and physicochemical conditions (fixed effects), we fit linear mixed models using *lme4* (Bates, 2010) and tested for significance with Type III ANOVA with Satterhwaite's method using *lmertest* (Kuznetsova at al., 2017). Bacterial community composition was incorporated into model formulas as the first two PCoA axes. Cell counts were incorporated into model formulas as the maximum number of cells counted per time point in each experiment, and values were log(x+1) transformed. Time was incorporated into model formulas as the time in days from the start of each experiment. Temperature, [DO], and pH were incorporated into model formulas as continuous, explanatory variables represented as the average value over the course of each experiment. Each experiment was included as a random intercept, and time was included as a random slope when its inclusion did not result in a singular fit of the model.

In McCartin et al. (2022), we fit biphasic linear models to the log-transformed coral eDNA concentrations to accurately estimate eDNA degradation rates across earlier

and later time points in eDNA persistence experiments. To investigate the effects of bacterial abundance and community composition on eDNA degradation, we fit linear mixed models to eDNA concentration during the second phase of eDNA degradation in each experiment. Log-transformed average coral eDNA concentration was the response variable; time, and the interactions of time with temperature, pH, and either cell counts, Shannon alpha diversity, or the first two principal coordinates axes were included as fixed effects; each experiment was included as a random intercept; and time was included as a random slope when its inclusion did not result in a singular fit of the model. We also fit a linear mixed model to investigate the correlation between the maximum number of cells counted over the course of all experiments (fixed effect) and their modeled decay rate constants during the second phase of eDNA degradation (response variable). Temperature, treated as a factor with groups of 4°C, 10°C, and 20°C, was included as a random intercept.

3.4 Results and Discussion

3.4.1 Physicochemical conditions modulated changes in the bacterial communities across eDNA persistence experiments.

All ASVs in the eDNA persistence experiments were classified to the Kingdom Bacteria. The bacterial communities were dominated (> 50% relative sequence abundance) by ASVs classified to the phylum Proteobacteria across all time points. Other ASVs that comprised at least 1% of the sequencing reads in any sample (hereafter "abundant ASVs") were classified into two other phyla: Campylobacterota and

Firmicutes. Twenty-six other phyla were represented by ASVs that comprised less than 1% of the sequencing reads in all samples (**Table B.1**).

During the first day of each experiment, bacterial communities were dominated by ASVs classified to the genus *Halomonas*. However, in eleven of twenty-two experiments, the bacterial communities shifted over time from communities dominated by *Halomonas* to diverse communities of ASVs classified into multiple genera. Analysis of compositions of microbiomes with bias correction (ANCOM-BC2) identified five bacterial genera that were significantly differentially abundant over time. One genus exhibited significant increases in abundance over time: *Marinobacter* (Log-fold change = 0.32968 ± 0.09125 per day, *Q-Value = 0.01293*). Four genera exhibited significant decreases in abundance over time: *Halomonas* (Log-fold change = -0.20 ± 0.03 per day, *Q-Value < 0.00001*), *Aliidiomarina* (Log-fold change = -0.24 ± 0.03 per day, *Q-Value < 0.00001*), *Salipaludibacillus* (Log-fold change = -0.23 ± 0.03 per day, *Q-Value < 0.00001*), and *Poseidonibacter* (Log-fold change = -0.15 ± 0.04 per day, *Q-Value = 0.00072*).

Increases in bacterial community diversity and changes in bacterial community composition were modulated by the physicochemical conditions of the experiments, namely temperature. Shannon alpha diversity was significantly positively correlated with the interaction of time and temperature (*P-Value = 0.0077*). All six experiments conducted at 20°C exhibited community turnover from a community dominated by *Halomonas* to a community dominated by other ASVs including the genera *Alteromonas*, *Colwellia*, and *Pseudoalteromonas,* which dominated the community at any single time point, along with several other less abundant bacterial genera (**Figure 3.1**). Community

turnover was apparent in just one of four experiments at 10°C, and just four of twelve experiments at 4°C. The speed of community turnover was faster at higher temperatures. Community turnover occurred after just 48 hours in experiments conducted at 20°C, but after at least four days in experiments conducted at 10°C and 4°C. In experiments conducted at 20°C there was little (~1 day), if any, lag between the time at which new genera were detected in the *16S* data and the time at which these new genera comprised the majority of the bacteria in the experiments. On the contrary, community turnover happened more gradually, over longer periods of time (multiple days) in experiments conducted at 10°C and 4°C. In two experiments at 4°C, certain ASVs increased in relative abundance gradually but did not outnumber *Halomonas* by the end of the experiments.

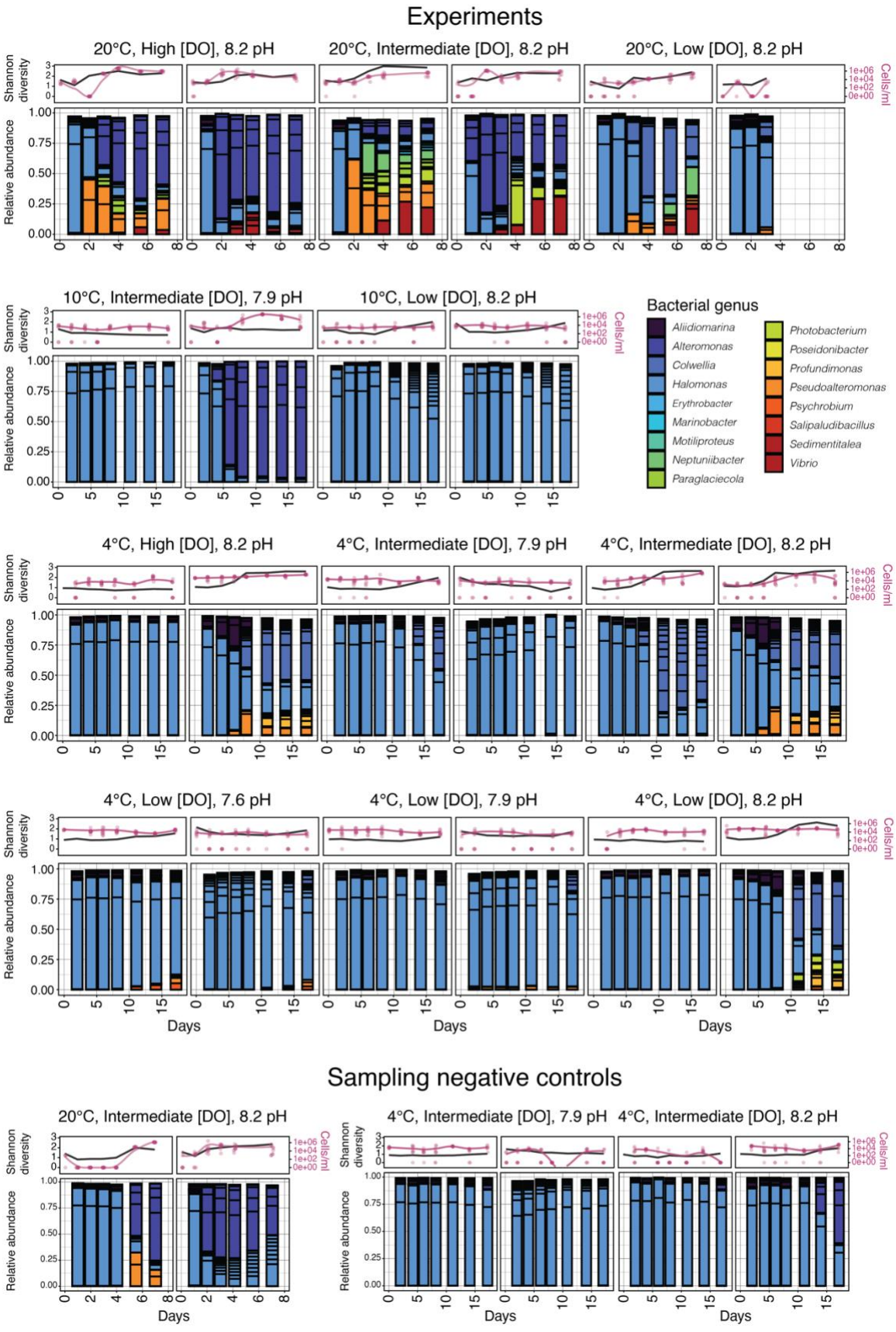
Experiments
20°C, High [DO], 8.2 pH
20°C, Intermediate [DO], 8.2 pH
20°C, Low [DO], 8.2 pH
10°C, Intermediate [DO], 7.9 pH
10°C, Low [DO], 8.2 pH
4°C, High [DO], 8.2 pH
4°C, Intermediate [DO], 7.9 pH
4°C, Intermediate [DO], 8.2 pH
4°C, Low [DO], 7.6 pH
4°C, Low [DO], 7.9 pH
4°C, Low [DO], 8.2 pH
Shannon diversity
Relative abundance
Cells/ml
Days
Bacterial genus
Aliidiomarina
Alteromonas
Colwellia
Halomonas
Erythrobacter
Marinobacter
Motiliproteus
Neptuniibacter
Paraglaciecola
Photobacterium
Poseidonibacter
Profundimonas
Pseudoalteromonas
Psychrobium
Salipaludibacillus
Sedimentitalea
Vibrio
Sampling negative controls
20°C, Intermediate [DO], 8.2 pH
4°C, Intermediate [DO], 7.9 pH
4°C, Intermediate [DO], 8.2 pH

Figure 3.1: Relative abundance of bacterial ASVs that comprised at least 1% of the sequencing reads in any single sample in 22 eDNA persistence experiments. Genus-level taxonomic classifications of the bacterial ASVs are visualized. Shannon alpha diversity and cell counts are plotted in the upper panels. Shannon alpha diversity is plotted as the black line through each estimate at each timepoint. Each individual cell count observation and a smoothing curve fit through the average cell count at each timepoint are plotted. The right y-axis (cell counts) is $\log_{10}$ transformed.

Not only were the prevalence and speed of community turnover higher across experiments with increased temperatures, but the compositions of the bacterial communities also differed across temperatures. Distance-based redundancy analysis found that 9.685% of the squared Bray-Curtis distances calculated between the relative abundances of bacterial genera was explained by the constrained variables: time, temperature, dissolved oxygen concentration, and pH (**Figure 3.2**). Temperature (*P-Value = 0.001*), pH (*P-Value = 0.003*), and time (*P-Value* = 0.034) were significant predictors of the squared Bray-Curtis distance between samples. Two bacterial genera, *Colwellia* and *Sedimentitalea,* were differentially abundant between experimental temperatures. Pairwise tests of significance as implemented with ANCOM-BC2 revealed that *Colwellia* was significantly less abundant in experiments conducted at 10°C than at 4°C (Log-fold change = -2.34 ± 0.79, *Q-Value = 0.03716*) and 20°C (Log-fold change = 3.16 ± 1.08, *Q-Value = 0.03716*). *Sedimentitalea* was significantly more abundant in experiments conducted at 20°C than at 4°C (Log-fold change = 4.37 ± 1.01, *Q-Value* =

0.00038), but not 10°C. We did not find any statistically significant differences in the abundances of specific genera with either average dissolved oxygen concentration or pH.

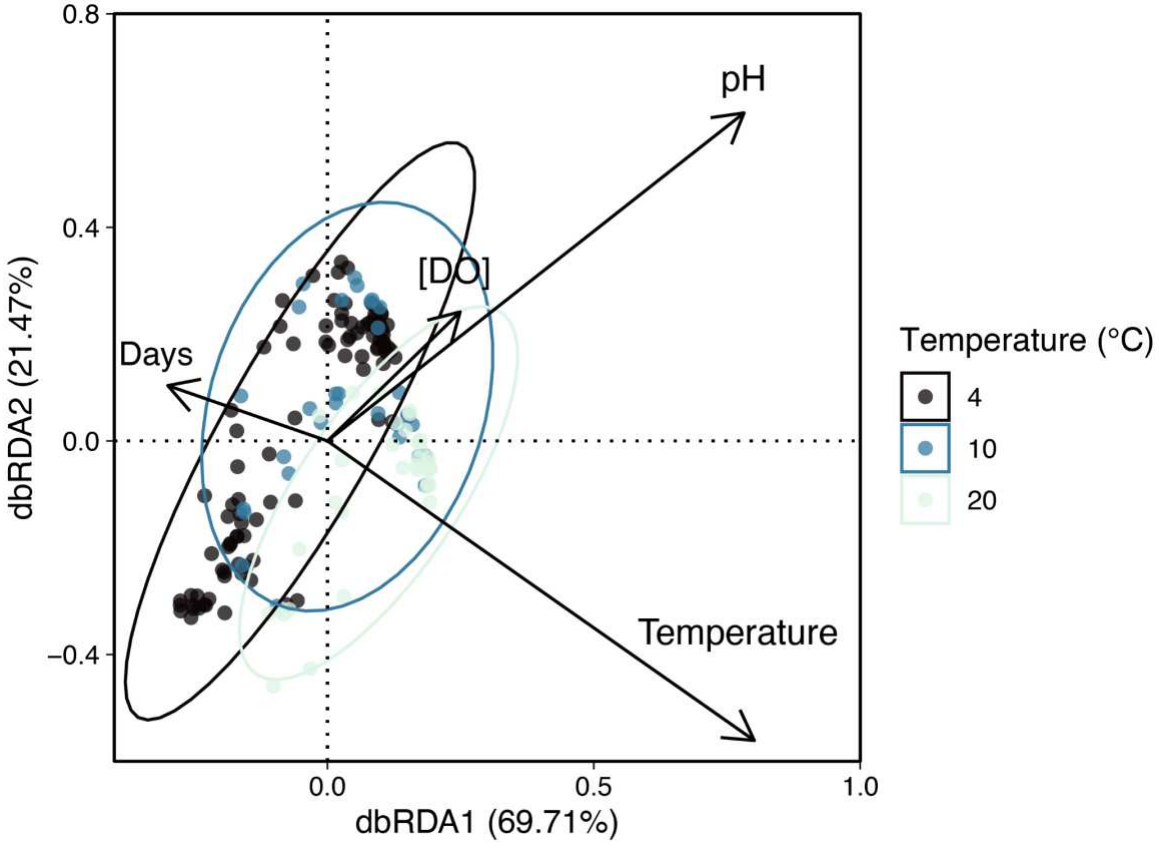

Figure 3.2: Distance-based redundancy analysis (dbRDA) ordination plots of *16S* bacterial communities visualized by time, temperature, dissolved oxygen concentration, and pH in eDNA persistence experiments. Bray-Curtis distances between samples were calculated based on a matrix of relative abundances of genera represented by ASVs that comprised at least 1% of sequence read abundance in any sample. Axes labels represent the percentage of constrained variation that is accounted for by each axis.

3.4.2 Bacteria were likely sourced from artificial seawater yet represent taxa that naturally occur in the marine environment.

Bac

terial community turnover was not limited to experimental tanks where coral eDNA was added. During the first 48 hours of the experiments, bacterial communities in the negative sampling control tanks were also dominated by bacterial ASVs classified to the genus *Halomonas*. As in the experimental tanks, the relative abundances of certain bacterial genera (e.g. *Alteromonas* and *Pseudoalteromonas*) increased over time in three of six negative control tanks. However, as compared to the experiments, fewer genera exhibited increases in relative abundance over time in the negative sampling controls. To this end, Shannon alpha diversity was significantly lower in the sampling negative controls than in the experimental tanks at the same conditions (*P-Values* < 0.00001).

The bacteria in the eDNA persistence experiments could have been derived from two sources: 1) the components of the artificial seawater, which consisted of two dry salts (NaCl and $MgSO_4$) and two proprietary aqueous salt solutions, and/or 2) the homogenized coral tissue added to each experimental tank. It is unlikely that the source of these bacteria was the ultrapure MilliQ water that we used to make the artificial seawater. Overlap in the identities of bacteria between the experiments and the sampling negative control tanks demonstrate that at least some, if not the majority, of the bacteria that proliferated in the experiments and in the negative sampling control tanks (e.g. *Alteromonas, Pseudoalteromonas*) were derived from the salt components of the artificial seawater. Other genera that were absent in the sampling negative controls but present in the experiments, notably *Colwellia* which at some time points dominated bacterial communities in the experimental tanks, may have either been 1) associated with the homogenized coral tissue added to experimental tanks, or 2) derived from the artificial

seawater at low initial abundance, then proliferated after the addition of the organic material and nutrients derived from the coral tissue.

Regardless of the provenance of bacteria in the eDNA persistence experiments, members of bacterial taxa that were detected through *16S* metabarcoding are largely known to be heterotrophic and to occur naturally in marine environments. The majority of the abundant ASVs were classified to the class Gammaproteobacteria (Phylum: Proteobacteria), including four genera in the order Oceanospirillales: *Halomonas*, *Motiliproteus*, *Neptuniibacter*, and *Profundimonas*. Members of the Oceanospirillales are either heterotrophic or chemoheterotrophic and are known from marine environments including deep-sea habitats such as plumes associated with the Deepwater Horizon oil spill, the Puerto Rico trench, and hydrothermal vents (Mason et al., 2012; Kim et al., 2013; Cao et al., 2014). Other abundant bacterial ASVs classified into the class Gammaproteobacteria included genera in the orders Alteromonadales: *Aliidiomarina, Alteromonas*, *Pseudoalteromonas*, *Colwellia, Psychrobium*, *Paraglaciecola*; Vibrionales: *Vibrio*, and *Photobacterium*; and Pseudomondales: *Marinobacter*. Members of these genera are heterotrophic and are known from marine environments from coastal ecosystems, sea ice, and the deep sea (Ivanova et al., 2004, Singer et al., 2011). Three other classes were represented in the experiments by ASVs that comprised at least 1% of the sequencing reads in any sample: Alphaproteobacteria, represented by *Erythrobacter* and *Sedimentitalea*; Bacillota, represented by *Salipaludibacillus*; and Epsilonproteobacteria, represented by the genus *Poseidonibacter*. Members of these genera are similarly known from marine environments, including the deep sea, and are heterotrophs or photoheterotrophs, in the case of some members of *Erythrobacter* (Yoon

et al., 2003; Wu et al., 2012; Breider et al., 2014; Zheng et al., 2016; Amoozegar et al., 2018; Guo et al., 2019).

3.4.3 Bacterial cell counts were correlated with changes in bacterial community composition.

The maximum number of cells counted at each timepoint was significantly *negatively* correlated with temperature (*P-Value = 0.00502*), but *positively* correlated with the interaction between time and temperature (*P-Value = 0.00003*), suggesting that over time bacterial cells were most abundant in experiments conducted at higher temperatures. This interpretation is consistent with the observation that the highest number of cells were counted in experiments conducted 10°C at 20°C. Cell counts were also *positively* correlated with Shannon alpha diversity (*P-Value < 0.00001*), and *negatively* correlated with the first PCoA axis (*P-Value < 0.00001*). We interpret that increases in cell counts coincided with the proliferation of a diverse suite of bacteria, the identities of which were modulated by temperature and pH. This interpretation is consistent with the fact that bacteria forming aggregations in samples from later time points in experiments conducted at 20°C and 10°C were characteristically rod-shaped (**Figure B.1**), coinciding with the typical morphologies of Gammaproteobacteria that exhibited high relative abundances in the *16S* metabarcoding data, such as *Alteromonas* and *Pseudoalteromonas* (Ivanova et al., 2004).

3.4.4 Increases in bacterial cell abundance and bacterial community turnover were correlated with accelerated eDNA degradation.

Here, we provide evidence that higher temperatures and oxygen concentrations increased the proliferation of bacteria, and that the composition of these bacterial communities were modulated by temperature and pH. Previously, we demonstrated from the same set of experiments that accelerated eDNA degradation rates occurred at higher temperatures (20°C versus 10°C and 4°C), and to a lesser extent at higher pH during the second phase of a biphasic exponential decay (McCartin et al., 2022). Indeed, experiments conducted at 20°C that exhibited the fastest rates of eDNA degradation also exhibited the highest bacterial cell counts (**Figure 3.3**). However, when data from experiments across all temperatures are considered, the interaction terms between time and temperature and/or time and pH were significantly correlated with eDNA concentration, but cell counts, Shannon alpha diversity, and the first two PCoA axes were not (**Tables 3.1-3.3**). Further, while considering each temperature as a random intercept, the maximum number of cells counted in the experiments was not significantly correlated with their modeled decay rate constants during the second phase of eDNA degradation (*P-Value = 0.643*).

From these results we infer that temperature was the driving factor controlling eDNA degradation rate, and that this effect was likely the result of synergy between temperature and the proliferation of heterotrophic bacteria. A synergistic interaction between temperature and microbial processes, rather than an additive interaction, would explain why experiments conducted at 20°C that also experienced proliferations in bacteria exhibited the fastest rates of eDNA degradation, but experiments at 4°C and 10°C that experienced proliferations in bacteria did not exhibit similarly drastic increases in eDNA degradation rate as compared to experiments with low numbers of cells. It is

worth noting however, that across experiments at both 4°C and 10°C, the highest decay rate constants were estimated from experiments that exhibited the largest numbers of bacterial cells as compared to experiments at the same temperatures. It is challenging to conclusively establish microbial processes as a driver of eDNA degradation in synergy with temperature from these data, since all experiments conducted at 20°C coincided with substantial increases in bacterial abundance. To conclusively establish the role of bacterial abundance in accelerating eDNA degradation at 20°C, sterilization of the seawater in the experimental tanks, perhaps using chemicals such as antibiotics, would have been necessary to collect data at 20°C in the absence of large numbers of bacterial cells. If bacteria were indeed responsible for the accelerated rate of eDNA degradation at 20°C, we would expect that experiments conducted in sterile conditions at 20°C would exhibit slower rates of eDNA degradation than those with a proliferation of bacteria. Comparing modeled rates in sterile experiments at 20°C to those from experiments conducted at 4°C and 10°C would also help to determine if temperature alone can accelerate eDNA degradation rate in the absence of microbes.

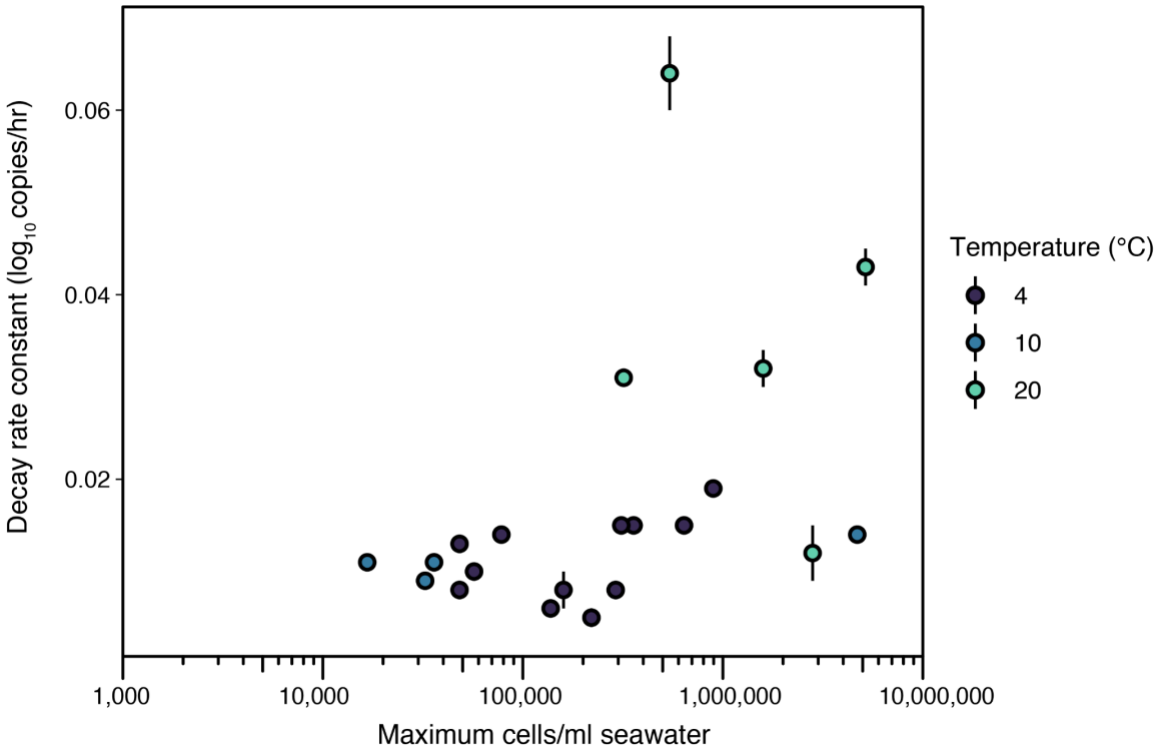

Figure 3.3: Relationships between decay rate constants and the maximum number of cells counted at any one time point in eDNA persistence experiments. Error bars represent the standard error of the decay rate constant estimate.

Table 3.1: Coefficients and Type III Analysis of Variance results for a linear mixed model with log-transformed eDNA concentrations as the response variable, and the interaction of time with cell counts as a fixed effect along with physicochemical conditions.

Coefficient	Estimate	Std. Error	Sum of Squares	Degrees of Freedom	F-Value	P-Value
(Intercept)	8.833	0.221	NA	NA	NA	NA
Days	0.788	0.693	0.254	9.621	1.290	0.284
Days:avg.temp	-0.022	0.004	5.316	32.441	26.995	<0.001*
Days:avg.pH	-0.122	0.088	0.374	9.886	1.900	0.198
Days:log1p(max_cells)	0.000	0.006	0.000	60.562	0.001	0.980

Table 3.2: Coefficients and Type III Analysis of Variance results for a linear mixed model with log-transformed eDNA concentrations as the response variable, and the interaction of time with estimated Shannon alpha diversity as a fixed effect along with physicochemical conditions.

Coefficient	Estimate	Std. Error	Sum of Squares	Degrees of Freedom	F-Value	P-Value
(Intercept)	8.749	0.212	NA	NA	NA	NA
Days	0.724	0.632	0.278	7.522	1.312	0.287
Days:avg.temp	-0.022	0.004	6.402	26.468	30.246	<0.001*
Days:avg.pH	-0.107	0.080	0.374	7.565	1.769	0.222
Days:Shannon	-0.030	0.022	0.392	14.448	1.854	0.194

Table 3.3: Coefficients and Type III Analysis of Variance results for a linear mixed model with log-transformed eDNA concentrations as the response variable, and the interaction of time with PCoA axes as fixed effects along with physicochemical conditions.

Coefficient	Estimate	Std. Error	Sum of Squares	Degrees of Freedom	F-Value	P-Value
(Intercept)	10.549	0.445	NA	NA	NA	NA
Days	271.409	90.718	2.417	12.000	8.951	0.011
Days:avg.temp	-6.162	2.473	1.677	12.000	6.210	0.028*
Days:avg.pH	-18.407	5.183	3.407	12.000	12.614	0.004*
Days:Axis.1	-0.444	0.342	0.456	12.000	1.689	0.218
Days:Axis.2	0.017	0.264	0.001	12.000	0.004	0.951

3.4.5 Inorganic [PO_4^{3-}] were not limiting in experiments.

Dissolved inorganic [PO_4^{3-}] in experimental samples ranged from 0.02 to 2.28 µmol/L (µM), values that are within the range of natural [PO_4^{3-}] abundance in deep waters in offshore, marine environments. Generally, [PO_4^{3-}] rose slightly over the first few days of the experiments and then stabilized or decreased over time (**Figure 3.4**). This general trend may be expected if [PO_4^{3-}] were linked to the addition of coral tissue and subsequent degradation of eDNA. Hypothetically, following the addition of the coral tissue, as the tissue degraded and cells lysed, particulate and dissolved organic P in the form of eDNA will be released. Subsequently, if this eDNA were scavenged for P, [PO_4^{3-}] would increase as it is remineralized into the experimental tanks from the eDNA. However, we found that [PO_4^{3-}] also increased over time in sampling negative control

tanks, which contained no coral tissue and thus no eDNA. Thus, increases in [PO_4^{3-}] cannot be linked to the addition of coral tissue to seawater, and we infer that the addition of the coral tissue did not contribute substantially to the overall P pool in the experimental tanks. Over time, [PO_4^{3-}] were significantly, negatively correlated with temperature (*P-Value = 0.0179*), consistent with marked declines in [PO_4^{3-}] in experiments conducted at 20°C. We hypothesize that these declines were due to increased cell densities at later time points at higher temperatures, as PO_4^{3-} was removed from its aqueous form and incorporated into biomass of the bacterial cells.

Salter (2018) found that the cycling of radiolabeled P in dissolved eDNA was accelerated in P-limited conditions. However, the range of [PO_4^{3-}] measured in that study was much lower overall, from 0.03 to 0.06 μM, than in our experiments. Zhao et al. (2022) conducted eDNA persistence experiments and found that in water from natural ecosystems where P was not limiting, [PO_4^{3-}] were not correlated eDNA degradation rate. Likewise, we conclude that in our experiments P was not limiting, and we infer that scavenging of particulate and dissolved organic P from coral eDNA was not a particularly relevant mechanism for bacterially mediated eDNA degradation in this experimental system. However, we still observed a strong correlation between eDNA degradation rate and the proliferation of heterotrophic bacteria at higher temperatures, suggesting that microbial degradation of eDNA is not exclusive to P-limiting conditions.

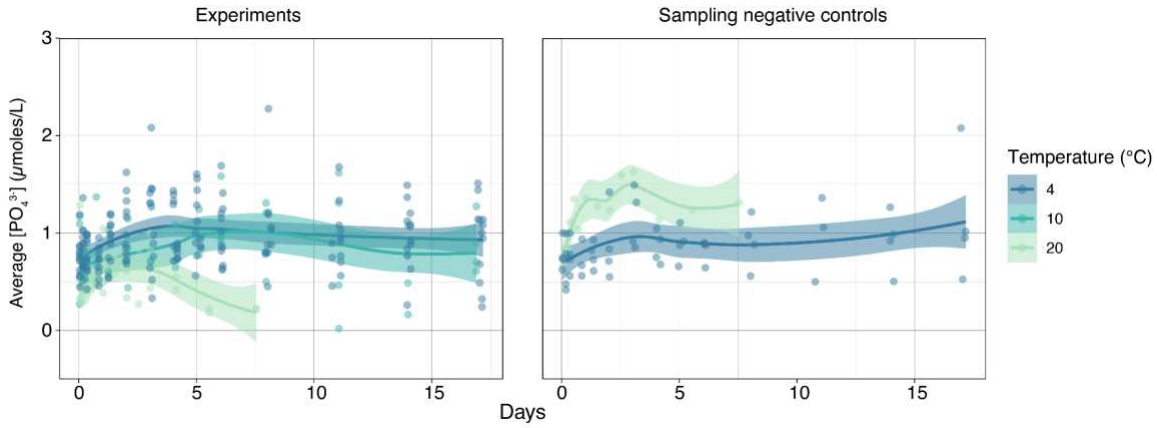

Figure 3.4: Changes in [PO_4^{3-}] over time in eDNA persistence experiments plotted by temperature. Each point represents the average concentration from duplicate samples analyzed from each time point in each experiment. A smoothing function was fit to the data, and the highlighted region represents the standard error.

3.4.6 A lack of data regarding microbial community and function precludes the accurate and confident assessment of the factors that control eDNA persistence in natural environments.

To our knowledge, this is the first study to incorporate metabarcoding of the microbial community with eDNA persistence experiments to detect changes in bacterial communities. Through the analysis of *16S* rRNA metabarcoding data, we identified that increases in bacterial abundance were coupled with changes in microbial community composition across our experiments. Metabarcoding not only permitted the identification of these potentially relevant changes in community composition, but also allowed for the comparison of our experimental samples to samples from natural environments where our coral species of interest, *Desmophyllum pertusum*, occurs. While the bacterial taxa detected in the experiments were heterotrophic and known from natural, marine

environments, bacterial communities in field samples were very different in composition (**Figure B.2**).

In future eDNA persistence studies it would be pertinent to include microbial community metabarcoding data not only to assess similarity between communities in experiments and natural environments, but also between separate sets of eDNA persistence experiments. Differences in the sources of water used in experimental studies explain variation across experimental results, but differences in bacterial community composition, a potentially relevant factor, cannot yet be investigated due to a lack of data (Jo and Minamoto, 2021). Conducting fluorescent cell counts requires additional, purposeful sample preservation, is time consuming, and also requires a unique analytical skill set. However, the routine collection of *16S* rRNA metabarcoding data would also be powerful, as we show that these data were correlated with bacterial abundance, data collection made use of DNA extracts that were already preserved for qPCR (i.e., additional sample collection was not necessary), and metabarcoding analysis is a common skill set among eDNA analysts. Other strategies, such as qPCR of the *16S* rRNA gene, as in Eichmiller et al. (2015), would also be useful in place of or in addition to metabarcoding. We caution against conflating total DNA concentration with microbial abundance, since genome sizes of microbes differ drastically, resulting in incomparable results across communities with different compositions.

Incorporating analyses of microbial community composition in future experimental studies is an achievable and necessary goal. However, the value of understanding microbial community composition is limited to identifying changes in taxonomic composition without a more comprehensive understanding of the putative

functions of microbial taxa that relate to the degradation of nucleic acids. To this end, no experimental eDNA persistence study has incorporated microbial metagenomic or metatranscriptomic sequencing to investigate changes in relevant putative functions or gene expression. From the literature that does exist outside of the immediate eDNA realm, evidence suggests that a taxonomically broad suite of bacteria possess genes that encode enzymes necessary for the catabolism and/or scavenging of eDNA, nucleotides, and nucleosides. For example, a recent study experimentally demonstrated that bacterial ASVs in the phylum Proteobacteria, Firmicutes, and Bacteroidota possess enzymes such as extracellular nucleases and nucleoside phosphorylases necessary to catabolize dissolved, extracellular DNA in marine sediments (Wasmund et al., 2021). Further investigation into the metabolic capabilities of bacterioplankton in freshwater and saltwater environments as they relate to eDNA degradation are necessary for a comprehensive understanding of the relevance of specific microbial taxa for eDNA degradation. To constrain the timescales of eDNA data from the field with the highest level of confidence, this understanding should ideally be integrated with several relevant data types from field sampling sites: 1) microbial community composition through metabarcoding; 2) measurements of microbial abundance through either cell counts or qPCR; and 3) measurements of relevant physicochemical factors: temperature, pH, and nutrient concentrations.

3.5 Concluding remarks

In McCartin et al. (2022), we experimentally demonstrated that across a wide range of temperatures, pH, and dissolved oxygen concentrations, the degradation rate of

eDNA from a coral in seawater was most strongly influenced by temperature, wherein higher temperatures of 20°C versus 10°C and 4°C accelerated eDNA degradation. Here, by combining cell counts using epifluorescence microscopy, *16S* metabarcoding, and eDNA concentration data from the same experiments, we link the proliferation of several bacteria genera with high temperatures that coincide with the accelerated degradation of eDNA. From the integration of these data, we conclude that the acceleration of eDNA degradation at higher temperatures in our experiments was likely driven by the bacterial community. The combinations of temperature, pH and dissolved oxygen concentration that we tested reflect natural conditions, and our experiments supported bacterial communities composed of taxa with members that are heterotrophic and known from marine habitats. Thus, we suggest that the accelerated degradation of eDNA in the marine environment is likely driven through the interaction of temperature with the bacterial community, and mechanistically through strengthened biotic, enzymatic processes rather than abiotic hydrolysis. Further research linking specific bacterial taxa and biomolecular pathways to the degradation of aqueous eDNA will lead to a more nuanced understanding of the mechanisms governing the degradation of eDNA by marine microbes.

3.6 Acknowledgements

I sincerely thank Lehigh undergraduate studies Maia Clayton and Mary Mahoney for conducting [PO_4^{3-}] measurements, and Penny Demetriades, Luis Caceres, Carly Hecht, Petra Oganovich, Sebastian Bedoya, Simone Keck, and Hailey Kirkendall for conducting cell counts. Without their hard work this work would not have been possible.

We also thank Weihua Wang from the Genomics Research Core at the University of Illinois Chicago for library preparation and sequencing.

This research was funded by the National Oceanic and Atmospheric Administration's Oceanic and Atmospheric Research, Office of Ocean Exploration and Research, under award NA18OAR0110289 to SH and JMM at Lehigh University.

3.7 References

Amoozegar, M. A., Shahinpei, A., Makzum, S., Rafieyan, S., Moshtaghi Nikou, M., Spröer, C., & Ventosa, A. (2018). Salipaludibacillus halalkaliphilus sp. nov., a moderately haloalkaliphilic bacterium from a coastal-marine wetland. *International Journal of Systematic and Evolutionary Microbiology*, *68*(7), 2214–2219.

Andruszkiewicz Allan, E., Zhang, W. G., C. Lavery, A., & F. Govindarajan, A. (2021). Environmental DNA shedding and decay rates from diverse animal forms and thermal regimes. *Environmental DNA (Hoboken, N.J.)*, *3*(2), 492–514.

Barnes, M. A., Turner, C. R., Jerde, C. L., Renshaw, M. A., Chadderton, W. L., & Lodge, D. M. (2014). Environmental conditions influence eDNA persistence in aquatic systems. *Environmental Science & Technology*, *48*(3), 1819–1827.

Bates, D., Mächler, M., Bolker, B., & Walker, S. (2014). Fitting Linear Mixed-Effects Models using lme4. In *arXiv [stat.CO]*. arXiv. http://arxiv.org/abs/1406.5823

Björkman, K., & Karl, D. (1994). Bioavailability of inorganic and organic phosphorus compounds to natural assemblages of microorganisms m Hawaiian coastal waters. *Marine Ecology Progress Series*, *111*, 265–273.

Björkman, K. M., & Karl, D. M. (2003). Bioavailability of dissolved organic phosphorus in the euphotic zone at Station ALOHA, North Pacific Subtropical Gyre. *Limnology and Oceanography*, *48*(3), 1049–1057.

Björkman, K., Thomson-Bulldis, A. L., & Karl, D. (2000). Phosphorus dynamics in the North Pacific subtropical gyre. *Aquatic Microbial Ecology: International Journal*, *22*, 185–198.

Breider, S., Scheuner, C., Schumann, P., Fiebig, A., Petersen, J., Pradella, S., Klenk, H.-P., Brinkhoff, T., & Göker, M. (2014). Genome-scale data suggest reclassifications in the Leisingera-Phaeobacter cluster including proposals for Sedimentitalea gen. nov. and Pseudophaeobacter gen. nov. *Frontiers in Microbiology*, *5*. https://doi.org/10.3389/fmicb.2014.00416

Callahan, B. J., McMurdie, P. J., Rosen, M. J., Han, A. W., Johnson, A. J. A., & Holmes, S. P. (2016). DADA2: High-resolution sample inference from Illumina amplicon data. *Nature Methods*, *13*(7), 581–583.

Cao, Y., Chastain, R. A., Eloe, E. A., Nogi, Y., Kato, C., & Bartlett, D. H. (2014). Novel psychropiezophilic Oceanospirillales species Profundimonas piezophila gen. nov., sp. nov., isolated from the deep-sea environment of the Puerto Rico trench. *Applied and Environmental Microbiology*, *80*(1), 54–60.

Caza-Allard, I., Laporte, M., Côté, G., April, J., & Bernatchez, L. (2022). Effect of biotic and abiotic factors on the production and degradation of fish environmental DNA: An experimental evaluation. *Environmental DNA (Hoboken, N.J.)*, *4*(2), 453–468.

Collins, R. A., Wangensteen, O. S., O'Gorman, E. J., Mariani, S., Sims, D. W., & Genner, M. J. (2018). Persistence of environmental DNA in marine systems. *Communications Biology*, *1*, 185.

Davis, N. M., Proctor, D. M., Holmes, S. P., Relman, D. A., & Callahan, B. J. (2018). Simple statistical identification and removal of contaminant sequences in marker-gene and metagenomics data. *Microbiome*, *6*(1), 226.

Dell'Anno, A., & Danovaro, R. (2005). Extracellular DNA plays a key role in deep-sea ecosystem functioning. *Science*, *309*(5744), 2179.

Eichmiller, J. J., Best, S. E., & Sorensen, P. W. (2016). Effects of Temperature and Trophic State on Degradation of Environmental DNA in Lake Water. *Environmental Science & Technology*, *50*(4), 1859–1867.

Govindarajan, A. F., McCartin, L., Adams, A., Allan, E., Belani, A., Francolini, R., Fujii, J., Gomez-Ibañez, D., Kukulya, A., Marin, F., Tradd, K., Yoerger, D. R., McDermott, J. M., & Herrera, S. (2022). Improved biodiversity detection using a large-volume environmental DNA sampler with in situ filtration and implications for marine eDNA sampling strategies. *Deep Sea Research Part I: Oceanographic Research Papers*, *189*, 103871.

Guo, X.-H., Wang, N., Yuan, X.-X., Zhang, X.-Y., Chen, X.-L., Zhang, Y.-Z., & Song, X.-Y. (2019). Poseidonibacter antarcticus sp. nov., isolated from Antarctic intertidal sediment. *International Journal of Systematic and Evolutionary Microbiology*, *69*(9), 2717–2722.

Ivanova, E. P., Flavier, S., & Christen, R. (2004). Phylogenetic relationships among marine Alteromonas-like proteobacteria: emended description of the family Alteromonadaceae and proposal of Pseudoalteromonadaceae fam. nov., Colwelliaceae fam. nov., Shewanellaceae fam. nov., Moritellaceae fam. nov., Ferrimonadaceae fam. nov., Idiomarinaceae fam. nov. and Psychromonadaceae fam. nov. *International Journal of Systematic and Evolutionary Microbiology*, *54*(Pt 5), 1773–1788.

Jo, T., Arimoto, M., Murakami, H., Masuda, R., & Minamoto, T. (2020). Estimating shedding and decay rates of environmental nuclear DNA with relation to water temperature and biomass. *Environmental DNA (Hoboken, N.J.)*, *2*(2), 140–151.

Jo, T., & Minamoto, T. (2021). Complex interactions between environmental DNA (eDNA) state and water chemistries on eDNA persistence suggested by meta-analyses. *Molecular Ecology Resources*, *21*(5), 1490–1503.

Jo, T., Murakami, H., Yamamoto, S., Masuda, R., & Minamoto, T. (2019). Effect of water temperature and fish biomass on environmental DNA shedding, degradation, and size distribution. *Ecology and Evolution*, *9*(3), 1135–1146.

Karl, D. M. (2014). Microbially mediated transformations of phosphorus in the sea: new views of an old cycle. *Annual Review of Marine Science*, *6*, 279–337.

Karl, D. M., & Björkman, K. M. (2015). Chapter 5 - Dynamics of Dissolved Organic Phosphorus. In D. A. Hansell & C. A. Carlson (Eds.), *Biogeochemistry of Marine Dissolved Organic Matter (Second Edition)* (pp. 233–334). Academic Press.

Kasai, A., Takada, S., Yamazaki, A., Masuda, R., & Yamanaka, H. (2020). The effect of temperature on environmental DNA degradation of Japanese eel. *Fisheries Science: FS*, *86*(3), 465–471.

Kim, K. K., Lee, J.-S., & Stevens, D. A. (2013). Microbiology and epidemiology of Halomonas species. *Future Microbiology*, *8*(12), 1559–1573.

Krause, E., Wichels, A., Giménez, L., Lunau, M., Schilhabel, M. B., & Gerdts, G. (2012). Small changes in pH have direct effects on marine bacterial community composition: a microcosm approach. *PloS One*, *7*(10), e47035.

Kuznetsova, A., Brockhoff, P. B., & Christensen, R. H. B. (2017). LmerTest package: Tests in linear mixed effects models. *Journal of Statistical Software*, *82*(13). https://doi.org/10.18637/jss.v082.i13

Lance, R., Klymus, K., Richter, C., Guan, X., Farrington, H., Carr, M., Thompson, N., Chapman, D., & Baerwaldt, K. (2017). Experimental observations on the decay of environmental DNA from bighead and silver carps. *Management of Biological Invasions: International Journal of Applied Research on Biological Invasions*, *8*(3), 343–359.

Lin, H., & Peddada, S. D. (2020). Analysis of compositions of microbiomes with bias correction. *Nature Communications*, *11*(1), 3514.

Martin, M. (2011). Cutadapt removes adapter sequences from high-throughput sequencing reads. *EMBnet.journal*, *17*(1), 10–12.

Mason, O. U., Hazen, T. C., Borglin, S., Chain, P. S. G., Dubinsky, E. A., Fortney, J. L., Han, J., Holman, H.-Y. N., Hultman, J., Lamendella, R., Mackelprang, R., Malfatti, S., Tom, L. M., Tringe, S. G., Woyke, T., Zhou, J., Rubin, E. M., & Jansson, J. K. (2012).

Metagenome, metatranscriptome and single-cell sequencing reveal microbial response to Deepwater Horizon oil spill. *The ISME Journal*, *6*(9), 1715–1727.

Mauvisseau, Q., Harper, L. R., Sander, M., Hanner, R. H., Kleyer, H., & Deiner, K. (2022). The Multiple States of Environmental DNA and What Is Known about Their Persistence in Aquatic Environments. *Environmental Science & Technology*, *56*(9), 5322–5333.

McCartin, L. J., Vohsen, S. A., Ambrose, S. W., Layden, M., McFadden, C. S., Cordes, E. E., McDermott, J. M., & Herrera, S. (2022). Temperature Controls eDNA Persistence across Physicochemical Conditions in Seawater. *Environmental Science & Technology*, *56*(12), 8629–8639.

McMurdie, P. J., & Holmes, S. (2013). phyloseq: an R package for reproducible interactive analysis and graphics of microbiome census data. *PloS One*, *8*(4), e61217.

Muyzer, G., de Waal, E. C., & Uitterlinden, A. G. (1993). Profiling of complex microbial populations by denaturing gradient gel electrophoresis analysis of polymerase chain reaction-amplified genes coding for 16S rRNA. *Applied and Environmental Microbiology*, *59*(3), 695–700.

Oksanen, J., Kindt, R., Legendre, P., O'Hara, B., Stevens, M. H. H., Oksanen, M. J., & Suggests, M. (2007). The vegan package. *Community Ecology Package*, *10*(631-637), 719.

Redfield, A. C. (1958). The Biological Control of Chemical Factors in the Environment. *American Scientist*, *46*(3), 230A – 221.

Rodriguez-Lanetty, M., Granados-Cifuentes, C., Barberan, A., Bellantuono, A. J., & Bastidas, C. (2013). Ecological Inferences from a deep screening of the Complex Bacterial Consortia associated with the coral, Porites astreoides. *Molecular Ecology*, *22*(16), 4349–4362.

Salter, I. (2018). Seasonal variability in the persistence of dissolved environmental DNA (eDNA) in a marine system: The role of microbial nutrient limitation. *PloS One*, *13*(2), e0192409.

Singer, E., Webb, E. A., Nelson, W. C., Heidelberg, J. F., Ivanova, N., Pati, A., & Edwards, K. J. (2011). Genomic potential of Marinobacter aquaeolei, a biogeochemical "opportunitroph." *Applied and Environmental Microbiology*, *77*(8), 2763–2771.

Shogren, A. J., Tank, J. L., Egan, S. P., August, O., Rosi, E. J., Hanrahan, B. R., Renshaw, M. A., Gantz, C. A., & Bolster, D. (2018). Water Flow and Biofilm Cover

Influence Environmental DNA Detection in Recirculating Streams. *Environmental Science & Technology*, *52*(15), 8530–8537.

Spens, J., Evans, A. R., & Halfmaerten, D. (2017). Comparison of capture and storage methods for aqueous macrobial eDNA using an optimized extraction protocol: advantage of enclosed filter. *Methods in Ecology and Evolution / British Ecological Society*. https://doi.org/10.1111/2041-210X.12683

Strickland, J., & Parsons, T. (1968). *A practical handbook of seawater analysis*. https://repository.oceanbestpractices.org/handle/11329/1994

Strickler, K. M., Fremier, A. K., & Goldberg, C. S. (2015). Quantifying effects of UV-B, temperature, and pH on eDNA degradation in aquatic microcosms. *Biological Conservation*, *183*, 85–92.

Tsuji, S., Ushio, M., Sakurai, S., Minamoto, T., & Yamanaka, H. (2017). Water temperature-dependent degradation of environmental DNA and its relation to bacterial abundance. *PloS One*, *12*(4), e0176608.

Wasmund, K., Pelikan, C., Schintlmeister, A., Wagner, M., Watzka, M., Richter, A., Bhatnagar, S., Noel, A., Hubert, C. R. J., Rattei, T., Hofmann, T., Hausmann, B., Herbold, C. W., & Loy, A. (2021). Genomic insights into diverse bacterial taxa that degrade extracellular DNA in marine sediments. *Nature Microbiology*, *6*(7), 885–898.

Wickham, H., Averick, M., Bryan, J., Chang, W., McGowan, L., François, R., Grolemund, G., Hayes, A., Henry, L., Hester, J., Kuhn, M., Pedersen, T., Miller, E., Bache, S., Müller, K., Ooms, J., Robinson, D., Seidel, D., Spinu, V., … Yutani, H. (2019). Welcome to the tidyverse. *Journal of Open Source Software*, *4*(43), 1686.

Wu, H.-X., Lai, P. Y., Lee, O. O., Zhou, X.-J., Miao, L., Wang, H., & Qian, P.-Y. (2012). Erythrobacter pelagi sp. nov., a member of the family Erythrobacteraceae isolated from the Red Sea. *International Journal of Systematic and Evolutionary Microbiology*, *62*(Pt 6), 1348–1353.

Yoon, J.-H., Kim, H., Kim, I.-G., Kang, K. H., & Park, Y.-H. (2003). Erythrobacter flavus sp. nov., a slight halophile from the East Sea in Korea. *International Journal of Systematic and Evolutionary Microbiology*, *53*(Pt 4), 1169–1174.

Zhao, B., van Bodegom, P. M., & Trimbos, K. (2021). The particle size distribution of environmental DNA varies with species and degradation. *The Science of the Total Environment*, *797*, 149175.

Zheng, Q., Lin, W., Liu, Y., Chen, C., & Jiao, N. (2016). A Comparison of 14 Erythrobacter Genomes Provides Insights into the Genomic Divergence and Scattered Distribution of Phototrophs. *Frontiers in Microbiology*, *7*, 984.

Zulkefli, N. S., Kim, K.-H., & Hwang, S.-J. (2019). Effects of Microbial Activity and Environmental Parameters on the Degradation of Extracellular Environmental DNA from a Eutrophic Lake. *International Journal of Environmental Research and Public Health*, *16*(18). https://doi.org/10.3390/ijerph16183339

CHAPTER 4

NUCLEAR EDNA METABARCODING PRIMERS FOR ANTHOZOAN CORAL BIODIVERSITY ASSESSMENT

4.1 Abstract

The distributions of anthozoan corals are under-characterized due to their wide bathymetric range, occurrences in remote locales, and difficulties of identification from morphology alone. Environmental DNA (eDNA) sequencing promises to be a non-invasive strategy to complement conventional approaches for mapping and monitoring coral communities. Primers for eDNA metabarcoding have been designed to amplify nuclear and mitochondrial DNA barcodes in shallow scleractinians and mitochondrial *MutS* in deep-sea octocorals. However, a comprehensive method for eDNA meta-barcoding from all anthozoan corals, including black corals, has not been developed. We leveraged a sequence database of global coral collections, from shallow water to the deep sea, to design new PCR primers for coral eDNA sequencing that target the *28S rRNA* gene. We tested the performance of these primers by amplifying and sequencing eDNA from water samples collected in the Gulf of Mexico near mesophotic and deep-sea corals that were also imaged, sampled, and sequenced. Sequencing libraries produced using the primers were highly enriched in coral eDNA, with up to 99.9% of the reads originating from corals. Further, the *28S* barcode amplified using the primers distinguished coral genera. We recovered amplicon sequencing variants (ASVs) identical to DNA barcodes derived from Sanger sequencing and genome skimming of corals sampled at the same field sites. This new eDNA meta-barcoding strategy permits targeted eDNA sequencing

of black corals, octocorals, and scleractinians at sites where they co-occur and expands our current toolkit for mapping and monitoring coral communities in shallow coral reefs and the deep sea.

4.2 Introduction

Anthozoan corals, including stony corals (Order: Scleractinia), black corals (Order: Antipatharia), and octocorals (Orders Malacalcyonacea and Scleralcyonacea), occur globally and are foundation species in shallow (less than 30 meters depth), mesophotic (30 to 150 m), and deep-sea (> 150 m) benthic ecosystems (Cordes et al., 2008; Slattery & Lesser 2021). Mesophotic and deep-sea coral ecosystems are ecologically distinct from shallow reefs yet face similar threats, including invasive species, ocean warming, pollution, destructive fisheries, and other bottom-damaging activities (Koslow et al., 2000; Fisher et al., 2014; Etnoyer et al., 2016; Rocha et al., 2018). Developing novel methods that can rapidly assess the distributions of coral communities with meaningful taxonomic resolution will expedite the assessment of coral biogeography, diversity, and resilience.

Environmental DNA (eDNA) sequencing complements conventional methods for assessing biodiversity and the distribution of invasive and ecologically important invertebrates in marine habitats, including corals (Everett & Park, 2018; West et al., 2020; Dunn et al., 2022, Nishitsuji et al., 2023). Water sampling for eDNA analysis is inherently non-destructive and thus is well suited for monitoring marine protected areas and areas where past disturbances have impacted deep-sea corals with slow growth and recovery rates. The most often used eDNA sequencing method is eDNA meta-barcoding,

wherein a DNA barcoding gene is amplified and sequenced from an environmental sample. eDNA meta-barcoding may be conducted using PCR primers that amplify DNA barcodes from specific taxa (e.g. Miya et al., 2015) or all metazoans (e.g. Leray et al., 2013). With a comprehensive reference database for a taxon of interest, primers can be designed to amplify taxonomically informative regions not yet amplified by other eDNA meta-barcoding protocols. Thus, taxonomically specific primers are necessary for generating sequencing data that can be used to assess coral diversity at a taxonomic resolution comparable to established methods that do not involve physical sampling (e.g. video transects).

Multiple primer sets have been designed to amplify taxonomically informative eDNA nuclear and mitochondrial DNA barcodes in shallow scleractinians (Brian et al., 2019; Nichols & Marko, 2019; Alexander et al., 2020; Shinzato et al., 2021) and the mitochondrial *MutS* gene (*mtMutS*) in deep-sea octocorals (Everett and Park, 2018). Due to a slow rate of evolution in octocorals and scleractinians, mitochondrial barcoding genes are not taxonomically informative across all orders of anthozoan corals (McFadden et al., 2011). Furthermore, *mtMutS* is not present in black corals or scleractinians, precluding the use of this gene for comprehensive anthozoan meta-barcoding (Shimpi and Bentlage 2023). Nuclear ribosomal RNA (*rRNA*) genes encode for the small (*18S rRNA*) and large (*5S, 5.8S* and *28S rRNA*) subunits of the ribosome and are present in tandem repeats that occur in many copies in the eukaryotic nuclear genome. Due to their high copy number, like mitochondrial genes, nuclear *rRNA* genes have also been targeted for eDNA meta-barcoding. In anthozoan corals, *28S* has been sequenced in previous

phylogenetic studies and has shown utility in discriminating taxa (e.g. Barbeitos et al., 2010; Brugler & France, 2013; McFadden et al., 2014; Cairns & Wirshing, 2015).

Here, we leveraged a database of sequences from global coral collections with broad bathymetric distributions (from shallow reefs to over 2,000 meters depth) to design new eDNA primers for meta-barcoding a taxonomically informative region of *28S rRNA* gene in all anthozoan corals. We assess the specificity of the primers to Anthozoa and the ability of the amplified DNA barcode to discern taxonomic relationships both *in silico* and through the meta-barcoding of field samples collected at mesophotic and deep-sea coral communities in the northwestern Gulf of Mexico. Furthermore, we investigate the utility of this novel nuclear eDNA meta-barcoding sequencing approach for anthozoan coral biodiversity assessment by pairing eDNA sampling with video observation and sequencing coral specimens collected at the same field sites.

4.3 Methods

4.3.1 Barcode Sequence Data Compilation

We obtained *28S* sequences from 1) a target-capture enrichment genomic dataset of global coral collections (Quattrini et al., 2020) and 2) samples of various mesophotic and deep-sea coral species collected in the northwestern Gulf of Mexico (GoMx).

Quattrini et al. (2020) conducted target-capture phylogenomic sequencing of anthozoans collected from the Atlantic, Indian, Pacific, and Southern Ocean basins. Partial contig assemblies from each specimen sequenced by Quattrini et al. (2020) were transformed into local BLAST (Altschul et al., 1990) databases, and BLASTN searches (Hexacorallia: -evalue .5; Octocorallia: -evalue 1e-5, -max_target_seqs 5 -max_hsps 5)

were executed using *28S* query sequences from a range of anthozoan species downloaded from GenBank. Out of the *28S* blast results for each specimen, those with the highest bit scores, lowest e-values, and minimum match lengths of 3,000 nt. were selected. Sequences were aligned by their taxonomic group (Octocorallia, Antipatharia, and Scleractinia) using MAFFT online v7 (Katoh & Standley, 2013), visually adjusted, trimmed, and exported using AliView v1.26 (Larsson, 2014).

Mesophotic and deep-sea corals were collected from the Gulf of Mexico from depths of 53 to 1,850 m during remotely operated vehicle (ROV) dives from 2018 to 2021 (**Table C.1**). Samples from the Flower Garden Banks National Marine Sanctuary were collected under permits FGBNMS-2017-007-A2 and FGBNMS-2019-003-A2 to S.H. DNA was extracted from these specimens using a salting-out protocol (dx.doi.org/10.17504/protocols.io.bypypvpw). An ~810 base pair (bp) sequence of *28S* was amplified and Sanger-sequenced from 48 octocoral and black coral species using previously published primers (McFadden and Ofwegen, 2012). Further detail is provided in the Supporting Information.

4.3.2 Primer design

Sequences from the target-capture dataset (143 sequences) and the Sanger sequencing data generated from the GoMx samples (48 sequences) were aligned using *Clustal Omega* (Sievers et al., 2011) and the default parameters in Geneious Prime version 2022.1.1 (https://www.geneious.com). Primers were designed to amplify a ~400 bp variable region of the trimmed alignment (**Figure 4.1**). Black corals and octocorals share substantial sequence similarity at the forward primer sequence such that a single

forward primer could be designed for both groups. However, a second primer set needed to be designed specifically for scleractinians due to divergence in scleractinian sequences at the forward primer binding site as compared to octocorals and black corals.

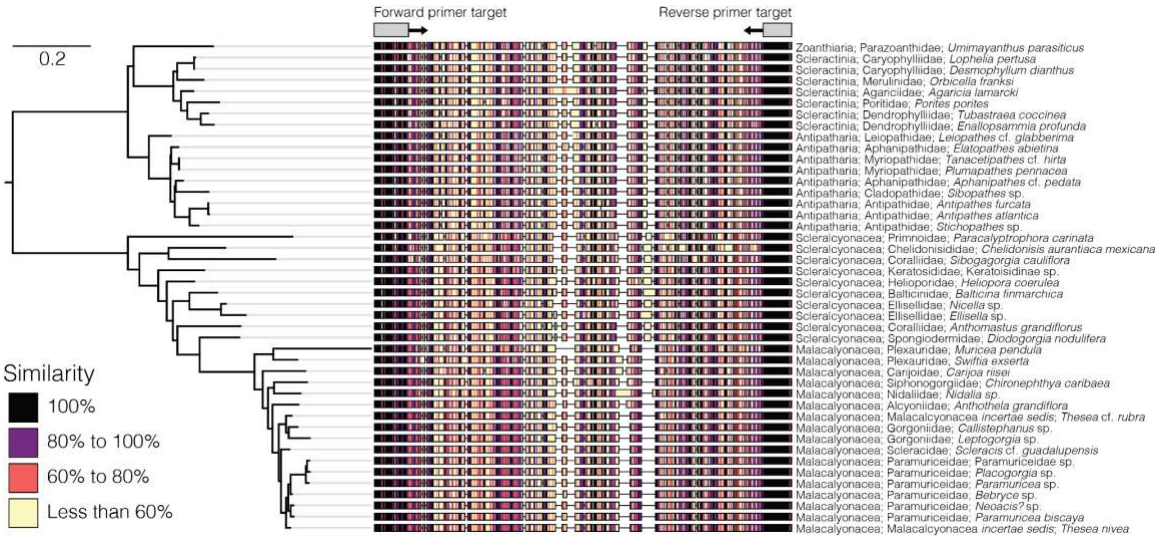

Figure 4.1: Sequence alignment of the barcoding region of the *28S* targeted for eDNA metabarcoding from a selection of zoantharian, octocoral, black coral, and scleractinian species. Sequences were aligned with MAFFT. The similarity of the aligned sequences was calculated as the percent identity shared at each position across all sequences. The scale bar represents the number of substitutions per site. The tree is rooted at the node representing the most recent common ancestor of hexacorals and octocorals. The tree was modeled using IQ-TREE2 (Minh et al., 2020) without bootstrapping. The best substitution model was found with modelfinder (Kalyaanamoorthy et al., 2017) based on Bayesian Information Criterion. The model is a transition model where AC=CG and AT=GT and base frequencies were unequal (TIM3), with empirical base frequencies (+F), and rate heterogeneity modeled using a gamma function (+G4).

Black coral and octocoral barcode sequences were aligned separately from scleractinians using MUSCLE (Edgar, 2004) and the default parameters in Geneious. Primers for black corals and octocorals were designed to complement the 95% consensus sequence of the aligned sequences using *Primer 3* (Untergasser et al., 2012; Version 2.3.7) in Geneious. Melting temperatures of candidate primers were calculated using the formula from Santa-Lucia (1998), with a 2 mM concentration of divalent salt cations ($MgCl_2$), an oligo concentration of 50 nM, a 0.2 mM concentration of dNTPS, and a 50 mM concentration of monovalent salt cations. The minimum, optimal, and maximum primer lengths, melting temperatures, and GC% were 18, 20, and 22 bp; 55, 60, and 65 degrees C; and 35, 50, and 65%, respectively. A GC clamp of 1 bp was set, and the maximum polynucleotide run was limited to 3 bp. Primers were designed to the alignment of scleractinians using the same parameters as for black corals and octocorals. Forward and reverse primer pairs were chosen with a preference for primers with a C or G in 3 of the 5 nucleotides at the 3-prime ends of the forward primer sequences to increase specificity to the target (Andruszkiewicz et al., 2020).

We introduced ambiguities into the forward primer sequence for black corals and octocorals to complement single nucleotide polymorphisms (SNPs) in sequences of black corals and the primnoid octocorals *Callogorgia gracilis* and *Paracalyptrophora carinata* that occur in the northwestern Gulf of Mexico. We introduced additional ambiguities into the forward primer sequence for scleractinians to complement SNPs present in the sequences of the deep-sea genus *Enallopsammia*, and the shallow Western Atlantic genera *Orbicella* and *Montastraea*. Primers with and without CS1 and CS2 Illumina universal adapters were synthesized by Eurofins Genomics using standard desalting. The

28S forward and reverse primer sequences were synthesized as mixtures with 50% of each nucleotide at each ambiguous position. We refer to the primers designed to target black coral and octocoral sequences as *Anth-28S-eDNA*, to reflect their broader diversity of targets and the primers designed to scleractinian sequences as *Scler-28S-eDNA*.

Table 4.1: Primer sequences designed for anthozoan coral eDNA meta-barcoding at the nuclear *28S* gene. The *Anth-28S-eDNA* primers were designed to target black coral and octocoral sequences, and the *Scler-28S-eDNA* primers target scleractinian sequences. For meta-barcoding, the forward and reverse primers were synthesized with CS1 and CS2 universal adapters, respectively, at the 5' ends to facilitate the binding of Access Array (Standard BioTools) indices unique to each sample during library preparation. The CS1 universal adapter is 5'-ACACTGACGACATGGTTCTACA-3', and the CS2 universal adapter is 5'-TACGGTAGCAGAGACTTGGTCT-3'. The %GC content reported for primers with ambiguities is the average of the possible primer sequences.

Primary target taxa	Primer sequences	T_m	%GC
Antipatharia and Octocorallia	*Anth-28S-eDNA-F:* 5'–CGTGAAACCGYTRRAAGGG–3'	55.7 – 62.3°C	56.3%
	Anth-28S-eDNA-R: 5'–TTGGTCCGTGTTTCAAGACG–3'	59.9°C	50%
Scleractinia	*Scler-28S-eDNA-F:* 5'–AKGGAAACGAATGGRCTMAG–3'	54.0 – 61.1°C	47.1%
	Scler-28S-eDNA-R: 5'–TCCTTGGTCCGTGTTTCAAG–3'	59.3°C	50%

4.3.3 Reference database compilation

Low coverage whole-genome sequencing (genome skimming) data were generated from specimens collected in the Gulf of Mexico following the methods described by Quattrini et al. (2024). Several of these specimens were also barcoded with Sanger sequencing. Briefly, DNA extractions were cleaned with a PowerClean Cleanup Pro Kit (Qiagen) following the manufacturer's protocol. Genomic DNA was enzymatically sheared, and libraries were prepared using the NEBNext Ultra II FS DNA Library Prep Kit for Illumina (New England Biolabs, Ipswich, MA). Libraries were sequenced with 150 bp paired end reads on an Illumina NovaSeq. Read pairs were quality-filtered and trimmed using *Trimmomatic* (Bolger et al., 2014) and merged using *BBMerge* (Bushnell et al., 2017) in Geneious Prime version 2023.1.2 using the default settings. Merged reads were aligned with the *Map to Reference* function to a complete *rRNA* operon sequence extracted from the *Xenia* sp. NCBI reference genome (scaffold NW_025813507.1) and a sequence of *Cladopathes* cf. *plumosa* from Barrett *et al.* 2020

that includes *18S, ITS1, 5.8S, ITS2* and the majority of *28S*. Consensus sequences from the assemblies were generated with a 90% identity threshold at each position, and the barcoding region was extracted from these consensus sequences. See Quattrini et al. (2024) for further methodological details.

To supplement the sequences generated in this study, we also compiled *28S* sequences from GenBank that aligned with the *28S* barcode. GenBank was queried using the terms “Antipatharia”, “Octocorallia” or “Scleractinia” and “28S” or “large subunit”. The resulting sequences were aligned with sequences generated in this study using *Clustal Omega* with default parameters, trimmed to the alignment, and extracted for inclusion in the reference sequence database.

To compare results using *28S* to *mtMutS* for octocoral eDNA analyses, octocoral *mtMutS* sequences were downloaded from GenBank using the search terms “Octocorallia” and “mutS” or “msh1”. Predicted amplicons using the *mtMutS* primers were extracted from these sequences with *cutadapt* by setting the forward primer and the reverse complement of the reverse primer as linked adapters with a minimum overlap of 20 bp and a maximum of 2 allowed mismatches to either primer.

4.3.4 *in silico* Assessments of Primer Complementarity and Taxonomic Resolution of the 28S rRNA Barcode

To determine the complementarity of the designed primers to the compiled coral *28S* barcode reference sequences, reference barcode sequences were imported into Geneious Prime, and the primers were queried against them, allowing two possible mismatches using the “Add Primers to Sequences” function. Annotations of the primer

matches to the *28S* barcode reference sequences for the *Anth-28S-eDNA* and *Scler-28S-eDNA* primers were exported as .csv files and joined with metadata for each sequence using the *tidyverse* packages (Wickham et al., 2019) in *R* v4.1.3.

To determine the taxonomic resolution of the *28S* barcodes amplified using the primers, predicted amplicons were extracted from the reference sequences using *cutadapt* with primer sequences set as required linked adapters with two possible mismatches to either the forward or reverse primer. *28S* barcodes identified from the reference sequence database using the *Anth-28S-eDNA* primers (for Octocorallia and Antipatharia) and the *Scler-28S-eDNA* primers (for Scleractinia) were separately aligned in Geneious using *MAFFT* and the default settings. Pairwise percent identities were calculated between all *28S* barcode sequences and exported as .csv files. The pairwise identity matrix was analyzed in R using the *tidyverse* packages and visualized using the *pandas, seaborn,* and *matplotlib.pyplot* python v3 libraries.

To compare to *28S*, we also determined the taxonomic resolution of the *mtMutS* barcodes amplified with the primers described in Everett and Park (2018). Barcodes were aligned with *MAFFT* and pairwise identities were calculated as for the *28S* barcodes. To minimize the influence of misidentified specimens, we only included sequences from samples identified to the species level.

4.3.5 *in silico* Assessment of Primer Specificity to Anthozoan Corals

To assess the specificity of the two primer sets to *28S* sequences of anthozoan corals, we used *cutadapt* to identify potential PCR products from the SILVA ribosomal large subunit (LSU) dataset (version 138.1; https://www.arb-silva.de/), which is a curated

reference database of prokaryotic and eukaryotic ribosomal RNA sequences. The primer sequences were set as required linked adapters and *cutadapt* was run with 0, 1 and 2 mismatches to either the forward or reverse primer (i.e. the "-e" flag was set to 0, 1 or 2). The minimum overlap was set to 19 bases (equal to the shortest primer sequence). Sequences that did not match were excluded from the output. Predicted amplicons were visualized by taxa and sequence length in *R* using *ggplot2*.

4.3.6 Testing the Performance of the *28S* Primers with eDNA Samples from the Gulf of Mexico

To test the performance of the *28S* primers, we meta-barcoded 50 field-collected eDNA samples from seven sites in the northwestern Gulf of Mexico at depths between 55 to 531 meters (**Figure 4.2**). Samples were collected during Remotely Operated Vehicle (ROV) dives or Niskin bottle rosette casts during expedition PS22-04 in August 2021 aboard the *R/V Point Sur*. We tested the *Anth-28S-eDNA* primers on water samples taken near mesophotic coral communities south of Stetson Bank, east of Bright Bank, and on Bright Bank within the Flower Garden Banks National Marine Sanctuary (FGBNMS). We also tested the *Anth-28S-eDNA* primers on water samples taken near deep-sea coral communities at Bureau of Ocean Energy and Management (BOEM) designated lease blocks GC354 and VK826. We tested the previously developed primers by Everett and Park that amplify *mtMutS* on the same samples (Everett & Park, 2018). The *Scler-28S-eDNA* primers were tested on water samples collected from mesophotic coral communities at East Flower Garden Bank (EFGB), east of Bright Bank, GC354, and VK826.

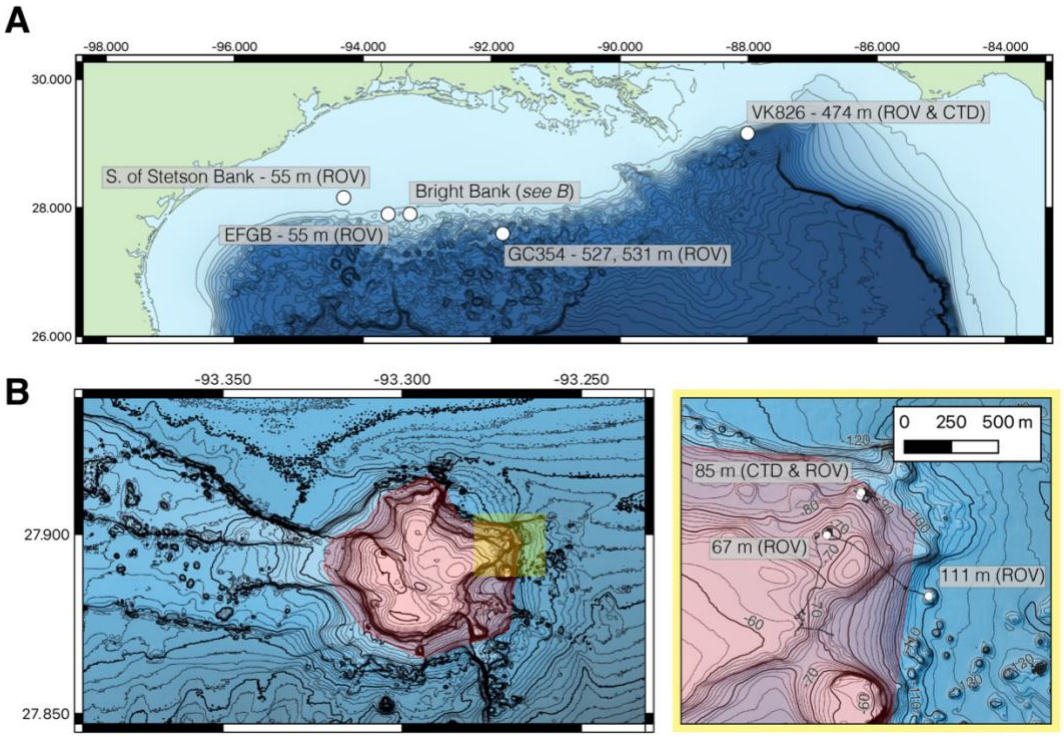

Figure 4.2: **(A)** eDNA sampling sites (white points) across the Northern Gulf of Mexico. Water sampling was conducted with Niskin bottles during remotely operated vehicle (ROV) dives and Niskin bottle rosette (CTD) casts. Bathymetry data is from the Global Multi-Resolution Topography Data Synthesis (GMRT.org) (Ryan et al., 2009), and contours represent 100-meter isobaths. EFGB stands for Eastern Flower Garden Bank. **(B)** At Bright Bank and to its east, eDNA samples were collected at three proximate sites at differing depths. Navigational fixes during ROV dives are shown in black and intersect contour lines. The spatial extent of the highlighted area on the right is indicated as the yellow shaded area on the map of Bright Bank on the left panel. Bathymetry data is from the USGS Multibeam Mapping of Selected Areas of the Outer Continental Shelf, Northwestern Gulf of Mexico (https://pubs.usgs.gov/of/2002/0411/index.html) (Gardner et al., 1998). Contours represent 10-meter and 2-meter isobaths. Sampling sites at EFGB

and at 67 and 85 meters depth at Bright Bank were conducted within the boundaries of the Flower Garden Banks National Marine Sanctuary (highlighted in red). The bathymetric map was created with QGIS.

4.3.7 eDNA Sampling During ROV Dives

Seawater was sampled during ROV dives using 1.7L General Oceanics Niskin bottles (Model 1010) mounted to the port side of the ROV *Global Explorer* (Oceaneering, Houston, TX). Two to four Niskin bottles were remotely triggered at a time to collect replicate water samples at the seafloor near corals seen in video. Once the ROV was recovered, water from each Niskin was drained through rubber tubing into a sterile, 2L stand-up Whirl Pak bag (Nasco). The seawater was then filtered over a 0.22 μm pore size polyethersulfone Sterivex filter using a Masterflex L/S peristaltic pump with Easy Load II pump heads and Masterflex L/S 15 platinum-cured silicone tubing. The Sterivex filter was connected to the tubing via a luer-lock nylon barb, and the pump was set to 100 RPM. The effluent was collected in a bucket, and the volume filtered was measured using a graduated cylinder. The average filtered volume was 0.91 ± 0.14 (SD) liters. Once the entire volume was filtered, the Sterivex filter was placed in a Sterile Whirl-Pak and frozen at -80°C. The filters were transported back to the laboratory at Lehigh University on dry ice and stored at -80°C prior to DNA extraction.

4.3.8 eDNA Sampling Using a Niskin Bottle Rosette

In the evenings after ROV dives were completed, conductivity, temperature, and depth (CTD) casts were conducted at ROV dive sites at Bright Bank and VK826 using a

Seabird 911plus CTD unit on a Niskin bottle rosette with twelve ~12 L General Oceanics and Ocean Test Equipment Niskin bottles. The ship was moved to the position on the seafloor of eDNA sampling during ROV dives, and the Niskin bottle rosette was lowered to the seafloor. Altitude from the seafloor was measured with an altimeter, and water samples were collected in duplicate or triplicate by remote triggering of the Niskin bottles as close to the seafloor as possible and at intervals in altitude from the bottom. After recovery of the rosette, samples were processed and preserved in the same way as the samples from Niskins mounted to the ROV, except that filtration was conducted directly from the Niskin bottle rather than after transferring the water to a Whirl-pak. To sample directly from Niskin bottles, a short segment of bleach-sterilized Masterflex L/S 24 C-flex tubing was connected to the bottle's petcock and stepped down to the L/S 15 tubing via a bleach-sterilized nylon barbed straight reducer. The average volume of the samples collected from these two casts was 3.3 ± 0.4 (SD) and 5.0 ± 0.7 (SD) liters, respectively.

After each sampling day, a sampling negative control was run by pumping 1 liter of high-purity water over a Sterivex filter using the sampling equipment sterilized for that day. This sampling negative control was treated in the same manner as the field samples to monitor for any potential sources of contamination in the field. A detailed description of efforts taken to mitigate the risk of sampling and laboratory contamination is included in the Supporting Information.

4.3.9 eDNA Extraction and Meta-barcoding Library Preparation

DNA was extracted from the frozen Sterivex filters using the Qiagen DNEasy Blood and Tissue Kit with a modified protocol for extraction from the filter capsule. This

method was first described by Spens et al. (2017), and modifications were subsequently detailed by Govindarajan et al. (2022). DNA was eluted in 100 µL of Qiagen Buffer AE. Sampling negative controls from each site were extracted alongside eDNA samples, and these extracts were also subjected to PCR, and any amplicons were sequenced.

Samples collected from mesophotic sites were amplified via PCR using the *Anth-28S-eDNA-F* primer without the R ambiguity at the 14th nucleotide, since we did not expect to recover eDNA from deep-sea scleralcyonaceans from these samples. To amplify *mtMutS* using the primers designed by Everett and Park (2018) from samples collected at GC354 and VK826, we used a 50/50 mix of the published reverse primer and a second reverse primer (5'-CAGTCTTCTAAATTGCAACCGGGAGAATA-3'). This primer is complementary to sequences of coralliid octocorals that occur at deep-sea depths (M. Everett, personal communication).

Duplicate PCR reactions were performed for each eDNA extraction. The reactions consisted of 2 µL of DNA, 10 µL of 2X Platinum SuperFi II MasterMix (ThermoFisher), 2 µL of each of the forward and reverse primers with CS1/CS2 universal adapters diluted in molecular grade water to 10 µM (final reaction concentration 1.0 µM), 0.6µL of 50 mM $MgCl_2$ (final concentration 3.25 mM), and 3.4 µL of molecular-grade water. For the *28S rRNA* primers, cycling conditions were as follows: initial denaturation at 98°C for 30 seconds; then 15 cycles of denaturation at 98°C for 10 seconds, the touchdown annealing step from 70°C to 56°C for 10 seconds, and elongation at 72°C for 15 seconds; followed by 25 cycles of denaturation at 98°C for 10 seconds, annealing at 55°C for 10 seconds, and elongation at 72°C for 15 seconds; and a final elongation at 72°C for 5 minutes. For the *mtMutS* primers, 30 cycles with an annealing temperature of

55°C following the touchdown cycles were performed to enhance amplification. PCRs were performed in 96 well-plates, and duplicate PCR negative controls (NTCs) were conducted in each plate of PCR reactions, carried through library preparation, and sequenced. Amplification success was assessed through electrophoresis by running 4 µL of each PCR product on a 1% agarose TBE gel stained with GelRed at 110V until the sample ran nearly to the entire gel length. Amplification success was scored based on the relative intensity of the band across samples and the visualization of any off-target products, as compared to the band corresponding to the predicted amplicon size. After visualization, the duplicate PCR products from each sample were pooled. Pooled PCR products were shipped to the Rush University Genomics and Microbiome Core Facility (GMCF) (Chicago, Illinois, USA) on dry ice for all subsequent library preparation steps and sequencing.

At GMCF, a second PCR was conducted to ligate unique indices to the pooled PCR products from each sample. This PCR reaction was conducted in 10 µL reactions with 5 µL of 2X repliQa HiFi ToughMix (QuantaBio, Beverly, MA, USA), 1 µL of the PCR product, 2 µL of the unique barcode index from the Access Array Barcode Library for Illumina (Standard BioTools, South San Francisco, CA), and 2 µL of molecular-grade water. Cycling conditions were as follows: initial denaturation at 98°C for 2 minutes; then 8 cycles of denaturation at 98°C for 10 seconds, annealing at 60°C 1 minute, and elongation at 68°C for 1 minute. Indexed, pooled PCR products from each sample were combined, cleaned using a 0.6X ratio of AMPure beads (Beckman Coulter, Indianapolis, IN), visualized on a TapeStation (Agilent Technologies, Santa Clara, CA), and further size-selected using Blue Pippin (Sage Science, Beverly, MA). The target fragment length

was on average 541 bp, including the primers, universal adapters, and Access Array indices. Libraries were first pooled and sequenced with equal volumes of each sample (2 μL) on an Illumina MiniSeq (150 bp paired-end reads) with a 15% phiX spike-in. For subsequent sequencing on an Illumina MiSeq, the volumes of each library in the pool were adjusted based on the comparative number of reads each sample produced from the MiniSeq run. The goal was to normalize the number of reads produced across all samples. Only 1 μL of sampling negative controls and PCR no-template controls were sequenced in the MiSeq run since these samples did not produce visible amplicons and yielded comparatively fewer reads than the eDNA samples in the MiniSeq run. Volume-adjusted libraries were pooled and re-sequenced on an Illumina MiSeq with v3 chemistry (300 bp paired-end reads) and a 15% phiX spike-in.

4.3.10 Bioinformatics Analysis

First, *FASTQC* (Andrews 2010) and *MultiQC* (Ewels et al. 2016) were used to summarize read quality and counts across the samples. Primers anchored to the 5' ends of the forward and reverse reads were trimmed from the sequences using *cutadapt* (Martin 2011) with a minimum overlap of 5 bases and the default settings otherwise. The reverse complement of primers at the 3' end was also trimmed if it was identified. Untrimmed read pairs were excluded from subsequent analysis. Sequences were processed using the *DADA2* pipeline (Callahan et al. 2016) to infer error-corrected amplicon sequence variants (ASVs) from the sequencing data. For filtering and quality trimming, forward reads were trimmed to 250 bases in length, reverse reads were trimmed to 175 bases in length, and the maximum number of expected errors per read was set to 2. Denoising,

wherein errors are inferred and corrected based on the error profile of the sequencing libraries, read pair merging and chimera identification and removal were conducted using the default settings. A remote BLASTN search was conducted to query the denoised ASVs against the entire GenBank nucleotide database. The hits were filtered from the resulting BLAST searches to identify denoised ASVs derived from anthozoan coral eDNA. ASVs were identified as derived from coral if the top hit (according to the lowest e-value) of the ASV was to a black coral, scleractinian or octocoral, and the ASV sequence was >90% identical to the subject sequence across its length. The ASV table output from DADA2 was then filtered to ASVs identified as corals and further curated using the LULU algorithm and a minimum match percent identity of 95% (Frøslev et al. 2017).

4.3.11 Taxonomic Classification of Coral Amplicon Sequence Variants

From the sequences generated in this study and those downloaded from GenBank, a reference database of barcode sequences (N = 735; **Table C.2**) of anthozoan corals, a zoantharian, several corallimorpharians, and an anemone was created for the taxonomic classification of *28S* anthozoan coral ASVs using the *assignTaxonomy* and *addSpecies* functions in *DADA2*. The reference barcode sequences were included in a .fasta file with the required header format for the *assignTaxonomy* function. A second .fasta file was compiled from sequences of coral species recorded in the western North Atlantic with the required header format for the *addSpecies* function, which classifies ASVs to the species level if a 100% identical match to a sequence in the reference database is identified. Sequences of corals not identified to the species level (e.g. *Bebryce* sp.) were only

included in this file if it could be verified that they were collected from the western North Atlantic. The species distributions in the reference database were assessed using the OBIS database (obis.org). Questionable occurrence records, for example, single occurrences of species in genera known otherwise exclusively from the Pacific, were not considered valid. Both the .fasta files for *assignTaxonomy* and *addSpecies* were trimmed to the target barcode region amplified using the *Anth-28S-eDNA* and *Scler-28S-eDNA* primers using *cutadapt* with 2 mismatches to create separate reference files for each of these primer sets.

Another reference database was created for the taxonomic classification of octocoral *mtMutS* ASVs to compare to the *28S rRNA* data. For the 5,068 *MutS* barcodes extracted from sequence data downloaded from GenBank (**Table C.3**), the taxonomic hierarchy for each sequence was gleaned from WoRMS using the *taxize* package in R (Chamberlain and Szocs, 2013), and a .fasta file with the taxonomy in the required header format was created for the *assignTaxonomy* function. Thirty-five additional *mtMutS* sequences from octocoral mitochondrial genomes were assembled and annotated from the genome skimming data (see Section 2.3) using MitoFinder (Allio et al. 2020). Together, with an additional *mtMutS* sequence for *Chelidonisis aurantiaca mexicana* generated by Quattrini et al. (2013), these sequences were aligned, trimmed to the region amplified by the octocoral eDNA primers, and properly formatted to determine 100% matches to corals collected from the Gulf of Mexico using the *addSpecies* function.

For both datasets, *28S* and *mtMutS*, ASVs were recovered with identical sequences to that of *Thesea nivea*. However, due to the uncertainty of the taxonomic placement of *Thesea* at the family level (Family: Malacalcyonacea *incertae sedis*), these

ASVs were not classified beyond the order level. The taxonomic identity of these ASVs was manually assigned as *Thesea nivea* for analyses of the taxonomic composition of eDNA samples.

4.3.12 Meta-barcoding Data Analysis and Visualization

To visualize phylogenetic relationships, *28S* barcode sequences were aligned using *MAFFT* and the default parameters in Geneious Prime. Maximum-likelihood phylogenetic trees were then created using IQTree (Nguyen et al., 2015) with ModelFinder (Kalyaanamoorthy et al., 2017). ASV tables and taxonomic assignments generated from the bioinformatic pipeline were analyzed in R using the *tidyverse* packages. Bar plot visualizations of eDNA read abundances and their classifications to the genus level across eDNA samples were generated using *ggplot2*.

To remove sequence reads that may have resulted from sampling or laboratory contamination, the maximum number of sequences enumerated in any negative control sample (sampling negative controls, target-specific PCR no-template controls, and library prep. PCR no-template controls) was determined for each genus from each sampling location and in each sampling replicate. If the number of reads from a sample replicate did not exceed the maximum for that genus in the negative controls, those reads were removed from the dataset for analyses. The maximum number of reads in any negative control sample for a genus was 18 reads, which were classified as the genus *Lateothela*.

We detected several ASVs classified to deep-sea or mesophotic taxa in samples outside their plausible depth range. In most cases, these detections were represented by few read numbers (maximum = 11 classified as *Desmophyllum dianthus*), so we removed

ASVs detected with sequencing read abundances equal to or less than 11 from each sample. In four sample replicates collected at GC354 at 527 meters depth, we detected eDNA from characteristically mesophotic species, namely *Stichopathes* spp. at high read abundances (>20,000 reads) but also *Tanacetipathes* sp., *Thesea nivea*, and *Swiftia* sp at lower read abundances (3 to 524 reads). It is unclear whether these sequences represent legitimate detections. There was no evidence for contamination of the sampling negative control associated with the ROV dive at GC354, and sequences detected in the other two sample replicates collected at this site consisted of characteristically deep-sea species. Nevertheless, out of an abundance of caution we excluded these four sample replicates from further analysis.

4.4 Results and Discussion

4.4.1 Complementarity of the meta-barcoding primers to anthozoan coral sequences

We analyzed the complementarity of the *Anth-28S-eDNA* and *Scler-28S-eDNA* primers to anthozoan coral sequences generated in this study and downloaded from GenBank (**Table C.2**). The *Anth-28S-eDNA* primers are broadly complementary to black coral, octocoral, and scleractinian sequences. The *Anth-28S-eDNA* primers are complementary with zero mismatches to all 68 black coral barcode sequences analyzed. These sequences represent all seven recognized black coral families and 22 accepted genera (according to WoRMS). While *28S rRNA* sequence data for several genera, including the deepest genus *Abyssopathes*, are not available, high sequence conservation at the forward and reverse primer binding sites across all seven antipatharian families supports their utility in yet-to-be-sequenced black coral species. We expect that the

primers are broadly applicable for meta-barcoding black coral eDNA across all ocean depths.

The *Anth-28S-eDNA* primers are complementary to the vast majority (84.7%, N = 409) of the 483 octocoral barcode sequences analyzed with zero mismatches and are complementary to sequences in 64 of 82 recognized octocoral families in 147 accepted genera with two or fewer mismatches. Specifically, the primers are complementary to sequences of all malacalcyonacean octocorals with two or fewer mismatches except for sequences from *Astrogorgia rubra* and *Pacifigorgia* sp. The primers have one or two mismatches to five sequences in the genera *Xenia*, *Hanah*, *Acrossota*, and *Pacifigorgia*. We designed the forward primer with ambiguities to accommodate sequence variation in scleralcyonacean octocorals present at our field sites. Nevertheless, the forward primer has greater than two mismatches to *Junceella fragilis*, *Dichotella gemmacea*, and four primnoid species. Additionally, the forward primer has at least one mismatch to sequences of a sea pen (*Pennatula* sp.), two bamboo corals (Family: Keratoisididae), and 31 species in the family Primnoidae.

Alterations to the forward primer sequence are possible and recommended if primnoid species with mismatches to the primers are known or expected to occur at sampling locations. For example, octocorals of the genus *Primnoa* have an A rather than a G at the 10th nucleotide in the forward primer sequence. From samples taken near habitats where *Primnoa* may occur, substituting an R for the A at the 10th position would correct for this mismatch while maintaining a range of melting temperatures (54.9°C – 62.3°C) within 5°C of the reverse primer.

While the *Anth-28S-eDNA* primers were designed to an alignment of black coral and octocoral sequences, we also found that the primers are complementary to 165 of the 174 scleractinian barcodes analyzed with 2 or fewer mismatches, and most sequences (92) have zero mismatches. The *Scler-28S-eDNA* primers, which were designed to an alignment of scleractinian sequences, are complementary to a larger number of scleractinian sequences (165) with zero mismatches and complement sequences from 24 out of 36 recognized families and 75 accepted scleractinian genera. Thus, while the *Anth-28S-eDNA* primers will amplify many scleractinian species, we recommend also using the *Scler-28S-eDNA* primers for eDNA meta-barcoding from locales where scleractinians are known to occur.

We tested the specificity of the primers to anthozoan corals *in silico* by extracting barcodes with two or fewer mismatches the forward or reverse primers from the entire SILVA large-subunit ribosomal RNA database. We found that with zero or one mismatch to the forward or reverse primer, off-target amplicons predicted using the *Anth-28S-eDNA* primers consisted largely of marine invertebrates. Besides anthozoans, sponges and hydrozoans had the highest number of predicted amplicons. Fungi sequences may be amplified using the primers if potential template sequences with two mismatches to the *Anth-28S-eDNA* primers are considered. However, the distribution of expected fungi amplicons is shorter (~200 bp) than that of marine invertebrates (**Figure C.1**). Thus, by visualizing the size distribution of the PCR product generated using the *Anth-28S-eDNA* primers (either through agarose gel or automated electrophoresis), it should be simple to assess the specificity of PCR reaction to corals and other marine invertebrates. When considering zero or one mismatch of the primers to potential template sequences, we

found that the *Scler-28S-eDNA* primers are highly specific to hexacorals; amplicons were only predicted from hexacorals. When two mismatches in potential template sequences are considered, sponges may also be amplified using the *Scler-28S-eDNA* primers.

4.4.2 The *28S rRNA* barcode distinguishes anthozoan coral sequences to the genus and species levels.

To assess the taxonomic resolution of the DNA barcode amplified with the *Anth-28S-eDNA* and *Scler-28S-eDNA* primer sets, we extracted and aligned predicted amplicons from anthozoan coral sequences generated in this study and downloaded from GenBank. We found that *28S* DNA barcodes predicted using the primers are non-identical across all anthozoan families. Further, *28S* barcodes are non-identical across all genera within 18 of 20 octocoral families, 9 of 11 scleractinian families, and 4 of 7 black coral families (**Figure 4.3**).

Identical barcodes exist across genera in a minority of cases. Within the octocoral family Primnoidae, identical barcodes exist 1) between *Candidella helminthophora* and *Parastenella pacifica* and 2) between *Pyrogorgia lemnos* and *Primnoa pacifica*. Within Paramuriceidae, barcode sequences of *Paramuricea* sp. and *Placogorgia* sp. are identical. Within the scleractinian family Dendrophylliidae, barcode sequences of *Cladopsammia gracilis* and *Tubastraea coccinea* are identical, unfortunately precluding the identification of the invasive *Tubastraea* from *Cladopsammia*, two genera that are already challenging to distinguish morphologically (Hoeksema et al. 2019). In Fungiidae, barcode sequences of *Zoopilus echinatus*, *Polyphyllia* and *Sandolitha* are identical, and barcode sequences of *Halomitra* sp. and *Lobactis scutaria* are also identical. Within the black coral family

Antipathidae, a barcode sequence of *Cirrhipathes anguina* collected from Hawai'i (GenBank: FJ626243.1) and a sequence of *Stichopathes* sp. collected from the Gulf of Mexico are identical. The *Stichopathes* specimen is morphologically similar to *Stichopathes pourtalesi* and was collected from this species' known depth range and habitat (Opresko et al. 2016). Within the deep-sea genus Schizopathidae, a sequence of *Bathypathes* sp. is identical to sequences of *Stauropathes arctica*. Within Cladopathidae, sequences of *Cladopathes* cf. *plumosa* and *Trissopathes* cf. *tetracrada* are identical.

Many of these problematic cases, especially within the black corals, reflect incongruences between phylogenetic relationships and taxonomic nomenclature rather than the rate of evolution of the *28S* barcode and its ability to distinguish taxonomic identity at the genus level. In black corals, phylogenetic evidence suggests that the genera *Stichopathes* and *Cirrhipathes* are polyphyletic (Bo et al. 2018, Quattrini et al. 2023). Likewise, Barret et al. (2020) suggested that validations of the genera within Schizopathidae and Cladopathidae are necessary based on mitochondrial genome sequencing data. Paraphyletic and polyphyletic taxa preclude the confident classification of ASVs derived from eDNA sequencing data. Unless a 100% identical match to a reference sequence is available, caution should be used when inferring occurrences from eDNA data within taxa where discrepancies between phylogenetic relationships and current taxonomy are known. Efforts focused on resolving the systematics of these anthozoan corals using phylogenomic methods will benefit biodiversity assessment and monitoring using eDNA sequencing. Whenever possible, voucher specimens deposited in accessible collections should accompany reference barcode sequences to confirm

morphological identifications, especially considering our evolving understanding of coral taxonomy.

To compare the taxonomic resolution of octocoral DNA barcodes amplified using the *Anth-28S-eDNA* primers and the *mtMutS* primers (Everett and Park 2018), we analyzed the pairwise identities of predicted *mtMutS* barcodes in the same manner as for *28S*. We found that *mtMutS* barcodes are identical in some cases across genera within ~30% (N=10) of the 34 families represented in the dataset (**Figure C.3**). While some of these cases may be due to misidentifications, others appear to be legitimate. For instance, in Primnoidae, which is well represented in both the *mtMutS* and *28S* barcode sequence databases, *mtMutS* barcodes are identical across thirteen genera, whereas *28S* barcodes are identical across just four genera. The *28S* barcode may distinguish taxa in more cases than the *mtMutS* barcode in part due to its longer length (~ 400 bp vs. ~300bp). The *28S* barcode is also, on average, more variable among genera of the same family (average mean pairwise identity = 89.0%) than the *mtMutS* barcode (average mean pairwise identity = 94.0%).

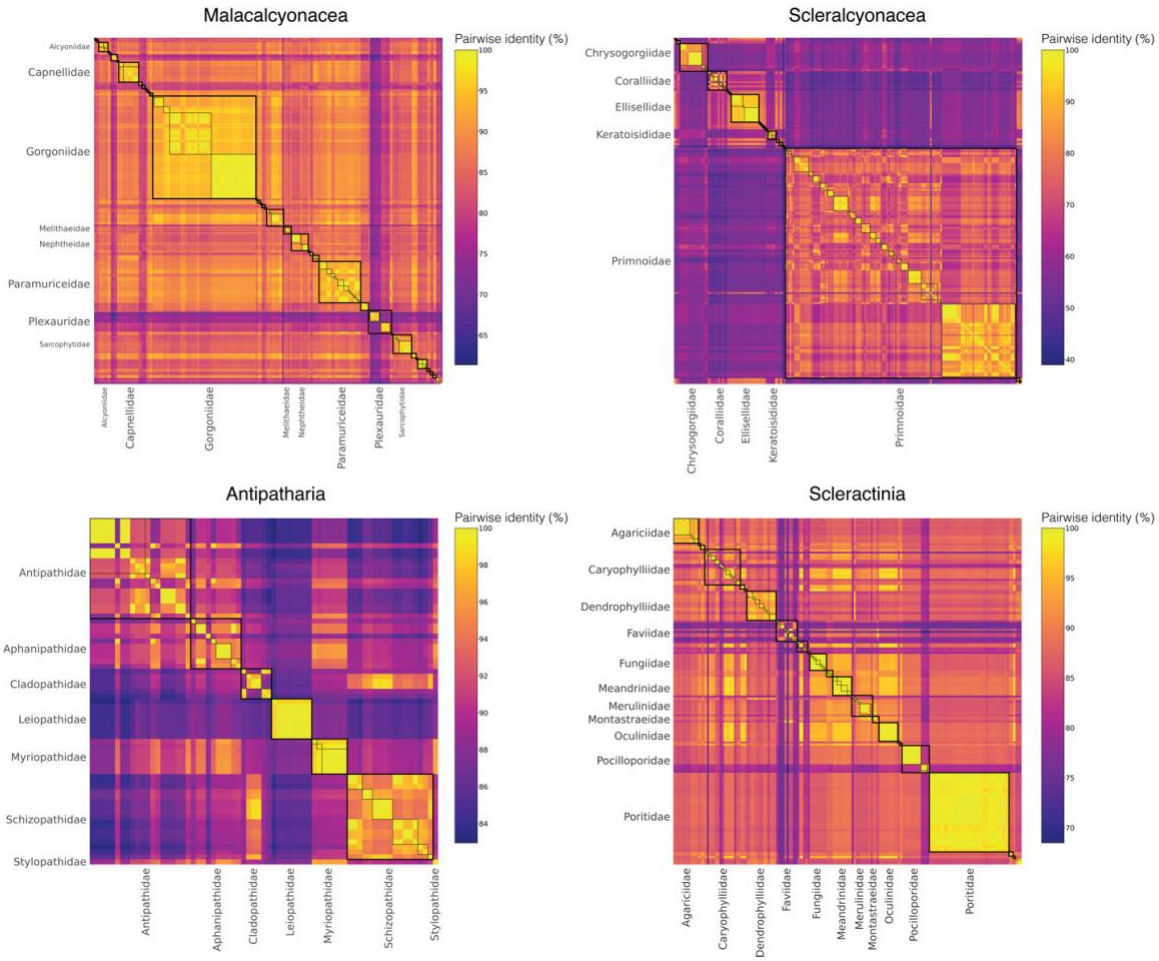

Figure 4.3: Matrices of pairwise identities between *28S rRNA* barcode sequences generated in this study and downloaded from GenBank. Boxes with thick black borders highlight comparisons within families, and boxes with thin black borders highlight comparisons within genera. Only families represented by the largest numbers of barcode sequences are labeled to highlight these comparisons and improve readability.

4.4.3 Sequencing libraries produced using the *28S rRNA* primers were enriched in coral eDNA

We successfully amplified the *28S* barcode from all field eDNA samples collected from the northwestern Gulf of Mexico using the *Anth-28S-eDNA* primers. On average,

68.0% of sequencing reads generated from each sample taken at the seafloor during ROV dives were classified as belonging to anthozoan corals. In some samples, up to 99.9% of reads were identified as coral (**Table C.4**). By producing sequencing libraries enriched with barcodes from coral eDNA, meta-barcoding using the *Anth-28S-eDNA* primers is a cost-effective approach for discerning anthozoan biodiversity as compared to primers that broadly target marine invertebrates. Other marine invertebrate ASVs recovered using the *Anth-28S-eDNA* primers included those with top BLAST hits to hydrozoans (16.9% of reads across all libraries), ctenophores (16.8%), sponges (2.3%), and anemones (< 0.1%). The *Scler-28S-eDNA* primer set was exceptionally specific to hexacorals. From the samples amplified using this primer set, virtually all (99.9%) of the sequencing reads were identified as belonging to scleractinians and black corals.

The levels of taxonomic specificity to anthozoan corals that we found using the *Anth-28S-eDNA* and *Scler-28S-eDNA* primer sets are comparable to those of previously published eDNA primer sets designed to anthozoan coral DNA sequences. Among the multiple primer sets designed to scleractinian sequences, Shinzato *et al.* designed highly specific primers that target mitochondrial *12S rRNA* and *COI* (Shinzato et al. 2021). Using their primers designed to *12S rRNA*, they found that 83.27% to 98.98% of the sequencing reads in the sequencing libraries from field samples were scleractinian. Using their primers designed to *COI*, 55.78% to 96.92% of the sequencing reads in their libraries were scleractinian. Using the primers designed to octocoral *mtMutS* sequences (Everett and Park 2018), we found that 100% of the sequencing reads were derived from octocorals in all samples that amplified. We cannot expect that the primers we designed to *28S rRNA* have the same specificity as the *mtMutS* primers since nuclear *28S* is present

in all eukaryotic genomes. However, we are encouraged to find that in samples taken at the seafloor, most sequencing reads recovered using our *28S rRNA* primers were from corals.

4.4.4 Sampling efficacy using a Niskin bottle rosette depended on proximity to the seafloor.

The distance above the seafloor at which a sample was taken during Niskin bottle rosette casts was negatively correlated with the percentage of sequencing reads produced in libraries using the *Anth-28S-eDNA* primers (Pearson's r = -0.50, *P-value* = 0.018; **Figure C.4**). Compared to samples taken at the seafloor, across samples taken at altitudes greater than 5.8 meters from the seafloor the average percentage of coral sequencing reads was just 0.8% and the remaining reads were derived from other taxa. Similarly, using the *Scler-28S-eDNA* primers, in sample duplicates taken ~20 meters above the seafloor, no band on an agarose gel was visible after PCR and just one coral read was recovered. While further systematic testing is necessary to constrain the vertical extent of benthic eDNA confidently, these preliminary results suggest that the efficacy of coral eDNA meta-barcoding relies on proximity to the seafloor. Practically, accurate characterization of seafloor bathymetry and the use of altimeter sensors are vital for successful coral eDNA capture using Niskin bottle rosettes in deep waters.

4.4.5 eDNA meta-barcoding with the *28S* primers detected coral genera and species in field samples.

From meta-barcoding eDNA field samples collected from mesophotic and deep-sea sites in the northern Gulf of Mexico, we recovered 112 coral ASVs using the *Anth-28S-eDNA* primers and 17 coral ASVs using the *Scler-28S-eDNA* primers. Of the 112 coral ASVs recovered using the *Anth-28S-eDNA* primers, 73% (n = 82) were classified as octocorals, 24% (n = 27) were classified as black corals, and 3% were classified as scleractinians (n = 3). Of the 17 coral ASVs recovered using the *Scler-28S-eDNA* primers, 65% (n = 11) were classified as black corals and 35% (n = 6) were classified as scleractinians. The black corals detected using the *Scler-28S-eDNA* primers were a subset of those detected using the *Anth-28S-eDNA* primers. Likewise, the scleractinians detected using the *Anth-28S-eDNA* primers were a subset of those detected using the *Scler-28S-eDNA* primers. The proportions of ASVs classified to each group met our expectations for each primer set, given the taxonomic breakdown of the sequences to which they were designed.

Using the *Anth-28S-eDNA* primers, we recovered ASVs classified to both octocoral orders, Malacalcyonacea (n = 58, 71%) and Scleralcyonacea (n = 24, 29%). Among those ASVs classified to the Malacalcyonacea, 69% (n = 40) were further classified to the family level and 62% (n = 36) were further classified to the genus level. Among those ASVs classified to the Scleralcyonacea, 96% (n = 23) were further classified to the family level, and 21 of these ASVs were further classified to the genus level. Using the *Anth-28S-eDNA* and *Scler-28S-eDNA* primers, we recovered 38 ASVs classified to the order Antipatharia and 8 to Scleractinia. All but one (n = 37) of the black coral ASVs were classified to the family level, and nearly all (n = 36) of those ASVs were further classified to the genus level. Of the 8 scleractinian ASVs, 7 were classified

further to the family and genus levels. Of all 129 coral ASVs, we found identical matches to 19 unique sequences in our reference database that we interpret as representing species-level detections. The high percentage of scleractinian, black coral, and scleralcyonacean octocoral ASVs that were classified at the genus level is comparable to a study of shallow-water benthic fauna that paired eDNA sampling and sequencing using scleractinian-specific markers with collections of representative morphospecies across belt-transect surveys (West et al., 2022). When paired with systematic, regional sampling and sequencing of voucher specimens to generate reference DNA barcodes, it should be expected for marine invertebrates that a high percentage of ASVs from eDNA sequencing data will be classifiable to the genus or species levels, as observed in vertebrates (Gold et al., 2022).

The percentage of malacalcyonacean octocoral ASVs classified to the family and genus levels was comparably lower than in other orders. Among the malacalcyonacean ASVs unclassified based the order level was a clade of sequences (8) with a maximum pairwise identity of just 93.4% (*BLASTN*) to any sequence in GenBank. These ASVs were placed phylogenetically in a clade sister to a clade consisting of ASVs classified to the genera *Lateothela*, *Chironephthya*, and *Nidalia* (**Figure C.4**). We interpret that these 8 ASVs unclassified past the order level represent a group of malacalcyonacean octocorals for which *28S* sequencing data does not currently exist, highlighting the importance of compiling a comprehensive reference database for taxonomic classification to the family level or to genus or species. We expect that further sampling and sequencing efforts of Malacalcyonacea from the Western Atlantic will resolve the taxonomic identity of more ASVs classified in this diverse order.

Given that most of the *28S rRNA* ASVs were classified to the genus level, we were able to make meaningful comparisons of the taxonomic composition of eDNA samples across sites and depths and to observations made during ROV dives. Like a number of other studies (Gösser et al., 2023; Dugal et al., 2022; West et al., 2022; Everett & Park, 2018), we found that coral eDNA sequencing data and video observations/collections are largely congruent, yet unique detections were gleaned using both methods.

Using eDNA sequencing, we detected coral genera observed in video and/or collected from the same field sites, and we confidently detected taxa that were not observed (**Figures 4.4** and **4.5**). At Bright Bank and to its east, we recovered substantial numbers of sequencing reads from the octocoral genera *Thesea* (Family: *incertae sedis*) and *Muricea* (Family: Plexauridae), respectively. While neither taxon was observed during ROV dives at these sites, *Muricea pendula* and *Thesea* spp. are common mesophotic octocorals in the Gulf of Mexico, and we have observed high densities during ROV surveys at nearby sites. We detected ASVs classified to the genera *Parasphaerasclera* and *Incrustatus*, at Bright Bank and VK826, respectively, while neither of these genera were observed or are known from the Atlantic Ocean. It is possible that due to their small and cryptic morphologies, these octocorals have been overlooked. These eDNA sequencing data are evidence for range extensions of these genera, which can be verified through regional collection efforts at mesophotic and deep-sea sites. We did not detect eDNA from some species observed and sampled during ROV dives and subsequently sequenced for inclusion in our reference database. Notably, at VK826, we did not detect eDNA from a mushroom coral in the sub-family

Anthomastinae. At Bright Bank, we observed a large colony of *Plumapathes pennacea* (Family: Myriopathidae). However, we did not detect eDNA identical to the sequence generated from a sample of this colony using genome skimming. This non-detection was significant because this colony was very large and supported numerous commensal organisms, including the pipefish *Aulostomus maculatus*.

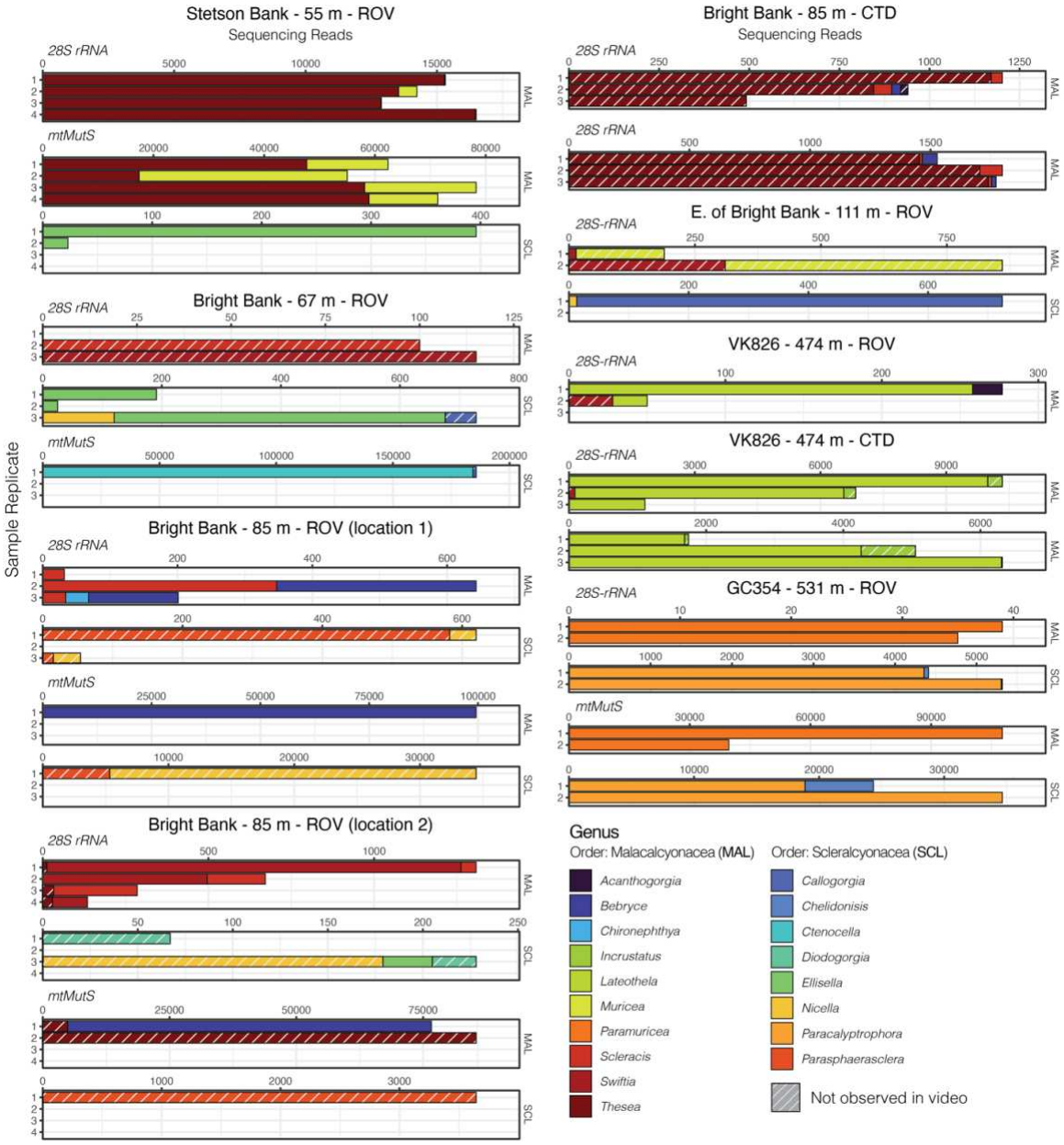

Figure 4.4: Octocoral eDNA sequence read abundances from replicate water samples taken during ROV dives and CTD casts near coral communities in the Northern Gulf of Mexico. Data are separated by the primer set used (*Anth-28S-eDNA* vs. *mtMutS*). Variable x-axis scales are used to aid in data visualization for all taxa.

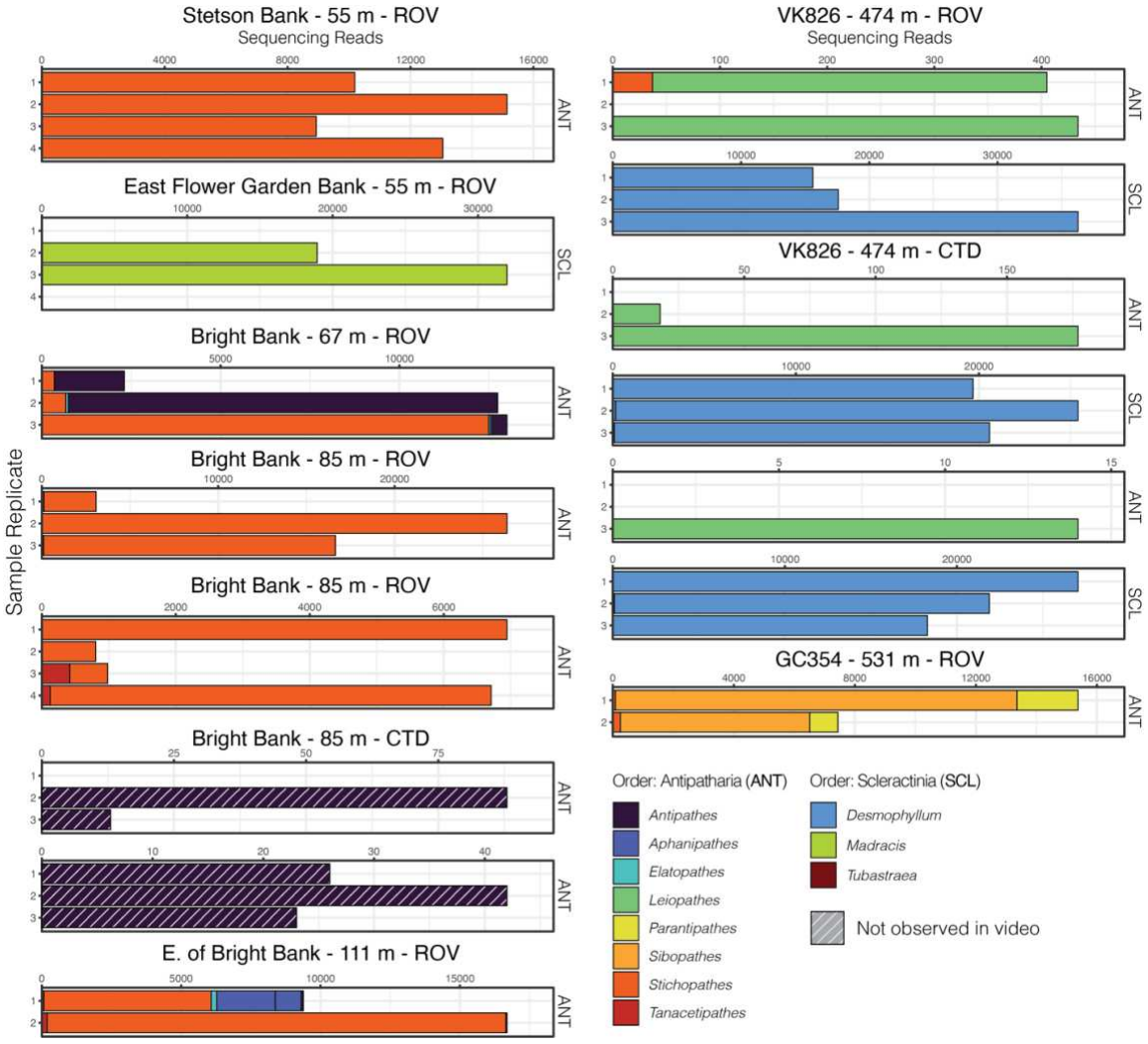

Figure 4.5: Black coral and scleractinian eDNA sequence read abundances from replicate water samples taken during ROV dives and CTD casts near coral communities in the Northern Gulf of Mexico. Data generated using both the *Anth-28S-eDNA* and *Scler-28S-eDNA* primers are summed. Sequence libraries from East Flower Garden Bank

were only generated using the *Scler-28S-eDNA* primers. Variable x-axis scales are used to aid data visualization. Sequence reads classified to the genus *Tubastraea* are not visible due to the low sequence read abundance.

4.4.6 *28S* and *mtMutS* coral eDNA markers are complementary for deep-sea coral eDNA sequencing.

Using the *mtMutS* primers, sequencing data was generated from all sample replicates collected at just two of the sampling locations, GC354 at 531 m and Stetson Bank at 55 m. These same sample replicates produced the highest percentage of coral reads using the *Anth-28S-eDNA* primers and had the largest proportions of octocoral reads relative to black coral reads. We detected one scleralcyonacean octocoral genus not detected with the *Anth-28S-eDNA* primers, *Ctenocella* (Family: Ellisellidae). Colonies with similar morphology to *Ctenocella* were observed at Bright Bank (although not sampled for confirmation of ID). Sequence reads classified to *Nicella* and *Ellisella* (Family: Ellisellidae) were detected at two sites where they were not detected using the *28S* primers. Furthermore, eDNA sequence read abundances produced with the *mtMutS* and *28S* primers differed. For instance, sequences classified to the family Paramuriceidae make up most of the sequence reads in sample duplicates from GC354 using the *mtMutS* primers. However, using the *28S rRNA* primers, sequences from *Paracalyptrophora* are the most numerous among the octocorals detected, and ASVs classified to Paramuriceidae total less than 80 sequencing reads.

From these data, we can infer that sequencing *mtMutS* is particularly suited to sites with abundant octocoral eDNA and that the *mtMutS* may be optimally designed for

detecting eDNA from scleralcyonacean octocorals. Thus, combining the *28S* and *mtMutS* primer sets could enhance octocoral eDNA detection and biodiversity characterization. If sequencing both markers is impractical or too expensive, we suggest that the *28S* primer set alone would provide the most comprehensive characterization of anthozoan coral biodiversity, including octocorals, black corals, and scleractinians.

4.5 Concluding remarks

Here, we present a new approach for metabarcoding eDNA from shallow, mesophotic, and deep-sea anthozoan corals by amplifying a variable barcode region of *28S*. By targeting the *28S rRNA* gene, we were able to design primers complementary to octocorals, black corals, and scleractinians. We predict that the barcode amplified using these primers distinguishes families in all cases and genera and species in most cases. Through meta-barcoding eDNA in field samples from mesophotic and deep-sea coral communities in the Gulf of Mexico, we demonstrate the utility of this new method for characterizing coral biodiversity.

eDNA sequencing is being rapidly adopted to assess biodiversity in nearly all of Earth's ecosystems, including the deepest depths of our oceans. While protocols and reference databases are well established for vertebrate taxa, such as fish, eDNA sequencing for corals is still in its infancy and will not reach its full potential until reference sequences are generated for more species and incongruencies between phylogenetics and current taxonomy are resolved. Nevertheless, with new molecular tools and the diminishing costs of amplicon and genomic sequencing, we are rapidly

approaching a more comprehensive understanding of the distributions and diversity of these ecologically important and vulnerable animals.

4.6 Acknowledgements

We specifically thank Captain Nicholas Allen and the crew of the *R/V Point Sur* for facilitating ROV deployment and recovery and the operation of Niskin bottle rosette casts. We thank the *Global Explorer* ROV team for their sample collection efforts. We also thank the staff of the Flower Garden Banks National Marine Sanctuary. We thank Dr. Stefan Green, Ashley Wu, and Cecilia Chau from the Genomics and Microbiome Core Facility at Rush Medical University for library preparation and sequencing. We thank Dr. Meredith Everett for her advice and for sharing coral eDNA sequencing protocols. We thank Dr. Chris Meyer, Dr. Sarah Tweedt, and Dr. Allen Collins for their helpful discussion at sea and onshore. We thank Dr. Dennis Opresko (NMNH) and Dr. Jeremy Horowitz for identifying collected black corals.

This research was funded by the National Oceanic and Atmospheric Administration's Oceanic and Atmospheric Research, Office of Ocean Exploration and Research, under award NA18OAR0110289 to S.H. at Lehigh University and sub-awards to A.M.Q. and C.S.M. at Harvey Mudd College. The fieldwork component of this study was funded by NOAA's National Centers for Coastal Ocean Science, Competitive Research Program under award NA18NOS4780166 to S.H. at Lehigh University

4.7 References

Alexander, J. B., Bunce, M., White, N., Wilkinson, S. P., Adam, A. A. S., Berry, T., Stat, M., Thomas, L., Newman, S. J., Dugal, L., and Richards, Z. T. (2020). Development of a multi-assay approach for monitoring coral diversity using eDNA metabarcoding. *Coral Reefs*, *39*(1), 159–171. https://doi.org/10.1007/s00338-019-01875-9

Allio, R., Schomaker-Bastos, A., Romiguier, J., Prosdocimi, F., Nabholz, B., and Delsuc, F. (2020). MitoFinder: Efficient automated large-scale extraction of mitogenomic data in target enrichment phylogenomics. *Molecular Ecology Resources*, *20*(4), 892–905. https://doi.org/10.1111/1755-0998.13160

Altschul, S. F., Gish, W., Miller, W., Myers, E. W., and Lipman, D. J. (1990). Basic local alignment search tool. *Journal of Molecular Biology*, *215*(3), 403–410. https://doi.org/10.1016/s0022-2836(05)80360-2

Andrews, S. (2010). FastQC: A Quality Control Tool for High Throughput Sequence Data. Available online at: http://www.bioinformatics.babraham.ac.uk/projects/fastqc/

Andruszkiewicz, E. A., Yamahara, K. M., Closek, C. J., and Boehm, A. B. (2020). Quantitative PCR assays to detect whales, rockfish, and common murre environmental DNA in marine water samples of the Northeastern Pacific. *PLoS ONE*, *15*(12), e0242689. https://doi.org/10.1371/journal.pone.0242689

Barbeitos, M. S., Romano, S. L., and Lasker, H. R. (2010). Repeated loss of coloniality and symbiosis in scleractinian corals. *Proceedings of the National Academy of Sciences*, *107*(26), 11877–11882. https://doi.org/10.1073/pnas.0914380107

Barrett, N. J., Hogan, R. I., Allcock, A. L., Molodtsova, T., Hopkins, K., Wheeler, A. J., and Yesson, C. (2020). Phylogenetics and Mitogenome Organisation in Black Corals (Anthozoa: Hexacorallia: Antipatharia): An Order-Wide Survey Inferred from Complete Mitochondrial Genomes. *Frontiers in Marine Science*, *7*, 440. https://doi.org/10.3389/fmars.2020.00440

Bo, M., Barucca, M., Biscotti, M. A., Brugler, M. R., Canapa, A., Canese, S., Iacono, C. L., and Bavestrello, G. (2018). Phylogenetic relationships of Mediterranean black corals (Cnidaria: Anthozoa: Hexacorallia) and implications for classification within the order Antipatharia. *Invertebrate Systematics*, *32*(5), 1102–1110. https://doi.org/10.1071/is17043

Bolger, A. M., Lohse, M., & Usadel, B. (2014). Trimmomatic: a flexible trimmer for Illumina sequence data. *Bioinformatics*, *30*(15), 2114–2120. https://doi.org/10.1093/bioinformatics/btu170

Brian, J. I., Davy, S. K., and Wilkinson, S. P. (2019). Elevated Symbiodiniaceae richness at Atauro Island (Timor-Leste): a highly biodiverse reef system. *Coral Reefs*, *38*(1), 123–136. https://doi.org/10.1007/s00338-018-01762-9

Brugler, M. R., Opresko, D. M., and France, S. C. (2013). Black Coral Systematics. *Zoological Journal of the Linnean Society*, *169*(2), 312–361. https://doi.org/10.1111/zoj.12060

Bushnell, B., Rood, J., and Singer, E. (2017). BBMerge – Accurate paired shotgun read merging via overlap. *PLoS ONE*, *12*(10), e0185056. https://doi.org/10.1371/journal.pone.0185056

Cairns, S. D., & Wirshing, H. H. (2015). Phylogenetic reconstruction of scleraxonian octocorals supports the resurrection of the family Spongiodermidae (Cnidaria, Alcyonacea). *Invertebrate Systematics*, *29*(4), 345–368. https://doi.org/10.1071/is14063

Callahan, B. J., McMurdie, P. J., Rosen, M. J., Han, A. W., Johnson, A. J. A., and Holmes, S. P. (2016). DADA2: High resolution sample inference from Illumina amplicon data. *Nature Methods*, *13*(7), 581–583. https://doi.org/10.1038/nmeth.3869

Chamberlain, S. A., and Szöcs, E. (2013). taxize: taxonomic search and retrieval in R. *F1000Research*, *2*, 191. https://doi.org/10.12688/f1000research.2-191.v2

Cordes, E. E., McGinley, M. P., Podowski, E. L., Becker, E. L., Lessard-Pilon, S., Viada, S. T., and Fisher, C. R. (2008). Coral communities of the deep Gulf of Mexico. *Deep-Sea*

Research Part I: Oceanographic Research Papers, *55*(6), 777–787. https://doi.org/10.1016/j.dsr.2008.03.005

Dugal, L., Thomas, L., Wilkinson, S. P., Richards, Z. T., Alexander, J. B., Adam, A. A. S., Kennington, W. J., Jarman, S., Ryan, N. M., Bunce, M., & Gilmour, J. P. (2022). Coral monitoring in northwest Australia with environmental DNA metabarcoding using a curated reference database for optimized detection. *Environmental DNA*, *4*(1), 63–76. https://doi.org/10.1002/edn3.199

Dunn, N., Savolainen, V., Weber, S., Andrzejaczek, S., Carbone, C., and Curnick, D. (2022). Elasmobranch diversity across a remote coral reef atoll revealed through environmental DNA metabarcoding. *Zoological Journal of the Linnean Society*, *196*(2), 593–607. https://doi.org/10.1093/zoolinnean/zlac014

Edgar, R. C. (2004). MUSCLE: multiple sequence alignment with high accuracy and high throughput. *Nucleic Acids Research*, *32*(5), 1792–1797. https://doi.org/10.1093/nar/gkh340

Etnoyer, P. J., Wickes, L. N., Silva, M., Dubick, J. D., Balthis, L., Salgado, E., and MacDonald, I. R. (2016). Decline in condition of gorgonian octocorals on mesophotic reefs in the northern Gulf of Mexico: before and after the Deepwater Horizon oil spill. *Coral Reefs*, *35*(1), 77–90. https://doi.org/10.1007/s00338-015-1363-2

Everett, M. V., and Park, L. K. (2018). Exploring deep-water coral communities using environmental DNA. *Deep-Sea Research Part II: Topical Studies in Oceanography*, *150*(September 2017), 229–241. https://doi.org/10.1016/j.dsr2.2017.09.008

Ewels, P., Magnusson, M., Lundin, S., & Käller, M. (2016). MultiQC: summarize analysis results for multiple tools and samples in a single report. *Bioinformatics*, *32*(19), 3047–3048. https://doi.org/10.1093/bioinformatics/btw354

Fisher, C. R., Hsing, P. Y., Kaiser, C. L., Yoerger, D. R., Roberts, H. H., Shedd, W. W., Cordes, E. E., Shank, T. M., Berlet, S. P., Saunders, M. G., Larcom, E. A., and Brooks, J. M. (2014). Footprint of deepwater horizon blowout impact to deep-water coral communities. *Proceedings of the National Academy of Sciences of the United States of America*, *111*(32), 11744–11749. https://doi.org/10.1073/pnas.1403492111

Frøslev, T. G., Kjøller, R., Bruun, H. H., Ejrnæs, R., Brunbjerg, A. K., Pietroni, C., and Hansen, A. J. (2017). Algorithm for post-clustering curation of DNA amplicon data yields reliable biodiversity estimates. *Nature Communications*, *8*(1), 1188. https://doi.org/10.1038/s41467-017-01312-x

Gardner, J.V., Mayer, L.A., Hughes Clarke, J.E., and Kleinier, A., 1998, High-resolution multibeam bathymetry of East and West Flower Gardens and Stetson Banks, Gulf of Mexico. Gulf of Mexico Science, v. 16, p. 131-143.

Gold, Z., Curd, E. E., Goodwin, K. D., Choi, E. S., Frable, B. W., Thompson, A. R., Walker, H. J., Burton, R. S., Kacev, D., Martz, L. D., and Barber, P. H. (2021). Improving metabarcoding taxonomic assignment: A case study of fishes in a large marine ecosystem. *Molecular Ecology Resources*, *21*(7), 2546–2564. https://doi.org/10.1111/1755-0998.13450

Gösser, F., Schweinsberg, M., Mittelbach, P., Schoenig, E., & Tollrian, R. (2023). An environmental DNA metabarcoding approach versus a visual survey for reefs of Koh Pha-ngan in Thailand. *Environmental DNA*, *5*(2), 297–311. https://doi.org/10.1002/edn3.378

Govindarajan, A. F., McCartin, L., Adams, A., Allan, E., Belani, A., Francolini, R., Fujii, J., Gomez-Ibañez, D., Kukulya, A., Marin, F., Tradd, K., Yoerger, D. R., McDermott, J. M., and Herrera, S. (2022). Improved biodiversity detection using a large-volume environmental DNA sampler with in situ filtration and implications for marine eDNA sampling strategies. *Deep Sea Research Part I: Oceanographic Research Papers*, *189*, 103871. https://doi.org/10.1016/j.dsr.2022.103871

Hoeksema, B. W., Hiemstra, A., and Vermeij, M. J. A. (2019). The rise of a native sun coral species on southern Caribbean coral reefs. *Ecosphere*, *10*(11). https://doi.org/10.1002/ecs2.2942

Kalyaanamoorthy, S., Minh, B. Q., Wong, T. K. F., Haeseler, A. von, and Jermiin, L. S. (2017). ModelFinder: fast model selection for accurate phylogenetic estimates. *Nature Methods*, *14*(6), 587–589. https://doi.org/10.1038/nmeth.4285

Katoh, K., and Standley, D. M. (2013). MAFFT Multiple Sequence Alignment Software Version 7: Improvements in Performance and Usability. *Molecular Biology and Evolution*, *30*(4), 772–780. https://doi.org/10.1093/molbev/mst010

Koslow, J. A., Boehlert, G. W., Gordon, J. D. M., Haedrich, R. L., Lorance, P., and Parin, N. (2000). Continental slope and deep-sea fisheries: implications for a fragile ecosystem. *ICES Journal of Marine Science*, *57*(3), 548–557. https://doi.org/10.1006/jmsc.2000.0722

Larsson, A. (2014). AliView: a fast and lightweight alignment viewer and editor for large datasets. *Bioinformatics*, *30*(22), 3276–3278. https://doi.org/10.1093/bioinformatics/btu531

Leray, M., Yang, J. Y., Meyer, C. P., Mills, S. C., Agudelo, N., Ranwez, V., Boehm, J. T., and Machida, R. J. (2013). A new versatile primer set targeting a short fragment of the mitochondrial COI region for metabarcoding metazoan diversity: application for characterizing coral reef fish gut contents. *Frontiers in Zoology*, *10*(1), 34. https://doi.org/10.1186/1742-9994-10-34

Martin, M. (2011). Cutadapt removes adapter sequences from high-throughput sequencing reads. *EMBnet.Journal*, *17*(1), 10–12. https://doi.org/10.14806/ej.17.1.200

McFadden, C. S., Benayahu, Y., Pante, E., Thoma, J. N., Nevarez, P. A., and France, S. C. (2011). Limitations of mitochondrial gene barcoding in Octocorallia. *Molecular Ecology Resources*, *11*(1), 19–31. https://doi.org/10.1111/j.1755-0998.2010.02875.x

McFadden, C. S., and Ofwegen, L. P. van. (2012). Stoloniferous octocorals (Anthozoa, Octocorallia) from South Africa, with descriptions of a new family of Alcyonacea, a new genus of Clavulariidae, and a new species of Cornularia (Cornulariidae). *Invertebrate Systematics*, *26*(4), 331–356. https://doi.org/10.1071/is12035

McFadden, C. S., Brown, A. S., Brayton, C., Hunt, C. B., and Ofwegen, L. P. van. (2014). Application of DNA barcoding in biodiversity studies of shallow-water octocorals: molecular proxies agree with morphological estimates of species richness in Palau. *Coral Reefs*, *33*(2), 275–286. https://doi.org/10.1007/s00338-013-1123-0

Miya, M., Sato, Y., Fukunaga, T., Sado, T., Poulsen, J. Y., Sato, K., Minamoto, T., Yamamoto, S., Yamanaka, H., Araki, H., Kondoh, M., and Iwasaki, W. (2015). MiFish, a set of universal PCR primers for metabarcoding environmental DNA from fishes: detection of more than 230 subtropical marine species. *Royal Society Open Science*, *2*(7), 150088. https://doi.org/10.1098/rsos.150088

Nichols, P. K., and Marko, P. B. (2019). Rapid assessment of coral cover from environmental DNA in Hawai'i. *Environmental DNA*, *1*(1), 40–53. https://doi.org/10.1002/edn3.8

Nishitsuji, K., Nagata, T., Narisoko, H., Kanai, M., Hisata, K., Shinzato, C., & Satoh, N. (2023). An environmental DNA metabarcoding survey reveals generic-level occurrence of scleractinian corals at reef slopes of Okinawa Island. *Proceedings of the Royal Society B*, *290*(1995), 20230026. https://doi.org/10.1098/rspb.2023.0026

Nguyen, L.-T., Schmidt, H. A., Haeseler, A. von, and Minh, B. Q. (2015). IQ-TREE: A Fast and Effective Stochastic Algorithm for Estimating Maximum-Likelihood Phylogenies. *Molecular Biology and Evolution*, *32*(1), 268–274. https://doi.org/10.1093/molbev/msu300

Opresko, D. M., Nuttall, M. F., and Hickerson, E. L. (2016). Black Corals of the Flower Garden Banks National Marine Sanctuary. *Gulf of Mexico Science*, *33*(1). https://doi.org/10.18785/goms.3301.05

Quattrini, A. M., Georgian, S. E., Byrnes, L., Stevens, A., Falco, R., and Cordes, E. E. (2013). Niche divergence by deep-sea octocorals in the genus *Callogorgia* across the continental slope of the Gulf of Mexico. *Molecular Ecology*, *22*(15), 4123–4140. https://doi.org/10.1111/mec.12370

Quattrini, A. M., Rodríguez, E., Faircloth, B. C., Cowman, P. F., Brugler, M. R., Farfan, G. A., Hellberg, M. E., Kitahara, M. V., Morrison, C. L., Paz-García, D. A., Reimer, J. D., and McFadden, C. S. (2020). Palaeoclimate ocean conditions shaped the evolution of corals and their skeletons through deep time. *Nature Ecology and Evolution*, *4*(11), 1531–1538. https://doi.org/10.1038/s41559-020-01291-1

Quattrini, A. M., McCartin, L. J., Easton, E. E., Horowitz, J., Wirshing, H. H., Bowers, H., Mitchell, K., Sei, M., McFadden, C. S., and Herrera, S. (2023). Skimming genomes for systematics and DNA barcodes of corals. *bioRxiv*. https://doi.org/10.1101/2023.10.17.562770

Rocha, L. A., Pinheiro, H. T., Shepherd, B., Papastamatiou, Y. P., Luiz, O. J., Pyle, R. L., and Bongaerts, P. (2018). Mesophotic coral ecosystems are threatened and ecologically distinct from shallow water reefs. *Science*, *361*(6399), 281–284. https://doi.org/10.1126/science.aaq1614

Ryan, W. B. F., S.M. Carbotte, J. Coplan, S. O'Hara, A. Melkonian, R. Arko, R.A. Weissel, V. Ferrini, A. Goodwillie, F. Nitsche, J. Bonczkowski, and R. Zemsky (2009), Global Multi-Resolution Topography (GMRT) synthesis data set, *Geochem. Geophys. Geosyst.*, 10, Q03014, doi:10.1029/2008GC002332.

SantaLucia, J. (1998). A unified view of polymer, dumbbell, and oligonucleotide DNA nearest-neighbor thermodynamics. *Proceedings of the National Academy of Sciences*, *95*(4), 1460–1465. https://doi.org/10.1073/pnas.95.4.1460

Shimpi, G. G., and Bentlage, B. (2023). Ancient endosymbiont-mediated transmission of a selfish gene provides a model for overcoming barriers to gene transfer into animal mitochondrial genomes. *BioEssays*, *45*(2), e2200190. https://doi.org/10.1002/bies.202200190

Shinzato, C., Narisoko, H., Nishitsuji, K., Nagata, T., Satoh, N., and Inoue, J. (2021). Novel Mitochondrial DNA Markers for Scleractinian Corals and Generic-Level Environmental DNA Metabarcoding. *Frontiers in Marine Science*, *8*, 758207. https://doi.org/10.3389/fmars.2021.758207

Sievers, F., Wilm, A., Dineen, D., Gibson, T. J., Karplus, K., Li, W., Lopez, R., McWilliam, H., Remmert, M., Söding, J., Thompson, J. D., and Higgins, D. G. (2011). Fast, scalable generation of high-quality protein multiple sequence alignments using Clustal Omega. *Molecular Systems Biology*, *7*(1), 539–539. https://doi.org/10.1038/msb.2011.75

Slattery, M., and Lesser, M. P. (2021). Gorgonians Are Foundation Species on Sponge-Dominated Mesophotic Coral Reefs in the Caribbean. *Frontiers in Marine Science*, *8*, 654268. https://doi.org/10.3389/fmars.2021.654268

Spens, J., Evans, A. R., Halfmaerten, D., Knudsen, S. W., Sengupta, M. E., Mak, S. S. T., Sigsgaard, E. E., and Hellström, M. (2017). Comparison of capture and storage methods for aqueous macrobial eDNA using an optimized extraction protocol: advantage of enclosed filter. *Methods in Ecology and Evolution*, *8*(5), 635–645. https://doi.org/10.1111/2041-210x.12683

Untergasser, A., Cutcutache, I., Koressaar, T., Ye, J., Faircloth, B. C., Remm, M., and Rozen, S. G. (2012). Primer3—new capabilities and interfaces. *Nucleic Acids Research*, *40*(15), e115–e115. https://doi.org/10.1093/nar/gks596

West, K. M., Stat, M., Harvey, E. S., Skepper, C. L., DiBattista, J. D., Richards, Z. T., Travers, M. J., Newman, S. J., and Bunce, M. (2020). eDNA metabarcoding survey reveals fine-scale coral reef community variation across a remote, tropical island ecosystem. *Molecular Ecology*, *29*(6), 1069–1086. https://doi.org/10.1111/mec.15382

West, K. M., Adam, A. A. S., White, N., Robbins, W. D., Barrow, D., Lane, A., and Richards, Z. (2022). The applicability of eDNA metabarcoding approaches for sessile benthic surveying in the Kimberley region, north-western Australia. *Environmental DNA*, *4*(1), 34–49. https://doi.org/10.1002/edn3.184

Wickham, H., Averick, M., Bryan, J., Chang, W., McGowan, L., François, R., Grolemund, G., Hayes, A., Henry, L., Hester, J., Kuhn, M., Pedersen, T., Miller, E.,

Bache, S., Müller, K., Ooms, J., Robinson, D., Seidel, D., Spinu, V., Takahashi, K., Vaughan, D., Wilke, C., Woo, K., and Yutani, H. (2019). Welcome to the Tidyverse. *Journal of Open Source Software*, *4*(43), 1686. https://doi.org/10.21105/joss.01686

CHAPTER 5

TRANSPORT OF BENTHIC MARINE EDNA AT AN OFFSHORE MESOPHOTIC BANK IN THE NORTHWESTERN GULF OF MEXICO

5.1 Abstract

Accurately constraining the transport of environmental DNA (eDNA) after it is shed from an animal is vital to appropriately geolocate species detections and biodiversity measurements from eDNA sequencing data. Modeling studies predict the horizontal transport of eDNA at concentrations detectable using quantitative PCR over scales of tens of kilometers, but more limited vertical transport. Field studies routinely find that eDNA metabarcoding data distinguishes biological communities at small spatial scales, over scales of tens of meters. Here, we leverage the unique bathymetry of an offshore, mesophotic bank and the benthic invertebrate community that it supports to determine the extent to which vertical and horizontal eDNA transport may affect the interpretation of species detections from eDNA metabarcoding data. We found that in a stratified water column, eDNA from benthic invertebrates was vertically constrained to depths close to the seafloor in the thermocline versus in the surface mixed layer above. However, when using primers that are taxonomically specific to corals, we found evidence for the horizontal transport of coral eDNA at distances at least ~1.5 km from where they can be reasonably expected to occur. On the contrary, there was minimal evidence for horizontal transport of benthic eDNA in data generated using primers that broadly targeted sequences from eukaryotes. These results highlight the importance of horizontal transport as well as considering methodological details, like the taxonomic specificity of PCR primers, when interpreting eDNA sequencing data.

5.2 Introduction

The analysis of environmental DNA (eDNA) from water samples is a powerful tool for animal species detection and biodiversity assessment in marine ecosystems, complementing conventional approaches by detecting taxa that would be otherwise missed (e.g. Govindarajan et al., 2021; Govindarajan et al., 2023; West et al., 2024). While the spatial resolution of biodiversity data generated using conventional methods, including trawls, net tows, and submersible observations, is well-defined, the spatial resolution of data generated through eDNA sequencing is less clear. Aqueous eDNA is subject to transport by currents until it either settles to the benthos or degrades into fragments that are too short to amplify using PCR-based methods (reviewed in Harrison et al., 2019). Uncertainty in the distances that eDNA can be transported after it is shed from an animal complicates the integration of species detections and biodiversity estimates using eDNA sequencing with those from conventional methods, due to the possible discrepancies in the spatial resolution of these two data types. Geolocating species detections and biodiversity measurements from eDNA sequencing data depends on accurately constraining the scale of eDNA transport from its source, a vital component of what has been referred to as the "ecology of eDNA" (Barnes & Turner, 2016).

In lotic environments eDNA may be transported up to tens of kilometers downstream from its source, and transport distance downstream depends not only on flow but also the river substrate (Deiner et al., 2014; Jerde et al., 2016; Shogren et al., 2016; Shogren et al., 2017; Snyder et al. 2023). These findings are derived from experiments in artificial streams or in experiments where a novel animal is introduced to the environment and the distance downstream that its eDNA is transported is quantified.

Hereafter we refer to the latter as “caged fish” experiments for brevity, though some have also used invertebrates as eDNA sources such as freshwater mussels (e.g. Sansom & Sassoubre, 2017). While fewer of these studies have been conducted in marine ecosystems, their results are enlightening. For example, Ely et al. (2021) found that eDNA concentrations decreased rapidly with distance from the source and were undetectable in many samples taken within 100s of meters. In contrast, Murakami et al. (2019) introduced a caged fish for 48 hours in a harbor and detected its eDNA up to 1 km from its location, albeit at low concentrations.

Most other inquiries into the transport distances of eDNA in marine and lacustrine habitats can be generally categorized into two main approaches: 1) modeling eDNA transport through Lagrangian particle tracking, or 2) conducting eDNA field sampling from different habitat types with distinct communities at known distances apart from each other and/or at different depths.

Lagrangian particle tracking studies have been especially useful for modeling eDNA transport over the large spatial scales that are relevant to studying biology in the ocean. By pairing particle tracking model simulations with the quantification of eDNA from field samples, these studies have predicted that detectable concentrations of eDNA may be transported up to tens of kilometers from its source. However, these models also predict that eDNA will be found in higher concentrations and detected with a higher probability closer to its source (Andruszkiewicz et al., 2019; Kutti et al., 2020). These predictions are consistent with the exponential decay of eDNA that these particle tracking models rely on. In the vertical dimension, results from modeling studies suggest that scales of transport are small (on the order of tens of meters) and depend on the rate of

eDNA settling and water column stratification (Andruskiewicz et al., 2019; Allan et al. 2021). Modeling studies rely on three inputs that must be derived independently to accurately model eDNA particle transport: 1) a model of ocean circulation with a fine enough spatial resolution to model particle transport at relevant spatial scales, 2) a rate(s) of eDNA degradation and 3) a rate(s) of eDNA settling. Results from eDNA persistence experiments now permit the accurate estimation of eDNA degradation rate across ranges of relevant physicochemical factors, namely temperature (Andruszkiewicz Allan et al., 2021; McCartin et al., 2022). However, rates of eDNA settling are largely unknown, and their estimation is hindered by a lack of understanding of the predominant form of eDNA in the environment, e.g. dissolved DNA molecules versus cells or particulates, which may differ depending on environmental conditions (Barnes et al., 2021).

Due to the dependencies of particle tracking models on the accurate estimation of these parameters, field studies are vital to validate model predictions. While modeling studies predict the horizontal transport of detectable eDNA concentrations over tens of kilometers, metabarcoding eDNA from water samples routinely differentiates biological communities across habitats connected by either near shore currents and/or tidal movement at scales of tens of meters to a few kilometers (Port et al., 2016; Jeunen et al., 2019; West et al., 2020; Dugal et al., 2023; Shea & Boehm, 2024). These results suggest that when considering the entire pool of eDNA from multiple taxa in a sample, biological communities can be differentiated based on eDNA in seawater that is either present at the highest concentrations and has the highest detection probability; theoretically this eDNA should represent eDNA from taxa close to where the sample is taken. This inference is

consistent with the predictions from particle tracking studies that eDNA concentrations and probabilities of detection will be highest closest to the source organism.

Horizontal transport of eDNA may still result in the detection of eDNA that has originated far from the sampling location. In one recent study, Shea and Boehm (2024) leveraged the natural tidal cycle and demonstrated that eDNA "communities" in tide pools separated by just 40 meters were more distinct from one another at the lowest stage of the tide. At higher stages of the tide, and thus just after flow between the tide pools had ceased, eDNA communities in the tide pools were more similar. Their study elegantly demonstrates that eDNA shedding from local fauna and the degradation of eDNA from distant fauna leads to distinct eDNA signals between locations, but that water flow between locations can blur these distinctions (Shea and Boehm, 2024).

eDNA metabarcoding studies have validated model predictions that the vertical transport of eDNA is weak in a stratified water column, across both very narrow depth ranges (meters) and broad depth ranges (hundreds to thousands of meters). Strong haloclines form in some fjords, where a freshwater layer exists at the very surface, and eDNA from these different layers is readily distinguished across depths of just a few meters (Jeunen et al., 2019; Robinson et al., 2023). Monuki et al. (2021) also found that samples from the surface were distinct from samples taken just 10 meters below the surface in a coastal kelp forest ecosystem (Monuki et al., 2021). Govindarajan et al. found differences in eukaryotic eDNA between water masses in the offshore Northwest Atlantic across depth ranges of tens to hundreds of meters (Govindarajan et al., 2021). In one study, a lack of differentiation in fish eDNA across the pycnocline may be attributed

to upwelling where the samples were collected, off the coast of California (Closek et al., 2019).

Even though these substantial efforts have been made, the transport distances of marine eDNA that is detectable in metabarcoding data remain largely unconstrained. No field studies have combined metabarcoding with known point sources of eDNA over multiple kilometers in the horizontal dimensions and across substantial depth ranges. In this study, we follow the principles of "caged fish" experiments by leveraging an isolated benthic invertebrate community that occurs at a bank offshore in the northwestern Gulf of Mexico, where diapiric intrusions of salt domes have formed steep-sloped carbonate banks along the edge of the continental shelf (Rezak et al., 1985). These banks support dense and diverse communities of benthic invertebrates at their peaks and slopes and provide habitat for reef-associated and commercially/recreationally important fish species (e.g. Red Snapper, *Lutjanus campechanus*, and groupers, *Mycteroperca* spp.) (Dennis & Bright, 1988). Across the depths at which these banks occur (as shallow as 17 meters to surrounding depths of over 200 meters), environmental conditions, including temperature, vary drastically. During the summer, temperature decreases rapidly with depth, resulting in shoaling of the surface mixed layer and the stratification of depth layers in the strong thermocline below (Lugo-Fernández, 1998). At these banks, benthic invertebrate communities and the demersal organisms associated with them turn over rapidly with depth, resulting in unique benthic invertebrate communities in each depth zone (Rezak et al., 1985; Sammarco et al., 2016). As a result of this structure by depth and the dearth of available hard bottom habitat elsewhere on the continental shelf, benthic communities at the banks are akin to isolated "islands" of biodiversity that do not occur

elsewhere except many kilometers away at the nearest bank that rises to the same depths above the sedimented, turbid shelf edge.

We sampled eDNA systematically at distances away (up to ~ 5 ½ kilometers) from one of these mesophotic banks, Bright Bank, and at different depths (from 20 to ~100 meters below sea level), to determine the extent of eDNA transport in the horizontal and vertical dimensions. Additionally, we compared data generated using PCR primers that broadly amplify a barcode in the *18S rRNA* gene from all eukaryotes with data generated using primers that specifically enrich *28S* in anthozoan corals to investigate the influence of this methodological choice on inferring the transport of eDNA from metabarcoding data.

5.3 Methods

5.3.1 Study site

Bright Bank is a carbonate bank within the Flower Garden Banks National Marine Sanctuary (FGBNMS) that is situated on the edge of the continental shelf ~120 miles south of the borders of the U.S. states of Louisiana and Texas. Bright Bank protrudes from a background depth of approximately 120 meters to 33 meters. At its shallowest point, there is a small mesophotic stony coral reef community (Hickerson et al., 2008). Most of the top of the bank lies at depths between 40 and 80 meters deep. The closest seafloor at depths shallower than 80 meters in the region are at Rankin & 28 Fathom Banks ~8 nautical miles (~15 km) to the west and Geyer Bank ~12 nautical miles (~22 km) to the east (**Figure 1A**).

At Bright Bank, the benthos is characterized by abundant carbonate encrusted with coralline crustose algae and interspersed sediments. At the top of the bank at 67 meters, benthic invertebrate morphotaxa observed during remotely operated vehicle (ROV) dives include sponges, incl. *Xestospongia muta* and *Siphonodycton* sp.; giant Caribbean Sea anemone, *Condylactis gigantea*; black corals, antipathids and *Plumapthes* cf. *pennacea*; octocorals, *Diodogorgia nodulifera*, *Nicella*, and *Ellisella*; and other, smaller benthic invertebrates associated with the benthos and with corals. At depths of ~85 meters near the eastern edge of the bank at site "*Swiftia*", the diversity of benthic invertebrate morphotaxa observed is lower than at the top of the bank (11 versus 18 unique morphotaxa), but black corals and octocorals, including those not observed at shallower depths, *Swiftia exserta* and *Chironepthya* sp., occur. From the 80-meter isobath, the bathymetry slopes steeply to the north, east and south, and more gently to the west where it gradually connects to Rankin and 28 Fathom Banks. To the east of Bright at depths below 100 meters, the coral community is different than at shallower depths on the bank and includes black corals and octocorals such as *Elatopathes abietina*, *Aphanipathes pedata*, *Acanthopathes thyoides*, and *Callogorgia gracilis* that have not been observed at shallower depths during ROV dives at Bright.

5.3.2 Study design

To determine the distribution of benthic invertebrate eDNA from Bright Bank, we conducted a series of Niskin bottle rosette casts over the course of three days from September 24-26, 2019, to sample eDNA extensively at the center of Bright Bank and in the water column nearby. Casts were conducted at stations corresponding to the center of

the bank, and then in each ordinal direction at distances 1.5 and 3 nautical miles from the bank's center to capture potential eDNA transport from the bank's center in all directions in the horizontal dimension (**Figure 1B**). An additional cast was conducted 1 NM east of the center of the reef bank, and two additional casts were conducted ~2 NM to the NNW (station "mooring") and NNE (station "*Swiftia*") where remotely operated vehicle (ROV) dives had previously occurred.

Casts were conducted during daylight hours, as early as 7:00 CST (local time) and as late as 19:05 CST. The Niskin bottle rosette was outfitted with twelve ~2L Niskin bottles and a Sea-Bird SBE 19plus V2 Conductivity Temperature Depth (CTD) unit (Seabird Scientific, Bellevue, Washington) that included sensors for pressure, conductivity, and temperature, as well as a WET Labs ECO-AFL/FL fluorescence sensor, a WET Labs ECO turbidity sensor, and an SBE 43 dissolved oxygen sensor. Downcast profiles were generated from .cnv files exported from the raw data using Seasoft software (Seabird Scientific) and plotted using the *R* package *ggplot2* in the *tidyverse* (Wickham et al., 2019) in *R* (version 4.3.1 *Beagle Scouts*) to visualize conditions with depth at each station.

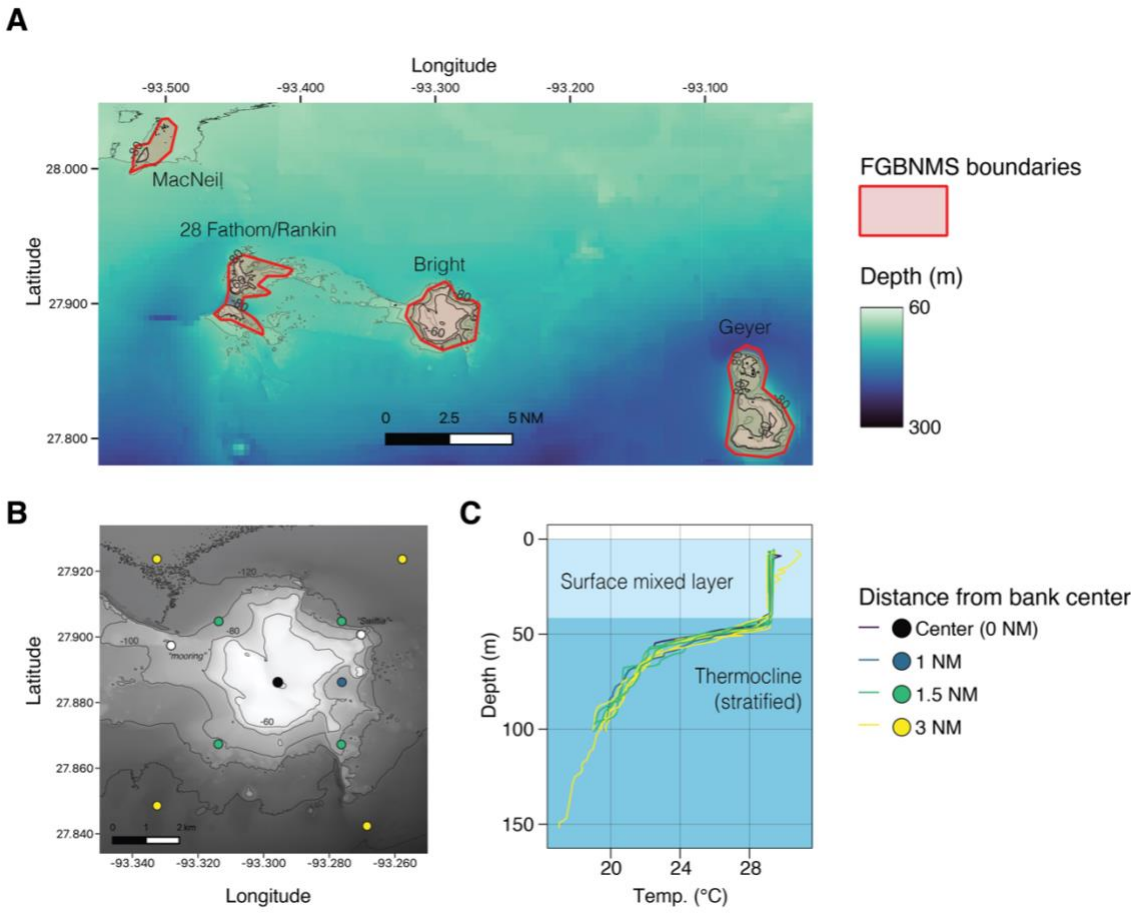

Figure 5.1: A) Bathymetric map of Bright Bank and nearby mesophotic banks in the northwestern Gulf of Mexico. Bathymetry data includes data from the USGS Multibeam Mapping of Selected Areas of the Outer Continental Shelf, Northwestern Gulf of Mexico (https://pubs.usgs.gov/of/2002/0411/index.html) (Gardner et al., 1998) and the General Bathymetric Chart of the Oceans (GEBCO; https://www.gebco.net/). 10-meter isobaths at depths from 100 to 60 meters in the high resolution data are indicated with contour lines. 60 and 80-meter isobaths are emboldened and labeled. The extent of the color ramp is from 300 to 60 meters, and all depths shallower than 60 meters are indicated by the same, light blue color. B) Bathymetric map of Bright Bank, the study site at the shelf edge in the northwestern Gulf of Mexico. Contour lines represent the 40, 60, 80, 100 and 120

meter isobaths. Colors of the stations correspond their distances from the center of Bright Bank, except for casts at the "*Swiftia"* and "mooring" stations. C) Downcast profiles of temperature from Niskin bottle rosette casts at distances away from the center of Bright Bank.

5.3.3 eDNA sampling

Water samples were taken with Niskin bottles during upcasts at all stations 0, 1, 1.5 and 3 NM from the center of Bright Bank at depths from ~100 meters to 20 meters. At the "Center" station (0 NM), the Niskin bottle rosette was lowered to a depth as close to the seafloor as possible (58 meters). Here, quadruplicate samples were taken near the seafloor, and at 40 meters depth and 20 meters in the water column. At stations 1.0, 1.5, and 3.0 NM from the Center of Bright, triplicate samples were taken in the water column at 100 meters depth or as close to the seafloor as possible (101 to 90 meters depth), and at 80 meters, 60 meters, and 40 meters in the water column. At the two stations "mooring" and "*Swiftia"*, all twelve Niskin bottles were triggered as close to the seafloor as possible at depths of 83 and 84 meters, respectively.

Water from the Niskin bottles was either first transferred to sterile 2L Whirl-Pak bags (Nasco Sampling, Madison, WI, USA) or filtered directly from the Niskin bottles. Filtration was conducted using peristaltic pump tubing (Masterflex, Vernon Hills, IL, USA) sterilized with a 10% solution of household bleach, Masterflex peristaltic pumps, and polyethersulfone filters. For all Niskin bottle rosette casts, except those conducted at the "Mooring" and "Swiftia" stations, water from each Niskin bottle was filtered over separate 0.22 µm polyethersulfone (PES) Sterivex filters (MilliporeSigma, Burlington,

MA USA). The average volume filtered per sample was 2.20 ± 0.21 L (1 SD). For the Niskin bottle rosette casts conducted at the "Mooring" and "Swiftia" stations, the entire volume from all 12 Niskin bottles was filtered over a single 0.20 µm PES membrane with an outer pre-filter mesh in a Mini Kleenpak capsule (Pall Corporation, Port Washington, New York, USA). The volumes filtered for these two samples were 28.2 and 30 liters, respectively. After each Niskin bottle rosette cast, an average of 2.37 ± 0.14 L of MilliQ water (the same water used to rinse tubing following bleach sterilization) was filtered over a Sterivex to serve as a sampling negative control for each set of samples from each Niskin bottle rosette cast. Additionally, 22 liters of MilliQ water was filtered over a Mini Kleenpak to serve as a sampling negative control for the Niskin bottle rosette casts conducted at the "Mooring" and "Swiftia" sites. Detailed descriptions of the measures taken to prevent contamination are reported in Govindarajan et al. (2022). In that study, eDNA samples were included from Niskin bottle rosette casts conducted during the same cruise for a separate analysis.

5.3.4 DNA extraction, metabarcoding library preparation, and sequencing

DNA was extracted from the Sterivex and Mini Kleenpak filters using the Qiagen DNEasy Blood & Tissue Kit (Qiagen, Hilden, Germany) and modified protocols for each filter type as described in Govindarajan et al. (2022). The protocol for extraction from Sterivex filters is adapted from the protocol originally described in Spens et al. (2017) and involves extracting directly from the filter capsules using larger volumes of the kit reagents. For the Sterivex samples, DNA was eluted in 80 µl of molecular-grade water and stored at -20°C. For the Mini Kleenpak samples, DNA was eluted in 80 µl of Qiagen

Buffer AE and stored at -20°C. DNA extractions from separate pieces of the Mini Kleenpak filters were pooled at equal volumes for downstream processing. For *18S* library preparation, DNA from the inner PES filter and outer filter mesh of the Mini Kleenpak filters was processed separately in two separate libraries. For *28S* library preparation, DNA from these two filter layers was processed together in a single library.

Metabarcoding libraries were prepared using primers that amplify a barcode in the V9 region of the *18S rRNA* gene in many eukaryotic taxa including marine invertebrates (Amaral-Zettler et al., 2009) and separately using primers designed to amplify a barcode in the *28S rRNA* gene in anthozoan corals. The latter also amplify *28S* in ctenophores, medusozoans, and sponges (McCartin et al., 2023). The primer sequences for *18S* are 5'-CCCTGCCHTTTGTACACAC-3' (forward) and 5'-CCTTCYGCAGGTTCACCTAC-3' (reverse), and the primer sequences for *28S* are 5'-CGTGAAACCGYTRRAAGGG-3' (forward) and 5'-TTGGTCCGTGTTTCAAGACG-3' (reverse). Library preparation for the *18S* marker is described in detail in Govindarajan et al. (2022), and library preparation for the *28S* marker was conducted following McCartin et al. (2023). Here, we will describe a few details that differed between library preparation using the two markers. For the *18S* libraries, DNA extractions were diluted 1:10 in molecular grade water prior to PCR amplification, whereas for the *28S* libraries samples were not diluted. KAPA HiFi HotStart Readymix (Kapa Biosciences, Wilmington, MA, USA) was used for the amplification of *18S*, whereas Platinum SuperFi II Mastermix (Thermofisher Scientific, Waltham, MA, USA) was used for the amplification of *28S*. Primer concentrations for the two primer sets also differed, with final concentrations of 200 nM for *18S* and 1,000 nM for *28S*, and cycling conditions differed depending on the

manufacturer's recommended protocols for the different mastermixes. 25 PCR cycles were conducted for the *18S* libraries, and 40 cycles of PCR were conducted for the *28S* libraries. The protocols differed between the two primer sets to optimize the PCR for *28S* to make the reaction as sensitive as possible for the detection of coral eDNA according to McCartin et al. (2023). Duplicate PCR reactions were conducted for each sample with each primer set, and the duplicate products were pooled after their visualization on a 1% agarose gel in TBE buffer stained with GelRed (Biotium, Fremont, California, USA). Each of the pooled PCR products using the *28S* marker were size selected using a 0.8X ratio of KAPA Pure magnetic beads (Kapa Biosciences, Wilmington, MA, USA) and eluted in 10 mM Tris-HCl to remove primer-dimers. PCR negative controls were included on each plate and processed in the same manner along with the sampling negative controls to monitor for contamination during library preparation.

The *18S* and *28S* primers included CS1 and CS2 adapter overhangs for sample barcoding using Access Array barcodes (Standard Biotools, San Francisco, CA). Sample barcoding using a second PCR reaction and subsequent sequencing were conducted at the University of Illinois Chicago's Genome Research Core for the *18S* libraries and Rush University Medical Center's Genomics and Microbiome Core Facility for the *28S* libraries. For both *18S* and *28S* libraries, a preliminary sequencing run with paired-end 150 bp reads on an Illumina MiniSeq was conducted using equal, pooled volumes of each barcoded library. The pooled volumes for each sample were adjusted based on the number of reads produced in the MiniSeq runs for subsequent sequencing on an Illumina MiSeq, to obtain even depths of coverage across samples. 1 µl of each negative control sample (including sampling negative controls and PCR negative controls) that did not

amplify (as visualized with gel electrophoresis) were pooled. The volumes of negative control samples that did amplify were adjusted in the same manner as for the Niskin bottle samples. Prior to sequencing, the pooled *18S* libraries were cleaned with a 1X ratio of Ampure magnetic beads (Beckman Coulter, Indianapolis, IN, USA). Pooled *18S* libraries were sequenced with three MiSeq runs (all samples were included in each run) using V2 chemistry with paired-end 250 bp reads. Pooled *28S* libraries were sequenced with one MiSeq run using V3 chemistry with paired-end 300 bp reads.

5.3.5 Bioinformatic processing

Primer sequences were trimmed from forward and reverse sequencing reads using *cutadapt* (Martin, 2011) with the following settings: forward and reverse primer sequences were anchored to the beginning of the forward and reverse reads, respectively; reverse complements of the reverse and forward primers were optionally trimmed from the forward and reverse reads, respectively, if they were identified; the minimum overlap length was set to five nucleotides (-O 5); the number of primer sequences matched was set to one (-n 1); the minimum length of trimmed reads retained was set to five nucleotides (--minimum-length 5); and untrimmed read pairs were discarded if either the forward or reverse primer sequences were not matched and trimmed from the forward and reverse reads, respectively. Read pairs were quality filtered, denoised to infer error-corrected amplicon sequence variants (ASVs), and merged using the *R* package *DADA2* (Callahan et al., 2016) in *R*. *18S* read pairs were filtered using the *filterAndTrim* function with a maximum of two expected errors allowed in either the forward or reverse read, and forward and reverse reads were truncated to 125 bp. *28S* read pairs were filtered using the

filterAndTrim function with a maximum of two expected errors allowed in either the forward or reverse read, and forward and reverse reads were truncated to 250 and 200 bp, respectively. Error profiles were learned, and read pairs were denoised and merged using the default settings, except that the pseudo-pool option was used for denoising with the *dada* function (pool = "pseudo"). Chimeras were removed from the resulting ASV tables using the *removeBimeraDenovo* function and the default settings. For the *18S* data, each sequencing run was processed separately, and then ASV tables were merged using the *gather* and *summarise* functions from the *tidyverse* (Wickham et al., 2019).

Taxonomic classification of ASVs was conducted using the *assignTaxonomy* function in *DADA2*, which implements a naïve Bayesian classifier (Wang et al., 2007). Custom reference database files were created from *18S* and *28S* data downloaded from MetaZooGene (https://metazoogene.org/database/) (O'Brien et al., 2024). For *18S*, global data for all taxa were downloaded to form the reference database on April 25, 2024. For *28S*, data from genus and/or species known from the North Atlantic were downloaded for all taxa other than anthozoan corals (Orders: Antipatharia, Scleractinia, Malacalcyonacea, and Scleralacyonacea) on June 20, 2024. A separate, custom reference database with sequences from these anthozoan coral taxa and their most up-to-date taxonomic nomenclature (McCartin et al., 2023) was concatenated to the *28S* data from MetaZooGene to build a comprehensive taxonomic reference database for all animals. For taxonomic classification, the default settings were used, which includes a minimum bootstrap cutoff score of 50. Following taxonomic classification, separate *phyloseq* (McMurdie and Holmes, 2013) objects were created from the ASV tables, taxonomic classification tables, and sampling metadata files for the *18S* and *28S* data. The resulting

phyloseq ASV tables were "decontaminated" of ASVs that were more prevalent in the negative control samples (both sampling and PCR negative controls) than in the field samples using the *R* package *decontam* and the "prevalence" method with the default settings (Davis et al., 2018).

5.3.6 Correcting for cross contamination between samples

In the *18S* data, >100,000 sequencing reads were produced in a library prepared from the sampling negative control corresponding to the Niskin bottle rosette cast 1.0 NM to the east of Bright Bank's center and in a library prepared from a PCR negative control from the same PCR plate as this negative sampling control. These libraries produced 117,894 and 116,000 reads, respectively, which were comparable numbers to libraries prepared from field samples. Cross contamination to the same degree was not apparent in the *28S* library prepared from the same sampling negative control (602 reads), nor from the *18S* library prepared from the other sampling negative control on the same PCR plate and just one column away (7 reads). The maximum number of reads in any of the other sampling negative controls or PCR negative controls was 334 reads. We assumed that cross contamination of the negative sampling control corresponding to the cast east of Bright Bank occurred during *18S* library preparation, and we removed all samples from this cast for the analysis of the *18S* data out of caution.

In the *28S* data, > 100 sequencing reads were produced from libraries prepared from several sampling negative controls. We detected 279 total sequencing reads in the sampling negative control corresponding to the cast 1.5 NM to the NW of Bright; animal ASVs detected in this sample were classified to the black coral genus *Antipathes*. We

detected 102 total sequencing reads in the sampling negative control corresponding to the cast 3.0 NM to the NW of Bright; animal ASVs detected in this sample were classified to *Antipathes* and the trachymedusae genus *Aglaura*. We also recovered 477, 602, and 5,077 total sequencing reads in the sampling negative controls corresponding to the CTD casts 1.5 NM to the NE, 1.0 NM to the E, and 1.5 NM to the SW of Bright Bank, respectively. Animal ASVs in these samples were classified to the octocoral genera *Muricea* and *Eunicea* (Family: Plexauridae).

The prevalence of these sequences in the sampling negative controls was concerning. However, we chose to retain sequences from these taxa for data analysis, because the detection of these taxa across samples could have very likely represented true detections, and false positive detections of these taxa would not have meaningfully influenced our broader interpretation of the data. Specifically, eDNA sequences from *Muricea* and *Eunicea*, which were most numerous among those taxa detected in the sampling negative controls, were largely constrained to samples from one depth in the CTD cast corresponding to the sampling negative control where they were detected. We infer that the negative control sample was likely contaminated from these few samples that represent valid detections of these genera. *Antipathes* was the most common coral genus across samples, based on both the number of sample replicates in which it was detected (52 of 115) and its average relative abundance across these samples (3.2%). Therefore, its presence in any sample below the surface mixed layer (it was not detected in any sample in the surface mixed layer) was plausible. False positive detections of these three coral taxa in the *28S* data, the trachymedusae *Aglaura* in the *28S* data, and any taxa detected in sampling negative controls at low sequence abundances in the *18S* data

(excluding the samples that were removed) may have marginally influenced some analyses that included all the data, for example ordination. However, broader interpretation of patterns in the distribution of eDNA with depth and with distance from the center of Bright Bank would not be changed. Nevertheless, we interpreted the detections of taxa across depths and sites in few sample replicates and in low relative abundances with caution, considering the detection of eDNA in sampling negative controls.

5.3.7 Data analysis

All downstream data analyses were performed in *R* (version 4.3.1 *Beagle Scouts*) using functions in *phyloseq* (McMurdie & Holmes, 2014) unless otherwise mentioned. Rarefied ASV richness was estimated from the ASV tables using *rarecurve* from *vegan* (Okansen et al., 2007) with a step size of 2,500 reads per random sample. Resulting rarefaction curves were plotted using *ggplot2* to visualize if the depth of sampling was sufficient to capture ASV diversity in each sample. To analyze β-diversity across sampling depths, first the *18S* and *28S* ASV tables were subset only to ASVs classified to the Animal kingdom that were further classified to the Phylum level. We filtered out animal ASVs that were not further classified to the Phylum level to avoid including ASVs that were erroneously classified as animals, and because classifications only to the Animal level were not relevant to our analyses of taxonomic composition across samples. Sequence read abundances for each ASV detected from replicate samples at each sampling depth and station were summed using *merge_samples2* from the *speedyseq* package. Summed read counts were then converted to relative abundances using

transform_sample_counts and were calculated as the proportion of sequencing reads represented by each ASV at each station and depth out of the total number of sequencing reads from ASVs assigned a taxonomic classification to an animal phyla. Bray-Curtis dissimilarities were calculated from both these relative abundance matrices, as well as matrices of presence/absence of the animal ASVs. Ordination was performed on the resulting dissimilarity matrices with Principal Coordinates Analysis (PCoA) using the *ordinate* function, and the positions of each sample in the first two principal coordinate axes were plotted using the *plot_ordination* function. Distance-based redundancy analyses (dbRDA) from the dissimilarity matrices were conducted using the *dbrda* function from *vegan* to determine if there were significant correlations between differences in sampling depth and location and Bray-Curtis dissimilarities. We fit a model that included sampling depth (in meters), latitude, longitude, and proximity to the seafloor as constraining variables. Proximity to the seafloor was scored as a categorical, binary variable depending on whether the sample was taken as close to the seafloor as possible, within 6 meters as calculated from the sampling depth indicated using the CTD data and bathymetric data of Bright Bank. Permutational analyses of variances implemented using the *anova* function in *vegan* were conducted with 999 permutations to determine if differences in these factors were significantly correlated with Bray-Curtis dissimilarities between samples calculated from the relative abundances of ASVs.

To visualize the taxonomic composition of eDNA sample replicates using the *18S* and *28S* markers with sampling depth and distance from the center of Bright Bank, the relative abundances of animal ASVs in each sample replicate were calculated as previously described and visualized using the *plot_bar* function. The differential

abundances of different taxonomic groups across eDNA samples were modeled using *DESeq2* (Love et al., 2014) and the extension for *phyloseq* objects as described in the online vignette (https://joey711.github.io/phyloseq-extensions/DESeq2.html). First, the differential abundance of sequencing reads in the *18S* and *28S* data classified to each Order were separately modeled with respect to sampling depth, to investigate the taxa driving trends overall in community dissimilarities across the thermocline. For this model, sampling depth was converted to a binary, categorical variable by grouping samples taken at depths of 20 and 40 meters (in the surface mixed layer) and samples taken at depths in the thermocline (60 to 100 meters). Next, the differential abundance of sequencing reads in the *18S* and *28S* data classified to each Family were separately modeled with respect to sampling depth and the distance of each sampling station from the center of Bright Bank in nautical miles. For these models, we subset the *18S* and *28S* data to only samples taken in the thermocline (depths of 60 meters or greater). Sampling depths and distances of the sampling stations from the center of Bright Bank were scaled by dividing each value by the standard deviation of each measurement. The interaction term for these two variables was not included in the model. For significance testing, p-values were adjusted using the Benjamini and Hochberg method to control the false-discovery rate, and 0.05 was used as the significance threshold.

We characterized invertebrate families as benthic, versus pelagic, according to whether these families have predominantly benthic adult forms (Brusca et al., 2022; Jumars et al. 2015). We did not consider hydrozoan families as benthic, because many hydrozoans in the orders Anthoathecata and Leptothecata detected in the data exist as pelagic medusa for a substantial period as adults. This resulted in the exclusion of some

eDNA likely derived from the colonial, sessile adult forms of some hydroid families, including milleporid fire corals. We acknowledge that eDNA from the families distinguished as benthic may also be derived from pelagic larvae.

Summary statistics, including ASV richness and relative abundance, were calculated and visualized using *tidyverse R* packages including *tidyr, dplyr*, and *ggplot2* (Wickham et al., 2019). Bathymetric maps were made both in *QGIS* as well as in *R* with the package *marmap* (Pante & Simon-Bouhet, 2013). Distances from isobaths to sampling stations were measured using the measure tool in *QGIS*. High resolution bathymetry data of Bright Bank was taken from a publicly available multibeam mapping survey generated by the U.S. Geological Survey (https://cmgds.marine.usgs.gov/data/pacmaps/wg-index.html) (Gardner et al., 1998), and bathymetry data from the Gulf of Mexico more broadly was derived from the General Bathymetric Chart of the Oceans (GEBCO; https://www.gebco.net/). Hindcast current data were generated by the HYCOM+NCODA Gulf of Mexico 1/25° analysis (https://www.hycom.org/data/gomu0pt04/expt-90pt1m000) and analyzed/visualized in *R* using the packages *netcdf* (Michna & Woods, 2013), *marmap*, and *lubridate* and *ggplot2* from the *tidyverse*.

5.4 Results

5.4.1 Water column profile

Consistently over the course of the three sampling days, there was a strong thermocline from approximately 45 to 60 meters depth that persisted below these depths with a less drastic rate of change (**Figure 5.1C**). This strong thermocline was expected

and typical for the northwestern Gulf of Mexico in late summer, and coincided with consistent decreases in salinity, decreases in dissolved oxygen concentration, peaks in fluorescence, and slight increases in turbidity across CTD casts (**Figure D.1**). From these data, we interpret that the shallowest depth of this strong thermocline corresponds to the chlorophyll maximum which occurs at the transition between the surface mixed layer and deeper, nutrient rich waters.

5.4.2 Amplicon sequence diversity and sequencing depth

After primer trimming, quality filtering, denoising, merging, and chimera removal, the average depth of sequencing per sample from the ~2L Niskin bottle samples was 118,676 ± 26,704 reads (1 SD) for the *18S* data and 45,971 ± 15,571 reads for the *28S* data. The average number of total ASVs per sample in the *18S* data (891 ± 217 ASVs) was over three-fold higher than in the *28S* data (254 ± 70 ASVs). Visualization of rarefaction curves demonstrates that these sequencing depths were sufficient to capture the majority of ASV richness in both the *18S* and *28S* libraries; however, sequencing was more comprehensive with greater sequencing depth using the *18S* barcode (i.e. rarefaction curves reached a true asymptote) (**Figure 5.2**).

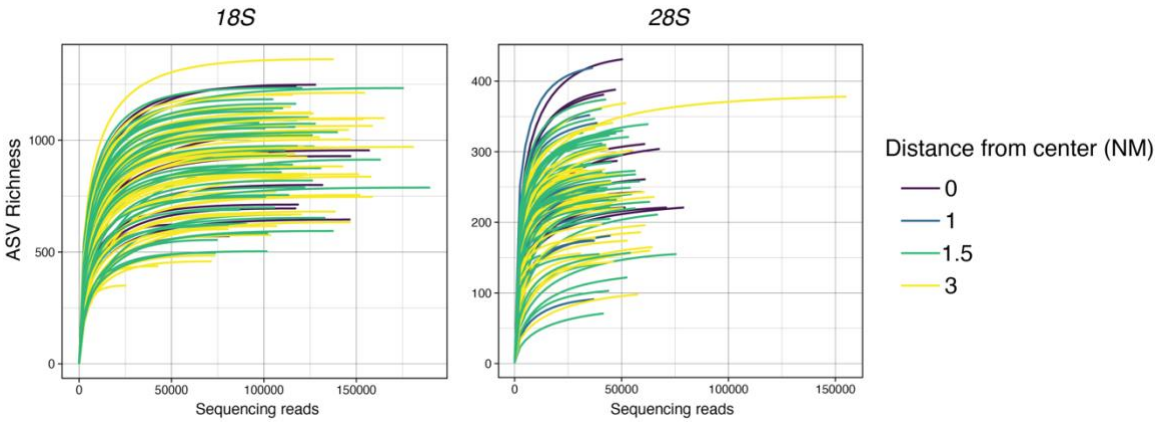

Figure 5.2: Rarefaction curves visualizing amplicon sequence diversity (ASV) in samples at steps of 2,500 sequencing reads for libraries generated using an *18S* and *28S* barcode. Each path line represents a single sample from a Niskin bottle collected during Niskin bottle rosette casts at the center or some distance from the center of Bright Bank in the northwestern Gulf of Mexico (visualized as the color of each path).

5.4.3 Taxonomic composition of eDNA in the 18S and 28S metabarcoding data

The percentage of ASVs classified as animals and assigned a taxonomic classification to the phylum level was higher in the *28S* data (25.2 ± 9.3%) (1 SD) than in the *18S* data (5.2 ± 1.4%). Hereafter, these ASVs are referred to succinctly as "animal ASVs". While the percentages of animal ASVs in the *18S* and *28S* data were quite low, on average animal ASVs were represented by more substantial percentages of the number of total sequencing reads in the *28S* (68.0 ± 19.6%) and *18S* (43.5 ± 20.7%) data across samples. Hereafter, these sequencing reads are referred to as "animal sequencing reads" and "relative abundances" refer to the proportion of reads with respect to the total number of animal sequencing reads in a sample.

In most samples in the *18S* data (104 of 107), Hexanauplia (Phylum: Arthropoda) was the most abundant animal class proportionally with a mean relative abundance of 86.8 ± 14.4% (1 SD) across samples (**Figure 5.3**). ASVs classified to Hexanauplia were predominantly classified as calanoid and cyclopoid copepods. The second most abundant animal class was Hydrozoa (Phylum: Cnidaria) (mean relative abundance 9.0 ± 13.9%), which were predominantly siphonophores. Other classes that comprised at least 5% of the animal sequencing reads in any individual sample were Appendicularia and Thaliacea

(Phylum: Chordata); Phascolosomatidea and Polychaeata (Phylum: Annelida); sagittoid chaetognaths; Tentaculata (Phylum: Ctenophora); and demosponges (Phylum: Porifera). On average, polychaetes comprised 1.2 ± 3.7% of the animal sequencing reads across samples, while the remaining classes comprised < 1% of the animal sequencing reads on average. The following animal phyla were also detected in the *18S* data at relative abundances < 5% in every sample: Mollusca, Bryozoa, Echinodermata, Platyhelminthes, Nemertea and Rotifera.

In the *28S* data, Hydrozoa was the most abundant animal class proportionally, comprising 78.7 ± 21.2% of the animal sequencing reads on average across samples. The second most abundant animal class in the *28S* data was Tentaculata (Phylum: Ctenophora) (mean relative abundance 13.0 ± 16.3%). Anthozoans and calcareous sponges comprised just 3.6 ± 6.6% and 3.6 ± 10.1% of the animal sequencing reads on average across samples. However, in 20 and 9 of 117 samples, respectively, these taxa comprised at least 10% of the animal sequencing reads. The remaining four classes that comprised at least 5% of the animal sequencing reads in any individual sample were Nuda (Phylum: Ctenophora), Scyphozoa (Phylum: Cnidaria), and Cephalopoda (Phylum: Mollusca). On average these taxa comprised less than 1% of the animal sequencing reads across samples. The following animal phyla were also detected in the *28S* data at relative abundances < 5% in every sample: Annelida, Chordata, and Arthropoda.

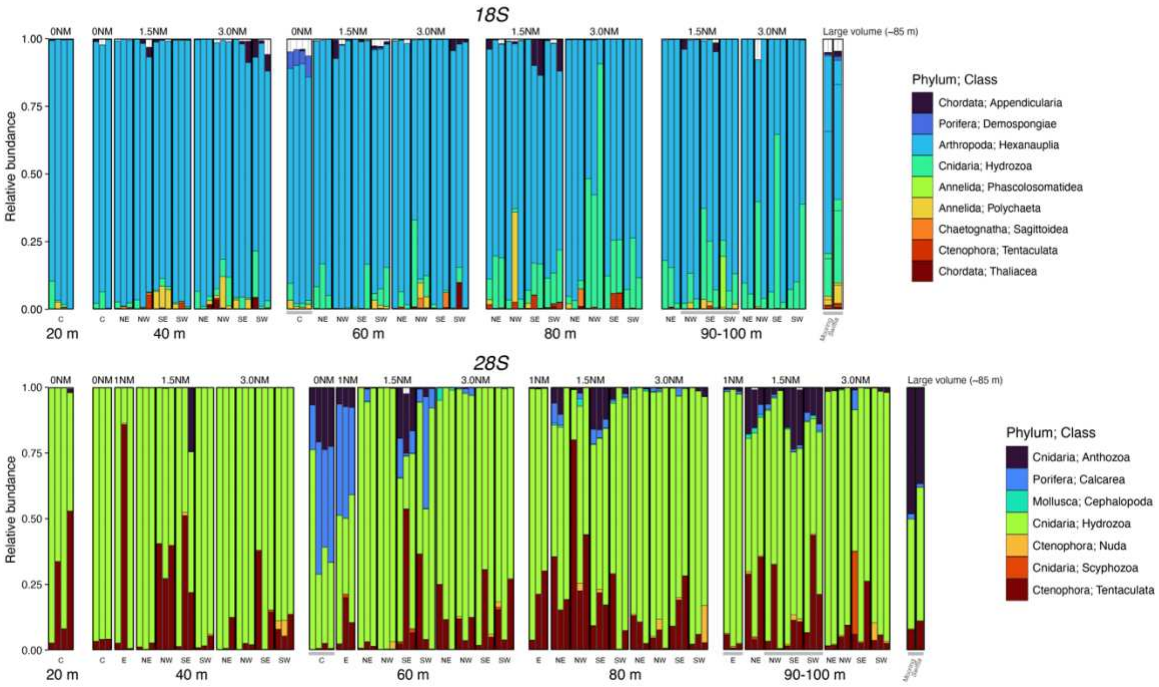

Figure 5.3: Relative abundances of eDNA sequencing reads from invertebrate animal classes across sampling replicates at different sampling depths, distances and directions from the center of Bright Bank. X axis labels indicate direction from the center of Bright Bank (C = Center, E = east, NE = northeast, NW = northwest, SE = southwest, and SW = southeast). Gray bars on the x axis indicate samples taken as close to the seafloor as possible.

5.4.4 β-diversity analysis across sampling stations and depths

Principal coordinates and distance-based redundancy analyses consistently revealed that Bray-Curtis dissimilarities calculated from the relative abundances of *18S* animal ASVs between eDNA samples were strongly correlated with differences in sampling depth, specifically whether or not samples were taken in (20 and 40 meters) versus below (60 meters and deeper) the surface mixed layer. Samples taken at depths in the surface mixed layer trended towards higher values on the first PCoA axis, which

accounted for 30.4% of the variation in Bray-Curtis dissimilarities in animal eDNA relative abundances between samples (**Figure 5.4**). Distance-based redundancy analysis found that 29.1% of the variation in squared Bray-Curtis dissimilarities calculated from relative abundances of animal ASVs were constrained by sampling depth, latitude, longitude, and proximity to the seafloor. Bray-Curtis dissimilarities between samples were significantly correlated with differences in sampling depth (*P-Value = 0.001*), but not with differences in latitude (*P-Value = 0.653*), longitude (*P-Value = 0.598*), or proximity to the seafloor (*P-Value = 0.154*).

Distance-based redundancy analyses based on the presence/absence of *18S* animal ASVs recapitulated the correlation between sampling depth and sample dissimilarities, finding that 28.0% of the variation in squared Bray-Curtis dissimilarities were constrained by the explanatory variables. Bray-Curtis dissimilarities between samples were significantly correlated not only with differences sampling depth (*P-Value = 0.001*), but also with proximity to the seafloor (*P-Value = 0.018*). However, they were not correlated with differences in latitude (*P-Value = 0.306*) or longitude (*P-Value = 0.189*).

Differences in the relative abundances of *28S* animal ASVs in samples taken in versus below the surface mixed layer were not as apparent from the PCoA. On the first two PCoA axes, samples collected from depths above the thermocline were not apparently more similar to one another than to samples taken at depths in the thermocline. Distance-based redundancy analysis found that 13.4% of the variation in Bray-Curtis dissimilarities between samples was constrained by depth, latitude, longitude and proximity to the seafloor. Bray-Curtis dissimilarities between samples were significantly correlated with differences in sampling depth (*P-Value = 0.017*), but not

with differences in latitude (*P-Value = 0.438*), longitude (*P-Value = 0.407*), or proximity to the seafloor (*P-Value = 0.217*).

In contrast to analyses based on the relative abundances of *28S* animal ASVs, ordination of Bray-Curtis dissimilarities calculated from the presence/absence matrix of *28S* animal ASVs more apparently revealed that depth explained variation in community dissimilarities. Samples collected at shallower depths trended towards more positive values on the first PCoA axis, which explained 14.4% of the variation in Bray-Curtis dissimilarities. Further, distance-based redundancy analysis found that 21.6% of the variation in squared Bray-Curtis dissimilarities was constrained by the explanatory variables, and that dissimilarities between samples were not only significantly correlated with differences sampling depth (P-Value = *0.001*), but also with differences in latitude (P-Value = *0.038*), and nearly with proximity to the seafloor (*P-Value = 0.085*). Bray-Curtis dissimilarities between samples were not significantly correlated with differences in longitude (*P-Value = 0.357*).

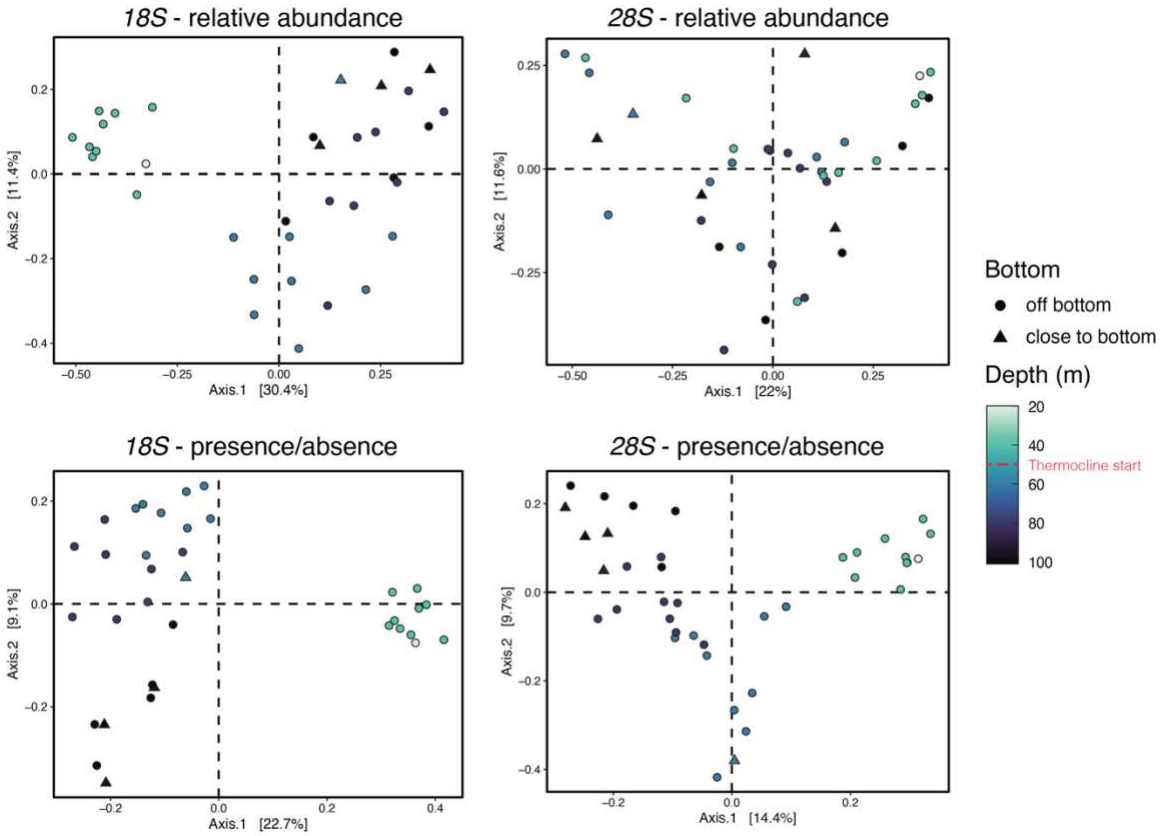

Figure 5.4: Visualizations of the first two PCoA axes for eDNA samples amplified using *18S* and *28S* primer sets. Ordinations are based on Bray-Curtis dissimilarities between samples calculated from the relative abundances (upper plots) and presence/absence (lower plots) of animal ASVs. Each point represents data across all sample replicates collected at each sampling station and depth.

5.4.5 Spatial distribution of invertebrate eDNA across depth layers

In the *18S* data, the sequence abundances of 6 invertebrate orders were significantly correlated with sampling depths in the surface mixed layer. Sequence abundances of eDNA from cyclopoid copepods were significantly higher in the surface mixed layer than at sampling depths below 40 meters ($\log_2$ fold change = 1.09 ± 0.28) (1 SE) (adjusted P-Value = 0.001). The sequence abundances of the remaining orders were

significantly lower in the surface mixed layer. These orders included several benthic taxa: black corals (Antipatharia) (Class: Anthozoa) (log_2 fold change = -5.57 ± 1.73, adjusted P-Value = 0.008), Sabellida (Class: Polychaeta) (log_2 fold change = -5.86 ± 1.46, adjusted P-Value = 0.00006), Spionida (Class: Polychaeta) (log_2 fold change = -24.6 ± 2.92, adjusted P-Value < 0.00001), and Terebellida (Class: Polychaeta) (log_2 fold change = -4.05 ± 1.16, adjusted P-Value = 0.003). Sequence abundances of siphonophores were also significantly negatively correlated with sampling depths in the surface mixed layer (log_2 fold change = -2.26 ± 0.39, adjusted P-Value < 0.00001).

The sequence abundances of several invertebrate orders were also significantly correlated with sampling depths in the surface mixed layer in the *28S* data. These include sessile, benthic taxa as well as zooplankton. The sequence abundances of all four orders of anthozoan corals were negatively correlated with sampling depths in the surface mixed layer: Antipatharia (log_2 fold change = -7.46 ± 0.77, adjusted P-Value < 0.00001), Scleractinia (log_2 fold change = -25.2 ± 1.96, adjusted P-Value < 0.00001), Malacalcyonacea (log_2 fold change = -25.4 ± 1.25, adjusted P-Value < 0.00001), and Scleralcyonacea (log_2 fold change = -7.45 ± 1.16, adjusted P-Value < 0.00001). The sequence abundances of sea anemones (Order: Actiniaria) were also significantly, negatively correlated with sampling depths in the surface mixed layer (log_2 fold change = -5.63 ± 2.25, adjusted P-Value = 0.03). Sequence abundances of two orders of calcareous sponges were also significantly, negatively correlated with sampling depths in the surface mixed layer: Leucosolenida (log_2 fold change = -10.6 ± 0.98, adjusted P-Value < 0.00001) and Clathrinida (log_2 fold change = -10.1 ± 1.09, adjusted P-Value < 0.00001). The sequence abundances of eDNA from Lobata (Phylum: Ctenophora) and

Narcomedusae (Phylum: Hydrozoa) were significantly, *positively* correlated with sampling depths in the surface mixed layer: Lobata (log_2 fold change = 1.25 ± 0.33, adjusted P-Value = 0.0003), and Narcomedusae (log_2 fold change = 2.33 ± 0.48, adjusted P-Value < 0.00001). Like in the *18S* data, the sequence abundances of siphonophores were significantly, negatively correlated with sampling depths in the surface mixed layer (log_2 fold change = -1.31 ± 0.35, adjusted P-Value = 0.0005). Additionally, sequence abundances of eDNA classified as belonging to cuttlefish (Order: Sepiida) were also significantly, negatively correlated with sampling depths in the surface mixed layer (log_2 fold change = -7.51 ± 0.65, adjusted P-Value < 0.00001).

5.4.6 Vertical and horizontal distribution of benthic invertebrate eDNA

As indicated by the negative correlations of the sequence abundances several benthic orders with depths in the surface mixed layer, eDNA from benthic invertebrate families was largely constrained to depths below the thermocline (**Figure 5.5**). The average number of benthic invertebrate families detected in the *18S* data was highest at the center of Bright Bank at depths of 60 meters close to the seafloor; on average 26.8 ± 4.5 (1 SD) families were detected across the four sample replicates. In the *28S* data, the number of benthic invertebrate families detected was also highest in samples taken at 60 meters in the center of the bank; on average 14.8 ± 0.5 benthic families were detected. Anthozoan coral eDNA was nearly entirely restricted to depths in the thermocline, except for the detection of octocoral eDNA in one sample replicate at a depth of 40 meters.

Considering samples taken only at depths in the thermocline, the sequence abundances of 4 and 17 benthic invertebrate families were significantly correlated with

sampling depth in the *18S* and *28S* data, respectively (**Figure 5.6A**). In the *18S* data, these taxa included 1 family of demosponges, 1 family of gastropods, and 1 family of bivalves with sequence abundances *negatively* correlated with sampling depth (i.e. more abundant at shallower depths below the surface mixed layer). The sequence abundances of 1 family of gastropods were significantly, *positively* correlated with sampling depth. In the *28S* data, the sequence abundance of 13 families of anthozoans and 7 families of sponges (including calcareous sponges and demosponges) were correlated with sampling depth. The sequence abundances from the majority of differentially abundant scleractinian coral families (3 of 4: Agariciidae, Astrocoeniidae, and Montastraeidae) were significantly, negatively correlated with greater sampling depths below the surface mixed layer. On the contrary, the sequence abundances of all seven differentially abundant octocoral families were significantly, *positively* correlated with greater sampling depth. Black corals were evenly split; sequence abundances of antipathids were *negatively* correlated with greater sampling depths while sequence abundances of aphanipathids were *positively* correlated with greater sampling depths. All differentially abundant families of sponges exhibited sequence abundances negatively correlated with greater sampling depth, as did sea anemones in the family Sagartiidae.

At depths in the thermocline, eDNA from benthic invertebrate families also decreased in diversity and relative abundance with distance from the center of Bright Bank. In samples taken away from the center of the bank and in the water column at 60 meters depth, the average number of benthic invertebrate families detected in the *18S* data was just 3.2 ± 1.6 at distances 1.5 NM from the center and 1.5 ± 1.2 at distances 3 NM from the center (**Figure 5.7**). The sequence abundances of 25 benthic invertebrate

families were significantly, negatively correlated with distance from the center of the bank (**Figure 5.6B**). The sequence abundances of just 1 family of polychaetes were significantly, *positively* correlated with distance from the center of Bright Bank.

Like in the *18S* data, the number of benthic families detected in the *28S* data at depths of 60 meters also decreased with increasing distance from the center of Bright. At distances 1 NM from the center of the bank, on average 9 ± 1 families were detected; at distances 1.5 NM from the center of the bank on average 4.8 ± 1.9 families were detected, and 3.0 NM from the center of the bank on average 1 ± 0.7 families were detected (**Figure 5.7**). The number of anthozoan coral genera detected, which comprised a large proportion of sequencing reads from benthic families in the *28S* data, also decreased with distance from the center of Bright in samples collected at 60 meters. At the center of the bank on average 6 ± 0.8 genera were detected; at distances 1 NM from the center of the bank on average 4.3 ± 0.6 families were detected; at distances 1.5 NM from the center of the bank on average 2 ± 1.0 families were detected; and at distances 3.0 NM from the center of the bank on average just 0.3 ± 0.5 families were detected. In the *28S* data the sequence abundances of 17 benthic invertebrate families, exclusively anthozoan corals and sponges, were significantly, negatively correlated with distance from the center of Bright Bank (**Figure 5.6B**).

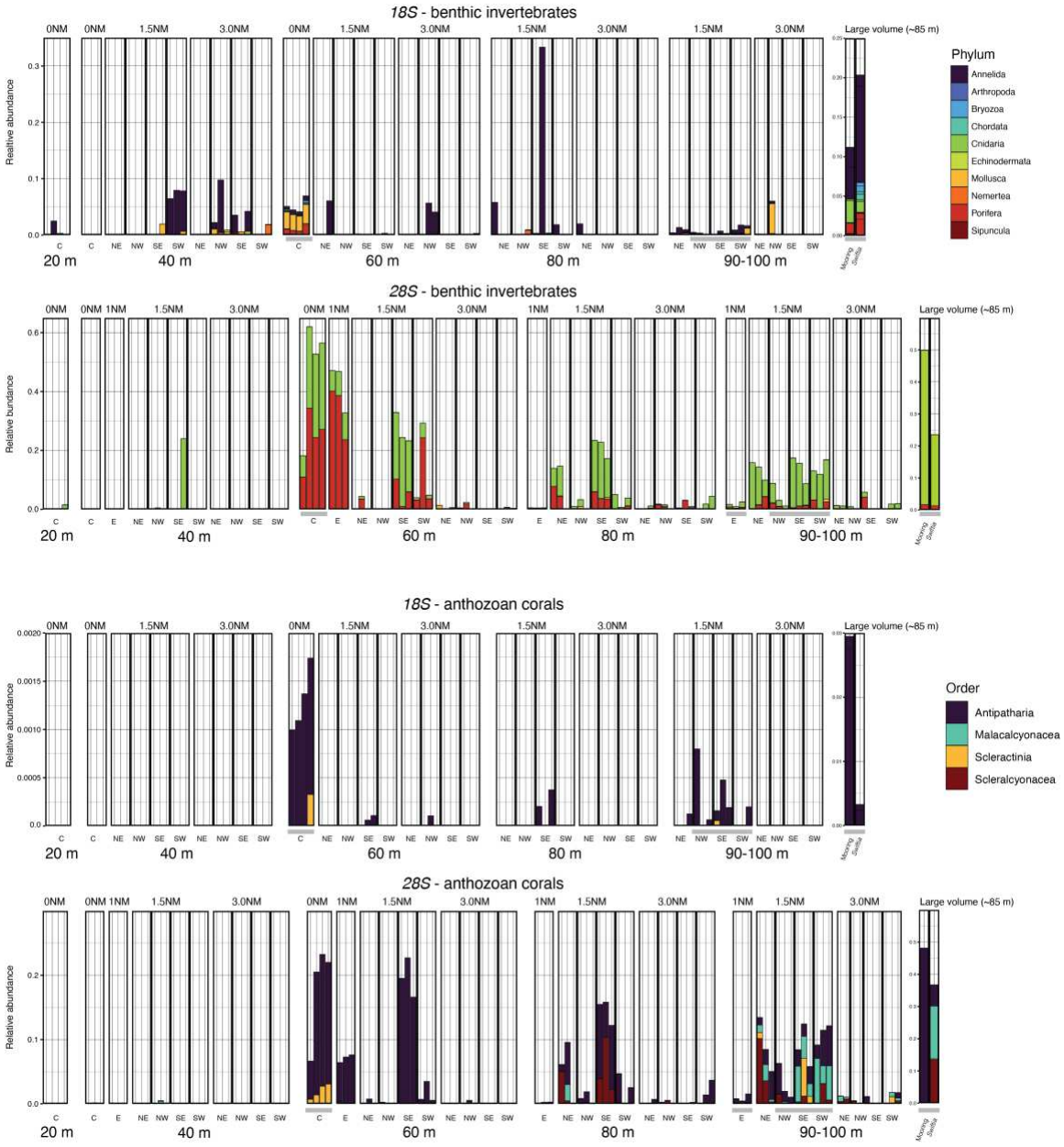

Figure 5.5: Relative abundances of eDNA from benthic invertebrate families across sampling replicates at different sampling depths, distances and directions from the center of Bright Bank. Note that relative abundances are plotted with different y-axis scales for large volume samples that correspond to each marker and taxonomic grouping. X-axis labels indicate direction from the center of Bright Bank (C = Center, E = east, NE =

northeast, NW = northwest, SE = southwest, and SW = southeast). Gray bars on the x axis indicate samples taken as close to the seafloor as possible.

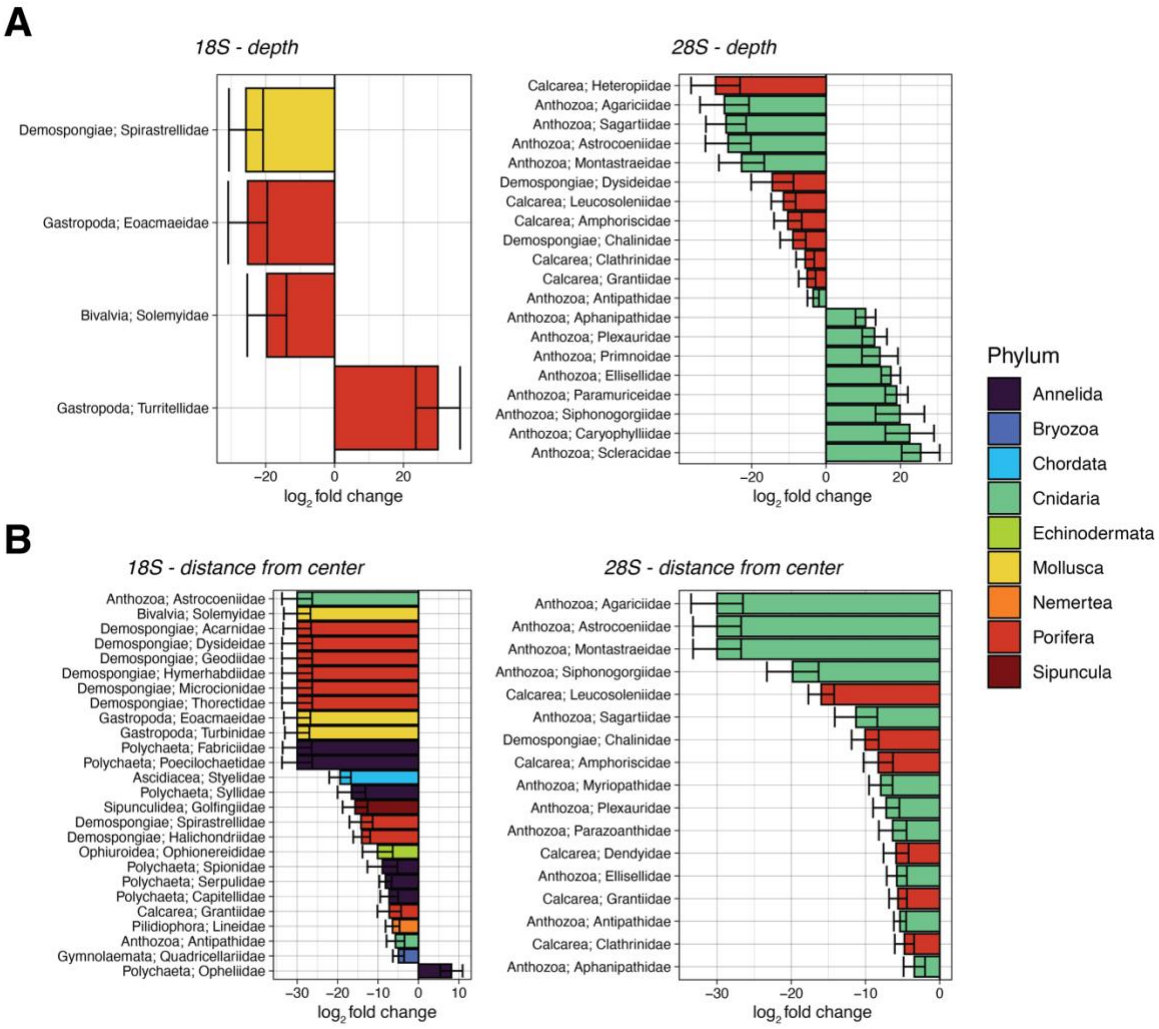

Figure 5.6: Modeled $\log_2$ fold changes in the sequence abundances of eDNA from benthic invertebrate families in samples taken below the surface mixed layer. Benthic families with sequence abundances that were significantly correlated ($\alpha = 0.05$) with distance from the center and/or sampling depth are shown. Error bars represent one standard error.

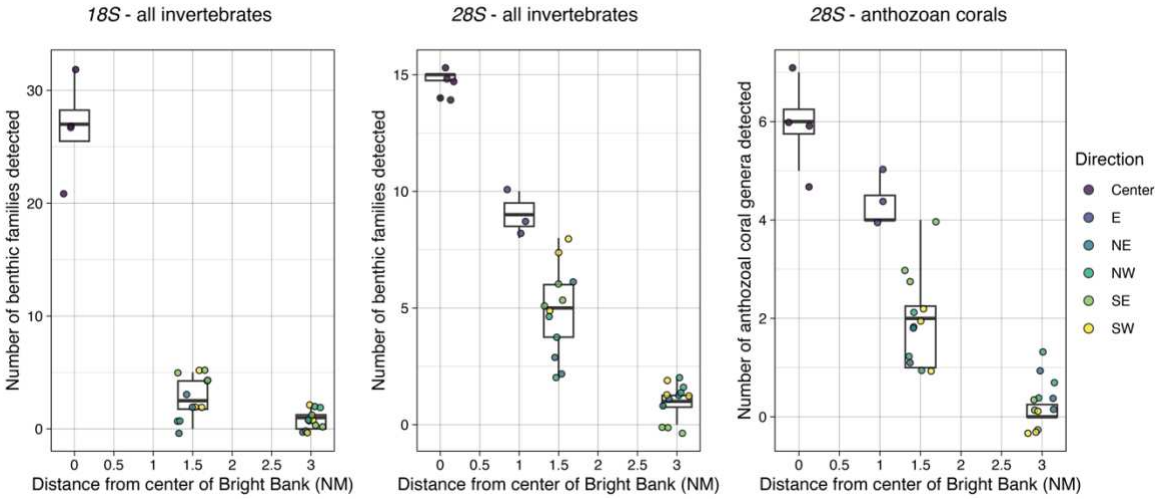

Figure 5.7: Taxonomic richness of benthic invertebrates detected in eDNA samples taken at 60 meters depth and at increasing distances from the center of Bright Bank. Each point represents a single sample replicate, and points are colored by their direction away from the bank's center.

5.4.7 Horizontal transport distances of coral eDNA from Bright Bank

In the *28S* data, but not in the *18S* data, eDNA from black corals was detected in all three sample replicates taken at 60 meters depth in the water column 1.0 and 1.5 NM to the east, southeast and southwest of Bright Bank (**Figure 5.8**). In fact, at samples taken at distances 1.5 NM from the center of Bright Bank to the southeast, the relative abundances of black coral eDNA (20.0 ± 3.1%) were higher than in samples taken at the center of Bright Bank near the seafloor, where black corals occur (16.1 ± 6.8%). Repeated detections of coral eDNA in samples taken in the water column were not limited to depths of 60 meters. At depths of 80 meters, we also detected eDNA from black corals and octocorals in the family Ellisellidae (genera *Ellisella* and *Nicella*) in all

three sample replicates at 80 meters 1.5 NM to the southeast of Bright Bank and at substantial total relative abundances (14.7 ± 10.1%).

Assuming that vertical transport was negligible due to water column stratification, we measured the minimum horizontal transport distances of coral eDNA to these three stations where coral eDNA was repeatedly detected. In samples taken 1.0 NM to the east at 60 meters, the 60 meter isobath is at minimum 490 meters away; in samples taken 1.5 NM to the southeast the 60 meter isobath is at minimum 1,460 meters away; in samples taken 1.5 NM to the southwest the 60 meter isobath is at minimum 1,110 meters away; and in samples taken 1.5 NM to the southeast at 80 meters, the 80 meter isobath is at minimum 480 meters away.

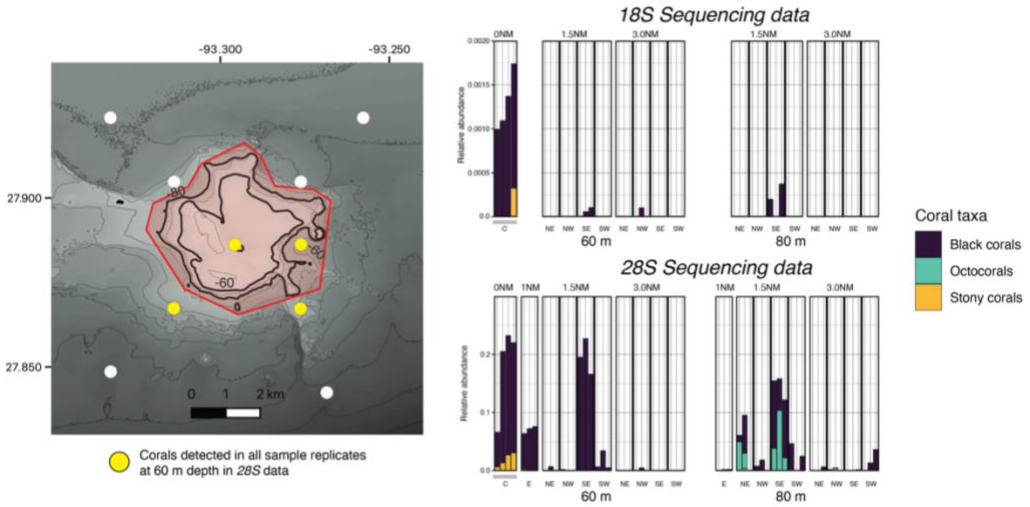

Figure 5.8: Detections of coral eDNA at depths of 60 and 80 meters at distances away from the center of Bright Bank. 60 and 80-meter isobath contours are emboldened and labeled. The boundaries of the FGBNMS are indicated with the red polygon. Points highlighted in yellow indicate sampling locations where coral eDNA was detected across all sample replicates at 60 meters depth. X-axis labels indicate direction from the center of Bright Bank (C = Center, E = east, NE = northeast, NW = northwest, SE = southwest,

and SW = southeast). Gray bars on the x axis indicate samples taken as close to the seafloor as possible.

5.5 Discussion

5.5.1 Vertical eDNA transport is limited in a stratified water column.

Here we present further evidence supporting the hypothesis that physical stratification in the water column hinders the vertical transport of eDNA between depth layers (Jeunen et al., 2019; Allan et al., 2021; Govindarajan et al., 2021; Monuki et al., 2021; Hoban et al., 2023; Robinson et al., 2023). In the *18S* and *28S* data, eDNA in samples collected in versus below the surface mixed layer were highly dissimilar based on the presence and absence of animal ASVs. Furthermore, eDNA from zooplankton, including copepods and siphonophores, and numerous benthic invertebrates, like corals and sponges, was significantly, differentially abundant between the surface mixed layer and thermocline below.

In both the *18S* and *28S* data, we detected eDNA from benthic families in samples taken in the surface mixed layer, but these detections were largely spurious and comprised a small proportion of the total sequencing reads in these samples. In the *18S* data, the most abundant of these benthic families detected in the surface mixed layer were opheliid polychaetes (at maximum nearly 10% of the sequencing reads across 7 samples at 40 meters deep), but this detection may plausibly reflect spawning aggregations of epitokes (Maciolek & Blank, 2006). Otherwise, the remaining benthic families detected in the surface mixed layer in the *18S* data were present in few sample replicates and at low relative abundances. These families include capitellid polychaetes, fireworms

(Family: Amphinomidae), nudibranchs (Family: Chromodorididae), file shells (Family: Limidae), and nemerteans (Family: Lineidae). In the *28S* data, eDNA from anthozoans was detected in three sample replicates taken in the surface mixed layer, from a zoanthid (Family: Parazoanthidae), an anemone, and an octocoral. Surprisingly, the zoanthid was detected at a high relative abundance, more than 20% of the sequencing reads in the sample.

Detections of benthic invertebrates in the surface mixed layer could represent the transport of eDNA either as waste from predators that feed near the benthos and then traverse the thermocline (e.g. fish) or as swimming larvae. The latter possibility remains a notable point of uncertainty and begs the question of whether larvae should be considered eDNA and can be practically distinguished from other forms of "real" eDNA. Size fractionation, by using a pre filter of a large pore size to remove larger eDNA particles including larvae, seems to be the most reasonable approach to remove larvae from water samples. However, using a pre filter would potentially come at the cost of losing eDNA in the form of particulates or other larger size fractions. Currently, the potential presence of larvae in marine eDNA sequencing data is one factor that may complicate the interpretation of species occurrence records using eDNA analysis.

Below the surface mixed layer, we found evidence that water column stratification further limited vertical transport. The sequence abundances of benthic invertebrate families were correlated with depth in samples taken in the thermocline. Among these families of corals in the *28S* data were several families of octocorals and black corals in the family Aphanipathidae, which were positively correlated with greater sampling depth. The differential abundances of these families were reflected in the

detection of a high diversity of octocorals and the detection of aphanipathid black corals in samples taken at depths > 90 meters and close to the seafloor. Coral genera that were not detected at shallower depths included *Callogorgia* (Order: Scleralcyonacea), as well as *Elatopathes* and *Aphanipathes* (Family: Aphanipathidae). In video collected during ROV dives, these three genera have only been observed at depths greater than 100 meters, reflecting the depths where they were detected in the eDNA data.

5.5.2 Evidence for the horizontal transport of coral eDNA over substantial distances in the 28S data

The distribution of eDNA shed from benthic invertebrate families was not only constrained by depth, but also by distance from the center of Bright Bank, where measurements of the diversity of benthic families were highest. At the center of Bright Bank near the seafloor, a diverse community of benthic invertebrates including polychaete worms, bryozoans, ascidian tunicates, anthozoan corals, molluscs, and sponges, were detected in all four sample replicates in the *18S* data. With distance from the center of Bright, the diversity of benthic invertebrate families detected in the water column at depths equivalent to the seafloor (~60 meters) decreased precipitously with distance from the bank. The average number of benthic families detected decreased ~8-fold within 1.5 NM of the center of the bank and ~18-fold within 3 NM of the bank center, coinciding with significant decreases in the abundance of eDNA from several benthic invertebrate families. In the *28S* data, the diversity of benthic invertebrates was comparably low (~15-fold less) at distances 3.0 NM from the center of Bright, and several calcareous sponges and anthozoan corals were differentially abundant with

distance from the center of the bank. However, the decrease in diversity over distances of 1.5 NM was less drastic than in the *18S* data; the average number of benthic families detected decreased just ~3-fold within 1.5 NM of the center of the bank.

Detections of coral eDNA in substantial relative abundances in the water column at distances up to 1.5 NM from the center of the bank most likely reflects the horizontal transport of eDNA from corals at Bright Bank in the east, southeast, and southwest directions. Vertical transport does not easily explain these data. The bottom depth at these stations 1 and 1.5 NM from Bright Bank exceeds 90 meters (30 meters deeper than where these samples were taken), and neither these data nor data from our previous work have demonstrated the vertical transport of coral eDNA upwards against the thermocline over tens of meters (McCartin et al., 2023). It is also not surprising that putatively transported eDNA would be shed from black corals in the family Antipathidae (*Stichopathes* spp. and *Antipathes* spp.). In eDNA samples taken from ROV dives at the seafloor at Bright Bank, and more broadly across the northern Gulf of Mexico, eDNA from *Stichopathes* spp. and *Antipathes* spp. is consistently more abundant than any other coral taxa at mesophotic depths (McCartin et al., 2023). If these corals shed the highest concentrations of eDNA as compared to other corals, it follows that eDNA from these corals would be detected the farthest away from their sources. In samples taken 1.5 NM to the southeast of Bright Bank at 80 meters depth we also detected eDNA from ellisellid octocorals (*Ellisella* spp. and *Nicella* spp.). The detection of ellisellid coral eDNA at this depth is also not surprising. In the large volume sample taken near the seafloor at depths of 84 meters (station "*Swiftia*") eDNA from ellisellid octocorals was also detected in substantial relative abundances in addition to eDNA from black corals. Thus, it is likely that coral

eDNA detected in samples at 80 meters deep 1.5 NM southeast of Bright originated from similar depths at the bank.

Under the assumption that vertical transport was negligible, we conservatively estimate that coral eDNA must have been transported up to ~1.5 km from the seafloor at Bright Bank to reach these sampling locations. These measurements are in line with those from a previous study that quantified the distribution of eDNA from a caged fish in two directions using qPCR (Murakami et al., 2021). In this study, water temperature was nearly the same as in our study (~ 20°C), meaning that eDNA degradation rates were likely also similar (McCartin et al., 2022). One substantial difference between their study and ours, is that they detected exponentially lower concentrations of eDNA concentration 1 km from the caged fish, while we detected coral eDNA at higher relative abundances at distances 1.5 NM from the center of Bright Bank. However, this discrepancy can be explained by differences between qPCR and metabarcoding. eDNA metabarcoding is not quantitative like qPCR, and the relative abundances of different taxa in a sample is dependent on other taxa in that same sample. Thus, while the detection of eDNA from a taxa in multiple sample replicates at substantial relative abundances can be interpreted as having a high probability of being a real detection, uncorrected relative abundances in metabarcoding data should not be conflated with concentrations from qPCR.

Considering eDNA transport at the kilometer scale in metabarcoding data may be surprising and perhaps unnerving. However, a back of the envelope calculation using eDNA persistence times from experimental studies and current speeds in the area reveals that the transport distances we observed are in fact entirely practical. Using the model in McCartin et al. (2022), at 22°C, the temperature at 60 meters at Bright Bank, we expect

eDNA concentrations to decrease by three orders of magnitude in four days (3.99 exactly). This three-fold decrease is a typical decrease from starting concentrations of experiments to concentrations near the limits of detection of qPCR. Thus, the following estimate assumes shed concentrations of eDNA from black corals are three-fold higher than the limit of detection of our *28S* metabarcoding protocol, which is admittedly unknown. Hindcasted currents at 60 meters depth at Bright Bank over the course of sampling during our study exceeded speeds of 0.1 m/s or .36 km/hour (**Figure D.2**). Considering the underlying assumptions and using this value as a conservative estimate for current speed, eDNA may be transported up to 8.64 kilometers per day in a straight-line distance. Thus, over four days it may be transported nearly 35 kilometers at detectable concentrations. Of course, these straight-line distances, which do not consider diffusion nor meandering current patterns, are overestimates; however, these calculations demonstrate that eDNA transport over the 1.5 km distance that we observed should not come as a surprise.

5.5.3 Comparison between expected current patterns and directions of coral eDNA transport

In the Gulf of Mexico, circulation patterns are driven by the protrusion and contraction of the loop current, riverine input, and the associated formation of mesoscale (twenty to hundreds of km in diameter) and submesoscale (< 10 km in diameter) eddies (Lugo-Fernández, 1998; Bracco et al., 2019). Typically, in September, currents in the upper 100 meters at East and West Flower Garden Banks (shelf-edge banks ~30 and 50 km west of Bright, respectively) are predominantly in the westward direction along the

shelf edge in the absence of eddies (Lugo-Fernández, 1998). Hindcasted currents revealed that currents at 60 and 80-meters depth at Bright Bank over the course of sampling during our study were consistently to the west and south and weakened over time.

We observed horizontal eDNA transport in part to the south and west, which is in line with these expected current patterns. Detection of eDNA to the east of Bright Bank is not expected. However, there is a pinnacle as shallow as 60 meters to the north of our sampling location 1.0 NM to east of the center of Bright Bank. Thus, it is plausible that the detection of benthic eDNA did not originate from the center of Bright Bank, but rather from this shallow feature. Discrepancies between the exact direction of eDNA transport and hindcasted current patterns likely exist due to the low resolution of the HYCOM data (1/25°). Modeling the circulation of current patterns to a sufficient resolution is a computationally intensive problem that is beyond the scope of this study (A. Bracco, personal communication). Complex interactions with the bathymetry of Bright Bank at small spatial scales may drive current patterns in ways that are undetected in models at coarse resolutions. Making a probabilistic map of hindcasted eDNA source locations would be impossible with these currently available circulation models. Thus, accurately constraining the position of eDNA sources at the same resolution as data from conventional methods (meters/tens of meters) is a tall task. Rather, leveraging the complementary natures of eDNA sequencing and conventional approaches whilst considering each of their inherent limitations (in the case of eDNA sequencing constraining the exact position of source organisms) will prove to be a more fruitful approach than expecting eDNA to replace conventional survey techniques.

5.5.4 eDNA sequencing with taxonomically specific primers is sensitive and complements data generated using primers that broadly amplify marine invertebrates.

In this study, we compare data generated through eDNA metabarcoding using a primer set designed to amplify a barcode in the V9 region of *18S* in all animals, and more broadly eukaryotes, and data generated using a primer set designed to specifically amplify a barcode in *28S* in anthozoan corals that is also complementary to several other marine invertebrate taxa. These two datasets provide complementary views of the pelagic and benthic invertebrate community.

The *18S* data is composed of eDNA from a diverse suite of 86 invertebrate orders distributed into 14 different phyla. Of these taxa, just 17 orders and 7 phyla are also included in the *28S* data. However, using the *28S* primers detected eDNA from 10 orders not detected in the *18S* dataset, including octocorals (Orders Malacalcyonacea and Scleralcyonacea). Further, using the *18S* primer set, the average relative abundance of eDNA from anthozoan corals was extremely low; at maximum fewer than 0.2% of the animal eDNA in any 2L eDNA sample was classified to Anthozoa. Even in the ~30 L samples taken close to the seafloor, the relative abundance of coral eDNA did not exceed 3%. By design, the *28S* libraries were comparatively enriched in eDNA from anthozoan corals; at maximum in the 2L samples nearly one fourth (24.6%) the animal eDNA in any sample was classified to Anthozoa. In the ~30 L samples taken close to the seafloor, the maximum relative abundance of coral eDNA was nearly 50%. The prevalence of eDNA from calcareous sponges in the *28S* data (more than half of the eDNA in a sample) was

not expected, but perhaps not surprising given that the primers match *28S* sequences from some sponges (McCartin et al., 2023).

By process of elimination, we propose that the low prevalence of coral eDNA across samples using the general *18S* primers is due to competition with DNA templates from other more abundant taxa. We aligned *18S* sequences of anthozoans in the MetaZooGene database and found that of the 91 sequences that contained the amplified V9 barcode, the primers were complementary to 84 of the sequences, including black corals, scleractinians and octocorals, with two or fewer mismatches. Therefore, it is unlikely that we failed to detect coral eDNA using this marker because the primers did not complement coral eDNA templates in our samples or because we did not have reference *18S* barcodes. We fully captured sequence diversity in the libraries generated using the *18S* primers, by conducting three separate runs on an Illumina MiSeq with all samples included in each run. Thus, it is also unlikely that the failure to detect anthozoan ASVs was due to insufficient sequencing depth. Competition with other eDNA templates and the failure to detect the less abundant coral eDNA is likely due to two processes that work in tandem: 1) a biological reality in which coral eDNA is more scarce than eDNA from other taxa in the sample and 2) amplification bias wherein over the course of the PCR reaction the proportion of eDNA from more abundant taxa is increased with each cycle, since eDNA from abundant taxa is more likely to amplify during earlier cycles (Kelly et al., 2019).

5.5.5 The spatial resolution of biodiversity measurements and species detections from eDNA metabarcoding data depends on PCR primer choice.

Understanding the expected distances of horizontal and vertical eDNA transport in the ocean is complicated yet necessary for constraining the spatial resolution of eDNA metabarcoding data. Here, we leveraged an isolated source of offshore benthic invertebrate eDNA in the Gulf of Mexico to constrain the expected vertical and horizontal distribution of marine eDNA. In agreement with several other studies, we found that vertical stratification in the water column limits transport across depth layers. In the horizontal dimension, while the diversity of eDNA from benthic invertebrates and the modeled abundances of eDNA sequences decreased with distance from the source, we also found strong evidence for the horizontal transport of eDNA over substantial distances, up to nearly 1.5 km. From a management perspective, this transport resulted in detecting eDNA from corals that likely originated inside the Flower Garden Banks National Marine Sanctuary outside of sanctuary boundaries.

Interestingly, we confidently identified horizontal transport of coral eDNA at substantial distances using primers that are taxonomically specific to coral *28S* and not in data generated using primers that broadly target eukaryotes. Using taxonomically specific primer sets, such as the MiFish *12S* primers and the *28S-Anth* primers used in this study, is a sensitive approach that also permits the accurate classification of eDNA to the genus and species levels (Miya et al., 2015; McCartin et al., 2023). Further, species-specific quantitative assays (e.g. qPCR and digital droplet PCR) permit the accurate quantification of very low concentrations of eDNA with high specificity. These characteristics are inherently beneficial for the respective purposes of these methods. However, here we demonstrate that the taxonomic specificity of PCR primers has a demonstrable effect on the inferred spatial distribution of eDNA metabarcoding data. With increasing taxonomic

specificity of PCR primers, sensitivity of detection and certainty in taxonomic identity is higher, but inferring the exact location of an animal detected in data generated using specific primers is more challenging. Pairing primers that target barcodes in a diversity of taxa (e.g. the *18S* primers herein or the Leray primers to *COI*) (Leray et al., 2013) with taxonomically specific primers for taxa of interest (e.g. fish, corals) is a comprehensive approach for biodiversity characterization at the community scale. However, inherent differences in the spatial resolution of biodiversity measurements and species detections inferred from data using each primer set must be considered to integrate these data for conservation and natural resource management.

5.6 Acknowledgements

We thank Rene Francolini and Katie Foley for their assistance with field work, as well as the captain and crew of *R/V Manta*, specifically Jimmy MacMillan for his assistance with Niskin bottle rosette deployments. We thank Weihua Wang from the Genomics Research Core at the University of Illinois Chicago, and Dr. Stefan Green, Ashley Wu, and Cecilia Chau from the Genomics and Microbiome Core Facility at Rush Medical University for library preparation and sequencing. We thank Dr. Wynn Meyer for her helpful comments on a draft of this manuscript. We also thank Dr. Allen Collins and Annemarie Wood for their helpful discussion regarding the interpretation of the zooplankton detections in the *28S* data.

This research was funded by the National Oceanic and Atmospheric Administration's Oceanic and Atmospheric Research, Office of Ocean Exploration and Research, under award NA18OAR0110289 to SH and JMM at Lehigh University. This

research is part of the Woods Hole Oceanographic Institution's Ocean Twilight Zone Project, funded as part of The Audacious Project housed at TED.

5.7 References

Allan, E. A., DiBenedetto, M. H., Lavery, A. C., Govindarajan, A. F., & Zhang, W. G. (2021). Modeling characterization of the vertical and temporal variability of environmental DNA in the mesopelagic ocean. *Scientific Reports*, *11*(1), 21273.

Amaral-Zettler, L. A., McCliment, E. A., Ducklow, H. W., & Huse, S. M. (2009). A method for studying protistan diversity using massively parallel sequencing of V9 hypervariable regions of small-subunit ribosomal RNA genes. *PloS One*, *4*(7), e6372.

Andruszkiewicz, E. A., Koseff, J. R., Fringer, O. B., Ouellette, N. T., Lowe, A. B., Edwards, C. A., & Boehm, A. B. (2019). Modeling Environmental DNA Transport in the Coastal Ocean Using Lagrangian Particle Tracking. *Frontiers in Marine Science*, *6*. https://doi.org/10.3389/fmars.2019.00477

Andruszkiewicz Allan, E., Zhang, W. G., C. Lavery, A., & F. Govindarajan, A. (2021). Environmental DNA shedding and decay rates from diverse animal forms and thermal regimes. *Environmental DNA (Hoboken, N.J.)*, *3*(2), 492–514.

Barnes, M. A., & Turner, C. R. (2016). The ecology of environmental DNA and implications for conservation genetics. *Conservation Genetics* , *17*(1), 1–17.

Barnes, M. A., Chadderton, W. L., Jerde, C. L., Mahon, A. R., Turner, C. R., & Lodge, D. M. (2021). Environmental conditions influence eDNA particle size distribution in aquatic systems. *Environmental DNA (Hoboken, N.J.)*, *3*(3), 643–653.

Bracco, A., Liu, G., & Sun, D. (2019). Mesoscale-submesoscale interactions in the Gulf of Mexico: From oil dispersion to climate. *Chaos, Solitons & Fractals*, *119*, 63–72.

Brusca, R.C., Giribet, G., & Moore, W. (2022) Invertebrates: Fourth Edition. *Oxford University Press.*

Callahan, B. J., McMurdie, P. J., Rosen, M. J., Han, A. W., Johnson, A. J. A., & Holmes, S. P. (2016). DADA2: High-resolution sample inference from Illumina amplicon data. *Nature Methods*, *13*(7), 581–583.

Closek, C. J., Santora, J. A., Starks, H. A., Schroeder, I. D., Andruszkiewicz, E. A., Sakuma, K. M., Bograd, S. J., Hazen, E. L., Field, J. C., & Boehm, A. B. (2019). Marine Vertebrate Biodiversity and Distribution Within the Central California Current Using Environmental DNA (eDNA) Metabarcoding and Ecosystem Surveys. *Frontiers in Marine Science*, *6*. https://doi.org/10.3389/fmars.2019.00732

Davis, N. M., Proctor, D. M., Holmes, S. P., Relman, D. A., & Callahan, B. J. (2018). Simple statistical identification and removal of contaminant sequences in marker-gene and metagenomics data. *Microbiome*, *6*(1), 226.

Deiner, K., & Altermatt, F. (2014). Transport distance of invertebrate environmental DNA in a natural river. *PloS One*, *9*(2), e88786.

Dennis, G. D., & Bright, T. J. (1988). Reef Fish Assemblages on Hard Banks in the Northwestern Gulf of Mexico. *Bulletin of Marine Science*, *43*(2), 280–307.

Dugal, L., Thomas, L., Meenakshisundaram, A., Simpson, T., Lines, R., Colquhoun, J., Jarman, S., & Meekan, M. (2023). Distinct coral reef habitat communities characterized by environmental DNA metabarcoding. *Coral Reefs, 42*(1), 17–30.

Ely, T., Barber, P. H., Man, L., & Gold, Z. (2021). Short-lived detection of an introduced vertebrate eDNA signal in a nearshore rocky reef environment. *PloS One*, *16*(6), e0245314.

Galili, T. (2015). dendextend: an R package for visualizing, adjusting and comparing trees of hierarchical clustering. *Bioinformatics, 31*(22), 3718–3720.

Gardner, J.V., Mayer, L.A., Hughes Clarke, J.E., & Kleinier, A. (1998). High-resolution multibeam bathymetry of East and West Flower Gardens and Stetson Banks, Gulf of Mexico. *Gulf of Mexico Science, 16,*131-143.

Govindarajan, A. F., Francolini, R. D., Jech, J. M., Lavery, A. C., Llopiz, J. K., Wiebe, P. H., & Zhang, W. (gordon). (2021). Exploring the Use of Environmental DNA (eDNA) to Detect Animal Taxa in the Mesopelagic Zone. *Frontiers in Ecology and Evolution*, *9*. https://doi.org/10.3389/fevo.2021.574877

Govindarajan, A. F., McCartin, L., Adams, A., Allan, E., Belani, A., Francolini, R., Fujii, J., Gomez-Ibañez, D., Kukulya, A., Marin, F., Tradd, K., Yoerger, D. R., McDermott, J. M., & Herrera, S. (2022). Improved biodiversity detection using a large-volume environmental DNA sampler with in situ filtration and implications for marine eDNA sampling strategies. *Deep Sea Research Part I: Oceanographic Research Papers*, *189*, 103871.

Govindarajan, A. F., Llopiz, J. K., Caiger, P. E., Jech, J. M., Lavery, A. C., McMonagle, H., Wiebe, P. H., & Zhang, W. (gordon). (2023). Assessing mesopelagic fish diversity and diel vertical migration with environmental DNA. *Frontiers in Marine Science*, *10*. https://doi.org/10.3389/fmars.2023.1219993

Harrison, J. B., Sunday, J. M., & Rogers, S. M. (2019). Predicting the fate of eDNA in the environment and implications for studying biodiversity. *Proceedings. Biological Sciences / The Royal Society*, *286*(1915), 20191409.

Hickerson, E. L., Schmahl, G. P., Robbart, M., Precht, W. F., & Caldow, C. (2008). The state of coral reef ecosystems of the Flower Garden Banks, Stetson Bank, and other banks in the northwestern Gulf of Mexico. *The State of Coral Reef Ecosystems of the United States and Pacific Freely Associated States*, 189–217.

Hoban, M. L., Bunce, M., & Bowen, B. W. (2023). Plumbing the depths with environmental DNA (eDNA): Metabarcoding reveals biodiversity zonation at 45-60 m on mesophotic coral reefs. *Molecular Ecology*, *32*(20), 5590–5608.

Jerde, C. L., Olds, B. P., Shogren, A. J., Andruszkiewicz, E. A., Mahon, A. R., Bolster, D., & Tank, J. L. (2016). Influence of Stream Bottom Substrate on Retention and Transport of Vertebrate Environmental DNA. *Environmental Science & Technology*, *50*(16), 8770–8779.

Kutti, T., Johnsen, I. A., Skaar, K. S., Ray, J. L., Husa, V., & Dahlgren, T. G. (2020). Quantification of eDNA to Map the Distribution of Cold-Water Coral Reefs. *Frontiers in Marine Science*, *7*. https://doi.org/10.3389/fmars.2020.00446

Jeunen, G.-J., Knapp, M., Spencer, H. G., Lamare, M. D., Taylor, H. R., Stat, M., Bunce, M., & Gemmell, N. J. (2019). Environmental DNA (eDNA) metabarcoding reveals

strong discrimination among diverse marine habitats connected by water movement. *Molecular Ecology Resources*, *19*(2), 426–438.

Jeunen, G.-J., Lamare, M. D., Knapp, M., Spencer, H. G., Taylor, H. R., Stat, M., Bunce, M., & Gemmell, N. J. (2020). Water stratification in the marine biome restricts vertical environmental DNA (eDNA) signal dispersal. *Environmental DNA (Hoboken, N.J.)*, *2*(1), 99–111.

Jumars, P. A., Dorgan, K. M., & Lindsay, S. M. (2015). Diet of worms emended: an update of polychaete feeding guilds. *Annual Review of Marine Science*, *7*, 497–520.

Kelly, R. P., Shelton, A. O., & Gallego, R. (2019). Understanding PCR Processes to Draw Meaningful Conclusions from Environmental DNA Studies. *Scientific Reports*, *9*(1), 12133.

Leray, M., Yang, J. Y., Meyer, C. P., Mills, S. C., Agudelo, N., Ranwez, V., Boehm, J. T., & Machida, R. J. (2013). A new versatile primer set targeting a short fragment of the mitochondrial COI region for metabarcoding metazoan diversity: application for characterizing coral reef fish gut contents. *Frontiers in Zoology*, *10*(1), 34.

Love, M. I., Huber, W., & Anders, S. (2014). Moderated estimation of fold change and dispersion for RNA-seq data with DESeq2. *Genome Biology*, *15*(12), 550.

Lugo-Fernández, A. (1998). Ecological Implications of Hydrography and Circulation to the Flower Garden Banks, Northwest Gulf of Mexico. *Gulf of Mexico Science*, *16*(2), 4.

Martin, M. (2011). Cutadapt removes adapter sequences from high-throughput sequencing reads. *EMBnet.journal*, *17*(1), 10–12.

McCartin, L. J., Vohsen, S. A., Ambrose, S. W., Layden, M., McFadden, C. S., Cordes, E. E., McDermott, J. M., & Herrera, S. (2022). Temperature Controls eDNA Persistence across Physicochemical Conditions in Seawater. *Environmental Science & Technology*, *56*(12), 8629–8639.

McCartin, L. J., Saso, E., Vohsen, S. A., Pittoors, N. C., Demetriades, P., McFadden, C. S., Quattrini, A. M., & Herrera, S. (2023). Nuclear eDNA Metabarcoding Primers for Anthozoan Coral Biodiversity Assessment. In *bioRxiv* (p. 2023.10.26.564240). https://doi.org/10.1101/2023.10.26.564240

McMurdie, P. J., & Holmes, S. (2013). phyloseq: an R package for reproducible interactive analysis and graphics of microbiome census data. *PloS One*, *8*(4), e61217.

Michna, P., & Woods, M. (2013). RNetCDF - A Package for Reading and Writing NetCDF Datasets. *The R Journal*, *5*, 29.

Miya, M., Sato, Y., Fukunaga, T., Sado, T., Poulsen, J. Y., Sato, K., Minamoto, T., Yamamoto, S., Yamanaka, H., Araki, H., Kondoh, M., & Iwasaki, W. (2015). MiFish, a set of universal PCR primers for metabarcoding environmental DNA from fishes: detection of more than 230 subtropical marine species. *Royal Society Open Science*, *2*(7), 150088.

Monuki, K., Barber, P. H., & Gold, Z. (2021). eDNA captures depth partitioning in a kelp forest ecosystem. *PloS One*, *16*(11), e0253104.

Murakami, H., Yoon, S., Kasai, A., Minamoto, T., Yamamoto, S., Sakata, M. K., Horiuchi, T., Sawada, H., Kondoh, M., Yamashita, Y., & Masuda, R. (2019). Dispersion and degradation of environmental DNA from caged fish in a marine environment. *Fisheries Science: FS*, *85*(2), 327–337.

Oksanen, J., Kindt, R., Legendre, P., O'Hara, B., Stevens, M. H. H., Oksanen, M. J., & Suggests, M. (2007). The vegan package. *Community Ecology Package*, *10*(631-637), 719.

Pante, E., & Simon-Bouhet, B. (2013). marmap: A package for importing, plotting and analyzing bathymetric and topographic data in R. *PloS One*, *8*(9), e73051.

Port, J. A., O'Donnell, J. L., Romero-Maraccini, O. C., Leary, P. R., Litvin, S. Y., Nickols, K. J., Yamahara, K. M., & Kelly, R. P. (2016). Assessing vertebrate biodiversity

in a kelp forest ecosystem using environmental DNA. *Molecular Ecology*, *25*(2), 527–541.

Rezak, R., Bright, T. J., & Mcgrail, D. (1985). Reefs and banks of the northwestern Gulf of Mexico: Their geological, biological, and physical dynamics.

Robinson, K. M., Prentice, C., Clemente-Carvalho, R., Hall, K., Monteith, Z. L., Morien, E., Olson, A. M., Pontier, O., Hessing-Lewis, M., Kellogg, C. T. E., & Lemay, M. A. (2023). Paired environmental DNA and dive surveys provide distinct but complementary snapshots of marine biodiversity in a temperate fjord. *Environmental DNA (Hoboken, N.J.)*, *5*(3), 597–612.

Sammarco, P. W., Nuttall, M. F., Beltz, D., Hickerson, E. L., & Schmahl, G. P. (2016). Patterns of Mesophotic Benthic Community Structure on Banks Off vs Inside the Continental Shelf Edge, Gulf of Mexico. *Gulf of Mexico Science*, *33*(1), 7.

Sansom, B. J., & Sassoubre, L. M. (2017). Environmental DNA (eDNA) Shedding and Decay Rates to Model Freshwater Mussel eDNA Transport in a River. *Environmental Science & Technology*, *51*(24), 14244–14253.

Shea, M. M., & Boehm, A. B. (2024). Environmental DNA metabarcoding differentiates between micro-habitats within the rocky intertidal. *Environmental DNA (Hoboken, N.J.)*, *6*(2). https://doi.org/10.1002/edn3.521

Shogren, A. J., Tank, J. L., Andruszkiewicz, E. A., Olds, B., Jerde, C., & Bolster, D. (2016). Modelling the transport of environmental DNA through a porous substrate using continuous flow-through column experiments. *Journal of the Royal Society, Interface / the Royal Society*, *13*(119), 20160290.

Shogren, A. J., Tank, J. L., Andruszkiewicz, E., Olds, B., Mahon, A. R., Jerde, C. L., & Bolster, D. (2017). Controls on eDNA movement in streams: Transport, Retention, and Resuspension. *Scientific Reports*, *7*(1), 5065.

Spens, J., Evans, A. R., & Halfmaerten, D. (2017). Comparison of capture and storage methods for aqueous macrobial eDNA using an optimized extraction protocol: advantage of enclosed filter. *Methods in Ecology and Evolution / British Ecological Society*. https://doi.org/10.1111/2041-210X.12683

Snyder, E. D., Tank, J. L., Brandão-Dias, P. F. P., Bibby, K., Shogren, A. J., Bivins, A. W., Peters, B., Curtis, E. M., Bolster, D., Egan, S. P., & Lamberti, G. A. (2023). Environmental DNA (eDNA) removal rates in streams differ by particle size under varying substrate and light conditions. *The Science of the Total Environment*, *903*, 166469.

Wang, Q., Garrity, G. M., Tiedje, J. M., & Cole, J. R. (2007). Naive Bayesian classifier for rapid assignment of rRNA sequences into the new bacterial taxonomy. *Applied and Environmental Microbiology*, *73*(16), 5261–5267.

West, K. M., Stat, M., Harvey, E. S., Skepper, C. L., DiBattista, J. D., Richards, Z. T., Travers, M. J., Newman, S. J., & Bunce, M. (2020). eDNA metabarcoding survey reveals fine-scale coral reef community variation across a remote, tropical island ecosystem. *Molecular Ecology*, *29*(6), 1069–1086.

West, K. M., Harry, A. V., Payet, S., Harvey, E., Travers, M. J., Rangers, D., Rangers, B.-J., Rangers, K., & Managers, Y. C. (2024). Comparative assessment of eDNA metabarcoding and longline deployments for elasmobranch surveying across a large tropical marine park network. *Aquatic Conservation: Marine and Freshwater Ecosystems*, *34*(4). https://doi.org/10.1002/aqc.4144

Wickham, H., Averick, M., Bryan, J., Chang, W., McGowan, L., François, R., Grolemund, G., Hayes, A., Henry, L., Hester, J., Kuhn, M., Pedersen, T., Miller, E., Bache, S., Müller, K., Ooms, J., Robinson, D., Seidel, D., Spinu, V., Takahashi, K., Vaughan, D., Wilke, C., Woo, K., & Yutani, H. (2019). Welcome to the tidyverse. *Journal of Open Source Software*, *4*(43), 1686.

CHAPTER 6

CONCLUSION

The objectives of this dissertation research were specifically to provide new tools for the analysis of eDNA from corals, and more generally to develop a conceptual framework for understanding spatiotemporal resolution of data generated through eDNA analysis. By accomplishing these objectives, the biodiversity of corals and their distribution can be rapidly and accurately assessed and monitored through eDNA analysis. Further, eDNA sequencing data can be interpreted with an appropriately nuanced appreciation for the influences of environmental and methodological factors on the spatiotemporal distribution of eDNA.

By conducting controlled, experimental studies, Chapters 2 and 3 establish that higher temperatures and microbial processes act in synergy to promote the degradation rate of marine eDNA. The broader implication of this finding for marine eDNA analysis is that eDNA may persist for longer periods of time and thus be transported over larger distances in the cold waters, like in the deep sea, than in warmer waters, like at mesophotic coral communities. This work was the first to concurrently examine the effect of multiple physicochemical (temperature, pH and dissolved oxygen concentration) and biotic factors (bacterial community composition and abundance) on marine eDNA degradation in a controlled experimental setting. These experiments pave the way for future efforts to pin down the exact biomolecular pathways through which marine eDNA predominantly degrades.

Chapter 4 presents new PCR primers for specifically sequencing the *28S* gene in anthozoan corals from eDNA samples. Through both *in silico* analysis and by

metabarcoding water samples take near mesophotic and deep-sea corals, the efficacy of metabarcoding with these primers is demonstrated. Library preparation using the primers enriched coral eDNA from samples across depths of 55 to 531 meters, and in some cases virtually all the eDNA in a sample was derived from corals. Other, off target marine invertebrates that were sequenced using this method included sponges, ctenophores, and medusozoans, demonstrating the potential utility of the primers for more taxa than originally intended. Future work to develop a broader *28S* metabarcoding strategy for these taxa in addition to corals is being pursued. By sequencing museum collections and recent collections from expeditions to places like Puerto Rico, the *28S* reference barcode database will continue to grow to comprehensively assess the biodiversity of deep corals and sponges in regions other than the Gulf of Mexico.

Chapter 5 directly investigated the implications of eDNA transport, in both the vertical and horizontal dimensions, for interpreting species detections from eDNA metabarcoding data. This work answers a complicated question in an elegant, practical manner. Does the detection of a species in eDNA sequencing data represent the presence of that species nearby to the sampling location, or could it represent eDNA that may have been transported to the sampling location over substantial distances? This work demonstrated that vertical transport of eDNA is limited in a stratified water column. However, eDNA was transported horizontally over substantial distances from its plausible source, and the detection of this horizontally transported eDNA depended on the sensitivity of the molecular laboratory protocol used. In data generated using the *28S* primers designed and tested in Chapter 4, there was strong evidence for the horizontal transport of coral eDNA in samples taken in the water column over distances of nearly

1.5 kilometers, assuming no vertical transport. On the contrary, in the same samples coral eDNA was not repeatedly detected in sequencing data generated using a primer set that broadly amplifies eukaryotes. Methods for eDNA metabarcoding and quantification exist along a gradient of sensitivity, from metabarcoding using primers designed to amplify eDNA from many taxa to quantitative and digital-droplet PCR assays using primers designed to a single species. From the results of this chapter, it can be expected that with increasing sensitivity and taxonomic specificity, the spatial resolution of eDNA data is coarser, and the importance of considering eDNA transport as a source of species detections is greater. Considering this methodological factor in addition to water temperature allows the analyst to more confidently determine the spatial accuracy of a species' detection in eDNA data generated from field samples. This determination is necessary to integrate species detections and biodiversity metrics from eDNA analysis with those from conventional approaches.

The work in these chapters is part of a greater eDNA revolution, as eDNA analysis continues to rapidly gain traction in both academic and government settings as a technique to characterize, monitor, and conserve biodiversity in the ocean at necessarily rapid timescales. While the analysis of eDNA is unequivocally a powerful tool for these purposes, a nuanced interpretation of these data is necessary for this tool's appropriate application. By determining both the environmental and methodological factors that govern the interpretation of eDNA data, through this work we can harness the power of eDNA analysis to map the distributions of marine species and monitor the biodiversity of marine ecosystems over time.

Publication and co-authorship notes

Chapter 2 was published in *Environmental Science & Technology* in 2022 with co-authors Dr. Samuel A. Vohsen, Susan W. Ambrose, Dr. Michael Layden, Dr. Catherine S. McFadden, Dr. Erik E. Cordes, Dr. Jill M. McDermott, Dr. Santiago Herrera. The digital object identifier for this publication is https://doi.org/10.1021/acs.est.2c01672.

Chapter 3 was co-authored with Dr. Samuel A. Vohsen, Penny Demetriades, Luis Caceres, Maia Clayton, Carly Hecht, Mary Mahoney, Petra Oganovich, Dr. Jill M. McDermott and Dr. Santiago Herrera. This chapter will be incorporated into another publication regarding the influence of microbes on the degradation of eDNA.

Chapter 4 was released as a preprint and has been submitted for publication with co-authors Emma Saso, Dr. Samuel A. Vohsen, Nicole Pittors, Penny Demetriades, Dr. Catherine S. McFadden, Dr. Andrea M. Quattrini, and Dr. Santiago Herrera. The digital object identifier associated with the preprint is https://doi.org/10.1101/2023.10.26.564240.

Chapter 5 was co-authored with Dr. Annette F. Govindarajan, Dr. Jill M. McDermott, and Dr. Santiago Herrera. This chapter will be released as a preprint and submitted for publication in late summer 2024.

APPENDIX A

SUPPORTING INFORMATION FOR CHAPTER 2

A.1 Supplementary Methods

A.1.1 *Coral Collection Methods*

Coral samples were collected at the seafloor (ambient temperature: ~ 8°C) using the remotely operated vehicle (ROV) *Jason* (operated by the Woods Hole Oceanographic Institution) and stored in a hydraulically operated, insulated bio-box until recovery of the submersible. Upon recovery, the samples were immediately transferred to aquaria with natural seawater inside a shipboard cold room kept at a constant temperature of 8°C. Partial water changes were made regularly while at sea using natural seawater collected from depth. Upon return to port, corals were transported overnight to Temple University and housed in a 550 L recirculating aquarium, where they were kept alive. Live fragments were removed from the aquarium, placed in sterile Whirl-Pak collection bags (Whirl-Pak, Madison, WI, USA), frozen, and transported on dry ice to Lehigh University (Bethlehem, PA, USA), and subsequently stored at -80°C until use.

A.1.2 Preparation of Source eDNA

A coral fragment was thawed in a sterile Whirl-Pak, and any ASW adhering to the coral tissue was allowed to drip off. The fragment was transferred to a new sterile Whirl-Pak. The tissue was removed from the skeleton into the Whirl-Pak using the water-jet dental flosser pre-filled with artificial seawater (ASW). The resulting mixture of coral tissue and ASW was homogenized using a FisherBrand 150 Handheld Homogenizer (ThermoFisher Scientific, Waltham, MA, USA). The homogenized slurry was transferred

to sterile 15 mL centrifuge tubes (Celltreat, Pepperell, MA, USA). This dilute tissue homogenate was frozen at stored at -80°C until it was used. The concentration of each tissue homogenate preparation was calculated by dividing the difference between the wet weight of the coral fragment and the bare skeleton by the total volume of ASW used from the water-jet dental flosser reservoir.

It was necessary to use frozen coral tissue rather than live coral as the source of eDNA for the experiments. Originally, we attempted to use water from live *Lophelia* housed at Temple University as the source of eDNA for the experiments. However, it took more than 24 hours for water to equilibrate to our desired experimental conditions (i.e. come to temperature from 8°C). As our data demonstrate, over this time period eDNA rapidly degraded (the "initial phase" of eDNA degradation). Not only would we have missed the initial phase, but this method would have also made comparisons among experiments at different temperatures impossible due to the varying times it would take to reach each desired temperature. For example, preliminary experiments at 20°C required many hours longer to reach target temperature than the 10°C experiments. Thus, we chose to use coral tissue homogenate as a way to correct this problem. We were able to equilibrate seawater to the target conditions before adding the source eDNA. This approach also allowed us to control the state of eDNA and use a consistent starting concentration in all experiments.

We confirmed that each preparation had similar concentrations of *Lophelia* DNA by filtering 500 mL of ASW with a small volume of the homogenate added over a 0.22 μM Sterivex filter. DNA was extracted from the filter, and quantitative PCR (qPCR) was performed as described later in the main text to quantify the concentration of *Lophelia*

DNA in each preparation. The volume of tissue homogenate added to each experiment was adjusted based on the results of this qPCR to ensure that starting concentrations for each experiment were comparable.

A.1.3 Primer Design and qPCR Assay Optimization

Primers were designed to be as specific to *Lophelia* as possible, have an annealing temperature close to 60°C, and minimize unwanted molecular interactions, such as self-complementarity. Forward and reverse primers were queried in GenBank by performing a BLASTN search to confirm specificity. In addition, we utilized the R package PrimerTree, which is designed to test the specificity of eDNA primers further and predict possible PCR products[1]. The only hits with 0 mismatches in both the forward and reverse primers were to *Desmophyllum dianthus* and *Solenosmilia variabilis*, both in the same family as *Lophelia* (Caryophylliidae). Thus, these primers are highly specific to caryophylliid scleractinians. However, they likely cannot distinguish among different caryophylliid species. Further testing on tissue samples from closely-related caryophylliids is necessary before using these primers if species-specific quantification is desired.

The primer concentrations for the qPCR assay were optimized by testing the assay on *Lophelia* tissue extracts with 300 and 500 nM primer concentrations. To remove potential PCR inhibitors before testing, the tissue extracts were cleaned using a Qiagen DNEasy PowerClean Cleanup Kit following the manufacturer's protocol with a final elution volume of 50 µL. Ten cleaned extracts were pooled to a final volume of 500 µL, and DNA concentration and purity were measured using a NanoDrop One

spectrophotometer (ThermoFisher). The measured concentration of the pooled extract was 55.5 ng/μL, and the 280/260 and 260/230 ratios were 1.87 and 2.20, respectively. 6 μL of five-fold dilutions of the template in water from 1:50 to 1:10,000 were amplified in triplicate with 500 and 300 nM primer concentrations using the cycling conditions and reagents described in the main text. With primer concentrations of 300 nM, all triplicates of each concentration amplified (18 of 18 total). Further, coefficients of variation (CV), as calculated in Klymus *et al.*[2], were low (0.032 to 0.120) among triplicates of all concentrations except the lowest concentration (CV = 0.764). With primer concentrations of 500 nM, a triplicate at two template dilutions, 1:100 and 1:10,000, failed to amplify. Additionally, coefficients of variation for 1:50 and 1:5,000 dilutions were high, 2.520 and 232.611, respectively. The respective efficiencies of the reactions at 300 nM and 500 nM were 75.32% and 72.23%. Thus, we determined that the optimum primer concentration was 300 nM.

A.1.4 Determination of the Limits of Quantification and Detection

A standard curve was created using purified plasmids containing the target fragment of *Lophelia* COI at multiple standard concentrations. The gene fragment was amplified from *Lophelia* tissue using conventional PCR, purified, and ligated to a plasmid vector using the pGEM-T Vector System and following the manufacturer's protocol (Promega, Madison, Wisconsin, USA). The pGEM-T vector contains a gene for ampicillin resistance. The plasmid was transformed into competent *E. coli* cells through a heat shock for 30 seconds at 43°C and a subsequent cooling on ice for 2.5 minutes. Following the heat shock, the cells were incubated at 37°C in nutrient broth, plated onto

nutrient agar with ampicillin, and incubated at 37°C overnight. The pGEM-T vector contains T7 and SP6 promoters that flank the insertion. A colony was picked, and the inserted fragment was PCR amplified using forward and reverse primers specific to these promoter regions to confirm that transformation was successful. The PCR products were imaged on a 1.5% agarose TBE gel dyed with GelRed (Biotium, Fremont, CA, USA) to confirm products of the correct amplicon size. These products were cleaned using a QIAQuick PCR Purification Kit (Qiagen, Hilden, Germany) and Sanger sequenced. After the transformation was confirmed, plasmids were purified from the picked colonies using the GeneJET Plasmid Miniprep kit (ThermoFisher Scientific).

The DNA concentrations of the purified plasmids were measured with the Qubit 1X High-sensitivity dsDNA assay. Purified plasmids were serially diluted ten-fold nine times from 0.42 ng/µL (778,000,000 copies per reaction) to 4.2 x 10^{-10} ng/µL (0.778 copies per reaction), yielding ten standards for creating a standard curve. The number of copies of the *Lophelia* COI fragment in each plasmid standard was calculated by multiplying the ratio of the mass of the amplicon in kDa to the known mass of the plasmid plus the mass of the inserted amplicon. The limits of quantification (LOQ) and limits of detection (LOD) of the qPCR assay were determined following the methods of Klymus *et al.*[2]. The discrete LOQ (the standard plasmid concentration at which the coefficient of variation exceeded 0.35) was 77.8 copies per reaction. The modeled LOD of the assay with three qPCR replicates was 3.4 copies per reaction. The qPCR run to determine the LOQ and LOD consisted of seven plasmid standards ranging from 4.2 x 10^{-4} ng/µL to 4.2 x 10^{-10} ng/µL (778,000 to 0.778 copies per reaction), each replicated ten times and two PCR negative controls. The qPCR reaction was conducted in the same

manner as described in the main text. The R^2 for this standard curve qPCR run was 0.99818, and the doubling efficiency was 87%. The slope of the line of best fit was -3.681 C_q per magnitude decrease in concentration and the intercept was 5.455 C_q.

A.1.5 qPCR Inhibition Testing

To test if eDNA extracts from our experiments were PCR-inhibited, we performed a dilution series using 6 eDNA samples. Samples were chosen that corresponded to the earliest time points in 6 separate experiments, when eDNA concentrations were highest. We chose samples that collectively spanned the temperature, pH and [DO] levels that we tested, and spanned the time over which we conducted the experiments (from June 2020 to March 2021) to account for different batches of artificial seawater. qPCR was performed as described in the main text, with 4 standard concentrations in triplicate, a PCR negative control in triplicate, and the 18 undiluted and diluted eDNA samples in triplicate. Undiluted extracts were diluted 1:10 and 1:100, such that effectively 0.6 µL, 0.06 µL and 0.006 µL of template was added into the reactions. The results of this dilution series test indicated that there was no PCR inhibition. Measured concentrations for each of the six samples decreased by an order of magnitude with each dilution, as expected (**Table S9**). The R^2 of the standard curve for the run was 0.98941, the efficiency was 0.86, the slope was -3.718 and the intercept was 4.262.

A.1.6 Quantification of caryophylliid eDNA concentrations at Viosca Knoll 826

On August 6, 2021, we conducted a remotely-operated vehicle (ROV) dive and two CTD casts at Viosca Knoll 826 (29°09.473' N, 88°00.931' W), a site at

approximately 470 meters depth in the Gulf of Mexico that supports high densities of *Lophelia*. The ROV *Global Explorer*, operated by Oceaneering, Morgan City, LA, USA, was deployed from the *R/V Point Sur* and situated the ROV on the seafloor directly adjacent and down current from a dense colony of live *Lophelia*. Three ~1.7L Niskin bottles mounted to the ROV and directly adjacent to the live coral colonies were remotely triggered. Following the ROV dive, two CTD casts were conducted as close to the site of the ROV dive as possible using a Seabird 911plus CTD rosette with twelve 12-litter Niskin bottles mounted to the rosette. Water samples were collected by the remote triggering of the Niskin bottles at altitudes of approximately 1 meter, 5 meters, 10 meters, and 20 meters above the seafloor. Water samples were filtered for eDNA using the same equipment and equipment sterilization protocols as the eDNA persistence experiments described previously. The average volume of ROV samples filtered for eDNA was 1.05 liters. The average volume of CTD samples filtered for eDNA was substantially greater, 5.08 liters, due to the larger volume of the Niskin bottles mounted on the CTD rosette. The samples were stored at -80°C without a preservation buffer at sea, transported on dry ice back to the lab, and then stored at -80°C before eDNA extraction.

To monitor for contamination in the field, deionized water generated on the *R/V Point Sur* using the Beckman B-Pure System and Thermofisher D0803 filter cartridges was filtered after the ROV dive and the second CTD cast. This sample served as a sampling negative control and was processed alongside eDNA samples. eDNA was extracted from the samples using the Qiagen Blood & Tissue Kit as already described. Caryophylliid COI fragment copies were quantified using the same qPCR assay as for the persistence experiments, except that 3.0 µL of the DNA extract was amplified, rather than

0.6 µL. Sampling negative controls, extraction negative controls, and PCR negative controls were processed alongside field samples to monitor for contamination in the lab. None of these negative control samples amplified.

A.2 Supplementary Figures

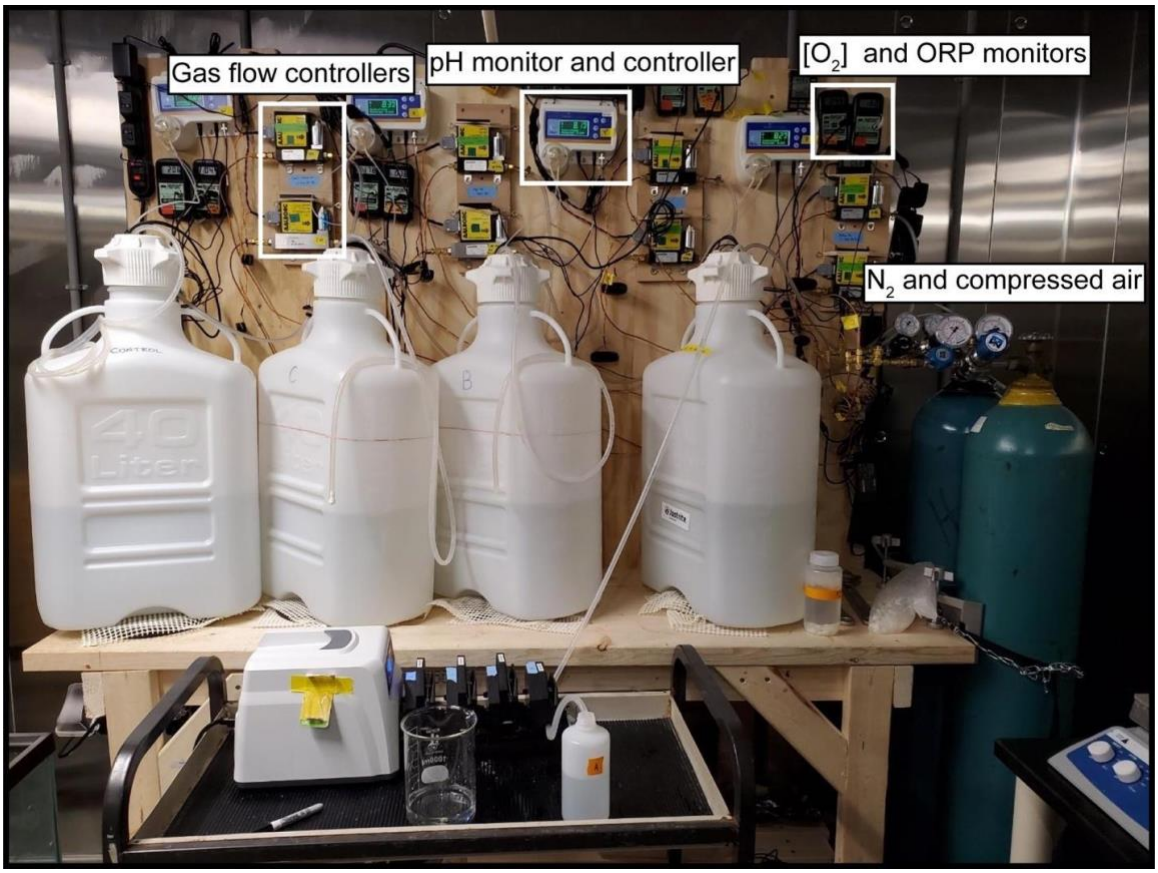

Figure A.1: Photograph of the experimental setup in the controlled-temperature room. Up to four experiments, including a control experiment, were conducted simultaneously.

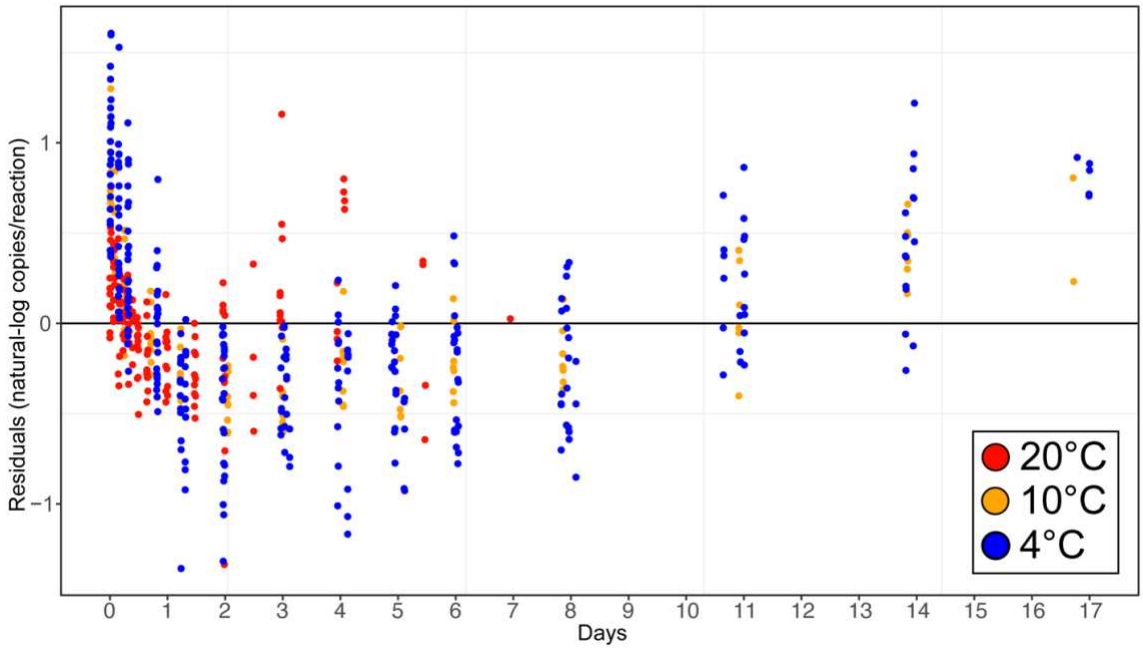

Figure A.2: Residuals over time from a simple exponential model fit as a linear model to natural-log transformed eDNA concentration data over the course of 22 eDNA persistence experiments. Points are colored by the temperature at which each experiment was conducted.

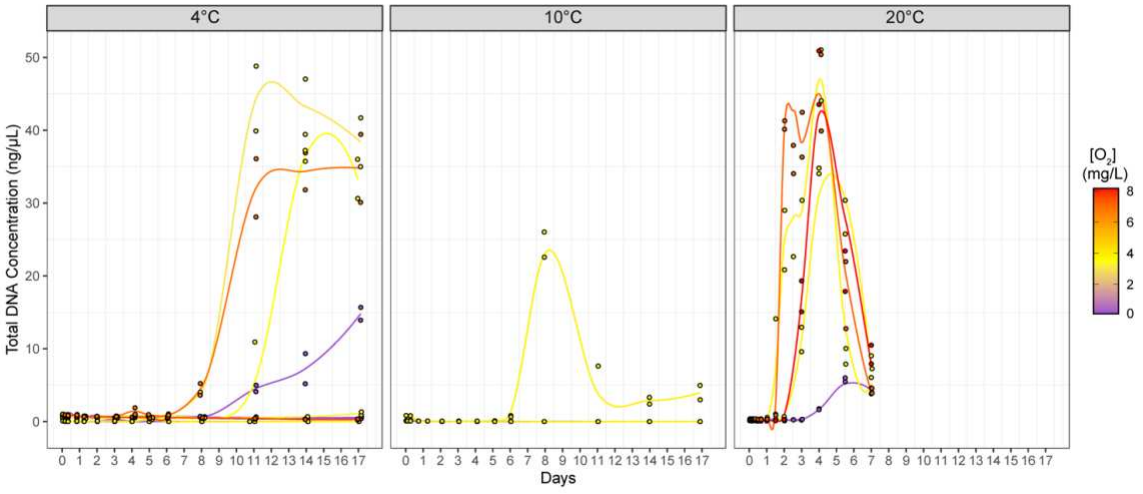

Figure A.3: Plots of total DNA concentrations (from any source) measured using Qubit fluorometry over the time course of 22 eDNA persistence experiments among a range of

temperatures, pH and [DO]. Each point represents a measurement from an individual DNA extraction. Points are fit with a loess smoothing curve to aid in the visualization of trends over time.

A.3 Supplementary Tables

Table A.1: Statistics summarizing the fits of linear models and segmented linear models to log-transformed eDNA concentration data over time to estimate exponential decay rate constants for single-phase and biphasic decay models. Between single-phase and biphasic models, lower BIC values and non-significant P-values are bolded. *pH for each experiment was measured at the ambient temperature in the cold room set for each experiment and at 1 bar.

Table A.1 is included in the supplementary Excel workbook.

Table A.2: Parameters for simple and biphasic exponential models of eDNA decay among 22 eDNA persistence experiments conducted under 11 unique sets of physicochemical factors. *pH for each experiment was measured at the ambient temperature in the cold room set for each experiment and at 1 bar. **Decay rate constants for the initial and second phases of eDNA degradation, as given by the fit of a biphasic exponential model, are separated by commas in that order.

Table A.2 is included in the supplementary Excel workbook.

Table A.3: Summary of the linear mixed model fit to the first phase data for twenty-one eDNA persistence experiments to investigate the role of temperature, pH, [DO] and relevant covariates in controlling eDNA degradation rate. The model formula was LN(eDNA Conc.) ~ Temp.*Time + pH*Time + [DO]*Time + ORP*Time + (1 + Time | Experiment).

Table A.3 is included in the supplementary Excel workbook.

Table A.4: Summary of the linear mixed model fit to the second phase data for twenty-one eDNA persistence experiments to investigate the role of temperature, pH, [DO] and relevant covariates in controlling eDNA degradation rate. The model formula was LN(eDNA Conc.) ~ Temp.*Time + pH*Time + [DO]*Time + ORP*Time + LN(Max total DNA concentration + 1)*Time + (1 + Time | Experiment).

Table A.4 is included in the supplementary Excel workbook.

Table A.5: Summary of the linear mixed model fit to the second phase data for eDNA persistence experiments conducted at pH 8.2, 4°C, and 20°C to investigate the role of [DO] on eDNA degradation rate. The model formula was LN(eDNA Conc.) ~ Temp.*Time + [DO]*Time + ORP*Time + LN(Max total DNA concentration + 1)*Time + (1 + Time | Experiment).

Table A.5 is included in the supplementary Excel workbook.

Table A.6: Summary of the linear mixed model fit to the second phase data for eDNA persistence experiments conducted at 4°C and 10°C, to investigate the role of pH and relevant covariates in controlling eDNA degradation rate. The model formula was LN(eDNA Conc.) ~ Temp.*Time + pH*Time + [DO]*Time + ORP*Time + LN(Max total DNA concentration + 1)*Time + (1 + Time | Experiment).

Table A.6 is included in the supplementary Excel workbook.

Table A.7: Data from previous studies and this study included in the analysis of $T_{99.9\%}$, or the calculated time point at which 99.9% of the starting concentration of eDNA degrades.

Table A.7 is included in the supplementary Excel workbook.

Table A.8: Concentrations of caryophylliid eDNA from seawater samples at Viosca Knoll 826, ~ 470 meters depth in the Gulf of Mexico. "ND" represents no detection or the instance wherein a qPCR triplicate did not amplify.

Table A.8 is included in the supplementary Excel workbook.

Table A.9: Measured concentrations of undiluted and diluted eDNA samples to test for PCR inhibition.

Table A.9 is included in the supplementary Excel workbook.

A.4 References

Cannon, M. V.; Hester, J.; Shalkhauser, A.; Chan, E. R.; Logue, K.; Small, S. T.; Serre, D. In Silico Assessment of Primers for EDNA Studies Using PrimerTree and Application to Characterize the Biodiversity Surrounding the Cuyahoga River. *Sci Rep-uk* 2016, *6* (1), 22908. https://doi.org/10.1038/srep22908.

Klymus, K. E.; Merkes, C. M.; Allison, M. J.; Goldberg, C. S.; Helbing, C. C.; Hunter, M. E.; Jackson, C. A.; Lance, R. F.; Mangan, A. M.; Monroe, E. M.; Piaggio, A. J.; Stokdyk, J. P.; Wilson, C. C.; Richter, C. A. Reporting the Limits of Detection and Quantification for Environmental DNA Assays. *Environ Dna* 2020, *2* (3), 271–282. https://doi.org/10.1002/edn3.29.

APPENDIX B

SUPPORTING INFORMATION FOR CHAPTER 3

B.1 Supplementary Figures

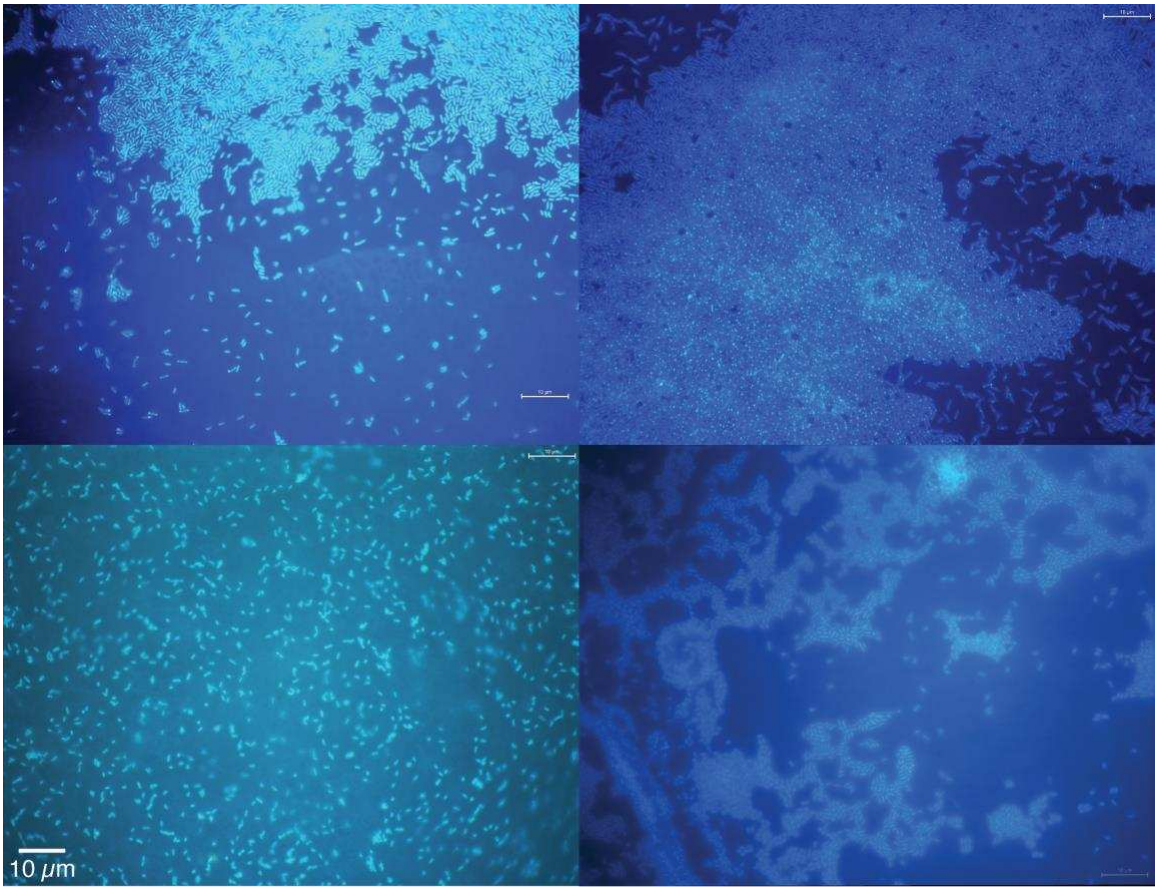

Figure B.1: Representative images of bacterial cells from eDNA persistence experiments conducted at temperatures of 20°C (top left), 10°C (top right), 4°C (bottom left), and in a sampling negative control tank at 20°C (bottom right). The bottom two images are stacked composites of multiple images taken at the same location with slight differences in the focal plane. Composite images were generated using Adobe photoshop and the brightness/contrast were adjusted using the auto setting. Each image was taken at 100X

magnification with a 10 µm scale bar included, and scale bars are consistent across the images. The scale bar on the bottom left with enlarged text is superimposed to aid in visualization.

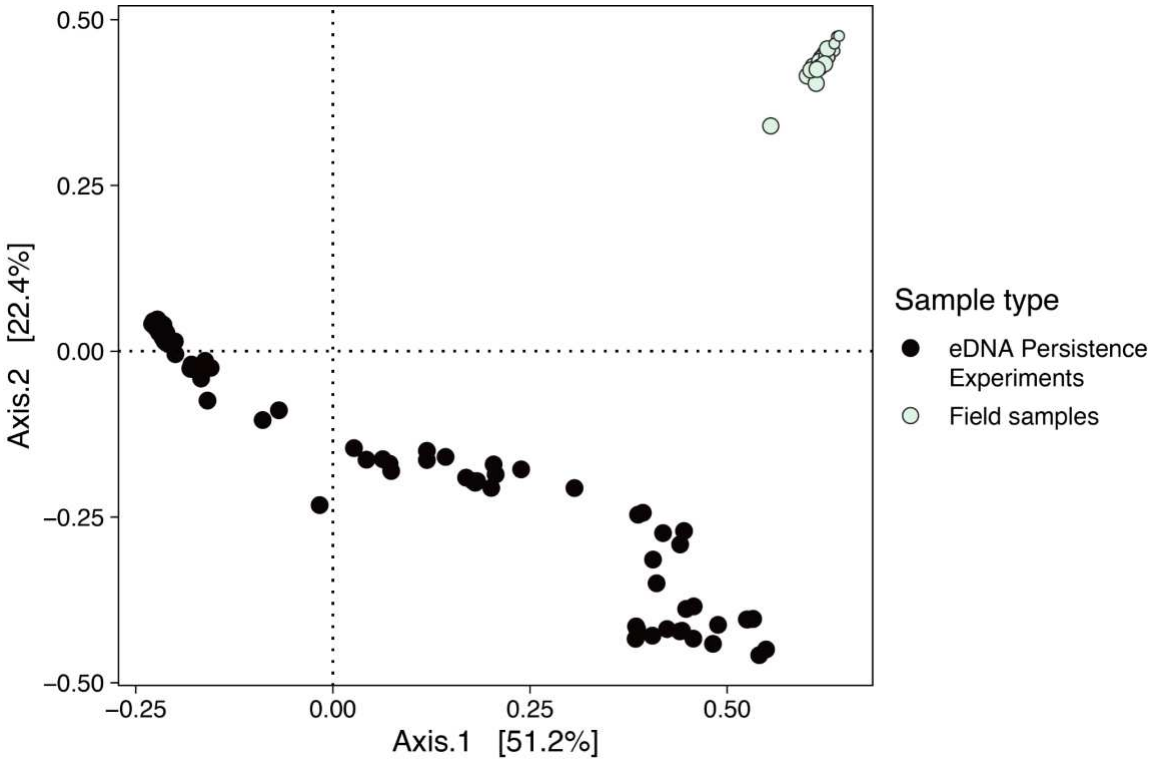

Figure B.2: Visualization of principal coordinates analysis (PCoA) of Bray-Curtis distances between experimental and field samples calculated based on the proportion of sequencing reads from each classified Genus in the dataset.

B.2 Supplementary Tables

Table B.1: Bacteria detected in *16S* metabarcoding data from samples taken during twenty two eDNA persistence experiments.

Rank-order abundance	Phylum	Sequencing reads	Proportion of sequencing reads
1	Proteobacteria	5692589	0.9872575
2	Firmicutes	39277	0.0068118
3	Campylobacterota	12800	0.0022199
4	Bacteroidota	10602	0.0018387
5	Desulfobacterota	3534	0.0006129
6	Actinobacteriota	3346	0.0005803
7	Dadabacteria	855	0.0001483
8	Patescibacteria	595	0.0001032
9	SAR324 clade (Marine group B)	332	0.0000576
10	Bdellovibrionota	325	0.0000564
11	Dependentiae	296	0.0000513
12	Marinimicrobia (SAR406 clade)	251	0.0000435
13	Acidobacteriota	213	0.0000369
14	Sumerlaeota	208	0.0000361
15	Calditrichota	179	0.0000310
16	Not classified to the phylum level	162	0.0000281
17	NB1-j	131	0.0000227
18	Cyanobacteria	82	0.0000142
19	Chloroflexi	67	0.0000116

20	Myxococcota	62	0.0000108
21	Gemmatimonadota	39	0.0000068
22	Verrucomicrobiota	35	0.0000061
23	Nitrospinota	20	0.0000035
24	Elusimicrobiota	19	0.0000033
25	Spirochaetota	11	0.0000019
26	Planctomycetota	9	0.0000016
27	Armatimonadota	7	0.0000012
28	Nitrospirota	7	0.0000012
29	WPS-2	6	0.0000010
30	Fusobacteriota	4	0.0000007

APPENDIX C

SUPPORTING INFORMATION FOR CHAPTER 4

C.1 Supplementary Methods

C.1.1 Sample collection and conventional DNA barcoding of coral samples from the northwestern Gulf of Mexico

ROVs were equipped with either a 4K or high-definition camera pan and tilt video camera, an Ultra-Short BaseLine (USBL) positioning beacon, and conductivity, temperature, and depth sensors. Branches or entire coral colonies were collected using "coral cutters" on the manipulator arm of the ROV. Samples were stowed in seawater in either an insulated "biobox" or a PVC cylinder with a rubber stopper until ROV recovery. Immediately after the ROV was recovered, the corals were transferred to cooled seawater, and subsamples of coral branches were either flash-frozen in liquid N_2 and stored at -80°C or immersed in 95% ethanol. Genomic DNA was purified from these samples by digestion with Proteinase-K, impurity removal with Ammonium Acetate, precipitation with isopropanol, washing with ethanol, and rehydration in 50 µL of Tris-HCl and EDTA (TE) buffer (dx.doi.org/10.17504/protocols.io.bypypvpw). DNA concentration and quality were assessed using a Nanodrop Spectrophotometer (Thermo Fisher Scientific).

PCR Primers (McFadden & Ofwegen, 2012) were synthesized by Eurofins Genomics, purified by standard desalting, and normalized to 100 µM in TE buffer (pH 8.0). PCR reactions were performed in 25 µL final volume using the Promega GoTaq G2 HotStart Colorless Mastermix in 8-strip tubes. Primer stocks in TE buffer were diluted to

10 µM in molecular-grade water, and 0.25 µL of each forward and reverse primer were added to each reaction for a final concentration of 100 nM. 1 µL of template DNA was amplified in each reaction. The total reaction volume was completed to 25 µL using molecular-grade water. Cycling conditions were as follows: initial denaturation at 95°C for 2 minutes; then 30 cycles of denaturation at 95°C for 30 seconds, annealing at 55°C for 45 seconds, and elongation at 72°C for 25 seconds; and a final elongation at 72°C for 5 minutes. PCR products were then held at 4°C short-term (hours) and frozen at 20°C. Amplification success was confirmed by visualization of the target product size on a 1% agarose gel stained with GelRed (Invitrogen) in TBE buffer run at 110 volts for nearly the entire length of the gel. Samples that did not amplify were diluted 1:10 in TE buffer and the PCR was repeated. If the reaction failed again, the DNA extracts were further purified using the DNEasy PowerClean Cleanup Pro Kit (Qiagen) following the manufacturer's instructions, and the PCR was repeated. PCR products were either purified before shipment using the QIAquick PCR Purification Kit following the manufacturer's protocol or purified at the sequencing facility as a paid service.

Sanger sequencing was conducted in both directions by Eurofins Genomics. Forward and reverse .ab1 chromatogram files were imported into Geneious Prime Version 2021.0.3 (https://www.geneious.com), and bases with an error probability limit of > 1% were trimmed from the ends of the sequences. Trimmed forward and reverse sequences were *de novo* assembled and the consensus sequences were extracted. Base calls were made as the highest peak in the aligned chromatograms. Consensus sequences were aligned using MUSCLE (Edgar 2004) with the default parameters. The resulting

alignment was visually inspected, and the aligned sequences were trimmed to an equal length by removing lower-quality bases at the 3' and 5' ends of the alignment.

C.1.2 PCR optimization

To achieve successful amplification of our samples using the *28S rRNA* primer sets, we tested three master mixes of increasing cost and specificity (as advertised by the manufacturers); increasing numbers of cycles; increasing primer concentrations; increasing concentrations of $MgCl_2$ and multiple annealing temperatures. Optimization reactions were performed on a subset of the eDNA samples collected from mesophotic and deep-sea sites. Specifically, these samples were collected at the seafloor using the ROV at Bright Bank and lease block VK826. Ultimately, we found that these samples were the most challenging to amplify among those tested herein, and thus the conditions presented represent the best strategy we found to encourage amplification across all the samples in our sample set. Purified genomic DNA from *Stichopathes* sp., *Tanacetipathes* sp., *Swiftia exserta*, *Callogorgia delta*, and *Lophelia pertusa* were also included in these reactions as positive controls for each order targeted: Antipatharia, Malacalcyonacea, Scleralcyonacea, and Scleractinia. In all cases, we used the manufacturer-suggested denaturation and elongation durations for the size amplicon we were targeting (approximately 400 bp) and used primers without the added CS1 and CS2 adapters. To assess the success of each reaction, 4 µL of each PCR product from the eDNA samples was visualized on a 1% agarose TBE gel stained with GelRed at 110V for nearly the entire length of the gel. Amplification success was assessed based on the intensity of the

band (strong, faint or absent) and the presence of any products of a different size than the intended product (i.e. off-target bands).

We tested the Promega GoTaq G2 HotStart Mastermix (Promega), KAPA HiFi HotStart Mastermix (KAPA), and Platinum SuperFi II MasterMix (SuperFi II) with primer concentrations of 500 nM, an annealing temperature of 55°C, and 30 to 35 amplification cycles. We found that while the coral tissue extractions amplified in all cases, the eDNA samples did not amplify with either the Promega or KAPA mastermixes. Using the KAPA mastermix, we also tested 1:10 dilutions of our samples under the suspicion that the samples may be inhibited, but we did not see any improvement with the dilution. The SuperFi II mastermix has been shown to be successful for the amplification of fish eDNA from deep-sea environments, where low concentrations of template eDNA are suspected (Kawato et al. 2021). Concordantly, using the Superfi II mastermix, we found that our eDNA samples amplified, albeit weakly, using this mastermix and primer concentrations of 500 μM, an annealing temperature of 55°C and 35 amplification cycles. Increasing the primer concentrations to 1.0 μM and $MgCl_2$ concentrations to 3.25 mM and 4.75 mM, resulted in stronger amplification. However, with stronger amplification we noted the increased prevalence of off-target bands in some samples. To potentially reduce the amplification of off-target templates while preserving amplification strength, we tested increasing annealing temperatures from 56°C to 59°C. Amplification was achieved at annealing temperatures to 58°C, however the presence of off-target bands was not resolved. Thus, to encourage specificity to our target as much as possible, we settled on using a ‘touchdown’ protocol,

with 15 cycles of annealing temperatures from 70°C to 56°C, prior to 25 cycles at 55°C (Korbie et al. 2008).

C.1.3 Contamination mitigation

eDNA filtration from ROV and CTD mounted Niskin bottles was conducted on the aft deck of the *R/V Point Sur* on a foldable table. The work surface was bleach sterilized by wiping it with a 10% solution of household bleach and high-purity water, letting it air dry, and then rinsing it with high-purity water. The water was obtained via a Beckman B-pure system in the wet lab on the ship. For sampling at the Viosca Knoll dive site, two Thermofisher D0803 cartridges were run in parallel to purify the water. For all other sampling, the downstream filter was exchanged for a Thermofisher D0809 ultrapure water cartridge. L/S 15 peristaltic pump tubing was sterilized by circulating 10% bleach solution through the tubing for at least five minutes. The tubing was rinsed by pumping fresh high-purity water through it for five minutes (approximately 1 liter). Tubing segments and nylon connectors were sterilized by submersion in a 10% bleach solution for at least 15 minutes and rinsed by submersion in high-purity water for 15 minutes. Nylon connectors were air-dried on a clean paper towel afterwards. Clean nitrile gloves were worn during sampling and the sterilization of sampling materials.

DNA extraction was conducted at a dedicated bench using dedicated pipettes. The work surface was bleach sterilized by wiping it with a 10% solution of household bleach and deionized water, letting it air dry, and then rinsing it with deionized water. Before extraction, pipettes were wiped with a 10% solution of household bleach UV-irradiated in a UV pipette carousel (nUVaClean). Tube racks were immersed in a 10% solution of

household bleach for at least 15 minutes, air-dried, and rinsed with deionized water. eDNA filtration blanks were extracted alongside and processed in the same manner as field samples. PCR reactions were conducted in a dedicated My-PCR Prep Station (Mystaire, Creedmoor, NC, USA) hood with positive airflow, air filtration through a HEPA filter, dedicated pipettes, and an overhead UV lamp. The work surface and pipettes were wiped with a bleach solution and rinsed in the same manner as the extraction materials, and the surface UV-irradiated for 15 minutes. PCR products were visualized on gels and pooled using dedicated pipettes at a separate laboratory bench for post-PCR work. PCR products were only handled at this bench. Sterile, filtered pipette tips were used at all stages of laboratory work.

C.1.4 ROV Video Annotation

Video was recorded using the 4K resolution camera with pan, tilt, and zoom functions. Recorded video was converted to high definition 1080p and annotated using the Video Annotation and Reference System (VARS) version 8.3.4 (Monterey Bay Aquarium Research Institute, Monterey, CA). Annotations with geolocation and depth data were compiled with frame grab images (.png file extension) to generate a catalog of all coral morphospecies observed at each ROV dive site. Morphospecies were identified to the lowest possible taxonomic level from the video imagery and according to published species guides for the region (Shuler and Etnoyer 2020; Opresko et al. 2016). Identifications were only made to more specific taxonomic levels than the video permitted if DNA sequencing data was generated for those morphospecies or if

collections were identified by taxonomic experts from material deposited to the Smithsonian National Museum of Natural History.

C.2 Supplementary Figures

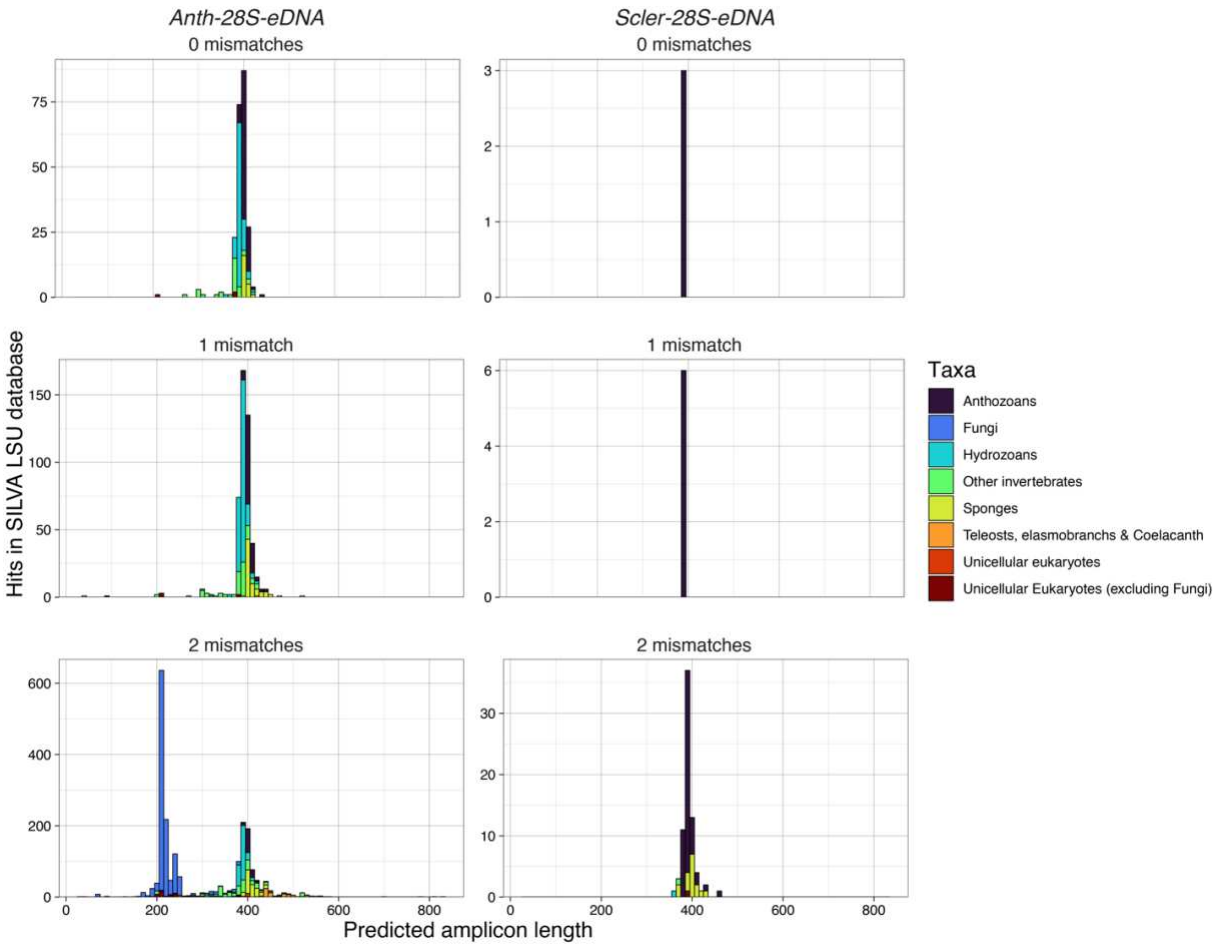

Figure C.1: Results of *in silico* taxonomic specificity testing of the *Anth-28S-eDNA* and *Scler-28S-eDNA* primers against the SILVA large subunit ribosomal RNA database. Amplicons were predicted by querying the database with the primers using *cutadapt* and zero, one, and two permitted mismatches to the primer sequences.

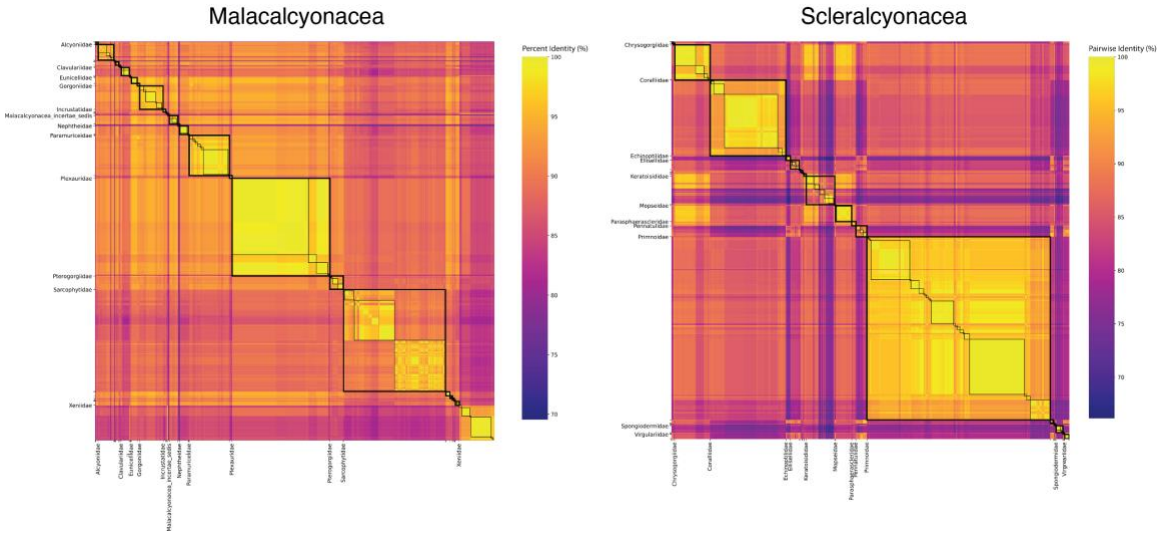

Figure C.2: Matrices of pairwise identities between predicted *mtMutS* barcode sequences amplified using the PCR primers described in Everett and Park (2018). Boxes with thick black lines delineate comparisons within families, and boxes with thin black lines delineate comparisons within genera. Only families represented by the largest numbers of barcode sequences are labeled to highlight these comparisons and improve readability.

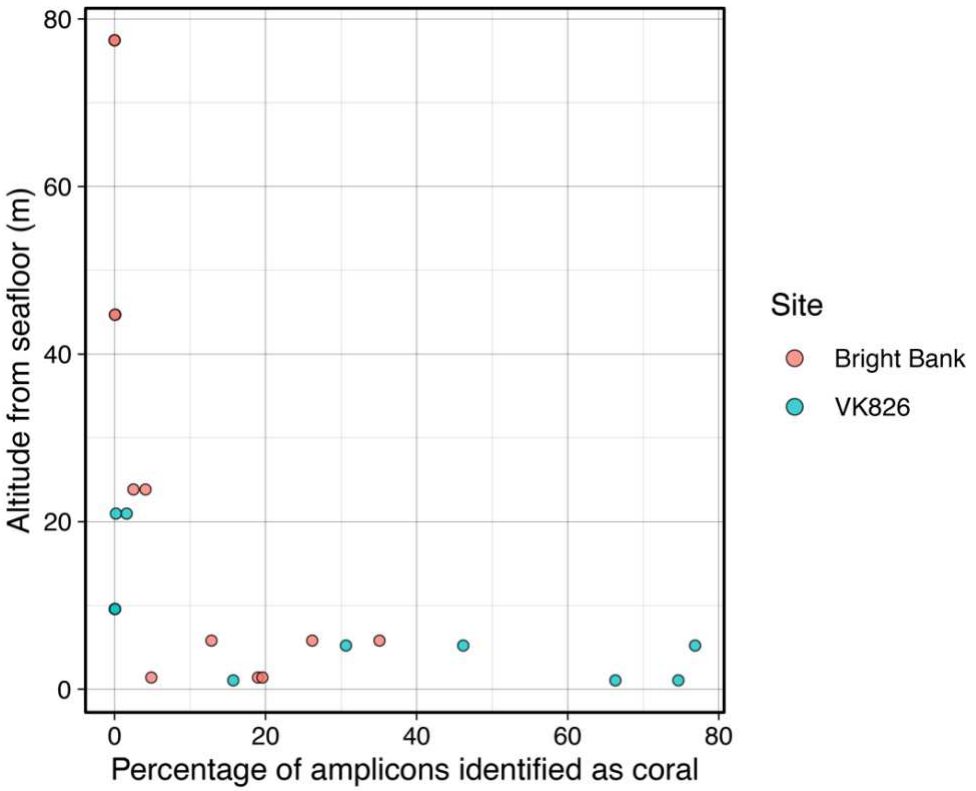

Figure C.3: Percentage of sequencing reads identified as coral across libraries generated from eDNA water samples taken at different altitudes from the seafloor. ASVs were identified as corals if the top BLASTN hit for that ASV was at least 90% identical to an anthozoan coral sequence in GenBank.

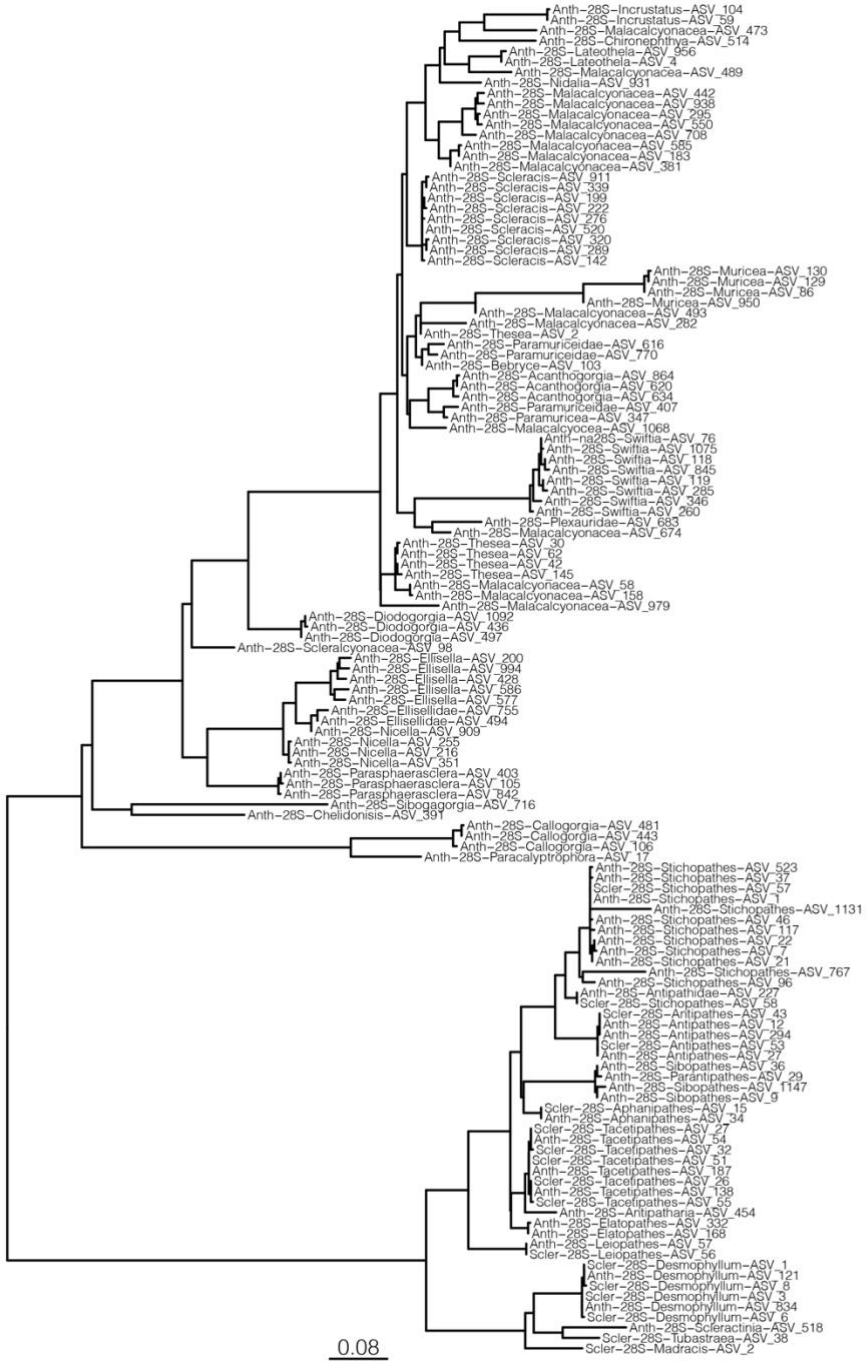

Figure C.4: Maximum-likelihood phylogenetic tree of amplicon sequence variants (ASVs) recovered from eDNA samples collected in the Gulf of Mexico and amplified using the *28S* primers described herein. ASVs were aligned with *MAFFT* and the phylogenetic tree was constructed using *IQTree* and *modelfinder* without bootstrapping.

The model with the lowest BIC is a General Time Reversible model with empirical base frequencies (+F), and rate heterogeneity modeled using a gamma function (+G4). Tips are labeled with the *28S* primer set used, ASV numerical identifier and their taxonomic classification. The tree is rooted at the note representing the most recent common ancestor to hexacorals and octocorals.

C.3 Supplementary Tables

Table C.1: Sample metadata for collections of corals made from field sites in the northwestern Gulf of Mexico that were DNA barcoded through conventional PCR/Sanger sequencing and/or genome skimming.

Table C.1 is included in the supplementary Excel workbook.

Table C.2: *28S* barcode sequences of anthozoan corals generated in this study and downloaded from GenBank for taxonomic classification, as well as analyses of primer complementary and the ability of the *28S* barcode amplified with the primers described herein to delineate taxonomic groups.

Table C.2 is included in the supplementary Excel workbook.

Table C.3: *mtMutS* sequences of octocorals generated in this study or downloaded from GenBank for taxonomic classification, as well as analyses of the ability of the *mtMutS* barcode amplified with the primers described in Everett and Park (2018) to delineate taxonomic groups.

Table C.3 is included in the supplementary Excel workbook.

Table C.4: eDNA sample metadata for eDNA samples analyzed using the *28S rRNA* and *mtMutS* primers in this study.

Table C.4 is included in the supplementary Excel workbook.

C.4 References

Edgar, R. C. (2004). MUSCLE: multiple sequence alignment with high accuracy and high throughput. *Nucleic Acids Research*, *32*(5), 1792–1797. https://doi.org/10.1093/nar/gkh340

Everett, M. V., and Park, L. K. (2018). Exploring deep-water coral communities using environmental DNA. *Deep-Sea Research Part II: Topical Studies in Oceanography*, *150*(September 2017), 229–241. https://doi.org/10.1016/j.dsr2.2017.09.008

Kawato, M., Yoshida, T., Miya, M., Tsuchida, S., Nagano, Y., Nomura, M., Yabuki, A., Fujiwara, Y., & Fujikura, K. (2021). Optimization of environmental DNA extraction and amplification methods for metabarcoding of deep-sea fish. *MethodsX*, *8*, 101238. https://doi.org/10.1016/j.mex.2021.101238

McFadden, C. S., & Ofwegen, L. P. van. (2012). Stoloniferous octocorals (Anthozoa, Octocorallia) from South Africa, with descriptions of a new family of Alcyonacea, a new genus of Clavulariidae, and a new species of Cornularia (Cornulariidae). *Invertebrate Systematics*, *26*(4), 331–356. https://doi.org/10.1071/is12035

Opresko, D. M., Nuttall, M. F., & Hickerson, E. L. (2016). Black Corals of the Flower Garden Banks National Marine Sanctuary. *Gulf of Mexico Science*, *33*(1). https://doi.org/10.18785/goms.3301.05

Shuler, A. & Etnoyer, P. (2020). Alcyonacean octocorals of the Pinnacle Trend: A photo-identification guide. *NOAA technical memorandum NOS NCCOS, 282*. https://dx.doi.org/10.25923/xzd1-z382

APPENDIX D

SUPPORTING INFORMATION FOR CHAPTER 5

D.1 Supplementary Figures

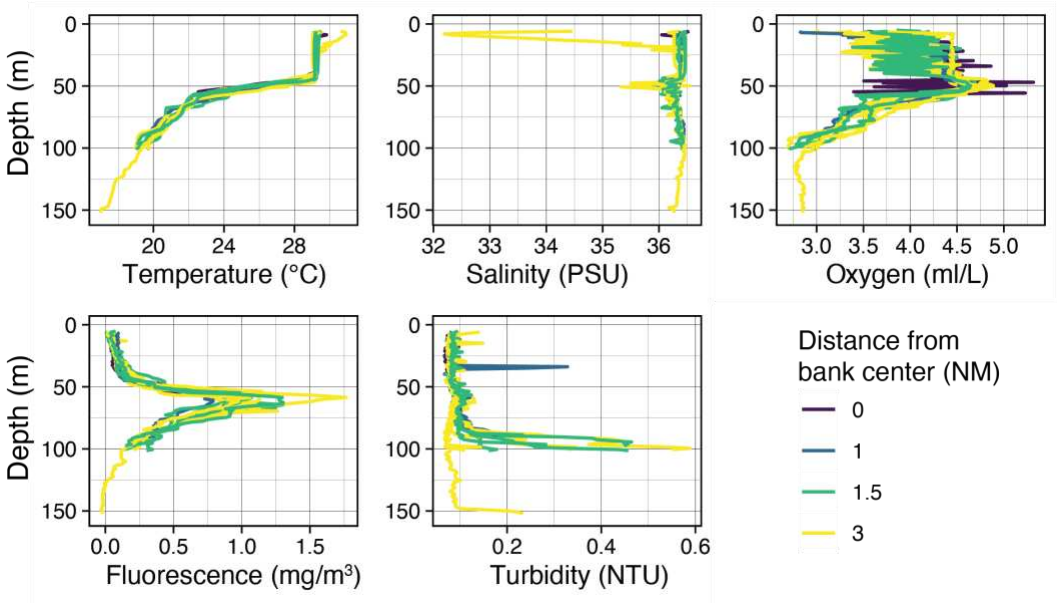

Figure D.1: Profiles of temperature, salinity, oxygen concentration, fluorescence, and turbidity by depth collected during downcasts of Niskin bottle deployments at and near Bright Bank.

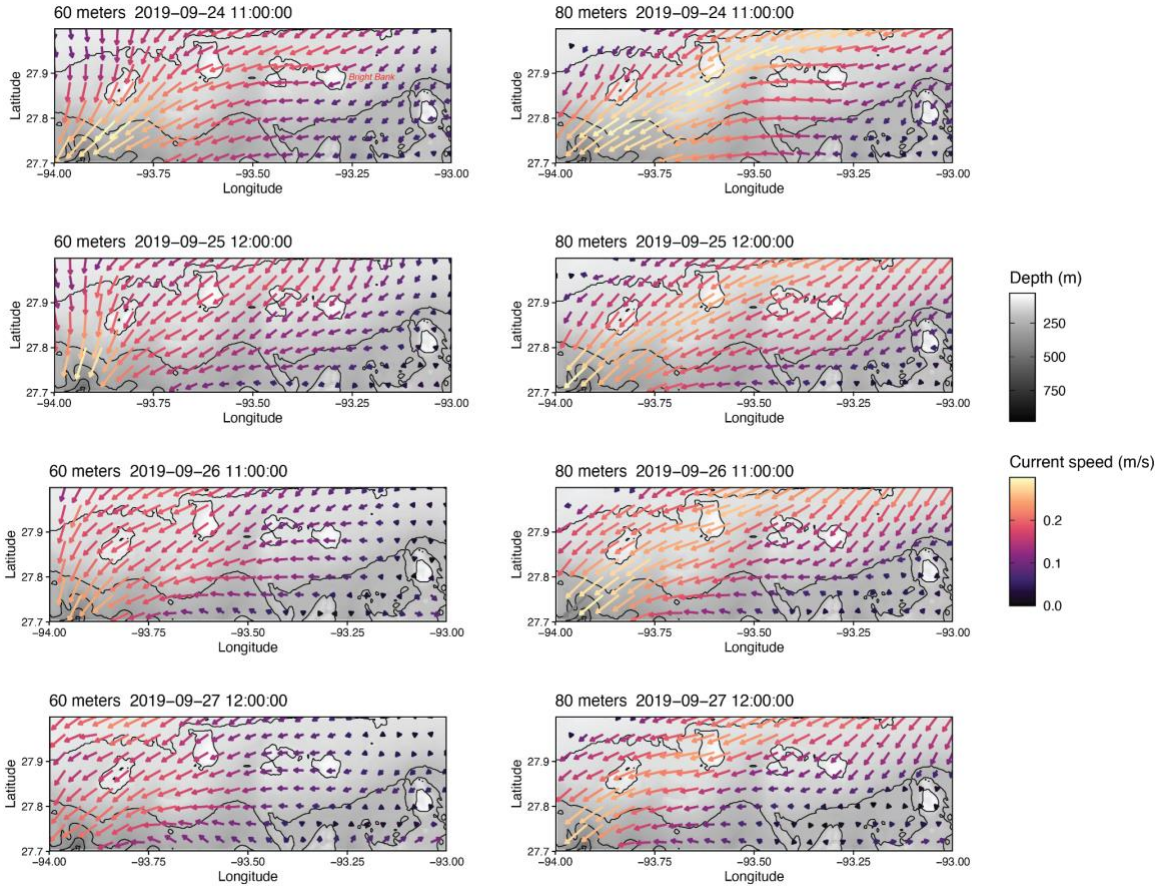

Figure D.2: Hindcasted currents at approximately 24 hour intervals over the course of eDNA sampling. Data are from the HYCOM + NCODA Gulf of Mexico 1/25° Analysis (https://www.hycom.org/data/gomu0pt04/expt-90pt1m000). The spatial extent along the shelf edge includes Bright Bank as well as West Flower Garden Bank and East Flower Garden Bank to the west. Contour lines represent 100 meter isobaths. Times are in universal coordinated time.

VITA

Luke J. McCartin
Birth date: April 1, 1995
Place of birth: Boston, Massachusetts, USA
Parents: Paul McCartin and Janet McCartin

Education

2019 – 2024	**PhD Biological Sciences**, GPA: 4.00 Department of Biological Sciences, Lehigh University, Bethlehem, PA
2013 – 2017	**B.S. Biological Sciences**, GPA: 3.68 Biology Department, University of Vermont, Burlington, VT

Research Appointments

May 2024 – August 2024	**Research Assistant**, Lehigh University, Herrera Lab
January – May 2024	**Thorne Fellow**, Lehigh Department of Biological Sciences
August – December 2023	**Pre-doctoral Research Fellow**, Smithsonian NMNH
June 2020 – August 2023	**Research Assistant**, Lehigh University, Herrera Lab
June 2017 – August 2019	**Research Assistant**, WHOI, Shank Lab
Summer 2016	**Undergraduate Summer Fellow**, University of Vermont, Brody Lab
May 2014 – August 2015	**Biological Science Technician**, USDA-APHIS-PPQ, Gould Lab

Publications

In review (1)

1. **L. J. McCartin**, E. Saso, S. A. Vohsen, N. C. Pittoors, P. Demetriades, C. S. McFadden, A. M. Quattrini & S. Herrera. (2023). *Nuclear eDNA Metabarcoding Primers for Anthozoan Coral Biodiversity Assessment*. https://doi.org/10.1101/2023.10.26.564240.

Published (8)

2. Quattrini, A. M., **McCartin, L. J.**, Easton, E. E., Horowitz, J., Wirshing, H. H., Bowers, H., Mitchell, K., Sei, M., McFadden, C. S., & Herrera, S. (2024). Skimming genomes for systematics and DNA barcodes of corals. *Ecology and Evolution*, *14*(5), e11254. https://doi.org/10.1002/ece3.11254.

3. T. P. Heyl, G. Panieri, D. J. Fornari, R. Mattingsdal, S. Sauer, H. Yao, **L. McCartin**, E. McElwee, & T.M. Shank. (2023). Implications of transient methane flux on associated biological communities in high-arctic seep habitats, Storbanken, Norwegian Barents Sea. *Deep Sea Research Pari I: Oceanographic Research Papers*. 201: 104156. https://doi.org/10.1016/j.dsr.2023.104156.

4. S. Herrera, W. W. Chadwick Jr., M. G. Jackson, J. Konter, **L. McCartin**, N. Pittoors, E. Bushta, & S. G. Merle. (2023). From basalt to biosphere: Early non-vent

community succession on the erupting Vailulu'u deep seamount. *Frontier's in Marine Science* 10. https://doi.org/10.3389/fmars.2023.1110062.

5. F. Govindarajan, A. Adams, E. Allan, S. Herrera, A. Lavery, J. Llopiz, **L. McCartin**, D. R. Yoerger, & W. Zhang. (2023). Advances in Environmental DNA Technology for Observing Ocean Twilight Zone Animal Biodiversity. *2nd Annual Supplement to Oceanography: Frontiers in Ocean Observing*. https://doi.org/10.5670/oceanog.2023.s1.27.

6. F. Govindarajan, **L. J. McCartin,** A. Adams, E. Allan, A. Belani, R. Francolini, J. Fujii, D. Gomez-Ibañez, A. Kukulya, F. Marin, K. Tradd, D. R. Yoerger, J. M. McDermott, S. Herrera. (2022). Improved biodiversity detection using a large-volume environmental DNA sampler with in situ filtration and implications for marine eDNA sampling strategies. *Deep-sea Research Part I – Topical Studies in Oceanography* 189: 103871. https://doi.org/10.1016/j.dsr.2022.103871.

7. **L. J. McCartin,** S. Vohsen, S. Ambrose, M. Layden, C. McFadden, E. Cordes, J. McDermott, S. Herrera. (2022). Temperature Controls eDNA Persistence Across Physicochemical Conditions in Seawater. *Environmental Science & Technology* 56, 12, 8629–8639. https://doi.org/10.1021/acs.est.2c01672.

8. **L. J. McCartin**, N. A. Nasseri, & A. K. Brody. (2019). Potential Consequences of Hosting an Ant-tended Treehopper, *Publilia concava*, for Tall Goldenrod, *Solidago altissima*. *American Journal of Undergraduate Research* 15, 4. https://doi.org/10.33697//ajur.2019.002.

9. J. R. Gould, B. Aflague, T. C. Murphy, **L. McCartin**, J. S. Elkington, K. Rim, & J. J. Duan. (2018). Collecting Nontarget Wood-Boring Insects for Host-Specificity Testing of Natural Enemies of Cerambycids: A Case Study of *Destarcus helophoroides* (Coleoptera: Bothrideridae), a Parasitoid of the Asian Longhorned Beetle (Coleoptera: Cerambycidae). *Environmental Entomology* 47, 6, 1440-1450. https://doi.org/10.1093/ee/nvy121.

Fellowships & Awarded Funding

Awarded

2023 Smithsonian Instruction Fellowship Program – Predoctoral Fellowship, $4,354 USD research allowance and $15,750 stipend

2019 Deep-Sea Biology Society. Travel award towards attendance of the 7th International Symposium on Deep-sea Corals, $927 USD for travel

2016 University of Vermont Office of Undergraduate Research. Summer Undergraduate Research Fellowship: Summer Research Award, $4,879 USD for research and stipend

Invited Talks

2024 Johns Hopkins Applied Physics Laboratory. 3rd National Workshop on Marine eDNA. *Temperature Controls the Degradation Rate of Marine eDNA*.

Smithsonian National Museum of Natural History Department of Invertebrate Zoology. "No Bones" Seminar Series. *Pairing Environmental DNA Sequencing and Genome Skimming to Characterize Anthozoan Coral Biodiversity in the Deep Western Atlantic*

2022 Smithsonian National Museum of Natural History Department of Invertebrate Zoology. "No Bones" Seminar Series. *Environmental DNA Sequencing to Study Deep Coral Communities*

Conference Presentations

2024 **Talk:** Luke McCartin, Emma Saso, Sam Vohsen, Nicole Pittoors, Penny Demetriades, Catherine McFadden, Andrea Quattrini & Santiago Herrera. *New eDNA Meta-barcoding Primers to Elucidate the Distribution of Diverse Anthozoan Corals.* Ocean Sciences Meeting. New Orleans, Lousiana.

2023 **Talk:** Luke McCartin, Emma Saso, Sam Vohsen, Nicole Pittoors, Penny Demetriades, Catherine McFadden, Andrea Quattrini & Santiago Herrera. *Nuclear Environmental DNA Sequencing to Study Mesophotic and Deep Anthozoan Corals.* 8th International Symposium on Deep-sea Corals. Edinburgh, Scotland.

Talk: Luke McCartin, Emma Saso, Sam Vohsen, Nicole Pittoors, Penny Demetriades, Catherine McFadden, Andrea Quattrini & Santiago Herrera. *Nuclear Environmental DNA Sequencing to Study Mesophotic and Deep Anthozoan Corals.* NOAA Open Ocean Restoration Plan, Natural Resource Damage Assessment. Mesophotic and Deep Benthic Communities. 3rd Habitat Assessment and Evaluation Workshop. Smithsonian NMNH, Washington, DC.

2022 **Talk:** L. McCartin, A. F. Govindarajan, J. McDermott, S. Herrera. *Zooplankton eDNA community composition is structured by depth in the epipelagic Gulf of Mexico.* SCOR MetaZooGene Symposium. Dublin, IRL.

Poster: L. J. McCartin, S. Vohsen, S. Ambrose, M. Layden, C. McFadden, E. Cordes, A. F. Govindarajan, J. McDermott, S. Herrera. *Temperature Controls Environmental DNA Persistence Across Physicochemical Conditions in Seawater.* 2nd National Workshop on Marine Environmental DNA. Costa Mesa, CA.

Talk: L. McCartin, S. Ambrose, S. Vohsen, E. Saso, E. Cordes, A. Govindarajan, C. McFadden, A. Quattrini, D. Yoerger, J. McDermott & S. Herrera. *Environmental DNA Sequencing to Study Deep Coral Reefs in the Gulf of Mexico.* The Gulf of Mexico Conference. Baton Rouge, LA.

2021 **Talk:** L. McCartin, S. Vohsen, S. Ambrose, A. Hallaj, M. Layden, E. Cordes, C. McFadden, J. McDermott & S. Herrera. *Physicochemical Controls on the*

Persistence of Marine Environmental DNA. ASLO 2021 Virtual Aquatic Sciences Meeting.

2019 **Lightning talk & poster:** L. McCartin, E. McElwee, T. Heyl, S. Auscavitch, E. Cordes, R. Rotjan & T. M. Shank. *Patterns of Coral Symbiont Distributions Among Deep Waters of Atolls, Islands, Reefs and Seamounts in the Phoenix Islands Protected Area*. 7th International Symposium on Deep-sea Corals. Cartagena, Colombia.

2017 **Poster:** L. McCartin, N. Nasseri & A. K. Brody. *The Ant-hemipteran Mutualism on Goldenrod.* University of Vermont Student Research Conference, Burlington, VT.

External Service

- Co guest editor with Dr. Annette Govindarajan, *Ocean Observing Supplement to Journal of Oceanography Volume 36 – Frontiers in Ocean Observing: Emerging Technologies for Understanding and Managing a Changing Ocean. Topic 6: Environmental DNA Technology*. https://doi.org/10.5670/oceanog.2023.s1.1
- Reviewer: *Environmental Biology of Fishes* (1 review), *Deep-Sea Research Part II* (1 review), and *Environmental DNA* (1 review).

Internal Service

- Reviewer, Lehigh University College of Arts & Sciences Dean's Fellowship
  Spring 2024
  Fall 2024

- Lehigh Biology Graduate Student Organization Officer
  2023-2024 Academic Year: *Treasurer*
  2022-2023 Academic Year: *Vice President*
  2021-2022 Academic Year: *President*
  2020-2021 Academic Year: *Secretary*

Research Cruise Participation

2023 Health Diagnostics of Deep-sea Corals, *R/V Falkor (too)*, San Juan, Puerto Rico

AT50-07, *R/V Atlantis*, Puntarenas, Costa Rica

2022 SALT3, *R/V Point Sur*, Gulfport, Mississippi

Illuminating Biodiversity, *NOAA Ship Nancy Foster,* San Juan, Puerto Rico

2021 Connectivity of Coral Ecosystems, *R/V Point Sur*, Gulfport, Mississippi

2019 Environmental DNA Exploration Cruise, *R/V Manta*, Galveston, Texas

2017 Deep-sea Corals of PIPA, *R/V Falkor*, Honolulu, Hawaii – Apia, Samoa

Professional Development

2024 Workshop on Molecular Evolution, University of Chicago's Marine Biological Laboratory, Woods Hole, MA.

Deep Submergence Science Committee (DeSSC) New Users Program, New Orleans, LA.

2022 2nd National Workshop on Marine Environmental DNA, Southern California Coastal Water
Research Project, Costa Mesa, CA.

Strategies and Techniques for Analyzing Microbial Population Structures (STAMPS), University of Chicago's Marine Biological Laboratory, Woods Hole, MA.

Societal Memberships

- Deep-Sea Biology Society

Mentorship

NMNH intern

- Annemarie Wood, 2023 graduate from Haverford College

Graduate students

- Milan Sengthep, Biology PhD Student, Lehigh University

Lehigh undergraduate students

- Penny Demetriades, Lehigh Class of 2022, Starting PhD at U. of Southern Alabama in Fall 2022
- Luis Caceres, Lehigh Class of 2024, RARE student, STEM-SI program
- Maia Clayton, Lehigh Class of 2023, Work study student
- Mary Mahoney, Lehigh Class of 2023, STEM-SI program
- Carly Hecht, Lehigh Class of 2023, Research for Credit
- Petra Oganovich, Lehigh Class of 2026, Research for Credit

Teaching Appointments & Jobs

Fall 2021	**Teaching Assistant:** Lehigh University, *Evolution*
Spring 2021	**Teaching Assistant:** Lehigh University, *Biology Core III*
Spring 2020	**Teaching Assistant,** Lehigh University, *Biostatistics and Microbiology lab*
Fall 2019	**Teaching Assistant:** Lehigh University, *Biology Core III*
June 2018 – August 2019	**Math & Science Tutor:** Solutions Learning Center, Osterville, MA
Spring 2017	**Biology Tutor:** University of Vermont Center for Academic Success
Fall 2016 – Spring 2017	**Undergraduate TA:** University of Vermont, biology teaching labs

Education & Outreach

2024 **Web article by Naomi Greenburg:** *Collecting Coral Codes: Environmental DNA Helps Scientists Assess Coral Biodiversity* on the Smithsonian NMNH Ocean Find Your Blue site https://ocean.si.edu/collecting-coral-codes-environmental-dna-helps-scientists-assess-coral-biodiversity
Expert Is in Takeover: Ocean Hall, Smithsonian National Museum of Natural History

2023 **Lecture:** Seaside Chats Webinar Series: National Marine Sanctuaries Education, *Coral Forensics in the Deep Flower Garden Banks*

2022 **Blog post:** *New Methodology for eDNA Collection to Study Deep-sea Ecosystems of Puerto Rico,* on the NOAA OER *Illuminating Biodiversity* expedition site https://oceanexplorer.noaa.gov/explorations/22puerto-rico-deepwaters/features/edna/edna.html
Expert Is in Takeover: Ocean Hall, Smithsonian National Museum of Natural History
Science Fair Judge: Southern Lehigh High School, Center Valley, PA

2021 **Lecture:** *Using Molecular Tools to Study Marine Biology*. SEA Semester: Marine Biodiversity and Conservation course, Woods Hole, MA.
Lecture: Dr. Amber Rice's Evolution Course, Lehigh University, Bethlehem, PA.

2020 **Science Fair Judge:** Southern Lehigh High School, Center Valley, PA

2019 **Lecture:** *Bird Banding on Wing Island,* Cape Cod Museum of Natural History Field Guide Training Program. Brewster, MA.

2017 **Blog post:** *Deep-sea Fish of PIPA* on the Schmidt Ocean Institute *Deep-sea Corals of PIPA* expedition site: https://schmidtocean.org/cruise-log-post/deep-sea-fish-pipa/